USZ Universitäts Spital Zürich

**Direktion Forschung und Lehre**

# Programm

## 19th Day of Clinical Research

Georg Friedrich Götz Preisverleihung 2020

27. August 2020

Universität Zürich[UZH]

**Assoziierte Kliniken**
Universitätsklinik Balgrist
Kinderspital Zürich
Psychiatrische Universitätsklinik Zürich
Zentrum für Zahnmedizin

## Committee Day of Clinical Research

Aguzzi Adriano, Prof. Dr.
Cinelli Paolo, PD Dr.
Distler Oliver, Prof. Dr.
Katan Kahles Mira, PD Dr.
Moch Holger, Prof. Dr.
Schneider Robin, MBA
Senti Gabriela, Prof. Dr.
Speck Roberto, Prof. Dr.
Van den Broek Maries, Prof. Dr.
von Eckardstein Arnold, Prof. Dr.
Weller Michael, Prof. Dr.
Zinkernagel Annelies, Prof. Dr.

## Table of contents



**Cover Figure**:
Prof. Dr. med. Adriano Aguzzi, Institutsdirektor, Institut für Neuropathologie, Universitätsspital Zürich

An advanced machine-learning technique (generative adversarial neural networks, or GAN) was applied to a 3D scan of a mouse brain and to a painting by Vincent Willem van Gogh. The GAN computed a painting based on a virtual longitudinal midline brain section.
Credits: Alessandro Crimi & Daniel Kirschenbaum

# Programm

## Donnerstag, 27. August 2020

Grosser Hörsaal Ost, USZ

08.15 **Eröffnung**
Prof. Dr. med. Gabriela Senti
Direktorin Forschung und Lehre, Universitätsspital Zürich

08.20 **Begrüssung**
Prof. Dr. med. Gregor Zünd
Vorsitzender der Spitaldirektion / CEO, Universitätsspital Zürich

08.25 **Begrüssung**
Prof. Dr. med. Rainer Weber
Dekan der Medizinischen Fakultät der Universität Zürich

### Session 1: Cardiovascular/Metabolism/Endocrinology
**Chairpersons: PD Dr. med. Elena Osto / PD Dr. med. Jelena-Rima Templin-Ghadri**

08.35 Wissenschaftliches Hauptreferat
**«Biology and mechanics of aortic aneurysm - two sides of the same coin»**
Prof. Dr. med. Alexander Zimmermann, Klinikdirektor, Klinik für Gefässchirurgie, Universitätsspital Zürich

08.55 **Decoding the vasodilatory effects of bile acid through TGR5 receptor**
A. Nasrallah, M. Kraljevic, A. Taheri, V. Marzolla, A. Jomard, C. Wolfrum, A. von Eckardstein, F. Ruschitzka, T. Lutz, E. Osto

09.05 **The methyltransferase SETD7 promotes myocardial ischemic injury by activating Hippo signalling**
S. Ambrosini, F. Montecucco, A. Akhmedov, S. Mohammed, T. Lüscher, S. Costantino, F. Paneni

09.15 **Novel echocardiographic methods for outcome prediction in patients with Arrhythmogenic Right Ventricular Cardiomyopathy**
S. Hosseini, Sh. Anwer, P. Heiniger, F. Gustafierro, N. Kuzo, R. Hess, C. Brunckhorst, F. Dura, A. Saguner, F. Tanner

**09.25 Coffee Break**

### Session 2: Hematology/Oncology (inkl. Götz-Preis-Verleihung Teil I)
**Chairpersons: PD Dr. med. Alexandre Theocharides / Prof. Dr. César Nombela Arrieta**

09.40 **Einführung und Würdigung des Preisträgers**
Herr Dr. med. Steffen Böttcher, durch Prof. Dr. med. Rainer Weber, Dekan der Medizinischen Fakultät

09.45 Kurzreferat von Dr. med. Steffen Böttcher
**«Die Entschlüsselung der funktionellen Konsequenzen von TP53Missense-Mutationen in der Krebsentstehung»**
Klinik für Medizinische Onkologie und Hämatologie, Universitätsspital Zürich

10.00 **Preisverleihung** durch Prof. Dr. med. Beatrice Beck Schimmer,
Direktorin Universitäre Medizin und Stiftungsratspräsidentin

10.10 Wissenschaftliches Hauptreferat
**«Intracavitary chemotherapy for mesothelioma from bench to bedside»**
Prof. Dr. med. Isabelle Schmitt-Opitz, Klinikdirektorin, Klink für Thoraxchirurgie, Universitätsspital Zürich

10.30 **Immunocytokines are a novel immunotherapeutic approach against glioblastoma**
T. Weiss, E. Puca, M. Weller, D. Neri, P. Roth

ANNULIERT

10.40 **Activation of CD271 (NGFR) intracellular death domain induces apoptosis and overcomes targeted therapy resistance in melanoma ex-vivo and in vivo models**
A. Saltari, A. Dzung, N. Tiso, M. Quadri, O. Eichhoff, A. Marconi, C. Pincelli, R. Dummer, M. Levesque

10.50 **A phase I clinical trial of malignant pleural mesothelioma treated with locally delivered autologous fibroblast activating protein (FAP)-targeting chimeric antigen receptor (CAR) T cells**
S. Hiltbrunner, C. Britschgi, C. Magnani, L. Bankel, T. Nguyen-Kim, P. Gulati, W. Weder, I.Opitz, O. Lauk, C. Caviezel, A. Tabor, P. Schröder, A. Knuth, C. Münz, C. Renner, R. Stahel, O. Boyman, U. Petrausch, A. Curioni-Fontecedro

## Session 3: Head Region / Neuroscience (inkl. Götz-Preis-Verleihung Teil II)
**Chairpersons: Dr. Lukas Imbach / Dr. Konrad Peter Weber**

11.05 **Einführung und Würdigung der Preisträgerin**
Frau Prof. Dr. sc. nat. Silvia Brem, durch Prof. Dr. med. Rainer Weber, Dekan der Medizinischen Fakultät

11.10 Kurzreferat von Prof. Dr. sc. nat. Silvia Brem
**«Lesenlernen und Lese- und Rechtschreibstörung: Neurowissenschaftliche Einblicke in die Entwicklung des Lesenetzwerkes im Gehirn»**
Klinik für Kinder- und Jugendpsychiatrie und Psychotherapie, Psychiatrische Universitätsklinik Zürich

11.25 **Preisverleihung** durch Prof. Dr. med. Beatrice Beck Schimmer,
Direktorin Universitäre Medizin und Stiftungsratspräsidentin

**11.30 Apéro Riche für Teilnehmer der Götz-Preis Verleihung**

11.35 Wissenschaftliches Hauptreferat
«**Genome-wide and brain-wide efforts to understand neurodegeneration»**
Prof. Dr. med. Adriano Aguzzi, Institutsdirektor, Institut für Neuropathologie, Universitätsspital Zürich

11.55 **Large patient cohort reveals increased plasma autoantibodies against tau protein aggregation domain in specific diseases**
A. Magalhães, A. Chincisan, M. Emmenegger, S. Hornemann, A. Aguzzi

12.05 **The Zurich Experience in Autologous Hematopoietic Stem Cell Transplantation for the Treatment of Multiple Sclerosis (aHSCT-in-MS) 18 Months after Approval**
I. Jelcic, A. Müller, P. Stathopoulos, N. Wolfensberger, J. Ruder, A. Thesenvitz, K. Ritter, A. Bachofner, M. Foege, A. Lutterotti, U. Schanz, R. Martin

12.15 **Whole genome RNAi screen identifies novel regulators of PrPC**
D. Heinzer, M. Avar, D. Pease, B. Doğançay, J. Yin, A. Chincisan, E. Schaper, M. Emmenegger, S. Hornemann, A. Aguzzi

**12.30 Lunch / Poster viewing**

## Session 4: Infection/Immunity/Inflammation/Systemic Diseases
**Chairpersons: Prof. Dr. Michael Scharl / Dr. Ilijas Jelcic**

14.00 Wissenschaftliches Hauptreferat
**«Clinical perspective on chronic - recurring staphylococcal infections»**
Prof. Dr. med. Annelies Zinkernagel, Leitende Ärztin, Klinik für Infektionskrankheiten und Spitalhygiene, Universitätsspital Zürich

14.20 **Sustained viral suppression with dolutegravir monotherapy during 9,899 patient weeks of follow-up in individuals starting combination antiretroviral therapy during primary HIV infection**
D. Braun, T. Turk, B. Hampel, T. Bühler, C. Grube, N. Lutz, C. Depmeier, H. Kuster, M. Flepp, K. Metzner, J. Böni, R. Kouyos, H. Günthard

14.30 **PTPN2 in dendritic cells exerts an anti-inflammatory role and is crucial for maintaining tissue tolerance**
L. Hering, E. Katkeviciute, M. Schwarzfischer, P. Busenhart, C. Gottier, D. Mrdjen, J. Komuczki, S. Lang, B. Becher, G. Rogler, M. Scharl, M. Spalinger

ANNULIERT

14.40 **Allergen-blocking antibodies: a novel concept of peanut-allergy immunotherapy**
M. Paolucci, N. Wuillemin, C. Arena, Y. Wäckerle-Men, T. Kündig, D. Bieli, T. Sonati, P. Johansen

## Session 5: Mixed Topics

**Chairpersons: Prof. Dr. med. Brigitte Leeners / Prof. Dr. Dominik Schaer**

14.55 Wissenschaftliches Hauptreferat
«**Patient journey analysis: a new paradigm for learning from health data»**
Prof. Dr. med. Michael Krauthammer, Managing Director, Medizininformatik, Universitätsspital Zürich

15.15 **Innovative trial design using digital approaches: an example from reproductive medicine**
G. Hamvas, A. Hofmann, V. Sakalidis, B. Goodale, M. Shilaih, B. Leeners

15.25 **Does oxycarbon improve cerebral oxygenation during apnea? A mono-center randomized cross-over trial inspired by aviation-research**
M. Schmidt, M. Studer, A. Kunz, S. Studer, J. Bonvini, M. Bueter, L. Kook, S. Haile, B. Beck-Schimmer, M. Schläpfer

15.35 **Health status, use of medication and recreational drugs during pregnancy: a cross-sectional survey in the Canton of Zurich**
E. Randecker, G. Gantner, D. Spiess, A.P. Simões-Wüst

**15.50 Coffee Break**

## Session 6: Klinische Forschungsschwerpunkte

16.05 **Präsentation**
**«Artifical intelligence in oncological imaging network»**
Prof. Dr. Dr. med. Andreas Boss; Leitender Arzt, Institut für Diagnostische und Interventionelle Radiologie, Universitätsspital Zürich
Prof. Dr. med. Nicolaus Andratschke, Leitender Arzt, Stv. Klinikdirektor, Klinik für Radio-Onkologie, Universitätsspital Zürich

16.25 **Präsentation**
**«Zurich initiative on novel cytokine-directed treatments for immune dysregulation (CYTIMM-Z)»**
Prof. Dr. med. Onur Boyman, Klinikdirektor, Klinik für Immunologie, Universitätsspital Zürich

## 16.50 Verleihung Day of Clinical Research-Preis

17.00 **Apéro**

ANNULIERT

## Cardiovascular / Metabolism / Endocrinology

### Basic Research

18
S. Ambrosini, F. Montecucco, A. Akhmedov, S. Mohammed, T. Lüscher, S. Costantino, F. Paneni
The methyltransferase SETD7 promotes myocardial ischemic injury by activating Hippo signalling

60
A. Hülsmeier, T. Hornemann
Association between lipid droplets and 1-deoxy-sphinglipid formation

61
L. Liberale, A. Akhmedov, N. Vlachogiannis, N. Bonetti, V. Nageswaran, M. Miranda, F. Montecucco, J. Beer, T. Lüscher, K. Stamatelopoulos, K. Stellos, G. Camici
Sirtuin 5 promotes arterial thrombosis through endothelial plasminogen activator inhibitor-1

66
Y. Puspitasari, C. Diaz-Canestro, I. Sudano, A. Flammer, N. Bonetti, P. Wuest, L. Liberale, S. Constantino, F. Paneni, J. Beer, F. Ruschitzka, M. Hermann, T. Luscher, G. Camici
The Role of Matrix Metalloproteinase-2 on Age-dependent Arterial Stiffness

72
A. Nasrallah, M. Kraljevic, A. Taheri, V. Marzolla, A. Jomard, C. Wolfrum, A. von Eckardstein, F. Ruschitzka, TA. Lutz, E. Osto
Decoding the vasodilatory effects of bile acid through TGR5 receptor

76
J. Jelisejevas, D. Hofer, A. Saguner, A. Breitenstein, J. Steffel
Retrospective analysis of left femoral access for leadless pacemaker implantations

94
G. Karsai, M. Lone, Z. Kutalik, T. Brenna, H. Li, D. Pan, A. von Eckardstein, t. Hornemann
FADS3 is a delta14Z sphingoid base desaturase that ameliorates the 1-deoxy-dihydroceramide associated toxicity

112
G. Panteloglou, P. Zanoni, L. Rohrer, J. Kuivenhoven, A. Rimbert, A. Tybjaerg-Hansen, N. Dalila, W. März, A. von Eckardstein
The coatomer (COP I) complex limits the cell-surface abundance of the LDL receptor and cellular LDL uptake

141
M. Lone, T. Hornemann
Tango to promiscuity: Role of SPTLC3 in generating sphingolipid diversity in Human cells

215
R. Chen, S. Saponara, T. Reding, R. Graf, S. Sonda
Peripheral serotonin-p21 axis contributes to metabolic changes during ageing

### Translational Research

73
M. Generali, E. Casanova, D. Kehl, D. Wanner, S. Hoerstrup, P. Cinelli, B. Weber*
Autologous endothelialized small-caliber vascular grafts engineered from blood-derived induced pluripotent stem cells

97
A. Jomard, O. Chavez-Talavera, A. Tailleux, P. Doytcheva, M. Bueter, A. Othman, A. Taheri, C. Wolfrum, T. Lutz, A. Von Eckardstein, F. Ruschitzka, B. Staels, E. Osto
Endothelial protective properties of Bile Acids bound to High-Density Lipoproteins: a novel therapeutic approach against obesity induced endothelial dysfunction

116
S. Saeedi Saravi, G. Camici, T. Lüscher, T. Michel, J. Beer
Age-dependent changes of aquaporin-1 modulate platelet/endothelial dysfunction in atherothrombosis

167
M. Kahr, M. Rothenbühler, P. Silber, D. Perrouchoud, H. Györgyi, M. Shilaih, B. Leeners
Association of physiological and psychological stress and menstrual cycle disorders

170
M. Lipiski, M. Eberhard, T. Fleischmann, S. Halvachizadeh, B. Kolb, F. Maisano, M. Kron, V. Falk, MY. Emmert, H. Alkadhi, N. Cesarovic
Computed Tomography-based evaluation of porcine cardiac dimensions to assist in pre-study planning and optimized model selection for pre-clinical research

183
I. Martinez Lopez, T. Papasotiropoulos, F. Schläpfer, S. Ulrich, M. Kirschner, I. Schmitt-Opitz
Biomarker identification for chronic thromboembolic pulmonary hypertension

**Clinical Trials**

10
J. Rössler, F. Schoenrath, S. Seifert, A. Kaserer, G. Spahn, V. Falk, D. Spahn
Iron deficiency is associated with higher mortality in patients undergoing cardiac surgery: a prospective study

70
M. Barbagallo, D. Naef, J. Beer, H. Hireche-Chikaoui
Right ventricular thrombi, a challenge in imaging diagnostics: a case series study

108
B. Kovacs, S. Reek, C. Sticherling, A. Linka, P. Ammann, N. Krasniqi, A. Müller, R. Kobza, J. Schlaepfer, T. Reichlin, L. Haegeli, K. Mayer, H. Burri, A. Saguner, J. Steffel, F. Duru
Which patients are most likely to benefit from the wearable cardioverter-defibrillator? – findings from the Swiss WCD registry

153
S. Anwer, P. Heiniger, S. Rogler, D. Cassani, J. Kebernik, N. Kuzo, L. Rebellius, G. Alexander, D. Schmid, M. Schuermann, A. Pazhenkottil, M. Meyer, R. Schoenenberger-Berzins, C. Gruner, F. Tanner
Circumferential deformation for diagnosis and risk assessment in left ventricular non-compaction

158
S. Costa, A. Gasperetti, D. Akdis, G. Suna, A. Medeiros-Domingo, C. Brunckhorst, F. Duru, A. Saguner
Familial ARVC in light of new genetic evidence: a case report

159
A. Gasperetti, S. Costa, D. Akdis, A. Breitenstein, D. Hofer, C. Brunckhorst, C. James, M. Casella, L. Chen, S. Kany, S. Schenker, H. Jensen, M. Shibu, P. Platonov, S. Willems, H. Calkins, C. Tondo, J. Steffel, F. Duru, A. Saguner
First-in-World Report of Outcomes of Catheter Ablation for Atrial Arrhythmias in Arrhythmogenic Right Ventricular Cardiomyopathy

162
N. Kuzo, B. Stähli, J. Kebernik, T. Nguyen-Kim, M. Eberhard, M. Schindler, F. Ruschitzka, F. Tanner
Normal Coronary Arteries as Negative Risk Marker in Patients with Severe Aortic Stenosis Undergoing Transcatheter Aortic Valve Replacement

205
S. Hosseini, S. Anwer, P. Heiniger, F. Gustafierro, N. Kuzo, R. Hess, C. Brunckhorst, F. Dura, A. Saguner, F. Tanner
Novel echocardiographic methods for outcome prediction in patients with Arrhythmogenic Right Ventricular Cardiomyopathy

211
M. Arnold, J. Schweizer, U. Fischer, L. Bonati, GD. De Marchis, K. Nedeltchev, T. Kahles, C. Cereda, G. Kägi, J. Monataner, G. Ntaois, C. Förch, A. Luft, K. Spanaus, A. von Eckardstein, M. Katan Kahles
Lipoprotein(a) is associated with large artery atherosclerosis (LAA) stroke etiology and recurrent cerebrovascular events: Results from the BIOSIGNAL Study

212
M. Arnold, C. Nakas, A. Luft, M. Christ-Crain, A. Leichtle, M. Katan Kahles
Independent prognostoc value of MRproANP levels in stroke patients is unaltered over time

## Hematology / Oncology

### Basic Research

5
E. Katkeviciute, L. Hering, A. Montalban-Arques, P. Busenhart, J. Conde Aranda, E. Naschberger, G. Leventhal, K. Atrott, S. Lang, O. Boyman, M. Stürzl, M. Scharl, M. Spalinger
PTPN2 deficiency increases the infiltration and cytotoxicity of CD8+ T cells and promotes the immunogenicity in hard to treat solid tumors

53
E. Cannizzaro, J. Lu, C. Boudesco, T. Zenz
Role of DDX3X in B cell lymphoma

89
A. Hariharan, M. Ronner, M. Sculco, E. Felley-Bosco
RNA editing and interferon signalling in mesothelioma

90
A. Gomariz, P. Helbling, S. Isringhausen, U. Suessbier, M. Manz, O. Goksel, C. Nombela-Arrieta
Deep Neural Networks for the Characterization of the BM Vasculature with Different Immunomarkers

95
M. Meerang, J. Kreienbühl, V. Orlowski, S. Müller, M. Kirschner, W. Weder, I. Schmitt-Opitz
Importance of Cullin4 Ubiquitin Ligase in Malignant Pleural Mesothelioma

120
M. Valletti, D. Eshmuminov, C. Gutschow, K. Kuno
Survival benefit in gastric cancer patients with chemotherapy-responsive peritoneal disease: a plea for a better local control

128
E. Felley-Bosco, J. Fonteneau, W. Qi, M. Ronner, A. Hariharan, C. Blanquart, H. Rehrauer
Contribution of RNA editing to mesothelioma heterogeneity

134
S. Sun, M. Ronner, F. Frontini, W. Qi, H. Rehrauer, A. Hariharan, M. Wipplinger, E. Felley-Bosco
Endogenous Retrovirus expression and activation of type-I interferons signaling in an experimental mouse model of mesothelioma development

135
N. Karavasiloglou, K. Matthes, M. Limam, D. Korol, M. Wanner, S. Rohrmann
Risk of subsequent invasive cancers in women diagnosed with breast cancer in situ: Results from the Cancer registry of Zurich, Zug, Schaffhausen and Schwyz

156
S. Steiner, T. Reding, D. Lenggenhager, M. Stopic, M.E. Healy, A. Gupta, G. Wanner-Seleznik, R. Graf
Gastrokine 1 and 2 in pancreatic carcinogenesis: one family with two distinct roles?

157
M. Wipplinger, M. Ronner, A. Okonska, A. Hariharan, E. Felley-Bosco
Identifying the regulatory role of Adenosine deaminase acting on dsRNA editing on RNA Binding Motif 8 protein in mesothelioma

169
JH. Jang, M. Haberecker, C. Curioni-Fontecedro, A. Soltermann, I. Gil-Bazo, F. Janker, H. Ilseon, K. Kwon, W. Weder, W. Jungraithmayr
CD26/DPP4 a novel prognostic marker for lung adenocarcinoma

192
I. Dubach, R. Buzzi, A. Yalamanoglu, F. Vallelian, D. Schaer
Comparative phenotype characterization of three hemolytic genes in the mouse

199
C. Meisel, C. Porcheri, T. Mitsiadis
The Role of Notch Signaling in Oral Cancers

200
PM. Helbling, A. Gomariz, K. Loosli, S. Isringhausen, T. Yokomizo, M. Manz, C. Nombela-Arrieta
Tissue-Scale Spatial Analysis of Hematopoietic Stem Cells and Stromal Niche Subtypes in the Fetal Liver Microenvironment

209
P. Schürch, A. Lakkaraju, L. Malinovska, T. Wildschut, V. Lysenko, A. Aguzzi, P. Picotti, A. Theocharides
CALR mutations in myeloproliferative neoplasms affect chaperone function and differentially impact on client proteins

216
C. Caiado, L. Kovtonyuk, M. G. Manz
Contribution of IL-1 Mediated Inflamm-ageing to Clonal Hematopoiesis Progression in Murine Models

**Translational Research**

42
C. Fritz, K. Zimmermann, M. Weller, C. Boudesco, T. Zenz, M. Rechsteiner, E. Haralambieva, S. Balabanov, U. Wagner
A Custom NGS-based Panel for Genetic Diagnostics of Lymphoid and Myeloid Malignancies

46
L. Bankel, W. Rebekka, K. Dedes, D. Franzen, P. Bode, H. Moch, M. Manz, C. Britschgi, B. Snijder
Single-cell ex vivo drug response testing on fluid samples from patients with solid tumors

51
F. Meier-Abt, W. Wolski, G. Tan, L. Gillet, S. Amon, A. Theocharides*, R. Aebersold*, M. Manz*
Repression of CXCL4/PF4 and activation of NFκB signaling suggests promotion of stem cell hyperproliferation in polycythemia vera patients

52
E. Breuer, M. Schneider, J. Eden, B. Pache, T. Steffen, M. Hübner, R. Lilian, A. Gupta, V. Kepenekian, G. Passot, P. Gertsch, O. Glehen, K. Lehmann
Mutations of Ras/Raf-Proto-Oncogenes impair Survival after Cytoreductive Surgery & HIPEC: Tumor biology remains king

69
L. Russo, L. Roth, A. Gupta, K. Lehmann
Improving loco-regional treatment of peritoneal metastasis

74
S. Hiltbrunner, S. Kasser, S. Freiberger, S. Kreutzer, N. Toussaint, L. Grob, M. Rechsteiner, A. Soltermann, A. Curioni-Fontecedro
Resistance mechanisms in non-small cell lung cancer patients upon anti-PD1 therapy

78
A. La Greca Saint-Esteven, J. van Timmeren, S. Tanadini-Lang, E. Konukoglu
HPV Status Prediction Using Deep Learning in Head-and-Neck Cancer Patients

80
I. Banik, M. Levesque, E. Busch, C. Dooley, E. Patton, T. Jana, P. Cheng
NRASQ61K melanoma is more aggresive than BRAFV600E melanoma in zebrafish models and can be rescued by p38 activation

86
L. Isenegger, P. Bode, C. Pauli, U. Camenisch, C. Matter, H. Moch, C. Britschgi
Phenotypic and Functional Validation of an in vitro Candidate Kinase Inhibitor Screen in Clear Cell Sarcoma

107
H. Meister, M. Weller, S. Pascolo, P. Roth, T. Weiss
Engineered mRNA-based multifunctional chimeric antigen receptor (CAR) T cells show anti-tumor activity in glioblastoma

115
S. Hussung, B. Pfefferle, F. Nollmann, R. Klar, A. Devisme, M. Boerries, U. Wittel, R. Fritsch
Ex vivo Drug Testing in Patient-Derived Pancreatic Cancer Organoids Challenges and Potential Applications

123
H. Gannon, T. Zoa, M. Kiessling, E. Levanon, W. Hahn, M. Meyerson
Dependency on the adenosine deaminase ADAR1

133
C. Millan, L. Prause, N. Hensky, T. Sulser, D. Eberli
Culture of Cancer Cells in 3D Hydrogels Induces Secretion of EVs that Promote Invasion and Chemoresistance

136
S. Hiltbrunner, R. Wechsler, A. Friedlaender, D. Akhoundova, L. Bankel, S. Kasser, S. Bihr, C. Britschgi, A. Addeo, M. Maathuis, A. Curioni-Fontecedro
Biomarkers for immunotherapy in non-small cell lung cancer patients based on retrospective data from USZ and HUG

138
O. Lauk, V. Orlowski, T. Neuer, B. Battilana, I. Schmitt- Opitz, M. Kirschner
Association between microRNAs and clinical, inflammatory factors in patients with malignant pleural mesothelioma undergoing multimodality therapy

139
Y. Zhang, F. Schläpfer, V. Orlowski, I. Schmitt-Opitz, M. Kirschner
MicroRNAs in chemotherapy response in malignant pleural mesothelioma

140
M. Kirschner, M. Meerang, O. Lauk, K. Furrer, I. Grgic, V. Orlowski, F. Tschanz, M. Guckenberger, M. Pruschy, W. Weder, I. Schmitt-Opitz
Efficacy of irradiation combined with intracavitary cisplatin-fibrin after lung-sparing surgery in an orthotopic rat model of mesothelioma

142
P. Knobel, V. Waller, M. Pruschy
Exploring ADAM17 as an immune checkpoint modulator

144
D. Vuong, M. Bogowicz, J. Unkelbach, S. Hillinger, S. Thierstein, E. Eboulet, S. Peters, M. Pless, M. Guckenberger, S. Tanadini-Lang
Quantitative image analysis to compare anatomical primary tumor location for surgical and non-surgical treatment regimens for locally advanced NSCLC (SAKK 16/00)

147
H. Gabrys, L. Basler, S. Hogan, M. Pavic, M. Bogowicz, D. Vuong, S. Tanadini-Lang, R. Förster, M. Huellner, R. Dummer, M. Guckenberger, M. Levesque
Radiomics for prediction of metastatic melanoma patient survival after immunotherapy

154
J. Müller, R. Myburgh, M. Manz
Combinatorial Chimeric Antigen Receptor T cells for the Treatment of Acute Myeloid Leukemia

161
M. Bogowicz, M. Pavic, O. Riesterer, F. Finazzi, H. Garcia Schüler, E. Holz-Sapra, L. Rudofsky, S. Glatz, L. Basler, M. Spaniol, M. Hüllner, M. Guckenberger, S. Tanadini-Lang
CT radiomics differentiates levels of radiocurability in tumor subvolumes in head and neck cancer

171
A. Saltari, A. Dzung, M. Quadri, N. Tiso, O. Eichhoff, A. Marconi, C. Pincelli, M. Levesque, D. Reinhard
Activation of CD271 (NGFR) intracellular death domain induces apoptosis and overcomes targeted therapy resistance in melanoma ex-vivo and in vivo models

182
V. Garcia, S. Hiltbrunner, P. Tallon de Lara, M. Messerli, D. Akhoundova, L. Bankel, C. Britschgi, S. Bihr, D. Pizzuto, M. Anisimova, I. Burger, a. Curioni-Fontecedro
An analysis of the effectiveness of immunotherapy in non-small cell lung cancer patients by tracking SUV lesion intensity

202
T. Weiss, E. Puca, M. Weller, D. Neri, P. Roth
Immunocytokines are a novel immunotherapeutic approach against glioblastoma

208
F. Arnold, B. Sobottka-Brillout, C. Britschgi, H. Moch, M. Zoche, A. Kahraman
MTPpilot: An Interactive Software-Tool for NGS Result Analyses for Molecular Tumor Boards

210
O. Lauk, T. Neuer, R. Werner, S. Hillinger, I. Inci, K. Furrer, I. Schmitt-Opitz
Risk factors for the occurrence of postoperative empyema in malignant pleural mesothelioma patients undergoing macroscopic complete resection

213
F. Meier-Abt, J. Lu, M. Gwerder, M. Roiss, W. Huber, R. Aebersold, T. Zenz
Proteomics of Trisomy 12 Chronic Lymphocytic Leukemia (CLL) as Part of Multi-Omics CLL Profiling

**Clinical Trial**

12
A. Kaserer, G. Kiavialaitis, J. Braun, A. Schedler, P. Stein, J. Rössler, D. Spahn, J. Studt
Impact of rivaroxaban plasma concentration on perioperative red blood cell loss

22
D. Busenhart, J. Erb, G. Rigakos, T. Eliades, S. Papageorgiou
Adverse effects of chemotherapy on the teeth and surrounding tissues of children with cancer: A systematic review with meta-analysis

125
S. Hiltbrunner, C. Britschgi, C. Magnani, L. Bankel, T. Nguyen-Kim, P. Gulati, W. Weder, I. Schmitt-Opitz, O. Lauk, C. Caviezel, A. Tabor, P. Schröder, A. Knuth, C. Münz, C. Renner, R. Stahel, O. Boyman, U. Petrausch, A. Curioni-Fontecedro
A phase I clinical trial of malignant pleural mesothelioma treated with locally delivered autologous fibroblast activating protein (FAP)-targeting chimeric antigen receptor (CAR) T cells

## Head Region / Neuroscience

### Basic Research

32
P. Biro, P. Hofmann, D. Gage, Q. Boehler, C. Chautems, J. Braun, D. Spahn, B. Nelson
REALITI became reality: simulated automated tracheal intubation based on image recognition

34
K. Frontzek, M. Bardelli, A. Senatore, RR. Reimann, M. Carta, R. Hussain, S. Jurt, M. Georg, G. Siligardi, O. Zerbe, C. Zhu, S. Hornemann, L. Simonelli, L. Varani, A. Aguzzi
Rationally designed neuroprotective antibodies against prions

35
A. Lakkaraju, E. Lemes, U. Herrmann, K. Frontzek, M. Losa, R. Marpakwar, A. Aguzzi
Identifying the determinants of spongiform phenotype in prion infections

36
A. Henzi, A. Senatore, A. Lakkaraju, A. Aguzzi
Effects of a dimeric PrP-Fc-fusion protein on mouse sciatic nerve

37
M. Carta, M. Losa, E. Kara, R. Moos, K. Frontzek, S. Kreutzer, A. Bratus-Neuenschwander, G. Russo, R. Reimann, S. Hornemann, C. Proukakis, A. Aguzzi
Somatic PRNP mosaicism in prion disease

38
Y. Liu, A. Aguzzi
Protective role of NG2 glia in chronic neurodegeneration

40
M. Avar, D. Heinzer, D. Pease, J. Yin, A. Lakkaraju, B. Dogancay, A. Chincisan, E. Schaper, M. Emmenegger, S. Hornemann, A. Aguzzi
High-throughput whole genome RNAi screen identifying modulators of prion propagation

48
L. Ebner, M. Samardzija, V. Todorova, D. Karademir, M. Thiersch, C. Grimm
Transcriptomic analysis of the mouse retina after acute and chronic hypoxia

59
A. Bentrup, M. Müller, A. Lakkaraju, E. Lemes, L. Pelkmans, A. Aguzzi
Mechanisms Leading to Cytoplasmic Vacuolation in Mammalian Cells

64
S. Valizadeh, M. Cheetham, L. Jancke, E. Battegay, R. Renzel, E. Efthymiou, L. Imbach
Automated decision support for EEG-based classification of epilpesy after first unprovoked seizure. A new approach using neuronal indices of dynamic effective connectivity

100
F. Capecchi, L. Imbach, M. Schubring-Giese
Stimulus induced repetitive periodic or ictal discharges (SIRPIDs) are associated with high prevalence of non-convulsive status epilepticus and high mortality

126
L. Imbach, R. Christian, M. Oertel, L. Stieglitz
A multimodal electrophysiological map of the anterior nucleus of the thalamus from intraoperative deep brain recordings in epilepsy patients

137
D. Karademir, V. Todorova, C. Grimm
CRISPR activation of an essential endogenous neuroprotective pathway in the mouse retina

143
E. Lemes, A. Lakkaraju, A. Bentrup, J. Sarabia del Castillo, M. Losa, L. Pelkmans, A. Aguzzi
Determinants of the toxicity of PIKfyve depletion

148
N. Schneider, F. Bernays, M. Ferster, C. Lustenberger, W. Karlen, R. Huber, C. Baumann, A. Maric
Acoustic stimulation may reduce impairments in vigilance induced by chronic sleep restriction

164
P. Pagella, L. Jimenez-Rojo, S. Weber, P. Saftig, C. Cantu, TA. Mitsiadis
ADAM10 acts as a modulator of notch signalling to regulate tooth enamel formation

189
R. Buzzi, K. Akeret, J. Klohs, R. Humar, M. Hugelshofer, DJ. Schaer
The red blood cell toxin heme as a therapeutic target after intracranial bleeding

193
K. Burelo, M. Sharifshazileh, G. Indiveri, J. Sarnthein
A spiking neural network algorithm detects high-frequency oscillations in intracranial EEG

198
S. Erdogan, C. Gonçalves Moreira, D. Bimbiryte, A. Sethi, C. Baumann, D. Noain
Role of slow-wave sleep delta power on amyloid beta accumulation in a mouse model of Alzheimer's Disease

**Translational Research**

13
J. Schaffenrath, T. Wyss Lozano Hoyos, M. Neidert, M. Delorenzi, L. Regli, A. Keller
Transcriptomic profiling of the glioblastoma-BBB

39
D. Heinzer, M. Avar, D. Pease, B. Doğançay, J. Yin, A. Chincisan, E. Schaper, M. Emmenegger, S. Hornemann, A. Aguzzi
Whole genome RNAi screen identifies novel regulators of PrPC

41
F. Catto, D. Kirschenbaum, F. Voigt, E. Dadgar-Kiani, S. Cohen, M. Vendruscolo, K. Jenkins, J. Lee, A. Aguzzi
Therapeutic assessment and holistic visualization of Alzheimer's disease in the brain

47
A. Magalhães, A. Chincisan, M. Emmenegger, S. Hornemann, A. Aguzzi
Large patient cohort reveals increased plasma autoantibodies against tau protein aggregation domain in specific diseases

63
E. Boran, T. Fedele, P. Hilfiker, L. Stieglitz, T. Grunwald, J. Sarnthein, P. Klaver
Neuronal firing in the medial temporal lobe reflects human working memory workload and capacity

84
AM. Reuss, A. Crimi, L. Frick, P. Nilsson, A. Aguzzi
ABSTRACT: Establishing a 3D histological grading system for early and late amyloid beta (Aβ) and tau pathology in Alzheimer's disease (AD) patients

174
C. Gonçalves Moreira, A. Müllner, P. Hofmann, V. Ginde, S. Erdogan, M. Scandella, M. Morawska, S. Masneuf, D. Noain, C. Baumann
Exploring CLASSOS as a potential therapeutic tool in TBI rats

180
R. Buzzi, M. Hugelshofer, K. Akeret, C. Schaer, H. Richter, R. Vaccani, V. Anagnostakou, P. Kronen, Z. Kulcsar, M. Dennler, R. Humar, E. Keller, P. Kircher, D. Schaer
Targeting cell-free hemoglobin-toxicity in the subarachnoid space after aneurysmal subarachnoid hemorrhage

184
E. Boran, V. Scharding, K. Niklaus, G. Ramantani, J. Sarnthein
High frequency oscillations are more specific biomarkers of epileptogenic tissue than interictal spikes in the intraoperative ECoG

185
E. Boran, J. Sarnthein, N. Krayenbühl, T. Fedele, G. Ramantani
High frequency oscillations in scalp EEG decrease after successful epilepsy surgery

194
M. Emmenegger, K. Frauenknecht, E. Capodaglio, P. Kumari, S. Grathwohl, J. Grimm, S. Hornemann, R. Riek, A. Aguzzi
Autoantibodies against major genetic risk factors for Alzheimer's Disease in unselected hospital-wide patient cohort

195
D. Gramatzki, A. Eisele, P. Roth, E. Le Rhun, E. Rushing, R. Stahel, M. Weller
Venous thromboembolic events in glioblastoma patients: an epidemiological study in the Canton of Zurich

197
I. Jelcic, A. Müller, P. Stathopoulos, N. Wolfensberger, J. Ruder, A. Thesenvitz, K. Ritter, A. Bachofner, M. Foege, A. Lutterotti, U. Schanz, R. Martin
The Zurich Experience in Autologous Hematopoietic Stem Cell Transplantation for the Treatment of Multiple Sclerosis (aHSCT-in-MS) 18 Months after Approval

**Clinical Trials**

130
M. Hilty, H. Hayward-Koennecke, C. Kaiser, F. von Kaenel, C. Esteban, S. Napolitano, F. Luchs, O. Mujkic, R. Iseli, S. Iseli, S. Broicher, O. Geisseler, G. Raetsch, E. Hafen, R. Martin, S. Bignens, A. Lutterotti
MitrendS –an app-based hand function test for multiple sclerosis

168
L. Barrios, P. Oldrati, D. Lindlbauer, M. Hilty, H. Hayward-Koennecke, C. Holz, A. Lutterotti
A Rapid Tapping Task on Commodity Smartphones to Assess Motor Fatigability

177
H. Hayward-Koennecke, C. Selles Moreno, M. Docampo, M. Morax, T. Ludersdorfer, V. Weichselbaumer, V. Treyer, M. Huellner, T. Mueller, C. Blumer, M. Sospedra Ramos, R. Martin, A. Lutterotti
First insights into biodistribution of a new tolerization approach using peptide-coupled autologous cells (ETIMSred study) in humans

## Infection / Immunity / Inflammation / Systemic Diseases

### Basic Research

6
L. Hering, E. Katkeviciute, M. Schwarzfischer, P. Busenhart, C. Gottier, D. Mrdjen, J. Komuczki, S. Lang, B. Becher, G. Rogler, M. Scharl, M. Spalinger
PTPN2 in dendritic cells exerts an anti-inflammatory role and is crucial for maintaining tissue tolerance

56
D. Heuberger, D. Ardizzone, R. Schüpbach
Co-factor-dependent activation of the platelet receptor protease-activated receptor 4

68
P. Wawrzyniak, P. Srikanthan, I. Hartling, C. Gemperle, N. Noureddine, D. Mathis, M. Hersberger
Anti-inflammatory effect of omega-3 fatty acids on activated CD4+T cells

75
B. Schmid, E. Bersuch, A. Künstner, A. Fähnrich, H. Busch, M. Glatz, P. Bosshard
Skin mycobiome sequencing reveals a high fungal diversity in patients with severe atopic dermatitis

79
S. Balakrishna, L. Salazar-Vizcaya, K. Kusejko, V. Kachalov, C. Thurnheer, J. Roth, A. Calmy, M. Cavassini, M. Battegay, P. Schmid, E. Bernasconi, F. Günthard, A. Rauch, R. Kouyos
Modelling the syphilis epidemic among HIV-positive and negative MSM in Switzerland

85
G. Ingoglia, A. Yalamanoglu, M. Pfefferlé, D. Schaer, F. Vallelian
Direct targeting of macrophages with an anti-CD40 antibody triggers a macrophage activation syndrome in mice

93
C. Wolf
Impact of posters and the role of leadership in improving professional appearance of staff in the hospital

103
K. Kusejko, K. Zens, K. Darling, N. Khanna, H. Furrer, P. Vetter, E. Bernasconi, P. Vernazza, H. Günthard, R. Kouyos, J. Nemeth
Potential impact of latent tuberculosis on reducing the frequency of opportunistic diseases in HIV-infected individuals

117
Z. Kotkowska, P. Johansen, C. Halin Winter, P. Schineis, E. Varypataki, I. Kolm-Djamei, T. Kündig
Photochemical internalization (PCI): a novel method for induction of cytotoxic CD8 T-cell responses with cancer vaccines

118
M. Mueller, M. Heinzelmann, B. Roth Z'graggen, M. Schlaepfer, B. Beck-Schimmer
Sevoflurane’s primary metabolite hexafluoroisopropanol attenuates the inflammatory response in human effector and target cells, mediated by inhibition of NF-κB p65 translocation

127
J. Wang, I. Jelcic, L. Mühlenbruch, V. Haunerdinger, N. Toussaint, Y. Zhao, C. Cruciani, W. Faigle, M. Foege, T. Binder, T. Eiermann, L. Schmitt-Opitz, L. Fuentes-Font, R. Reynolds, W. Kwok, J. Nguyen, J. Lee, A. Lutterotti, C. Münz, H. Rammensee, M. Hauri-Hohl, M. Sospedra, S. Stevanovic, R. Martin
Tightly Linked HLA-DR15 Alleles Cooperate in Shaping an Autoreactive T Cell Repertoire in Multiple Sclerosis

131
L. Jörimann, A. Inderbitzin, C. Schenkel, D. Braun, C. Grube, H. Kuster, K. Metzner, H. Günthard
Characterization of the HIV-1 latent reservoir in early treated individuals

145
A. Kelley, H. Kuster, K. Neumann, C. Leemann, P. Rindler, K. Kusejko, D. Braun, R. Kouyos, K. Metzner, H. Günthard
Time Trends of Replication Capacities of Transmitted Founder Viruses in Zurich

146
T. Schweizer, F. Andreoni, E. Marques Maggio, S. Dudli, A. Zinkernagel
Staphylococcus aureus – host interactions in a porcine ex vivo spondylodiscitis model

165
L. Kovtonyuk, F. Caiado, E. Slack, E. Manz, H. Takizawa, M. Manz
Inflammageing of Hematopoietic Stem Cells is driven by IL-1

166
M. Gruenbach, E. Schlaepfer, B. Escher, M. Schlapschy, A. Skerra, G. Schreiber, R. Speck, S. Bredl
Biological activity of different IFN-a subtypes - just an interplay between the dose and affinity?

172
J. Jang, D. Linus, F. Janker, Y. Yamada, C. Opelz, W. Weder, W. Jungraithmayr
The role of CD26 in fibrous formation in chronic lung allograft dysfunction

173
K. Klein, T. Schweizer, K. Siwy, B. Lechmann, P. Kronen, A. Karol, A. Zinkernagel, B. Von Rechenberg, Y. Achermann, S. Darwiche
Establishment of an acute implant-associated Staphylococcus aureus bone infection model in sheep designed to evaluate novel osteomyelitis treatments

175
M. Pfefferlé, G. Ingoglia, C. Schaer, A. Yalamanoglu, I. Dubach, R. Buzzi, G. Tan, N. Schulthess, K. Hansen, R. Humar, D. Schaer, F. Vallelian
Phenotypic and functional characterization of anti-inflammatory erythrophagocytes in the liver of hemolytic mice

176
N. Häffner, J. Bär, V. Dengler Haunreiter, S. Mairpady Shambat, A. Zinkernagel
Colony heterogeneity of S. aureus agr knock out strains is independent of intracellular pH

181
D. Vdovenko, W. Wijnen, M. Zarak Crnkovic, P. Blyszczuk, M. Bachmann, S. Costantino, C. Diaz-Canestro, F. Paneni, G. Camici, T. Lüscher, U. Eriksson
Controversial role of IL-23 in cardiac autoimmunity

188
B. Schmid, O. Hausmann, Y. Achermann, K. Wuertz-Kozak
The role of Cutibacterium acnes in intervertebral disc inflammation

191
A. Yalamanoglu, M. Pfefferlé, G. Ingoglia, I. Dubach, R. Buzzi, N. Schulthess, K. Hansen, D. Schaer, F. Vallelian
Antibody-induced CD40 signaling stimulates acute liver crisis in a mouse model of sickle cell disease

203
P. Frey, J. Bär, J. Bergada, K. Lemon, A. Zinkernagel, S. Brugger
Quantifying variations in cellular fitness of bacteria with and without antimicrobial resistance: a high-throughput method

214
F. Staubli, S. Dudli, I. Heggli, S. Fucentese, O. Distler, F. Brunner, A. Jüngel
Altered expression of neurotrophins and receptors in the skin of patient with Complex Regional Pain Syndrome (CRPS)

**Translational Research**

50
K. Becker, K. Haldimann, S. Hobbie
Repurposing of apramycin as a parenteral therapeutic for the treatment of Gram-negative systemic infections in humans

71
Iv. Jelcic, C. Esposito, J. Sarabia del Castillo, N. Caduff, F. Al Nimer, J. Wang, Il. Jelcic, A. Lutterotti, C. Münz, M. Sospedra, L. Pelkmans, R. Martin
In depth characterization of the autoreactive B-T cell interactome in Multiple Sclerosis

82
M. Paolucci, N. Wuillemin, C. Arena, Y. Wäckerle-Men, T. Kündig, D. Bieli, T. Sonati, P. Johansen
Allergen-blocking antibodies: a novel concept of peanut-allergy immunotherapy

111
H. Klein, P. Niggemann, P. Buehler, F. Lehner, R. Schweizer, D. Rittirsch, N. Fuchs, M. Waldner, P. Steiger, P. Giovanoli, T. Reding, R. Graf, J. Plock
Pancreatic Stone Protein Predicts Sepsis in Severely Burned Patients Irrespective of Trauma Severity

150
T. Mlambo, M. Alessandrini, R. Myburgh, L. Baroncini, S. Bredl, M. Manz, P. Salmon, R. Speck, K. Krause
A novel combinatorial approach combining CAR T cell therapy, PD1 knockdown and CCR5 disruption as a once-off treatment for HIV

152
C. Meier, K. Freiburghaus, C. Bovet, J. Schniering, O. Distler, C. Nakas, B. Maurer
Serum Branched-Chain Amino Acids as Biomarkers for Progressive Systemic Sclerosis-Associated Interstitial Lung Disease

187
C. Mamie, R. Bruckner, S. Lang, N. Shpigel, M. Turina, A. Rickenbacher, Y. Chvatchko, G. Rogler, M. Scharl
Expression of MMP-9 in resected intestinal fistula from patients with fistulizing Crohn's disease and from human xenograft mouse model for intestinal fistula

196
M. Emmenegger, A. Chincisan, Ch. Zografou, N. Wuillemin, D. Bieli, L. Saleh, A. Von Eckardstein, A. Aguzzi
Identification and mechanistic elucidation of IgG antibodies against a major peanut allergen in Cystic Fibrosis patients

201
S. Brugger, S. Eslami, M. Pettigrew, I. Fernandez Escapa, M. Henke, Y. Kong, K. Lemon
Dolosigranulum pigrum picks sides in nasal microbiota via cooperation and competition

207
M. Schwyzer, K. Martini, S. Skawran, M. Messerli, T. Frauenfelder
Pneumonia detection in chest X-ray dose-equivalent CT: Impact of dose reduction on the detectability by Artificial Intelligence

**Clinical Trials**

4
D. Braun, T. Turk, B. Hampel, T. Bühler, C. Grube, N. Lutz, C. Depmeier, H. Kuster, M. Flepp, K. Metzner, J. Böni, R. Kouyos, H. Günthard
Sustained viral suppression with dolutegravir monotherapy during 9,899 patient weeks of follow-up in individuals starting combination antiretroviral therapy during primary HIV infection (EARLY SIMPLIFIED):a randomized, controlled, multi-site, non-inferiority trial

55
D. Birrer, K. Horisberger, A. Rickenbacher, M. Turina
Kono-S anastomosis in Crohn's disease: Short-term results of a wide antimesenteric functional end-to-end anastomosis for ileocecal resection

204
S. Andresen, S. Balakrishna, D. Nicca, H. Günthard, A. Schmidt, A. Calmy, K. Darling, M. Stöckle, P. Schmid, E. Bernasconi, A. Rauch, R. Kouyos, L. Salazar-Vizcaya
Behavioural patterns to identify key populations for syphilis prevention

## Mixed Topics

### Basic Research

25
S. Mohammed, S. Costantino, A. Akhmedov, K. Gergely , S. Ambrosini, P. Madeddu, G. Spinetti, T. Luscher, F. Paneni
Chromatin modifications by the methyltransferase SETD7 modulate angiogenic response in diabetes: insights for epigenetic-based therapies

27
D. Canepa, E. Arvaniti, V. Tosevski, S. Märsmann, B. Eggerschwiler, M. Claassen, H. Pape, E. Casanova, P. Cinelli
Comprehensive Mass Cytometry Analysis of Human Adipose Derived Stem Cells for Clinical Applications

30
C. Waschkies, D. Heuberger, F. Kivrak Pfiffner, P. Wolint, M. Calcagni, P. Giovanoli, J. Buschmann
Functional gas challenges to probe vasoreactivity and hypoxia in MC-38 colon and A549 lung adeno-carcinoma cell grafts grown on the chorioallantoic membrane of the chick embryo in ovo using MRI

31
F. Strauss, A. Gil, D. Thoma, U. Jung, M. Kim, K. Paeng, R. Jung, S. Fickl
Effect of hard and soft tissue grafting and individualization of healing abutments at immediate implants – an experimental study in the canine

65
P. Nocchi, D. Canepa, S. Märsmann, B. Eggerschwiler, Y. Neldner, H. Pape, P. Cinelli, E. Casanova
Dissecting the role of the ectonucleotidases CD39 and CD73 in fate decision of human adipose-derived stem cells

67
E. Casanova, L. Stähli, A. Rodriguez Palomo, S. Tiziani, O. Gröninger, S. Märsmann, D. Canepa, B. Eggerschwiler, Y. Neldner, H. Pape, M. Liebi, P. Cinelli
Comparison of bioengineered PLGA/aCaP scaffolds with aligned and random fiber orientation for improved bone regeneration

81
A. Potapenko, L. Rohrer, A. von Eckardstein
Scavenger receptor SR-BI splice variants 1 and 2 differ by cellular localization and interaction with HDL and LDL in endothelial cells

87
P. Hejduk, C. Rossi, A. Ciritsis, K. Borkowski, A. Boss
Automatic and standardized quality assessment of digital mammography with deep convolutional neural networks

106
F. Scholkmann, T. Restin, M. Reinehr
Indications for an additional and overlooked vascular system of the human placenta: Preliminary results from an ongoing study

114
I. Condado Morales, R. Moos, A. Aguzzi, S. Hornemann
Microfluidic Approaches for the Sensitive Detection and Characterisation of Prion Aggregates

119
A. Moncsek, C. Wu, S. Benke, E. Friebel, B. Becher, B. Müllhaupt, J. Mertens
Understanding the contribution of immune cells to fibrosis progression in NASH

129
S. Souzan Salemi, S. Sheryl Preda, T. Tullio Sulser, D. Daniel Eberli
Effect of myostatin inhibitor on smooth muscle regeneration

149
I. Heggli, S. Epprecht, A. Juengel, B. Betz, S. Spirig, F. Wanivenhaus, F. Brunner, M. Farshad, O. Distler, S. Dudli
Dysregulated Adhesion of Modic Type I Change Bone Marrow Stromal Cells

163
L. Krattiger, B. Simona, M. Ehrbar
Establishment of a screening platform for the testing of pro- and antiangiogenic compounds

179
R. Buzzi, D. Schaer, R. Humar
Tracing the biodistribution of exogenously administered proteins in vivo using the TCO-tetrazine bioorthogonal reaction: A demonstration using cell-free hemoglobin

186
S. Dudli, D. Haenni, I. Heggli, A. Juengel, U. Ziegler, M. Betz, J. Spirig, F. Wanivenhaus, F. Brunner, M. Farshad, O. Distler
Histomorphometry of Modic changes

206
B. Eggerschwiler, E. Casanova Zimmermann, D. Canepa, H-C. Pape, P. Cinelli
Molecular properties and phenotypic outcomes of bone marrow-derived mesenchymal stem cells in patients with reduced bone mass density

**Translational Research**

14
J. von Atzigen, P. Wolint, C. Calcagni, P. Giovanoli, J. Buschmann
Paracrine Effects on Angiogenesis of 3D-Microtissues compared to Single Cells in the Chick Aortic Arch Assay

15
S. Hofmann, P. Wolint, M. Calcagni, P. Giovanoli, M. Brunelli, J. Buschmann
Towards an artificial tendon construct

16
I. Schneider, W. Baumgartner, O. Gröninger, WJ. Stark, S. Märsmann, M. Calcagni, P. Cinelli, P. Wolint, J. Buschmann
Is a predominant YAP expression in the nucleus of adipose-derived stem cells a sufficient indication for osteogenic commitment triggered by shear stress?

17
L. Otto, P. Wolint, A. Woloszyk, A. Becker, A. Boss, R. Böni, M. Calcagni, P. Giovanoli, M. Emmert, J. Buschmann
Is the secretome of human stem cells cultivated as microtissues or single cells as potent as the cells themselves? – A calcification and vascularization study in the CAM assay

33
M. Raeber, R. Rosalia, D. Schmid, U. Karakus, O. Boyman
Interleukin-2 signals converge in a lymphoid–dendritic cell pathway fostering anti-cancer immunity

49
S. Klinnert, A. Trkola, H. Günthard, A. Plückthun, K. Metzner
CRISPR/Cas9 based adenovirus payloads that eliminate HIV-1 infected cells

57
L. Roth, L. Russo, C. Pauli, E. Breuer, R. Graf, P. Clavien, A. Gupta, K. Lehmann
The impact of hyperthermic intraperitoneal chemotherapy (HIPEC) on the anticancer immune response

58
K. Slankamenac, D. Müller, A. Herzog, H. Kupferschmidt, A. von Eckardstein, D. Keller
Spectrum of acute drug toxicity during the most popular house and techno party in the world

62
M. Benker, S. Obahor, R. Werner, C. Caviezel, S. Hillinger, D. Schneiter, I. Schmitt-Opitz, I. Inci
Impact of preoperative comorbidities on postoperative complication rate and outcome in surgically resected NSCLC patients

88
S. Santos, M. Mennet, O. Potterat, U. von Mandach, M. Hamburger, A. Simões-Wüst
Bryophyllum pinnatum compounds inhibit the oxytocin-induced rise of intracellular calcium concentration in human myometrial cells

109
R. Schweizer, A. Taddeo, M. Waldner, H. Klein, N. Fuchs, P. Kamat, S. Targosinski, A. Barth, M. Drach, V. Gorantla, P. Cinelli, J. Plock
Adipose-derived Stromal Cell Therapy Combined with a Short Course Non-Myeloablative Conditioning Promotes Long-term Graft Tolerance in Vascularized Composite Allotransplantation

110
R. Schweizer, M. Waldner, S. Oksuz, W. Zhang, C. Komatsu, J. Plock, V. Gorantla, M. Solari, L. Kokai, K. Marra, J. Rubin
Evaluation of Porcine versus Human Mesenchymal Stromal Cells from Three Distinct Donor Locations for Cytotherapy after Rapid Expansion with Endothelial Growth Medium

113
L. Roth, X. Muller, R. Graf, Y. Tian, B. Imthurn, P. Imesch, F. Taran, N. Ochsenbein, M. Choschzick, P. Clavien, P. Dutkowski, O. De Rougemont
Ischemia Reperfusion Injury in Uterus Transplantation

132
J. Schniering, H. Gabrys, M. Brunner, M. Maciukiewicz, C. Blüthgen, D. Kenkel, O. Distler, M. Guckenberger, M. Bogowicz, D. Vuong, K. Karava, T. Frauenfelder, S. Tanadini-Lang, B. Maurer
Computed tomography-based radiomics as novel diagnostic tool for detection and staging of interstitial lung disease in systemic sclerosis – transferability from experimental to human lung fibrosis

160
L. Clack, A. Wolfensberger, M. Faes Hesse, M. Meier, H. Sax
Tailored implementation of non-ventilator-associated pneumonia (nvHAP) prevention bundle as part of a type 2 hybrid implementation-effectiveness study

178
E. Randecker, G. Gantner, D. Spiess, A. Simões-Wüst
Health status, use of medication and recreational drugs during pregnancy: a cross-sectional survey in the Canton of Zurich

190
S. Shim, J. Unkelbach, N. Saltybaeva, N. Berger, M. Marcon, H. Alkadhi, A. Boss
Evaluation of image quality, lesion detection and radiation dose in spiral breast CT equipped with a photon-counting detector

**Clinical Trials**

7
A. Kaserer, J. Rössler, K. Slankamenac, M. Arvanitakis, D. Spahn, P. Giovanoli, P. Steiger, J. Plock
Impact of allogeneic blood transfusions on clinical outcomes in severely burned patients

9
F. Schmid, R. Gomolka, A. Hötker, C. Rossi, D. Eberli
MRI-based Evaluation of Urinary Sphincter Function by Diffusion Tensor Imaging

19
D. Gero, M. Schneider, M. Suter, R. Peterli, R. Vonlanthen, T. Turina, B. Bueter
Sleeve gastrectomy or gastric bypass: a „post-code" lottery? – A comprehensive national analysis of the utilization of bariatric surgery in Switzerland between 2011-2017

20
D. Gero, B. File, N. Hinrichs, M. Müller, I. Ulbert, Z. Somogyvári, M. Bueter
Mental and emotional representations of "weight loss": free-word association networks in members of bariatric surgery-related social media communities

23
V. Koretsi, T. Eliades, S. Papageorgiou
Oral Interventions for Obstructive Sleep Apnea: An Umbrella Review of the Effectiveness of Intraoral Appliances, Maxillary Expansion, and Maxillomandibular Advancement

24
N. Pedrazzi, S. Schweizer, T. Gentzsch, H. Klein, P. Giovanoli, J. Plock
Characteristics, Management and Outcome of Electrical Injuries and Burns at a Swiss Burns Center

83
J. Prange, D. Mohr-Haralampieva, R. Alves de Sousa, N. Steinke, F. Schmid, D. Eberli
Translational Medicine: From the lab bench to patient-ready GMP production

98
G. Hamvas, A. Hofmann, V. Sakalidis, B. Goodale, M. Shilaih, B. Leeners
Innovative trial design using digital approaches: an example from reproductive medicine

101
J. Ehrsam, S. Hillinger, O. Lauk, D. Schneiter, I. Schmitt-Opitz, M. Schuurmans, I. Inci
Surgical management of bronchial stump complication in cadaveric lobar lung transplantation

102
J. Ehrsam, D. Schneiter, S. Hillinger, C. Caviezel, I. Schmitt-Opitz, M. Schuurmans, I. Inci
Cause of death after lung transplantation – a single center analysis

104
J. Ehrsam, S. Hillinger, I. Schmitt-Opitz, D. Schneiter, I. Inci
Risk of Malignancy after Lung Transplantation: A Single Center Experience

105
J. Ehrsam, S. Hillinger, I. Schmitt-Opitz, D. Schneiter, I. Inci
Charlson-Deyo-Comorbidity-Index Predicts Long-Term Survival in Lung Transplantation

121
M. Schmidt, M. Studer, A. Kunz, S. Studer, J. Bonvini, M. Bueter, L. Kook, S. Haile,
B. Beck-Schimmer, M. Schläpfer
Does oxycarbon improve cerebral oxygenation during apnea? A mono-center randomized cross-over trial inspired by aviation-research

217
A. Vent, C. Surber, N. Graf, C. Buset, V. Figueiredo, G. Schönbächler, J. Hafner
Lidocaine 1%, epinephrine 1:100'000 with sodium hydrogen carbonate (bicarbonate) admixture in mixing ratio 3:1 is less painful than in mixing ratio 9:1: A double-blind, randomized, placebo-controlled, crossover trial

**4**

D. Braun[3, 4], T. Turk[3, 4], B. Hampel[2, 3], T. Bühler[3], C. Grube[3], N. Lutz[3], C. Depmeier[5], H. Kuster[3], M. Flepp[1], K. Metzner[3, 4], J. Böni[4], R. Kouyos[3, 4], H. Günthard[3, 4]

**Sustained viral suppression with dolutegravir monotherapy during 9,899 patient weeks of follow-up in individuals starting combination antiretroviral therapy during primary HIV infection (EARLY SIMPLIFIED):a randomized, controlled, multi-site, non-inferiority trial**

*Center of Infectious Diseases Zurich[1], Checkpoint Zurich[2], Division of Infectious Diseases and Hospital Epidemiology, University Hospital Zurich, University of Zurich[3], Institute of Medical Virology, University of Zurich[4], Kalkbreitepraxis Zurich[5]*

**Introduction:**
Dolutegravir (DTG) monotherapy has been criticized because of the risk of long-term failure. Our EARLY-SIMPLIFIED trial showed that at week 48 DTG monotherapy was non-inferior to combination antiretroviral therapy (cART) in patients who started cART during primary (HIV-1 infection (PHI) and had a HIV-1 RNA <50 cp/mL plasma for >48 weeks (Braun et al, CID 2019). Here we report on the intermediate results at week 108 and beyond.

**Methods:**
EARLY SIMPLIFIED is a randomized, open label, non-inferiority trial. Inclusion criteria were documented PHI, start of cART <180 days after estimated date of infection, and HIV-1 RNA <50 cp/mL plasma for >48 weeks. Exclusion criteria were previous virological failure and resistance associated mutations to INSTIs. We randomly assigned patients (2:1) to DTG monotherapy 50 mg QID or to continuation of standard cART. The trial will continue for 4 years in total (ClinicalTrials.gov, NCT02551523).

**Results:**
101 patients were assigned to DTG monotherapy (n=68) or continuation of cART (n=33). After week 48 data had been analyzed, 16 patients from the cART group demanded to switch to DTG monotherapy. One patient from the DTG monotherapy group switched back to cART because of extensive weight gain. There was no virological failure occurring in both groups during the 9,899 and 4,316 person weeks of follow-up (PWFU) in the per-protocol population for the DTG monotherapy and the cART group, respectively. One patient from the DTG monotherapy group was excluded from the per-protocol analysis because he did not fulfill the criteria of PHI.

**Conclusion:**
No virological failure was observed during the observational period of 9,899 PWFU after switching to DTG monotherapy in patients who started cART during PHI and were fully suppressed for at least 48 weeks. DTG monotherapy might be a safe and sustainable maintenance therapy in patients who started cART during PHI

**5**

E. Katkeviciute[2], L. Hering[2], A. Montalban-Arques[2], P. Busenhart[2], J. Conde Aranda[2], K. Atrott[2], E. Naschberger[4], G. Leventhal[1], , S. Lang[2], O. Boyman[3], M. Stürzl[4], M. Scharl[2, 5], M. Spalinger[2]

**PTPN2 deficiency increases the infiltration and cytotoxicity of CD8+ T cells and promotes the immunogenicity in hard to treat solid tumors**

*Department of Civil and Environmental Engineering, Massachusetts Institute of Technology (MIT), Cambridge, MA, USA[1], Department of Gastroenterology and Hepatology, University Hospital Zurich, Zurich, Switzerland[2], Department of Immunology, University Hospital Zurich, University of Zurich, Zurich, Switzerland[3], Division of Molecular and Experimental Surgery, Translational Research Center, Department of Surgery, University Medical Center Erlangen, Germany[4], Zurich Center for Integrative Human Physiology, University of Zurich, Zurich, Switzerland[5]*

**Introduction:**
Recently, protein tyrosine phosphatase non-receptor type 2 (PTPN2) has emerged as a potential cancer immunotherapy target. However the role and mechanism how PTPN2 affects human colorectal carcinoma pathogenesis has not yet been fully determined. Here, we show that PTPN2 expression correlates with the low immunogenicity of colon tumors and is involved in suppressing T cell infiltration and activation.

**Methods:**
Using four colon tumor mouse models and human colon tumor samples we analyzed the effect of PTPN2 on tumor-infiltrating lymphocytes. We analysed immune cells in spleen, mesenteric lymph nodes (mLN), skin draining lymph nodes (sLN), lamina propia and tumours in PTPN2 fl/fl-CD4Cre and their littermate control mice using flow cytometry and immunohistochemistry (IHC). Human samples were analysed using qPCR and IHC.

**Results:**
We observed that increased PTPN2 expression in human colon tumor tissue inversely correlated with decreased levels of immune response mediators. In turn, PTPN2-deficient mice exhibited reduced tumor burden and significantly increased levels of CD44+ effector/memory CD4+ and CD8+ T cells. Additionally, we observed higher CD8+ T cells infiltration into tumors and increased expression levels of interferon gamma and granzyme B in the tumor tissue of PTPN2fl/fl-CD4Cre mice compared to their littermate controls. Furthermore, depletion of PTPN2-deficient CD8+ T cells led to the loss of the tumor reduction, highlighting the importance of these cells. Transfer of PTPN2 CD8+ T cells into tumor baring RAG mice, again reduced tumor growth, showing the therapeutic potential of PTPN2 protein inhibition and CD8+ T cells importance. Finally, combination of immunotherapy (anti PD-1) together with the PTPN2-deficiency resulted in pronounced tumor reduction, eventual clearance of tumors, and immune memory formation.

**Conclusion:**
Our results demonstrate a role for PTPN2 in the pathogenesis of colorectal carcinoma in vivo. This effect is likely mediated via promoting anti-cancer immune responses by modulating T-cell activation, infiltration and cytotoxicity and immune checkpoint molecule expression. Taken together, our results demonstrate a great potential for PTPN2 in the therapy of human CRC.

**6**

L. Hering[1], E. Katkeviciute[1], M. Schwarzfischer[1], P. Busenhart[1], C. Gottier[1], D. Mrdjen[2], J. Komuczki[2], S. Lang[1], B. Becher[2], G. Rogler[1], M. Scharl[1], MR. Spalinger[1]

**PTPN2 in dendritic cells exerts an anti-inflammatory role and is crucial for maintaining tissue tolerance**

*Department of Gastroenterology and Hepatology, University Hospital Zürich, University of Zürich, Zürich, Switzerland[1], Institute of Experimental Immunology, University of Zürich, Zürich, Switzerland[2]*

**Introduction:**
Dendritic cells (DCs) link innate and adaptive immunity and their controlled activation is crucial for protection against pathogens while preventing tissue inflammation. Variants within the gene locus encoding protein tyrosine phosphatase non-receptor type 2 (PTPN2) are associated with the development of inflammatory disorders and PTPN2 deletion results in severe systemic inflammation. The role of PTPN2 in T cells has been investigated in depth, but its role in DCs remains unclear.

**Methods:**
Here, we investigated the DC-specific importance of PTPN2 for maintaining normal tissue immune cell composition and prevention of inflammatory events. For this aim, we generated mice lacking PTPN2 specifically in DCs (PTPN2xCD11cCre mice).

**Results:**
DC-specific loss of PTPN2 promoted infiltration of inflammatory monocytes, neutrophils and effector/memory T cells into skin, lung, liver, and kidney in young mice, resulting in the onset of systemic inflammation and severe tissue damage in aged mice. Further, deletion of PTPN2 in DCs caused a shift in DC populations by increasing the proportion of CD11b+ cDC2 among DCs even before onset of overt tissue inflammation. Loss of PTPN2 in DCs resulted in increased activation of DCs via activation of the IFNgamma-STAT1 pathway as well as microbial stimuli, resulting in increased expression of co-stimulatory molecules CD80 and CD86, which promoted aberrant T cell activation and finally resulted in loss of tissue tolerance. Conversely, PTPN2xCD11cCre mice in RAG-/- background were protected from the onset of spontaneous tissue inflammation, demonstrating an important role of T cells for the disease phenotype in PTPN2xCD11cCre mice.

**Conclusion:**
In conclusion, our results show that dysfunction of PTPN2 in DCs shifts the immune reaction towards a pro-inflammatory response and demonstrates a crucial DC-specific role for PTPN2 in preventing generalized inflammation and for maintaining tissue tolerance.

**7**

A. Kaserer[4], J. Rössler[4], K. Slankamenac[2], M. Arvanitakis[1], DR. Spahn[4], P. Giovanoli[1], P. Steiger[3], J. Plock[1]

**Impact of allogeneic blood transfusions on clinical outcomes in severely burned patients**

*USZ - Department of Plastic Surgery and Hand Surgery[1], USZ - Emergency Department[2], USZ - Institute for Intensive Care Medicine[3], USZ - Institute of Anesthesiology[4]*

**Introduction:**
Allogeneic blood transfusions are common in the treatment of severely burned patients as surgery may lead to major blood loss. However, transfusions are associated with a number of adverse events. Therefore, the purpose of our study was to investigate the impact of allogeneic blood transfusions on clinical outcomes in severely burned patients.

**Methods:**
This retrospective study included all adult patients admitted to the burn center of the University Hospital Zurich between January 2004 and December 2014, with burn injuries greater than 10% of total body surface area and requiring both surgical and intensive care treatment. Primary Endpoints were infectious or thromboembolic complications and mortality and secondary endpoints were length of hospital and ICU stay. Simple and multivariable logistic and linear regression models, adjusted for injury severity and confounders, were applied.

**Results:**
413 patients met inclusion criteria of which 212 patients (51%) required allogenic blood products. After adjustment for injury severity and confounders, red blood cell transfusion was independently associated with wound infection (OR 13.5, 95% CI 1.7 to 107, p=0.014), sepsis (OR 8.3, 4.2 to 16.3; p<0.001), pneumonia (OR 4.7, 2.2 to 10.0; p<0.001), thrombosis (OR 3.0, 1.2 to 7.4; p=0.015), central line infection (OR 34.7, 4.6 to 260; p=0.001) and a longer ICU and hospital stay (difference 17.7, 95% CI 12.1 to 23.4, p<0.001 and 22.0, 15.8 to 28.2, p<0.001, respectively). Fresh frozen plasma transfusion was independently associated with a longer ICU and hospital stay (difference 13.7, 95% CI 5.5 to 21.8, p=0.001 and 13.5, 4.6 to 22.5, p=0.003, respectively). Platelet transfusion was independently associated with systemic inflammatory response syndrome (OR 4.5, 1.3 to 15.5; p=0.018) and mortality (OR 5.8, 2.1 to 16.0; p=0.001).

**Conclusion:**
Transfusion of allogeneic blood products is associated with an increased infection rate and thromboembolic morbidity and a longer hospital stay in severely burned patients.

**9**

F. Schmid[2], R. Gomolka[1], A. Hötker[1], C. Rossi[1], D. Eberli[2]

**MRI-based Evaluation of Urinary Sphincter Function by Diffusion Tensor Imaging**

*Department of Radiology, University Hospital Zurich[1], Department of Urology, University Hospital Zurich[2]*

**Introduction:**
We are about to establish a regenerative treatment using muscle precursor cells (MPCs) for stress urinary incontinence. Non-invasive measurement of muscular sphincter function as well as in-vivo tracking of MPCs is challenging by current imaging methods. The aim of our study was to confirm the applicability of diffusion tensor imaging (DTI) in evaluation of female urinary sphincter function and its ability to distinguish between rest and contraction.

**Methods:**
MRI scanning of the lower pelvis was performed at 3T in 10 young and healthy female volunteers (age 21-36 y, BMI 20.8±3.6 kg/m2) between June and July 2019. The scanning protocol consisted of high-resolution T1 image for anatomical reference and DTI. DTI was performed in four experiment phases lasting 30 seconds each: twice during rest (denoted 'r1' and 'r2') and twice during contraction ('c1' and 'c2'), alternately. DTI analysis was done by means of Syngo.via Neuro 3D workflow (Siemens Healthcare, Germany). Manual segmentation of the urinary sphincter as well as the levator ani muscle was performed in 3-4 regions of interest (ROIs) per scan by two independent raters. The values of mean diffusivity (MD) and fractional anisotropy (FA) were automatically derived from the ROIs. Kruskal-Wallis One-Way ANOVA and subsequent Dunn's post-hoc test was applied in search for significant differences between MD and FA values among the experiment phases. To confirm repeatability of performed measurement, Spearman's correlation was calculated between MD and FA values comparing two rest and two contraction states separately. Intraclass correlation coefficient (ICC) was calculated to report on agreement between raters.

**Results:**
Kruskal-Wallis test showed statistically significant differences between MD values among all the experiment phases based on the measurements of two independent readers ($X2(3,76) = 17.16$, $p<0.001$ and $X2(3,76) = 15.88$, $p<0.01$, respectively), whereas no statistically significant differences were found between FA values. Dunn's test revealed significant differences between MD values from the experiment phases in both raters: r1 vs. c1 ($p<0.05$), r1 vs. c2 ($p<0.01$), r2 vs. c1 ($p<0.03$), r2 vs. c2 ($p=0.02$, all FDR corrected). No difference was found between MD values from two rest and two contraction states solely. Moderate to strong Spearman's correlation was found between MD and FA values in rest and in contraction phases by both readers (rho = 0.45 to 0.83, $p<0.05$ to $p<0.001$). A high degree of reliability was found between the measurements of the two raters, with ICC of 0.85 (95% CI from 0.46 to 0.99) in MD values and 0.79 (95% CI from 0.71 to 0.99) in FA values, respectively.

**Conclusion:**
Our findings demonstrate a promising strategy for the functional evaluation of relevant pelvic floor muscle structures for urinary continence by means of DTI, and reliably differentiate between rest and contraction. Such strategy may improve the assessment of urinary continence and facilitate the diagnosis or the follow up in patients with SUI after stem cell therapy.

**10**

J. Rössler[4], F. Schoenrath[2, 3], S. Seifert[1], A. Kaserer[4], G. Spahn[4], V. Falk[2, 3], D. Spahn[4]

**Iron deficiency is associated with higher mortality in patients undergoing cardiac surgery: a prospective study**

*Department of Biostatistics at the Epidemiology, Biostatistics and Prevention Institute, University of Zurich, Zurich, Switzerland[1], Department of Cardiothoracic and Vascular Surgery, German Heart Centre Berlin, Berlin, Germany[2], German Centre for Cardiovascular Research, Partner Site Berlin, Berlin, Germany[3], Institute of Anaesthesiology, University of Zurich and University Hospital Zurich, Zurich, Switzerland[4]*

**Introduction:**
Iron deficiency is frequent in patients undergoing cardiac surgery. The relevance of iron deficiency, however, is ill defined. Therefore, our study aimed to investigate the impact of iron deficiency (ferritin <100 mg/L) with or without concomitant anaemia on clinical outcome after cardiac surgery.

**Methods:**
In this prospective observational study, 730 patients undergoing elective cardiac surgery were assigned into four groups according to their iron status and anaemia. Mortality, serious adverse events (SAEs), major cardiac and cerebrovascular events (MACCEs), allogenic blood transfusion requirements, and length of hospital stay were assessed during a 90-day follow-up period. The effect of iron deficiency on these outcomes was first calculated in models adjusting for anaemia only, followed by two multivariate models adjusting for anaemia and either the EuroSCORE II or any possible confounders.

**Results:**
The presence of iron deficiency (ferritin <100 mg/L) was associated with an increase in 90-day mortality from 2% to 5% in patients without anaemia, and from 4% to 14% in patients with anaemia. Logistic regression resulted in an odds ratio of 3.5 (95% confidence interval: 1.5-8.4); P=0.004. The effect persisted in both multivariate models. Moreover, iron deficiency was associated with an increased incidence of SAEs, MACCEs, transfusion, and prolonged hospital stay.

**Conclusion:**
Preoperative iron deficiency (ferritin <100 mg/L) was independently associated with increased mortality, more SAEs, and prolonged hospital stay after cardiac surgery. These findings underline the importance of preoperative iron deficiency screening in the context of a comprehensive patient blood management programme, and highlight its importance as a research topic in cardiac surgery.

**12**

A. Kaserer[3], G. Kiavialaitis[3], J. Braun[1], A. Schedler[3], P. Stein[3], J. Rössler[3], DR. Spahn[3], J. Studt[2]

**Impact of rivaroxaban plasma concentration on perioperative red blood cell loss**

*Department of Biostatistics, Epidemiology, Biostatistics and Prevention Institute, University of Zurich, Switzerland[1], Department of Medical Oncology and Haematology, Division of Haematology, University of Zurich and University Hospital Zurich, Zurich, Switzerland[2], Institute of Anaesthesiology, University of Zurich and University Hospital Zurich, Zurich, Switzerland[3]*

**Introduction:**
This study investigates the impact of preoperative calculated rivaroxaban (RXA) plasma concentration on perioperative red blood cell (RBC) loss.

**Methods:**
In this retrospective single-center study, we identified patients with RXA intake according to a preoperative determination of RXA levels within 96 hours before surgery. RXA plasma concentration at the beginning of surgery was then calculated from the last RXA intake using a single-compartment pharmacokinetic model with four categories of RXA concentration (≤20, 21-50, 51-100, and >100 µg/L). Patients were classified into surgery with high (≥500 mL) or low (<500 mL) expected blood loss. Perioperative bleeding was determined by calculating RBC loss.

**Results:**
We analyzed 308 surgical interventions in 298 patients during the period from January 2012 to July 2018. Among patients undergoing surgery with low expected blood loss, RBC loss varied from 164 mL (standard deviation [SD], 189) to 302 mL (SD, 397) ($p = 0.66$), and no association of calculated RXA concentration with RBC loss was observed. In patients undergoing surgery with high expected blood loss, we found a significant correlation of calculated RXA concentration with RBC loss (Pearson's correlation coefficient, 0.29; $p = 0.002$). RBC loss increased with rising RXA concentration from 575 mL (SD, 365) at RXA concentration of 20 µg/L or less up to 1400 mL (SD, 1300) at RXA concentration greater than 100 µg/L. RXA concentration greater than 100 µg/L was associated with a significant increase of in RBC loss of 840 mL (95% confidence interval, 360-1300; $p < 0.001$). Transfusion of RBC and fresh frozen plasma units tended to increase in patients with RXA concentrations greater than 100 µg/L. The proportion of patients treated with prothrombin complex concentrate and coagulation factor XIII concentrate increased significantly with higher RXA concentrations.

**Conclusion:**
Only in surgery with high expected blood loss, a calculated RXA concentration of greater than 100 µg/L was associated with a significant increase of perioperative RBC loss.

**13**

J.B. Schaffenrath[1], T. Wyss Lozano Hoyos[2], M. Neidert[1], M. Delorenzi[2], L. Regli[1], A. Keller[1]

**Transcriptomic profiling of the glioblastoma-BBB**

*Department of Neurosurgery, USZ[1], Swiss Institute of Bioinformatics, Université de Lausanne[2]*

**Introduction:**
Glioblastoma multiforme (GBM) is the most common primary brain tumor with high severity and low therapeutic success. Effective therapy starts with sfufficient drug delivery, which is limited by the special protecting properties of brain vasculature – the blood brain barrier (BBB). Most of prescribed drugs are effectively removed from the brain by ABC transporters expressed by BBB endothelial cells (EC). Extending the knowledge about the molecular composition of GBM BBB-ECs will hopefully bring insights into biology of GBM vasculature, and help to design better treatment strategies with elevated delivery efficiency.

**Methods:**
In this study, we aim to characterize the transcriptome of the human BBB in health and GBM. Human ECs are isolated from GBM and non-tumorous (autopsy, epilepsy) brain tissue using an immunoprecipitation approach. The isolation of ECs include enzymatic tissue dissociation followed by negative selection with anti-CD15 and anti-CD45 antibodies to exclude leukocytes and circulating progenitor cells. ECs are isolated using anti-CD31 antibody. After enrichment for ECs, RNA is isolated and subjected to RNA sequencing.

**Results:**
Analysis of RNA sequencing data from 5 GBM and 6 control cases enriched for ECs was performed. An unsupervised hierarchical clustering analysis showed similarity of samples according to their origin - GBM or control tissue.
Bioinformatics analysis of our dataset revealed deregulation of several endothelial SLC transporters in GBM compared to control (e.g. upregulation of SLC36A1, SLC1A4; downregulation of SLC1A1, SLC2A1). Furthermore, few ABC transporters are upregulated whereas only one ABC transporter (ABCB1) seems to be downregulated in GBM compared to controls.
Moreover, our dataset indicates changes in BBB`s characteristic closed cell-cell junctions in GBM (e.g. downregulation of OCLN, JAM2), a different composition of GBM vascular cells (e.g. smooth muscle cells, pericytes, fibroblasts) and differences in vascular zonation (downregulation of arterial markers e.g. SYT15, BMX, SEMA3G).

**Conclusion:**
RNA sequencing analysis suggests deregulation of several BBB characteristics upon GBM formation (e.g. transporters, junctional molecules, leukocyte adhesion molecules).
Some of these changes may be exploited to increase focal drug delivery into tumor site by using drugs addressing upregulated transporters in GBM for transit.

**14**

J. von Atzigen[1], P. Wolint[1], C. Calcagni[1], P. Giovanoli[1], J. Buschmann[1]

**Paracrine Effects on Angiogenesis of 3D-Microtissues compared to Single Cells in the Chick Aortic Arch Assay**

*Plastic Surgery and Hand Surgery[1]*

**Introduction:**
The use of mesenchymal stem cells for regenerative medicine has become popular during the last decade. Indeed, many cell-based and tissue engineering approaches take stem cells as a central cue to support healing, enable accelerated regeneration and suppress inflammatory reactions. Among different factors involved, (re-)vascularization of a graft or tissue engineered construct may be of high importance in order to avoid necrosis at the place of action. Stem cells are well-known for their support of angiogenesis and are therefore often used to enhance the vascularization. Nevertheless, stem cell expansion must be timely accurate and harmonized with operations for cell-based therapies. If the secretome of stem cells would be affecting wound healing, regeneration and vascularization in the same way as the cells, then the supernatant of stem cells could be collected independently; stored and used whenever needed.

**Methods:**
Human adipose-derived stem cells (ASCs) from three different donors were cultivated either as single cells (SCs) or as 3D-microtissues (MTs) of 250 or 8000 cells/ MT (250-MTs or 8000-MTs). After 3 days, the supernatant was collected and used as secretome for further experiments.The aorta was isolated from 14 days old chicken. The aorta was cut into 0.5 – 2.0 mm wide rings that were washed with PBS and further placed in Matrigel®. Then either secretome from SCs, 250-MTs or 8000-MTs was added (medium without secretome was the control). After 1, 4 and 7 days, sprouts growing out from the aortic ring were photographed with a bright field microscope. Number of microvessels, junctions and branches were assessed, as well as length of microvessels and branches.

**Results:**
There was a high inter-donor variability. Nevertheless, some comparisons had the same results for all three donors: Compared to the secretome of 250-MTs, the secretome of SCs enhanced angiogenesis significantly better. For two out of three donors, it was additionally found that the SC-secretome acted more pro-angiogenic than the 8000-MT secretome. Finally, if 250-MTs were compared to 8000-MTs, two out of three donors exhibited an enhanced vascularization with the 8000-MTs secretome.

**Conclusion:**
The secretome of mesenchymal stem cells could be used as a viable option to enhance vascularization instead of using the cells themselves. From our three donors studied, we conclude that the secretome of single cells is more potent with respect to angiogenesis than the MT-derived secretome. As we had two extreme sizes of MTs, 250 and 8000 cells/ MT, respectively, it might be valuable to study more intermediate sizes of MTs, collect their secretome and compare them with our findings. There is need to perform more experiments to verify if the secretome of other MT sizes, such as for example 1000 cells/ MT, might be still better than the secretome of SCs.

**15**

S. Hofmann[2], P. Wolint[2], M. Calcagni[2], P. Giovanoli[2], M. Brunelli[1], J. Buschmann[2]

**Towards an artificial tendon construct**

*EMPA[1], Plastic Surgery and Hand Surgery[2]*

**Introduction:**
Tendon injuries are among the most occurring musculoskeletal injuries. Due to their low cell densities and low metabolic activity, tendons only heal very slowly. After critical size defects, tendons have to be reconstructed, at best with a tendon construct that is fast and well integrated into the surroundings and leads to a strong and long-term stable graft.

**Methods:**
A novel coaxially electrospun scaffold based on PVDF/hfp-PDMS has been recently developed at EMPA St. Gallen. The core/shell fiber meshes have been fabricated either as aligned or as random fiber mesh. Human adipose-derived stem cells (ASCs) were seeded onto these scaffolds and cultivated for one week. Afterwards, RNA of the ASCs was extracted and quantitative real-time PCR was performed for typical tenogenic marker genes, inflammatory genes and genes of matrixmetalloproteases (MMPs).

**Results:**
Core/shell microfibers of PVDF/hfp-PDMS enhanced tenogenic marker genes of ASCs compared to ASCs cultivated without scaffold. As for inflammatory marker genes, IL-8 was upregulated, while IL-6 was downregulated on PVDF/hfp-PDMS compared to ASCs without scaffold. However, against our expectation, promotion of tenogenic markers was particularly exhibited on random fiber meshes and not on aligned fibers.

**Conclusion:**
Random core/shell fibers fabricated on the basis of PVDF/hfp-PDMS enhanced tenogenic marker gene expression to a higher extent compared to aligned fibers of the same material. Nevertheless, compared to stem cells cultivated without this scaffold in a polystyrene culture dish, tenogenic marker genes were significantly upregulated. We conclude that the novel coaxially electrospun fiber mesh of PVDF/hfp-PDMS might be acting as a viable option for an artificial tendon construct.

**16**

I. Schneider[3], W. Baumgartner[3], O. Gröninger[2], WJ. Stark[2], S. Märsmann[1], M. Calcagni[3], P. Cinelli[1], P. Wolint[3], J. Buschmann[3]

**Is a predominant YAP expression in the nucleus of adipose-derived stem cells a sufficient indication for osteogenic commitment triggered by shear stress?**

*Clinic for Traumatology[1], ETH Zürich[2], Plastic Surgery and Hand Surgery[3]*

**Introduction:**
Various stem cell niches are responsible for the differentiation commitment towards a certain phenotype. Cues that trigger differentiations are found in specific soluble factors, matrix elasticity, shear forces, and other specific characteristics in the microenvironment of a stem cell. This highly complex situation is difficult to experimentally split into single factors, adding up to a certain commitment; and researchers are looking for simple, but effective markers to know more about stem cell commitment.

**Methods:**
We used human adipose-derived stem cells (ASCs) and cultivated them either as single cell suspension or as microtissues (MT) with 1000 cells/ MT. After that they were seeded on electrospun PLGA/aCaP nanocomposites (aCaP = nanoparticles of amorphous calcium phosphate), a typical bone-biomimetic scaffold. After 2 weeks under static culture where the MTs decayed back to single cells, they were cultured for another two weeks in a perfusion bioreactor in order to apply shear forces to the stem cells that had grown into the pores of the electrospun mesh.
After these 4 weeks, YAP immunohistochemical staining was performed and the ratio of YAP intensity in the nucleus was compared to the intensity found in the cytoplasma to yield a nucleus: cytoplasmatic ratio. Theoretically, higher YAP ratios are related to a higher tension the cell is exposed to[1, 2].
In addition, gene expressions of typical marker genes for osteogenic commitment were assessed for all conditions. Furthermore, markers for adipogenic, chondrogenic and endothelial cell differentiation were determined.

**Results:**
As expected, the YAP nucleus: cytoplasmatic ratio was significantly higher for scaffolds cultivated under shear stress compared with static cultivation, no matter whether the ASCs had been cultivated as microtissues or single cells initially. However, when different static conditions were compared, such as microtissues (without PLGA/aCaP), microtissue-derived ASCs on PLGA/aCaP and single cells on PLGA/aCaP, we found that on the surface of microtissues, the YAP ratio was significantly higher compared with microtissue-derived cells on the scaffold PLGA/aCaP. Single cells seeded on PLGA/aCaP exhibited slightly higher YAP ratios than microtissue-derived ASCs, however, lower ratios than found for cells on the surface of microtissues.
Although higher YAP ratios were observed for cells under shear stress, gene expression of ASCs showed an adipogenic commitment rather than the expected osteogenic commitment under these specific conditions.

**Conclusion:**
YAP immunohistochemical staining revealed nucleus: cytoplasmatic ratios that indicated a higher tension for cells under shear stress; nevertheless, an adipogenic commitment was found under the specific conditions. We conclude that other factors such as the stem cell source, which was adipose tissue in this case, might be more important directives and may influence the fate of stem cells to a higher extent than the tension evoked by perfusion. Hence, YAP staining, as practical as it may be to detect different degrees of tensions in cells, is not a sufficient marker to elucidate the final stem cell commitment.

**17**

L. Otto[3], P. Wolint[3], A. Woloszyk[2], A. Becker[1], A. Boss[1], R. Böni[4], M. Calcagni[3], P. Giovanoli[3], M. Emmert[2], J. Buschmann[3]

**Is the secretome of human stem cells cultivated as microtissues or single cells as potent as the cells themselves? – A calcification and vascularization study in the CAM assay.**

*Institute for Diagnostic and Interventional Radiology[1], Institute of Regenerative Medicine, University Zurich[2], Plastic Surgery and Hand Surgery[3], White House center for Liposuction, Zurich[4]*

**Introduction:**
Bone tissue engineering demands for rapidly calcifying scaffolds, for example by adult stem cells differentiating towards the osteoblastic phenotype. Moreover, bone grafts should be well vascularized in order to provide sufficient nutrients and oxygen, particularly in critical size grafts. Natural bone is mainly composed of calcified collagen where the microenvironment affects stem cells' fate and differentiation. The calcification capacity as well as the vascularization of collagen seeded with stem cells may depend on the cell format, such as single cell suspension or microtissues.

**Methods:**
Human adipose-derived stem cells (ASCs) from two donors were seeded on commercially available collagen scaffold (Matricel®) to study the calcification of collagen. The cells were either seeded as single cells (SCs) or as microtissues (MTs). Moreover, the scaffold was also soaked with the secretome of MTs and SCs, respectively. Finally, in order to address mere chemical calcification (precipitation), the cell-free scaffold was cultivated in culture medium, PBS or water, respectively, before on-plantation on the chorioallantoic membrane of the chicken embryo (CAM assay) for one week. Micro-CT analysis of ex vivo samples was performed to assess micro-calcifications. Histological assessment included Van Kossa staining (extent of calcification) and H&E (vascularization).

**Results:**
The secretome of MTs was as potent as MT cells. As for SC-secretome, it had similar effects like SCs only in terms of calcification; otherwise, effects by SC-secretome were smaller than for SCs. Compared with SCs, MTs led to a higher calcification; this was also true for the secretome of MTs compared with the secretome of SCs, but only on the surface of the collagen scaffolds. Vascularization was higher in MT-seeded scaffolds compared with SC-seeded ones.

**Conclusion:**
Calcification capacity as well as vascularization are influenced by the cell format the seeded stem cells are applied. Three-dimensional MTs favor calcification and lead to a higher vessel density in collagen scaffolds planted onto the CAM assay. It may be worthwhile to apply stem cells as MTs in bone tissue engineering to promote two basic and important processes for functionally adequate bone grafts: calcification and vascularization.

**18**

S. Ambrosini[1], F. Montecucco[2], A. Akhmedov[1], S. Mohammed[1], T. Lüscher[1], S. Costantino[1], F. Paneni[1]

**The methyltransferase SETD7 promotes myocardial ischemic injury by activating Hippo signalling**

*Center for Molecular Cardiology, University of Zürich, Switzerland[1], First Clinic of Internal Medicine, Department of Internal Medicine and Centre of Excellence for Biomedical Research (CEBR), University of Genoa, Genoa, Italy[2]*

**Introduction:**
Despite significant advances in coronary revascularization, acute myocardial infarction remains the leading cause of heart failure and death worldwide. The Hippo pathway is a master regulator of cell survival during myocardial ischemia. Upon cellular stress, activation of Hippo signaling leads to cytosolic retention and degradation of the pro-survival transcription factor YAP. Post-translational modifications, namely methylation, critically affect protein functionality in conditions of cellular stress. The SET domain-containing lysine methyltransferase 7 (SETD7) - which induces a specific mono-methylation of both histone and non-histone proteins - has recently emerged as key player in the pathogenesis of vascular disease. However, the role of SETD7 in the heart is largely unknown.

**Methods:**
Neonatal rat ventricular myocytes (NRVM) were exposed to normal glucose levels or glucose deprivation (GD) for 15 h, in the presence of the selective SETD7 inhibitor [*(R)*-PFI-2] or its inactive enantiomer [*(S)*-PFI-2]. Western blot and real time PCR were employed to investigate the effects of energy stress on SETD7 and the Hippo pathway, while apoptosis was assessed by Caspase-3 activity assay. YAP localization was examined by confocal microscopy while its mono-methylation was assessed by immunoblotting. SETD7 knockout (*SETD7*$^{-/-}$) mice and wild-type (WT) littermates underwent 1 h of left anterior descending (LAD) coronary artery ligation followed by 24h of reperfusion. Infarct size was assessed by TTC staining and shown as infarct size per ventricle surface (I/V). Cardiac function was investigated at 24h by conventional and Tissue Doppler Imaging echocardiography.

**Results:**
GD for 15h in NRVMs led to both YAP phosphorylation and mono-methylation, and subsequent cytosolic retention, as assessed by confocal microscopy. Reduced nuclear content of YAP was confirmed by downregulation of YAP-dependent pro-survival genes, namely *Ctgf* and *Fgf2*. GD-induced YAP inactivation was associated with an increase in SETD7 expression. Interestingly, pharmacological inhibition of SETD7 by *(R)*-PFI-2 blunted YAP mono-methylation, thus restoring nuclear retention of YAP and transcription of anti-apoptotic genes in GD-treated NRVMs leading to an increase in cell survival. In line with our in vitro findings, *SETD7*$^{-/-}$ mice showed decreased infarct size as compared to WT littermates (I/V: 16.27%±2 vs. 20.54%±3, $p<0.005$, respectively). Consistently, cardiac function, as assessed by ejection fraction (EF: 46%±2 vs. 38%±5, $p<0.001$), fractional shortening (FS: 22%±1 vs. 18%±3, $p<0.001$) as well as by TDI, was preserved in mice lacking SETD7 as compared to WT animals.

**Conclusion:**
Pharmacological modulation of SETD7 by *(R)*-PFI-2 may represent a novel therapeutic approach to prevent myocardial ischemic damage.

**19**

D. Gero[3], M. Schneider[3], M. Suter[1], R. Peterli[2], R. Vonlanthen[3], T. Turina[3], B. Bueter[3]

**Sleeve gastrectomy or gastric bypass: a „post-code" lottery? – A comprehensive national analysis of the utilization of bariatric surgery in Switzerland between 2011-2017**

*CHUV Service de Chirurgie Viscérale[1], Department of Visceral Surgery, Clarunis: St.Clara Hospital and University Hospital Basel, Basel, Switzerland[2], USZ - Klinik Viszeralchirurgie[3]*

**Introduction:**
Over the last decade, a considerable worldwide trend shift was observed in bariatric surgery (BS), with sleeve gastrectomy (SG) becoming the most frequently performed operation followed by Roux-en-Y gastric bypass (RYGB). However, the main indications for one or the other procedure show large inter-center variations and warrant further investigations. The aim of this study was to identify recent nation-wide trends in the use of BS. We hypothesized that procedure-specific differences exist in patient demographics and in inpatient complication rates, and that the decision for or against SG or RYGB may be influenced by non-medical factors as well, such as private insurance or loco-regional trends.

**Methods:**
This study is an observational, retrospective, nationwide analysis of all BS-related hospitalizations in Switzerland between 01/01/2011 and 12/31/2017. Anonymized data were provided by the Swiss Federal Statistical Office. The database was queried for elective bariatric procedures based on ICD-10 codes and national surgical codes, with a main focus on primary BS. Subgroups were compared with t-test, determinants of implementation of SG versus RYGB were explored by multivariate logistic regression using the R software.

**Results:**
In total, 26'355 bariatric operations were performed in Switzerland between 2011-2017. Overall, RYGB was the prevailing BS procedure, although its annual proportion decreased from 80% in 2011 to 70% in 2017 ($P < 0.001$). Meanwhile the use of SG increased from 14 to 23%, while the proportion of revisional BS procedures varied between 2-4%. Patient related factors with a significant impact on procedural choice in favor of SG were male sex, younger (<20 years) or older age (>60 years) and presence of metabolic comorbidities. Gastro-esophageal reflux disease increased the chances of RYGB. Non-medical factors also impacted procedure selection: non-private insured patients were more likely to undergo a SG and more importantly, there were strong geographical differences in procedure selection that even outweighed patient-related factors with patients in German- and Italian-speaking areas having the highest likelihood (OR 4.2 and 3.7) to receive a SG. The overall rate of inhospital postoperative complications decreased from 10 to 7% from 2011 to 2017. Until discharge, primary RYGB and SG had similar incidence of gastrointestinal leakage (1.7%), bleeding (2.2%), wound infection (1.7%), pneumonia (0.8%) and mortality (0.05%), however, a significantly higher incidence of re-operations (8.1 vs 6.8%) and ileus (0.7 vs 0.1%) was observed following RYGB.

**Conclusion:**
The detection of paramount geographic differences in primary BS procedure selection indicates a lack of objective rationales and suggests that non-medical factors also impact on decision between SG and RYGB. We assume that factors not captured in this database, such as the level and place of training of the surgeon, the annual caseload of the center, the recommendation of the referring physicians and of social-media communities may impact the choice of the primary BS procedure. Therefore our findings may reflect the role of patients' involvement and of surgical doctrines in medical decision making.

**20**

D. Gero[2], B. File[3], N. Hinrichs[2], M. Müller[2], I. Ulbert[1], Z. Somogyvári[3], M. Bueter[2]

**Mental and emotional representations of "weight loss": free-word association networks in members of bariatric surgery-related social media communities**

*Faculty of Information Technology and Bionics, Pázmány Péter Catholic University, Budapest, Hungary [1], USZ - Klinik Viszeralchirurgie[2], Wigner Research Centre for Physics, Hungarian Academy of Sciences, Budapest, Hungary[3]*

**Introduction:**
Mindset and communication barriers may hinder the acceptance of bariatric surgery (BS) by the eligible patient population. Our objective was to improve the understanding of expectations, opinions, emotions and attitudes toward weight-loss among patients with obesity.

**Methods:**
Survey data collected from BS-related social media communities (N=1482). Participants were asked to write 5 words that first came to their mind about "weight loss", and to select 2 emotions which best described their corresponding feelings. Demographic and obesity-related data were collected. Cognitive representations were constructed based on the co-occurrence network of associations, using validated data-driven methodology.

**Results:**
Respondents were Caucasian (98%), female (94%), aged 42.5±10.1 years, current/highest lifetime body mass index=36.9±9/50.7±8.7 kg/m2. The association network analysis revealed two cognitive modules: benefit-focused (health, attractiveness, happiness, agility) and procedure-focused (effort, diet, sport, surgery). Patients willing to undergo BS were more benefit-focused (Odds ratio (OR)=2.4, P=0.02) and expressed more 'hope' (OR=142, P<0.001). History of BS was associated with higher adherence to the procedure-focused module (OR=2.3, P<0.001), and with increased use of the emotions 'gratitude' (OR=107, P<0.001), 'pride' (OR=15, P<0.001), and decreased mention of 'hope' (OR=0.03, P<0.001).

**Conclusion:**
Patients with obesity tend to think about weight loss along two cognitive schemes, either emphasizing its expected benefits or focusing on the process of achieving it. Benefit-focused respondents were more likely to consider BS, and to express hope rather than gratitude or pride. Novel communication strategies may increase the acceptance of BS by incorporating weight loss-related cognitive and emotional content stemming from patients' free associations.

**22**

D. Busenhart[1], J. Erb[1], G. Rigakos[2], T. Eliades[1], S. Papageorgiou[1]

**Adverse effects of chemotherapy on the teeth and surrounding tissues of children with cancer: A systematic review with meta-analysis**

*Clinic of Orthodontics and Pediatric Dentistry, Center of Dental Medicine, University of Zurich, Zurich, Switzerland[1], Third Oncology Department, Hygeia Hospital, Athens, Greece[2]*

**Introduction:**
The aim of this systematic review was to assess evidence on dental adverse effects associated with chemotherapy (CH) administered to children with cancer.

**Methods:**
Eight databases were searched without restrictions up to March 2017 for studies reporting on dental effects of CH administered for childhood cancer. After elimination of duplicates, data extraction, and risk of bias assessment according to the Cochrane guidelines, random-effects metaanalyses of Relative Risks (RR) and Mean Differences (MD) and their 95% Confidence Intervals (CI) were performed, followed by meta-regression and sensitivity analyses.

**Results:**
The literature search identified a total of 15 non-randomized case-control studies including at least 2315 patients (mean age at diagnosis or CH of 6.6 years; 36% male) followed for up to 22.9 years after CH. Meta-analysis indicated that CH was associated with increased risk for tooth agenesis compared to healthy controls (RR=2.47; 95% CI=1.30 to 4.71; P=0.006). This translated to every seventh child with CH having agenesis of at least one tooth that would not otherwise have. Additionally, CH was significantly associated with increased risk of tooth discoloration, arrested tooth development, enamel hypoplasia, microdontia, premature apexification, and decreased salivary flow rate, as well as worse oral hygiene and greater caries experience compared to controls. However, the strength of evidence was very low due to the inclusion of non-randomized study designs with high risk of bias.

**Conclusion:**
Current evidence from childhood cancer survivors indicates that chemotherapy is associated with considerable dental adverse effects that might be associated with greater burden of disease and treatment costs.

**23**

V. Koretsi[2], T. Eliades[1], S. Papageorgiou[1]

**Oral Interventions for Obstructive Sleep Apnea: An Umbrella Review of the Effectiveness of Intraoral Appliances, Maxillary Expansion, and Maxillomandibular Advancement**

*Clinic of Orthodontics and Pediatric Dentistry, Center of Dental Medicine, University of Zurich, Zurich, Switzerland[1], Department of Orthodontics, University of Regensburg, Regensburg, Germany[2]*

**Introduction:**
The effectiveness of intraoral appliances (IOA), maxillary expansion (ME), and maxillomandibular advancement (MMA) in the treatment of children and adults with obstructive sleep apnea (OSA) has not yet been adequately assessed.

**Methods:**
An umbrella review was performed based on established guidelines for evidence-based medicine. Data synthesis was performed only from randomized controlled trials with Paule-Mandel random-effects meta-analyses / meta-regressions using mean differences (MDs) and 95% confidence intervals (CIs) and was followed by the qualitative evaluation of the meta-evidence.

**Results:**
29 systematic reviews were included, 7 of which provided quantitative data. IOA were effective in improving apnea hypopnea index (AHI) compared to both, placebo appliances (12 trials; 525 patients; MD = –11.70; 95% CI: [–15.38; –8.01]; $p<0.001$) and no treatment (1 trial; 24 patients; MD = –14.30; [–21.59; –7.01]; $p<0.001$). Only the former comparison was supported by robust meta-evidence. Effectiveness of IOA as measured by the Epworth Sleepiness Scale, on the other hand, was not supported by robust meta-evidence. No randomized or prospective controlled trials were found on the effectiveness of ME (conventional or surgically assisted) and MMA.

**Conclusion:**
Intraoral appliances are effective in reducing AHI and their use is substantiated by robust evidence. There is no evidence from high-quality research to support treatment with ME (conventional or surgically assisted) or MMA in patients with OSA.

**24**

N. Pedrazzi[1], S. Schweizer[1], T. Gentzsch[1], H. Klein[1], P. Giovanoli[1], J. Plock[1]

**Characteristics, Management and Outcome of Electrical Injuries and Burns at a Swiss Burns Center**

*Universitätsspital Zürich[1]*

**Introduction:**
Electrical injuries are less frequent compared to other burn injuries, but very destructive with high morbidity and mortality, and associated with prolonged ICU and hospital stays and need for repeated procedures. The aim of this study was to determine epidemiology, management and outcome in patients with electrical injuries treated in a modern burns center.

**Methods:**
Patient charts over 15 years were analyzed retrospectively to identify patients with electrical injuries admitted into the burns center at the University Hospital Zürich between January 2005 and October 2019. Epidemiologic parameters, patient characteristics, injury type, management and outcome were reviewed.

**Results:**
89 patients were identified, with an average of six patients per year. Electrocution was predominant in males (86.5%), while 66.3% of patients had occupational injuries and 33.7% non-occupational ones, of which 11.2% due to attempted suicide. Patients had a wide age distribution (17 to 78 years old, median 47.5 years), the majority (50.6 %) in the age group 21–40 years. 46% of patients had at least one comorbidity at the time of the accident. 24.7% suffered from pre-existing psychiatric conditions, including active addiction (12.4%). 21 patients suffered low-voltage (<1000V), and 65 high-voltage injuries (43 cases flash, 38 direct contact and 8 unknown mechanism) and 3 unclear (no witnesses). Length of ICU and hospital stays ranged from 0 to 152 days (median 76 days), and 1 to 190 days (median 95.5 days), respectively. 43.8% of patients had specialized rehabilitation (range 0-357 days, median 178.5 days).Most common afflicted anatomical regions were upper extremities (91%), lower extremities (59.5%), trunk (51.7%) and head (51.7%). The mean TBSA was higher in patients with high-tension accidents (30.4%) compared to low-tension (9.8%). Several procedures were done per patient (total of 515). Low voltage injured had an average of 3.5 surgeries, of which 89.2% during the first acute admission and 10.8% during elective readmissions. High voltage patients had an average of 6.7 operations, 87.6% during the first acute admission, 9.6% during elective hospitalization and 2.8% emergency readmissions. Escharotomy and fasciotomies were performed in 40.5% and 24.7% of the patients, often on the day of admission. Further surgical care included reiterated debridement, necrectomy, tangential excision (56.2%) followed by meshed split-thickness skin grafting (69.7%). Flap-based reconstruction was required in 21 patients (23.6%): 17 patients had local flaps (76% high voltage) and 12 patients had free flaps (83.3% high voltage). The total flap failure rate was 9%, with fourflap failures out of forty-four flap-surgeries. Total amputation rate was 13.5% and predominantly affect the upper extremities. Complications included sepsis (47.2%), pulmonary (44.9%), cerebral (41.6%), rhabdomyolysis (29.2%), and renal failure (20.2%). Mortality was 9% in low voltage and 19% in high voltage injured. Most common cause of death was multiple organ failure (35%), septic shock (21%), cardiocirculatory arrest (7%), cerebral complications (7%).

**Conclusion:**
Electrical injuries (especially high voltage) are still cause of elevated morbidity (amputations and complications) and mortality, mostly involve young men in their earning period,towards which prevention should be focused on. Reconstruction remains frequently challenging.

**25**

S. Mohammed[3], S. Costantino[3], A. Akhmedov[3], K. Gergely [4], S. Ambrosini[3], P. Madeddu[1], G. Spinetti[2], T. Luscher[3, 5], F. Paneni[3, 6]

**Chromatin modifications by the methyltransferase SETD7 modulate angiogenic response in diabetes: insights for epigenetic-based therapies**

*Bristol Royal Infirmary, University of Bristol, London, UK [1], Cardiovascular research unit, IRCCS Multimedica, Milan, Italy[2], Center for Molecular Cardiology, University of Zürich, Switzerland[3], Institute for Clinical Chemistry, University Hospital, Zurich, Switzerland[4], Research, Education & Development, Royal Brompton and Harefield Hospital Trust, London, UK[5], University Heart Center, Cardiology, University Hospital Zürich, Switzerland[6]*

**Introduction:**
Peripheral artery disease (PAD) is highly prevalent in people with diabetes (DM), and associates with a high rate of limb amputation and poor prognosis. Surgical and catheter-based revascularization have failed to improve outcome in DM patients with PAD. Hence, a need exists to develop new treatment strategies able to promote blood vessel growth in the ischemic limb of DM patients. Epigenetic changes – namely DNA methylation and histone modifications - have recently shown to regulate the expression of genes involved in angiogenesis. Mono-methylation of histone 3 at lysine 4 (H3K4m1) - a specific epigenetic signature induced by the methyltransferase SETD7 – favours a chromatin conformation which enables the transcription of genes involved in endothelial inflammation and oxidative stress. The present study was designed to investigate whether SETD7-dependent epigenetic changes modulate angiogenesis in the setting of hyperglycaemia.

**Methods:**
Primary human aortic endothelial cells (HAECs) were exposed to normal glucose (NG, 5 mM) or high glucose (HG, 20 mM) concentrations for 48 hours. Mannitol (20 mM) was used as an osmotic control. SETD7 protein and H3K4me1 levels were investigated by Western blot and Chromatin immunoprecipitation (ChIP). Knockdown of SETD7 was achieved by small interfering RNA (siRNA) and scrambled-siRNA was used as a negative control. Pharmacological blockade of SETD7 was performed by using the highly selective inhibitor (R)-PFI-2, while its inactive enantiomer, (S)-PFI-2, was used as a control. Scratch and tube formation assays were performed to investigate the impact of SETD7 on angiogenic properties of HAECs. RNA sequencing (RNA-seq) and Ingenuity Pathway Analysis (IPA) were employed to unveil putative genes regulated by SETD7 in HAECs exposed to NG and HG. In vivo experiments were performed on Lepdb/db mice carrying the genetic deletion of the methyltransferase SETD7 (Setd7-/--Lepdb/db). Gastrocnemius muscle samples from patients with and without T2D were employed to translate our experimental findings.

**Results:**
HG exposure in HAECs led to a time-dependent increase of both SETD7 gene and protein expression, as compared to NG. SETD7 upregulation in HG-treated HAECs was associated with an increase of H3K4me1 levels as well as with impaired endothelial cell migration and tube formation. Of interest, both gene silencing and pharmacological blockade of SETD7 rescued hyperglycemia-induced impairment of angiogenic properties in HAECs. RNA-seq in HG-treated HAECs with and without SETD7 depletion unveiled an array of differentially expressed genes, which were mainly involved in blood vessel growth and angiogenic response, as shown by IPA analysis. Among dysregulated genes, ChIP assays showed that SETD7 specifically mono-methylates H3K4m1 in proximity of Semaphorin-3G (SEMA-3G) promoter, thus regulating its expression. Indeed, SEMA-3G overexpression impaired angiogenic properties in SETD7-depleted HAECs. Endothelial sprouting was defective in aortas from Lepdb/db as compared to WT mice, whereas angiogenic response was preserved in Setd7-/--Lepdb/db mice. Finally, SETD7/SEMA-3G axis was upregulated in muscle specimens from T2D patients

**Conclusion:**
Targeting SETD7 represents a novel epigenetic-based therapy to boost neovascularization in T2D patients with PAD.

**27**

D. Canepa[1], E. Arvaniti[2], V. Tosevski[3], S. Märsmann[1], B. Eggerschwiler[1], M. Claassen[2], HC. Pape[1], E. Casanova[1], P. Cinelli[1]

**Comprehensive Mass Cytometry Analysis of Human Adipose Derived Stem Cells for Clinical Applications**

*Department of Trauma, University Hospital Zurich[1], Institute of Molecular Systems Biology ETH Zurich[2], Mass Cytometry Facility Zurich[3]*

**Introduction:**
The impressive progress in the field of stem cell research in the past decades has provided the ground for the development of cell-based therapies. Mesenchymal Stem cells (MSCs) isolated from adult tissues represent in this context an appealing cell source for regenerative medicine. However, MSCs consist of a heterogeneous, not yet well-characterized population of different stem/progenitor cells and such variability complicates their use in regenerative applications. In 2006 the International Society for Cellular Therapy published the minimal criteria for defining MSCs: (1) adhere to plastic, (2) express CD73, CD90, CD105 and lack the expression of most of the hematopoietic stem cells markers and, (3) trilineage differentiation capacity (adipocytes, chondrocytes, and osteocytes). However, MSC preparations established with this method still exhibit heterogeneity. It would be therefore essential to analyze the expression of more markers in toto and at single cell level in order to fully understand the complexity of the cellular composition of MSC preparations. This knowledge is essential for improving the use of MSCs in potential outcomes in cell therapy.

**Methods:**
Recent advances in single-cell technologies have opened the way for high-dimensional, -throughput and -resolution measurements of biological systems. In this study, we made use of the novel technology of cytometry by time-of-flight (CyTOF) to explore the cellular composition of 17 human ASCs, interrogating 31 markers at single cell level. Subcellular composition of the ASCs was investigated in their naïve state as well as during trilineage commitment via unsupervised dimensionality reduction as well as supervised representation learning approaches.

**Results:**
Visualization of the distribution of the markers in the ASC lines with the dimensionality reduction method Uniform Manifold Approximation and Projection (UMAP) highlighted intra- and inter-donor heterogeneity in marker expression. To investigate whether this heterogeneity mirrored the ability of the cells to differentiate, all 17 ASCs were differentiated in the trilineage. Differentiation was quantified and based on the results, we divided the ASCs in “good”, “intermediate”, and “bad” differentiating cells for each lineage. To investigate how the differences in trilineage differentiation between the ASC lines correlate with the heterogeneity at single cell level, we next performed CyTOF over four days of trilineage differentiation. By using a suprvisonised learning approach, CellCNN (Concolutional Neuronal Network), we were able to detected a cell subpopulation with increased frequency in “good” lines over the 4 days of osteogenic differentiation characterized by high alkaline phosphatase (ALP+) and low CD73 expression. We could further demonstrate in vitro that the sorted ALP+/CD73+ subpopulation exhibited enhanced osteogenic potential and its presence is fundamental for osteogenic lineage commitment. We finally show that this subpopulation was present in freshly isolated human dipose-derived stromal vascular fractions (SVFs) and that could be ultimately used for cell therapies.

**Conclusion:**
The data obtained reveal for the first time at single cell level the heterogeneity of ASCs from several donors and highlight how cellular composition impact the trilineage differentiation capacities.
Identifying populations with enhanced differentiation potential would serve as a diagnostic tool to predict clinical outcomes and would improve therapeutic approaches. In sum, our study paves the way for an improved and targeted use of ASCs for clinical applications.

**30**

C. Waschkies[1, 2], D. Heuberger[4], F. Kivrak Pfiffner[3], P. Wolint[1, 5], M. Calcagni[5], P. Giovanoli[5], J. Buschmann[1, 5]

## Functional gas challenges to probe vasoreactivity and hypoxia in MC-38 colon and A549 lung adeno-carcinoma cell grafts grown on the chorioallantoic membrane of the chick embryo in ovo using MRI

*Center for Surgical Research, University Hospital Zurich, Switzerland[1], Institute for Biomedical Engineering, ETH and University of Zurich, Switzerland[2], Institute for Regenerative Medicine, University of Zurich, Switzerland[3], Institute of Intensive Care Medicine, University Hospital Zurich, Switzerland[4], Plastic Surgery and Hand Surgery, University Hospital Zurich[5]*

**Introduction:**
Tumor models based on the chorioallantoic membrane (CAM) are an intermediate step between cell culture and more complex mammalian in vivo models [1]. MRI has only started to harness this potential, and tumor grafts and their metastases have been characterized morphologically [2, 3]. Recently, it was demonstrated that functional gas challenge is feasible on the CAM [4] and here, using T1 and T2*, we explore the response of MC-38 colon and A549 adeno-carcinoma cell grafts to hypercapnic and hypercapnic-hyperoxic gas challenges pertaining to the grafts vascular and oxygenation phenotypes [5, 6].

**Methods:**
Fertilized Lohman white LSL chick eggs were opened on incubation day (ID) 3.5 and on ID 7 5 x $10^5$ matrigel embedded MC-38 colon or A549 lung adenocarcinoma cells were planted onto the CAM. MRI was performed in ovo on ID 14 in 5-6 samples for each graft type on a 4.7T Bruker PharmaScan system, with chicken embryos sedated by pre-cooling the egg at 4°C for 90 min, a protocol previously described [2]. T1w anatomical reference images obtained and quantitative T1 and T2* maps were compared between periods of air, hypercapnia (5% CO2, 20% O2, 75% N2) and hypercapnic hyperoxia (i.e. carbogen, 5% CO2, 95% O2). Gases were delivered through a plastic tubing to the CAM.

**Results:**
Quantitative T2* and T1 MR images were obtained from MC-38 colon and A549 lung adenocarcinoma cell grafts. Region of interest analysis within the graft revealed a significant decrease in T1 in the A549 grafts under hypercapnic hyperoxia; T2* was not affected for both graft types and under both gas challenges, and T1 was neither affected in MC-38 grafts under both gas challenges. The CAM serves as a breathing organ during chick embryo development, and we showed in a previous study that these markers are also applicable for the grafts on the CAM: Under medetomidine anesthesia A549 grafts revealed increased T2* values upon hypercapnic hyperoxia, while MC-38 grafts displayed a decreasing trend in T1, results that are in contrast to what we observed under the present cooling protocol for sedation. Graft size and T1/T2* heterogeneity were similar to the previous study.

**Conclusion:**
Our study reveals a differential response to hypercapnic and hypercapnic-hyperoxic functional gas challenge in A549 tumor grafts planted on the CAM. Effects from sedation protocol need to be consolidated with more samples. Using MRI, tumor grafts can be studied non-destructively in ovo for their differential response to functional gas challenges probing vascular reactivity and oxygenation status.

References:
[1] Nowak_Sliwinska et al. (2014) Angiogenesis 17: 779-804
[2] Zuo et al. (2014) NMR Biomed 28: 440-447
[3] Herrmann et al. (2018) Molecular Imaging 17: 1-9
[4] Waschkies et al. (2019) EMIM Poster #730
[5] Baudelet et al. (2006) NMR Biomed 19: 69-76
[6] O'Connor et al. (2015) Cancer Res 76(4) : 787-95

**31**

F. Strauss[2], A. Gil[2], D. Thoma[2], U. Jung[3], M. Kim[3], K. Paeng[3], R. Jung[2], S. Fickl[1]

**Effect of hard and soft tissue grafting and individualization of healing abutments at immediate implants – an experimental study in the canine.**

*Julius-Maximilians-University Würzburg[1], University of Zurich[2], Yonsei University[3]*

**Introduction:**
Immediate implant placement in conjunction with hard or soft tissue graft along with immediate provisionalization are additional procedures aiming at stabilizing the peri-implant tissues. However, the evidence regarding the added benefit of these procedures is still lacking. The aim of the present study was, therefore, to evaluate the effects of intra-alveolar socket grafting, subepithelial connective tissue grafting, and individualized abutments on peri-implant hard and soft tissue outcomes following immediate implant placement.

**Methods:**
This randomized experimental study employed 5 mongrel dogs, with 4 sites per dog (total of 20 sites). The mesial roots of P3 and P4 were extracted in each hemimandible and immediate dental implants were placed. Each site was randomly assigned to 1 of 4 different treatment groups: standardized healing abutment (control group), alloplastic bone substitute material (BSS) + standardized healing abutment (SA group), BSS + individualized healing abutment (IA group), and BSS + individualized healing abutment + a subepithelial connective tissue graft (IAG group). Clinical, histological, and profilometric analyses were performed. The intergroup differences were calculated using the Bonferroni test, setting statistical significance at $P<0.05$.

**Results:**
Clinically, the control and SA groups demonstrated a coronal shift in the buccal height of the mucosa (0.88±0.48 mm and 0.37±1.1 mm, respectively). The IA and IAG groups exhibited an apical shift of the mucosa (−0.7±1.15 mm and −1.1±0.96 mm, respectively). Histologically, the SA and control groups demonstrated marginal mucosa heights of 4.1±0.28 mm and 4.0±0.53 mm relative to the implant shoulder, respectively. The IA and IAG groups, in contrast, only showed a height of 2.6 mm. In addition, the height of the mucosa in relation to the most coronal buccal bone crest or bone substitute particles was not significantly different among the groups. Volumetrically, the IA group (−0.73±0.46 mm) lost less volume on the buccal side than the control (−0.93±0.44 mm), SA (−0.97±0.73 mm), and IAG (−0.88±0.45 mm) groups.

**Conclusion:**
The control group demonstrated the most favorable change of height of the margo mucosae and the largest dimensions of the peri-implant soft tissues. However, the addition of a bone substitute material and an individualized healing abutment resulted in slightly better preservation of the peri-implant soft tissue contour.

**32**

P. Biro[2], P. Hofmann[3], D. Gage[2], Q. Boehler[3], C. Chautems[3], J. Braun[1], D. Spahn[2], B. Nelson[3]

**REALITI became reality: simulated automated tracheal intubation based on image recognition**

*Epidemiology, Biostatistics and Prevention Institute, University of Zurich[1], Institute of Anesthesiology, University Hospital Zurich[2], Multi-Scale Robotics Lab, Swiss Federal Institute of Technology (ETH) Zurich[3]*

**Introduction:**
Tracheal intubation is an essential medical procedure that can be challenging for health care providers with limited airway management experience, such as emergency physicians or paramedics. Therefore, there is a definite need for new techniques to facilitate this vital procedure. The acronym REALITI stands for 'Robotic Endoscope Automated via Laryngeal Imaging for Tracheal Intubation', which is a novel system that uses a video-endoscopic stylet to guide a mounted tracheal tube into the trachea by automatically steering its flexible tip. As proposed by the IFA/USZ team, the MSRL/ETH team developed and assembled a REALITI prototype. This handheld device is a motorized 2-degrees-of-freedom endoscope that can bend its tip in any direction. This motion can be either manually controlled by a joystick, or automatically steered using anatomical reference features detected in the endoscopic camera image. The user retains control of the device during the intubation procedure and can switch between manual or automated action at any point. The prototype demonstrated the ability to guide the tracheal tube into the airway in a simulated setting.

**Methods:**
Fourteen individuals from both teams, IFA/USZ and MSRL/ETH, were recruited to perform tracheal insertions of the REALITI prototype into an airway manikin under standardized conditions. Each participant performed 12 successive tracheal insertions of the device. We assessed: a) the total number of successful tracheal insertions (procedures completed in < 180 seconds), b) the effective time to complete tracheal insertions, and c) the subjective degree of ease of performance according to a Likert scale ranging from 0 (very difficult) to 10 (very easy). The results are presented as descriptive statistics.

**Results:**
From the 168 planned tracheal insertions, 5 were aborted due to device malfunctions. All remaining 163 insertions resulted in successful tracheal positioning of the device within a time range of 3.8 to 133 seconds (s). The time to complete tracheal insertions resulted in a median and IQR of 16.3 seconds (12.5–22.0 s). The percentages of successful tracheal insertions arranged according to time periods of 30 seconds is as follows: 89.6% of insertions were successfully completed in 30 s, 97.5% in 60 s, 98.2% in 120 s, and 100% in 150 s. No esophageal insertion occurred. The participants assessed the ease of handling the REALITI device to be at 6.3 ± 1.6 (mean ± SD).

**Conclusion:**
The 100% success rate of tracheal insertions in less than 3 minutes using REALITI shows the use of image recognition of anatomical structures along the intubation pathway can be a valuable function when guiding a video endoscope into the trachea. In sufficiently pre-oxygenated patients, a successful placement of a tracheal tube into the trachea within 180 s is considered sufficient to avoid hypoxemia and related morbidity/mortality. The large proportion of insertions achieved within 60 s in 98.2% of all trials, including those performed by unexperienced non-medical users, was comparable to the performance levels of experienced anesthesiologists during their routine clinical activity. Thus, the REALITI prototype has demonstrated its ability to facilitate successful tracheal intubations even in the case of less experienced healthcare providers.

**33**

M. Raeber[1], R. Rosalia[1], D. Schmid[1], U. Karakus[1], O. Boyman[1]

**Interleukin-2 signals converge in a lymphoid–dendritic cell pathway fostering anti-cancer immunity**

*Department of Immunology, University Hospital Zurich, Zurich[1]*

**Introduction:**
Dendritic cells (DC) are a subgroup of professional antigen-presenting cells considered indispensable in orchestrating T cell responses to intracellular pathogens and tumors. Tumor-infiltrating DCs correlate with effective anti-cancer immunity and improved responsiveness to anti-PD-1 checkpoint immunotherapy. However, the upstream drivers of DC expansion and intratumoral accumulation are ill-defined. We find that interleukin-2 (IL-2)-mediated, innate and adaptive lymphoid cell-driven DC-poiesis in mice and humans imprints signatures of improved anti-cancer immunity. Thus, IL-2 immunotherapy-mediated stimulation of DCs contributes to anti-cancer immunity by rendering tumors more immunogenic.

**Methods:**
To investigate the effects of recombinant human IL-2 (Proleukin) on DCs, peripheral blood mononuclear cells collected within the Charact-IL-2 investigator-initiated clinical trial (ClinicalTrials identifier: NCT03312335) were characterized with high-parameter flow cytometry before and after IL-2 treatment. To further explore the mechanism of IL-2-driven DC expansion different IL-2-treated mouse models including in vivo antibody-mediated cell depletion models as well as knock-out, transgenic and bone marrow chimeric mouse models were extensively analyzed with flow cytometry, enzyme-linked immunosorbent assay, and RNA sequencing. For further functional studies cell-cycle analysis, in vitro antigen-uptake assays, and in vivo transplantable and transgenic tumor models were used.

**Results:**
We report that IL-2 administration in both human and mouse resulted in pronounced expansion of type-1 and type-2 DCs; these included migratory and cross-presenting DC subsets, although neither their precursors nor mature DCs expressed functional IL-2Rs. In mechanistic studies, IL-2 signals stimulated innate lymphoid cells, natural killer, and T cells to synthesize FMS-like tyrosine kinase 3 ligand (FLT3L), colony-stimulating factor 2 (CSF2), and tumor necrosis factor (TNF); these cytokines redundantly caused DC expansion and activation, which resulted in improved antigen processing and correlated with favorable anti-tumor responses.

**Conclusion:**
The advent of immune checkpoint inhibitors transformed modern oncology by exerting durable responses in selected metastatic cancers. Yet, only patients with highly immune cell-infiltrated, or so-called “hot” tumors, respond to immune checkpoint blockers. The present study shows a complementary difference and unappreciated advantage of interleukin-2 (IL-2) immunotherapy compared to anti-programmed cell death protein 1 (PD-1) immune checkpoint inhibitor treatment. Thus, IL-2 immunotherapy expanded tumor-infiltrating antigen-presenting DCs, and favored the conversion of poorly immunogenic into immunogenic tumors. These insights might help find ways of overcoming primary and secondary tumor-resistance to immune checkpoint inhibitors and provide a strong rationale for combinatorial strategies.

**34**

K. Frontzek[5], M. Bardelli[2], A. Senatore[5], R. Reimann[5], M. Carta[5], R. Hussain[1], S. Jurt[4], M. Georg[3], G. Siligardi[1], O. Zerbe[4], C. Zhu[5], S. Hornemann[5], L. Simonelli[2], L. Varani[2], A. Aguzzi[5]

**Rationally designed neuroprotective antibodies against prions**

*B23 Beamline, Diamond Light Source[1], Università della Svizzera italiana, Institute for Research in Biomedicine[2], University of Cambridge, Department of Chemistry[3], University of Zurich, Department of Chemistry[4], University of Zurich, Institute of Neuropathology[5]*

**Introduction:**
Prions multiply through the seeded propagation of the scrapie prion protein $PrP^{Sc}$, which uses its cellular counterpart $PrP^{C}$ as a substrate. The interaction of incoming $PrP^{Sc}$ with membrane-resident $PrP^{C}$ causes spongiform encephalopathies. Antibodies binding the globular domain (GD) of $PrP^{C}$ can halt this process, but they can also induce allosteric changes in its flexible tail (FT) that activate toxic intracellular cascades. Intriguingly, similar events occur in prion-infected brains, and substances that relieve the damage of infectious prions can also alleviate the toxicity of anti-$PrP^{C}$ antibodies including POM1. This suggests that POM1 and prions act through similar mechanisms, and that understanding POM1 toxicity might clarify how prions damage the brain.

**Methods:**
Molecular dynamics (MD) simulations and nuclear magnetic resonance (NMR) spectroscopy were used to study transient interactions of anti-$PrP^{C}$ antibodies in complex with $PrP^{C}$. We mutagenized each one of the POM1 residues showing significant interaction with $PrP^{C}$ to alanine and expressed the mutants as single-chain variable fragment antibodies. *Ex vivo* testing of $PrP^{C}$ mutants was undertaken by transduction of cerebellar organotypic slice cultures from *Prnp*$^{0/0}$ (Zurich 3) mice with $PrP^{C}$-expressing adeno-associated viruses. A synthetic human Fab phagemid library (Novartis Institutes for BioMedical Research) was used for phage display. For *in vivo* testing of antibodies, mice received intracerebral antibody injections and toxicity was assessed on volumetric diffusion-weighted magnetic resonance imaging and histology. Cerebellar organotypic slice cultures (COCS) from *Tga*20 mice overexpressing the prion protein were used as *ex vivo* system faithfully reproducing prion pathology.

**Results:**
We show that antibody POM1 induces the H-latch, an intramolecular R208-H140 hydrogen bond within $PrP^{C}$ that rigidifies its epitope while flexibilizing its α2-α3 and β2-α2 loops. Cells expressing a $PrP^{R208A}$ mutant unable to form the H-latch were resistant to POM1 toxicity; conversely, expression of a $PrP^{2Cys}$ mutant mimicking the H-latch was constitutively toxic. We therefore engineered POM1 mutants retaining their epitope specificity, yet unable to form the H-latch. These antibodies were innocuous when injected intracerebrally, conferred resistance to POM1 toxicity, and repressed neurodegeneration of prion-infected cerebellar organotypic cultures, suggesting that they prevented the docking of infectious prions to $PrP^{C}$. Finally, we developed phage-displayed antibody fragments binding wild-type $PrP^{C}$, but not $PrP^{2Cys}$. These reagents conferred protection against prions and, similar to innocuous pomologs, were not able to induce the H-latch.

**Conclusion:**
These findings identify a defined $PrP^{C}$ conformation as necessary and sufficient for neurotoxicity. The structural clarification of anti-$PrP^{C}$ neuroprotection may enable the rational design of efficacious anti-prion drugs.

**35**

A. Lakkaraju[1], E. Lemes[1], U. Herrmann[1], K. Frontzek[1], M. Losa[1], R. Marpakwar[1], A. Aguzzi[1]

**Identifying the determinants of spongiform phenotype in prion infections**

*Institute of Neuropathology, University Hospital of Zurich, Zürich, Switzerland[1]*

**Introduction:**
Prion diseases are protein misfolding and aggregating disorders (PMA) implicated in Creutzfeldt-Jakob disease (CJD) and several transmissible spongiform encephalopathies of humans and animals. It is characterized by the accumulation and deposition of an abnormal conformer (PrPSc) of the endogenous prion protein (PrPC). In addition to generic neuropathological changes (astrogliosis, neuronal loss, deposition of amyloid plaques), prion-infected brains feature a characteristic "spongiosis" which is caused by the accumulation of intraneuronal/intraneuritic vacuoles containing membrane fragments and, sometimes, degenerating organelles which are of uncertain biogenesis and content. Previous studies have documented the accumulation of PrPSc in multivesicular bodies after prion infection, suggesting impairment of the endo/lysosomal machinery. Depletion of PIKfyve and/or FIG4, which are involved in synthesis of phospholipid PI(3,5)P2 a key cog of endo/lysosomal machinery, induces vacuolation similar to spongiosis. We therefore decided to investigate whether the breakdown of the endolysosomal fusion machinery is the cause of spongiosis in prion infections.

**Methods:**
To address the mechanistic details of spongiosis, we use animal models (mice), organotypic slice cultures and cell lines. Techniques such as immunohiostochemistry, electron microscopy and in vitro biochemical assays were utilized in all these model systems, to identify determinants of vacuolation. Rescue experiments have been performed by treating the cell lines and mouse organotypic cultured slices with a water -soluble version of PI(3,5)P2. Mice models were used to assess time course of events preceding the generation of vacuoles and the downstream effects of vacuolation.

**Results:**
We monitored the protein levels of PIKfyve and FIG4 in the brains of prion-infected tga20 mice (overexpressing PrPC) infected with the Rocky Mountain Laboratory strain 6 (RML6) of prions. PIKfyve was significantly downregulated at 90 days post-infection and profoundly depleted in terminally sick mice. The mRNA levels of PIKfyve was unaltered, suggesting that posttranslational events led to destabilization. ER stress plays an important role in the toxicity in prion infections and time course analyses in prion-infected mice revealed PIKfyve depletion post ER stress induction. Interestingly PIKfyve was deacylated in prion infection, which further led to its ubiquitination and degradation. Loss of PIKfyve was associated with upregulation of lysosomal genes in a Transcription factor EB dependent manner, mimicking a lysosomal storage disease. Treatment with GSK2606414, which alleviates the ER stress induced by PERK pathway or overexpression of acyl transferases zdhhc9 and 21, restored acylation and steady state PIKfyve levels. Restoration of PI(3,5)P2 levels in cell culture models and cultured organotypic slices by treating them with a water soluble analog of PI(3,5)P2 rescued vacuolation and lysosomal defects.

**Conclusion:**
Our data suggests that spongiform change in prion infections may directly result from the suppression of the PIKfyve kinase, resulting in the impairment of endolysosomal machinery and formation of progressively larger vacuoles. In our study, activation of chronic ER stress preceded the depletion of PIKfyve. We observed that ER stress induces deacylation of PIKfyve thereby destabilizing it and promoting its degradation. Furthermore vacuolation and lysosomal defects could be rescued in our in vitro and ex vivo model systems using either water soluble analog of PI(3,5)P2 or overexpressing zdhhc9 and 21.

**36**

A. Henzi[1], A. Senatore[1], A. Lakkaraju[1], A. Aguzzi[1]

**Effects of a dimeric PrP-Fc-fusion protein on mouse sciatic nerve**

*Institute of Neuropathology, University Hospital of Zurich[1]*

**Introduction:**
Mice devoid of the normal prion protein (PrP) develop a chronic demyelinating polyneuropathy of the peripheral nervous system (PNS), suggesting a role of PrP in myelin maintenance. A peptide derived from the N-terminal flexible tail (FT) region of PrP was described as an activating ligand of Gpr126, increasing the expression of myelination related genes in Schwann cells in vitro and in vivo. Our aim was to exploit the function of PrP in myelin maintenance for the treatment of various PNS diseases such as chronic inflammatory demyelinating polyneuropathy or Charcot Marie Tooth disease. We have coupled FT to an Fc-γ antibody fragment, resulting in the FT2Fc-fusion protein. FT2Fc activates Gpr126 in vitro and has a terminal serum half-life of 50h in vivo. As a proof principle study, we have chronically administered this dimeric PrP-Fc-fusion protein to PrP knockout mice (ZH3). We used a prophylactic treatment design, with the start of treatment before the onset of demyelination in ZH3 mice (5 weeks). However, after 17 weeks of treatment, no difference between treated mice and control mice could be detected in electrophysiological testing, morphological analysis or protein analysis of sciatic nerves.

**Methods:**
ZH3 mice were treated with FT2Fc or control treatment (buffer or mouse IgG) for 17 weeks. Electrophysiological measurement were performed on the sciatic nerve in vivo. Then, the nerves were collected for analysis of morphology and protein.

**Results:**
No difference in motor and compound (sensory) nerve conduction velocity could be detected when comparing FT2Fc treated mice to control mice. Morphological analysis of toluidine blue stained semithin sections from sciatic nerves showed no qualitative difference and no difference in number of myelinated axons between. Protein markers of damage (GFAP, cJun) were similar in treated and control sciatic nerves.

**Conclusion:**
Our aim was to exploit the promyelinating property of PrP for the treatment of demyelinating diseases of the peripheral nervous system. However, the prophylactic proof of principle study in ZH3 mice showed neither a beneficial nor a detrimental effect of our compound, FT2Fc. This might be due to pharmacological or pharmacokinetic reasons, in particular a failure of FT2Fc to reach Gpr126 in the nerve. Or, the demyelinating phenotype of ZH3 mice at the investigated time point may be too mild for a rescue to be detectable.

**37**

M. Carta[2, 4], M. Losa[2, 4], E. Kara[2], R. Moos[4], K. Frontzek[4], S. Kreutzer[3], A. Bratus-Neuenschwander[3], G. Russo[3], R. Reimann[4], S. Hornemann[4], C. Proukakis[1], A. Aguzzi[4]

**Somatic PRNP mosaicism in prion disease**

*Department of Clinical and Movement Neurosciences, UCL Queen Square Institute of Neurology, London, United Kingdom[1], Equal contribution[2], Functional Genomics Center Zurich, ETH Zurich and University of Zurich, Zurich, Switzerland[3], Institute of Neuropathology, University Hospital Zurich, University of Zurich, Zurich, Switzerland[4]*

**Introduction:**
Prion diseases are progressive infectious neurodegenerative diseases associated with prions, which are believed to be composed of a misfolded version of the cellular prion protein (PrPC), a GPI-anchored protein that is found in many kinds of mammalian cells, particularly in the nervous system. This misfolded conformation allows prions to transform non-pathogenic PrPC into the misfolded infectious form PrPSC. Most cases of human prion disease are sporadic (sporadic Creutzfeldt-Jakob disease, sCJD), whereas a minority are caused by mutations in the prion protein gene PRNP or are a consequence of iatrogenic or oral infection with human or bovine prions. Despite decades of research, it is currently unclear which factors trigger the spontaneous generation of prions in sCJD.
Recent data show that in neurons, somatic mutations accumulate with age and are associated with neurodegeneration. Somatic mutations in PRNP may lead to the formation of mutant prion protein variants that favour the generation or propagation of prions, causing outbreak of sCJD. Furthermore, amplification of PRNP may lead to overexpression of PrPC, favouring aggregation.
To assess whether mosaicism within PRNP contributes to the pathogenesis of sCJD, we sequence DNA in neurons and cerebrospinal fluid obtained from prion disease patients and non-diseased controls. We aim to look for mutant forms of human PRNP including known pathogenic mutations, copy-number variants and integrated reverse-transcribed splice variants, and to characterise transcriptomic alterations.

**Methods:**
We employ flow cytometry to sort NeuN+/- nuclei and analyse DNA content. Non-prion-seeding nucleic acids in a combined decontamination and purification step. Cell-free DNA is extracted from patient cerebrospinal fluid (CSF). Specificity of flow cytometry is evaluated using RT-qPCR of selected transcripts. PRNP is sequenced using 1. an Agilent SureSelect probe hybridisation panel (brain gDNA and cfDNA) and 2. targeted enrichment using CRISPR/Cas9 (gDNA). We employ ddPCR to search for evidence of PRNP copy number variation in gDNA. RNA sequencing is employed to profile the transcriptome of the sorted populations.

**Results:**
We have established a nuclear sorting and nucleic acid purification pipeline to specifically obtain gDNA and RNA from neuronal and non-neuronal nuclei in post-mortem brain samples. Non-prion-seeding nucleic acids can be obtained from nuclei, bulk brain and CSF, from which PRNP can be amplified using PCR.

**Conclusion:**
There are currently around 40 Mendelian PRNP mutations that are known to be associated with genetic prion disease. The presented methods will enable us to assess whether PRNP mosaicism exists in sporadic prion disease and whether known mutations, copy number variants, gene recombination or other somatic mutations are associated with the generation and propagation of prions. In addition, we anticipate that RNA sequencing will yield novel findings on transcriptomic alterations that occur in sporadic prion disease.

**38**

Y. Liu[1], A. Aguzzi[1]

**Protective role of NG2 glia in chronic neurodegeneration**

*Institute of Neuropathology, University of Zurich[1]*

**Introduction:**
Single cell sequencing and neuropathological examinations of human brain tissues and animal models have identified NG2 glia, also known as oligodendrocyte progenitor cells, as one of the major cell types reacting to brain damages in neurodegenerative diseases. However, the contribution of NG2 glia to neurodegeneration and progression of neurodegenerative diseases is still largely unclear. Here, we study the role of NG2 glia in chronic neurodegeneration induced by prion infections through manipulating their abundance in cultured brain slices and in adult mouse brain.

**Methods:**
For ex vivo experiments, NG2 glia were transiently or long-term depleted from prion-infected and control brain slices with a novel, platelet derived growth factor signaling inhibition based approach. For in vivo experiments, NG2 glia were transiently depleted from the brains of prion infected and control mice at different disease stages. Levels of neurodegeneration were examined by immunofluorescence and biochemical analyses.

**Results:**
Loss of NG2 glia enhanced prion-induced neurodegeneration both in cultured brain slices and in vivo. Development of prion disease in adult mice was accelerated when NG2 glia were transiently depleted at 12 weeks and 16 weeks, but not 20 weeks, after prion infection.

**Conclusion:**
NG2 glia are protective against chronic neurodegeneration and play a key role in the progression of prion disease.

**39**

D. Heinzer[1], M. Avar[1], D. Pease[1], B. Doğançay[1], J. Yin[1], A. Chincisan[1], E. Schaper[1], M. Emmenegger[1], S. Hornemann[1], A. Aguzzi[1]

**Whole genome RNAi screen identifies novel regulators of PrPC**

*Institute of Neuropathology, University Hospital Zurich, Schmelzbergstrasse 12, 8091 Zurich[1]*

**Introduction:**
Although the physiological role of the cellular prion protein ($PrP^C$) remains controversial, its involvement in prion diseases is indisputable. During the progression of prion diseases, $PrP^C$ serves as an essential substrate for its misfolded isoform $PrP^{Sc}$ to maintain propagation. Additionally, $PrP^C$ itself is shown to be indispensable in mediation of neurotoxic signaling. Therefore, reduction of $PrP^C$ alone can provide a viable therapeutic approach to combat prion diseases. Hence, uncovering regulators of $PrP^C$ could yield novel insights into the cellular machinery responsible for its expression and provide novel targets for further studies against these invariably fatal disorders.

**Methods:**
We established a cell-based high-throughput platform to determine $PrP^C$ levels after downregulation of each individual gene of the human genome. In a 384-well plate format, U-251 MG cells are treated with siRNAs, incubated for 72h and a FRET-based readout is be performed using two antibodies coupled to a FRET-pair and targeting different epitopes of $PrP^C$. This method represents a one-pot reaction with no further sample preparation or washing steps to detect genes, which upon downregulation, lead to enhanced or decreased $PrP^C$ expression. Candidates which significantly regulate expression levels were further challenged by means of a secondary screen to determine high-confidence hits.

**Results:**
In a primary screen using a set of three pooled siRNAs targeting the same transcript, we could identify 743 genes that efficiently regulate $PrP^C$ levels. An overall z'-factor of 0.55 over 166 plates demonstrated the robustness of the approach. The 743 genes from the primary screen were further challenged in a secondary screen with the individual siRNAs uncovering 54 high-confidence hits, which upon downregulation with at least 2 out of 3 distinct siRNAs regulated $PrP^C$ levels. Moreover, we could mechanistically validate PUM1, a RNA binding protein, to regulate $PrP^C$ expression via binding to the 3'UTR of the mRNA.

**Conclusion:**
The 54 hits will be further validated using orthogonal methods such as CRISPRi and the mechanistic of $PrP^C$ regulation will be investigated. Additionally, the hits working on protein level will be assessed in their capability to interfere with $PrP^{Sc}$ formation in a novel human cell model for prion propagation. Thereby, we aim to exploit these novel regulators of $PrP^C$ as possible targets for therapeutic intervention in prion disease.

**40**

M. Avar[1], D. Heinzer[1], D. Pease[1], J. Yin[1], A. Lakkaraju[1], B. Dogancay[1], A. Chincisan[1], E. Schaper[1], M. Emmenegger[1], S. Hornemann[1], A. Aguzzi[1]

**High-throughput whole genome RNAi screen identifying modulators of prion propagation**

*Institute of Neuropathology[1]*

**Introduction:**
Misfolding of the cellular prion protein ($PrP^C$) results in the well-characterized scrapie isoform ($PrP^{Sc}$) which is the underlying cause of prion diseases. However, many events that govern its uptake into the cell, its propagation remain wholly enigmatic. Additionally, whether mammalian cells have a machinery to process and potentially degrade $PrP^{Sc}$ is not understood. Through interrogation of the impact of downregulation of every gene in the mouse genome with an RNAi screen, we sought to identify genetic players in clearance of prions and modulators of $PrP^{Sc}$ formation. This may shed light on possible pathways that may offer opportunities in prevention or causal treatment of prion diseases.

**Methods:**
We first developed a novel readout for detection of $PrP^{Sc}$ and utilized it for performing a cell-based high throughput screen. In a 384-well plate format, chronically infected mouse hypothalamic neuronal cells, scGT1-7, were subjected to 17584 pooled sets, each consisting of three distinct siRNAs targeting the same gene, incubated for 72h and treated with phosphoinositide phospholipase C (PI-PLC) to remove surface $PrP^C$. Following treatment, a FRET based readout using two antibodies, targeting different epitopes of $PrP^C$ were used. Identified targets were then further validated using selective screenings for their specificity for different prion strains as well as their effect on $PrP^C$ levels.

**Results:**
In the initial screening round we could identified 2500 genes that had a mild to strong effect on $PrP^{Sc}$. An overall z'-factor of 0.65 over 136 plates demonstrated the robustness of the approach. We then sought to assess whether the effect was acting through modulating $PrP^C$ levels. In this counterscreen, we could identify 161 specific regulators of prions. In a next step, we sought to use a different method for prion detection, as well as a different prion strain. Majority of the hits showed an effect on prion levels.

**Conclusion:**
Using a high throughput cellular screen, 161 master regulating genes for prion propagation could be identified. Currently, we are focusing on 11 genes that showed the highest effect and validating them through a multi-leveled approach, taking advantage of CRISPRi/CRISPRa and CRISPRo. Additionally, the effect of modulating these genes will be assessed in a new human cell model that allows prion propagation.

**41**

F. Catto[2], D. Kirschenbaum[2], F. Voigt[1], E. Dadgar-Kiani[3], S. Cohen[4], M. Vendruscolo[4], K. Jenkins[4], J. Lee[3], A. Aguzzi[2]

**Therapeutic assessment and holistic visualization of Alzheimer's disease in the brain**

*Brain research Institute, University of Zürich, Zürich, Switzerland [1], Institute of Neuropathology, University Hospital Zürich, Zürich, Switzerland [2], Neurology and neurological sciences Bioengineering, Neurosurgery, and Electrical Engineering, Stanford University, Stanford, USA.[3], Wren Therapeutics, Cambridge, UK [4]*

**Introduction:**
Alzheimer's disease (AD) is the most common neurodegenerative disease leading to dementia, but clinical trials for disease-modifying treatments for this disorder have had so far a 100% rate of failure. The amyloid hypothesis has motivated the development of many therapeutic candidates targeting different steps in the metabolism of the amyloid-beta peptide (Aβ), including production of the native protein, proteolytic cleavage, and misfolding and aggregation, with most of these approaches aiming to achieve a global reduction in the concentration of Aβ aggregates or a corresponding delay in the overall Aβ aggregation rate. Experiments preceding clinical trials typically use mouse models which are genetically modified to harbor human Aβ. Therapeutic effects on Aβ plaque loads in pre-clinical mouse studies are typically assessed only in a limited area of the mouse brain, whereas large parts of this heterogeneous organ are ignored. This traditional approach results often in underpowered studies with significant possibilities for artifactual conclusions, in addition to a lack of insight into the regional variations across the brain of any purported therapeutic effect, which may be of fundamental relevance in predicting and rationalizing clinical outcomes. To overcome these challenges, we present here a complete microscopic visualization of the mouse brain under different therapeutic interventions against AD. In particular, we report preliminary whole-brain results from the study of a small molecule inhibitor of Aβ aggregation that has been selected to act specifically in suppressing the nucleation of new Aβ aggregates.

**Methods:**
We use the well-established APPPS1 mouse model, which recapitulates hallmarks of AD, including Aβ pathology, and makes it possible to monitor disease progression and the efficacy of AD therapeutics in reducing plaque pathology. We perform whole-brain clearing with CRYSTAL, we stain Aβ plaques with luminescent conjugated polythiophenes (LCPs) and we image and map whole-brain plaque loads at different time points upon various drug treatments. Additionally, we perform biochemical assays, and transcriptomic analyses to validate the findings.

**Results:**
Region variation in the reduction of plaque burden from an Aβ aggregation inhibitor: our preliminary results indicate that at appropriate doses the inhibitor can reduce the overall plaque density in the brain over varying treatment times. Importantly, the most significant reductions of plaque burden occur in specific brain regions, with similar distributions in the two hemispheres.

**Conclusion:**
The inhibitor shows distinct therapeutic propensities to different areas of the brain. This information is highly valuable in predicting the clinical impact of this small molecule both as a monotherapy and potentially in combination with other therapeutics whose mechanism of action results in complementary spatiotemporal profiles of aggregate reduction. Importantly, these results could not have been obtained without the use of the 3D histology method that we have developed of entire mouse brains. The results imply that traditional pre-clinical analyses may need to be revisited by the scientific community, not least given the extreme failure rate of AD clinical trials, often without clear rationales for the lack of therapeutic effects.

**42**

C. Fritz[2], K. Zimmermann[2], M. Weller[1], C. Boudesco[1], T. Zenz[1], M. Rechsteiner[2], E. Haralambieva[2], S. Balabanov[1], U. Wagner[2]

**A Custom NGS-based Panel for Genetic Diagnostics of Lymphoid and Myeloid Malignancies**

*University Hospital Zurich, Department of Hematology and Oncology, Zurich, Switzerland[1], University Hospital Zurich, Department of Pathology and Molecular Pathology, Zurich, Switzerland[2]*

**Introduction:**
Over 900,000 people worldwide are diagnosed with blood cancer every year (World Cancer Research Fund International). It can be detected with different molecular diagnostic techniques. Next-generation-sequencing is quickly emerging as an accepted method for routine genetic diagnostics due to its sensitivity and speed, also for blood cancers.

**Methods:**
We tested and validated a custom NGS panel covering oncogenic hotspots or all exons of 107 genes involved in myeloid and lymphoid malignancies. The panel is based on anchored multiplex PCR chemistry running on the Illumina NextSeq platform. Panel performance was assessed by sequencing 14 DNA samples from blood or bone marrow aspirate with 8 corresponding FFPE samples from patients with myeloid malignancies. These samples carry different pathogenic mutations previously found by Sanger sequencing or a different NGS panel. We also sequenced DNA from 13 Lymphoma cell lines (some fresh and some from paraffin cell blocks) with previously identified mutations and two well-characterized and commercially available control samples: the Acrometrix Oncology Hotspot Control (AOHC) and the Horizon Oncospan gDNA (HOG).

**Results:**
The analysis of the AOHC and HOG variants was carried out in triplicates. Comparing the detected with the expected variants resulted in very high recall values (>98%) and very good correlation of variant allele frequencies. For the myeloid part of our custom panel, we could show very good correspondence between the variants found in patient samples based on the new platform and the Illumina TruSight Myeloid Sequencing Panel and/or Sanger sequencing. Finally, in order to characterize the lymphoid specific genes in our new panel, we conducted variant calling for well-characterized lymphoma cell lines. Although we found considerable discrepancies at first between our results and the variants listed for these cell lines in the literature (COSMIC), we were able to rule out these discrepancies using Sanger sequencing with the exception of one mutation. The resulting recall value was > 95% for those samples, with sufficient DNA quality.

**Conclusion:**
We developed, validated and implemented a custom NGS-based strategy for lymphoid and myeloid cancer diagnostics that extended our previous workflows. The design allows the flexibility to report all genes in cases where all are needed or only a subset of genes for either myeloid or lymphoid samples.

**46**

L. Bankel[2], W. Rebekka[5], K. Dedes[1], D. Franzen[4], P. Bode[3], H. Moch[3], M. Manz[2], C. Britschgi[2], B. Snijder[5]

**Single-cell ex vivo drug response testing on fluid samples from patients with solid tumors**

*Department of Gynecology, University Hospital Zurich[1], Department of Medical Oncology and Haematology, University Hospital Zurich[2], Department of Pathology and Molecular Pathology, University Hospital Zurich[3], Department of Pulmonology, University Hospital Zurich[4], Institute of Molecular Systems Biology, ETH Zürich[5]*

**Introduction:**
In patients with metastatic malignancies there is a strong need for better predictive markers. Fluids containing tumor cells, such as pleural effusion, ascites or cerebrospinal fluid, are easily accessible and could potentially provide information on drug responses with a minimally invasive procedure.

**Methods:**
Here, we use image-based single-cell ex vivo drug response testing (pharmacoscopy) on fluid samples from patients with solid tumors to investigate drug response variability on an intra- and interpersonal level. Briefly, a mixed population of malignant and healthy cells are isolated from a fluid probe and incubated with a drug panel for 24 hours. Afterwards, cells are fixed and stained with fluorescent antibodies and imaged by automated confocal microscopy. A convolutional neural network (CNN) is then used to infer cell types directly from single-cell images based on both morphology and marker expression. This data is correlated with clinical data such as treatment response and survival.

**Results:**
As of today, a total of 42 probes from 29 patients were collected, covering different solid tumor (predominantly non-small cell lung cancer and ovarian cancer) and sample types. Of those, 28 biopsies (66%) had a sufficient viability and cancer cell content to be successfully processed and analyzed. Our CNN, which was trained on example images from all biopsies, accurately distinguished cancer cells from healthy immune cells. Furthermore, it was able to separate macrophages from other immune cells by morphology alone. Comparison of drug responses across the cohort revealed high correlation between the drug response profiles of biopsies taken from the same patients within a short period of time. Taken together, these results highlight the technical feasibility and robustness of pharmacoscopy on body fluids.
To assess the predictive power of treatment recommendations derived from pharmacoscopy in an observational clinical trial setting, ex-vivo drug responses will be mapped to clinical response data. Currently, this study is at an early stage and for the majority of patients, response data are not available, yet. However, we want to highlight one case of a patient with BRAF p.V600E mutated adenocarcinoma of the lung, which revealed promising results. Once the oncogenic driver mutation was detected during the routine diagnostic work-up, the patient was started on combined tyrosine kinase inhibition with dabrafenib (BRAF inhibitor) and trametinib (MEK inhibitor), according to current treatment guidelines. In parallel pharmacoscopy predicted an ex vivo response to dabrafenib. This eventually correlated well with the clinical course of the patient, who responded with a subtotal partial response on FDG-PET/CT scan.

**Conclusion:**
Pharmacoscopy with the help of a CNN seems to be a feasible diagnostic tool to guide treatment decisions in patients with metastatic solid tumors at an early stage of treatment. As a next step, integration of drug response and morphological profiles with molecular measurements such as transcriptomics or proteomics will provide further insights into the molecular mechanisms underlying drug response variability.

**47**

A. Magalhães[1], A. Chincisan[1], M. Emmenegger[1], S. Hornemann[1], A. Aguzzi[1]

**Large patient cohort reveals increased plasma autoantibodies against tau protein aggregation domain in specific diseases**

*University Hospital Zurich, Institute of Neuropathology, Zurich, Switzerland[1]*

**Introduction:**
In Alzheimer's disease (AD) patients, pathologically phosphorylated tau aggregates are a major component of neurofibrillary tangles and cerebrospinal fluid levels of phosphorylated and total tau are increased. Therefore, the tau protein is being explored as a candidate for immunotherapy for AD in mice models and in early clinical trials in humans. However, there is conflicting evidence regarding the levels of tau autoantibodies in the blood of healthy subjects and AD patients. To explore the potential value of tau antibodies as diagnostic biomarkers and therapeutics, we designed a high-throughput screen for naturally occurring tau aggregation domain (tauK18) IgG autoantibodies.

**Methods:**
We used an automated microELISA high-throughput platform to screen more than 24'000 residual plasma samples from patients of the Institute of Clinical Chemistry. Data from the screen were used to perform an epidemiological study of tau autoantibodies by correlating patient sample reactivity with clinical data. Anti-tau antibodies from reactive patients' samples were purified and used to evaluate the specificity of the antibodies for tauK18. Specifically, the reactivity of the antibodies were tested by antigen-competition ELISA and also compared to commercially available antibodies using Western Blot and immunofluorescence staining.

**Results:**
We found 2% (478 samples out of 24'000) of distinctly reactive patients (-logEC50 >= 2) for monomeric tauK18. This percentage is conspicuously higher than the general reactivity of about 0.05% for other targets used in the screen. The correlation between the patient reactivity and the clinical data showed that anti-tau antibody positive patients were on the average older than non-reactive patients. Reactive patients also had a statistically significant increased prevalence for the following diseases: iron-deficiency anemia, chronic kidney disease, cystitis, other specified bacterial infections and diseases of the urinary system. We also showed by competition ELISA that selected purified natural antibodies from positive samples could be successfully competed with soluble tauK18, indicating that the antibodies bind specifically to tauK18. In addition, antibodies recognized tauK18 when spiked into human plasma by Western blotting. Purified antibodies were also able to immunofluorescently stain SH-SY5Y_tau441 cells, overexpressing tau, but not SH-SY5Y wild-type cells.

**Conclusion:**
We show for the first time that, in a large-cohort of patients, plasma titers of autoantibodies against the aggregation domain of tau increase with age and also in several diseases including kidney and urinary system diseases and bacterial infections. We conclude that there is clinical significance of tau autoantibodies in elderly patients and patients with specific diseases. The validation assays showed that the anti-tauK18 antibodies purified from reactive patient plasma samples are specific and sensitive for the detection of tauK18.

**48**

L. Ebner[2], M. Samardzija[2], V. Todorova[2], D. Karademir[2], M. Thiersch[1], C. Grimm[2]

**Transcriptomic analysis of the mouse retina after acute and chronic hypoxia**

*Institute of Veterinary Physiology[1], Lab for Retinal Cell Biology[2]*

**Introduction:**
Age-dependent changes in the retina include the accumulation of lipofuscin in the retinal pigment epithelium (RPE) and the formation of drusen. This drusen formation, together with a thickening of the Bruch's membrane lead to reduced choroidal blood flow and extenuated vascular density potentially limiting oxygen supply to photoreceptors. Therefore, we and others suggest a strong correlation between reduced choroidal blood flow, creating chronic hypoxic conditions in the retina and the development and progression of age-related macular degeneration (AMD).

**Methods:**
To gain better insight into cellular response of the retina to hypoxic conditions and the differences between acute and chronic hypoxia we characterised four different hypoxic conditions, including acute and chronic as well as normobaric and hypobaric hypoxia. RNA-sequencing was performed on retina samples of all conditions and will enable us to deeply analyse hypoxic gene regulation and identify new or uncommon hypoxia-regulated genes. Additionally, we performed high-throughput single-cell analysis (Drop-Seq) on mouse retinas after acute normobaric hypoxia, which allows us to identify specific cell clusters and analyse transcriptomic differences on a single-cell level. Besides transcriptional analysis, immunohistochemical and morphological differences were evaluated, since especially cone and rod segment length might be influenced by chronic hypoxic conditions.

**Results:**
RNA-Sequencing data showed upregulation of hypoxia-associated genes in all hypoxia groups compared to normoxia controls. In comparison to the other conditions, the acute normobaric hypoxia showed the strongest responses to hypoxia. Immunohistochemical and ultra-thin section analysis showed reduced rod segment length in animals experiencing chronic normobaric hypoxia and acute hypobaric hypoxia, while cone photoreceptor segment length was significantly reduced in acute hypobaric hypoxic conditions compared to the controls.

**Conclusion:**
Together, RNA-Sequencing and Drop-Seq of different acute and chronic hypoxic retinas will provide us with a deeper understanding of hypoxic adaptation, stress reactions and metabolic shifts in the retina upon hypoxic exposure and might contribute to identify possible therapeutic targets.

**49**

S. Klinnert[2, 3], A. Trkola[3], H. Günthard[2, 3], A. Plückthun[1], K. Metzner[2, 3]

**CRISPR/Cas9 based adenovirus payloads that eliminate HIV-1 infected cells**

*Department of Biochemistry, University of Zürich, Zürich, Switzerland[1], Division of Infectious Diseases and Hospital Epidemiology, University Hospital Zurich, Zurich, Switzerland[2], Institute of Medical Virology, University of Zurich, Zurich, Switzerland[3]*

**Introduction:**
The HIV-1 latent reservoir remains the main barrier to achieving a cure. Despite the availability of highly effective antiretroviral drugs that suppress viral replication to undetectable levels, the pandemic is not contained yet due to varying accessibility of therapy, poor drug adherence and development of resistance. Hence, research on vaccine development and cure strategies is still needed. One promising cure strategy involves the use of the CRISPR/Cas9 system to introduce deleterious mutations in or even excise proviral DNA in HIV-1 infected cells.

**Methods:**
We tested seven gRNAs that target different HIV-1 genomic regions, i.e., LTR, gag and pol. We determine inhibition of HIV-1 replication by CRISPR/Cas9 and the different gRNAs individually and in combination in HEK293T cells. Co-transfection of these cells with the Cas9/gRNA plasmid and an HIV-1 expression plasmid, and subsequent measurement of the HIV-1 capsid protein p24 in cell supernatant by ELISA enabled determination of virus production and its inhibition. Moreover, by treating TZM-bl cells with the virus containing supernatant of the HEK293T cells, we were able to measure HIV-1 infectivity via a luciferase readout. To determine whether single- und dual-gRNA/Cas9 treated cells show InDels or deletions between the gRNA target sites, we amplified an amplicon that spans the target sites and sequenced it.

**Results:**
gRNAs LTR4, LTR5, TAR and p24 showed 92-99% viral inhibition, whereas gRNAs LTR3, Gag1 and IN1 showed no inhibition. Combination of effective with ineffective gRNAs revealed a minor decrease in HIV-1 inhibition except for gRNAs LTR4 and TAR, which showed robust inhibition, also when combined with ineffective gRNAs. InDel/Deletion analysis revealed that in the TAR+p24-gRNA treated cells the sequence between the two gRNA target sites was deleted and the single-gRNA treated cells showed InDels at the respective Cas9 cleavage site.

**Conclusion:**
Our results suggest that the selected TAR and p24 gRNA sites in the HIV-1 genome are promising targets to achieve viral suppression and potentially proviral inactivation.
Next, we want to test both gRNAs and the CRISPR/Cas9 system as payloads of adenoviruses that are specifically retargeted to CD4 expressing cells via CD4-specific DARPINs. Since CD4+ T-cells represent the major part of the HIV-1 latent reservoir, investigating this approach in primary HIV-1 latency models or latently HIV-1 infected patient derived cells might lead to the development of a curative gene therapy against HIV-1 infections.

**50**

K. Becker[1], K. Haldimann[1], S. Hobbie[1]

**Repurposing of apramycin as a parenteral therapeutic for the treatment of Gram-negative systemic infections in humans**

*University of Zurich[1]*

**Introduction:**
Aminoglycoside antibiotics such as gentamicin, tobramycin and amikacin constitute an important therapeutic component in the combination therapy of Gram-negative bacterial infections such as UTI, sepsis or pneumonia. However, antimicrobial resistance to aminoglycoside therapy is on the rise and has already reached concerning prevalence in some countries. Apramycin differs from all of the standard-of-care aminoglycosides in its chemical structure retaining antibacterial activity against almost all aminoglycoside resistance mechanisms of clinical relevance.

**Methods:**
Here we used standard methodology to study the preclinical profile of apramycin with regards to its therapeutic potential in Gram-negative systemic infections.

**Results:**
Apramycin demonstrated broad-spectrum activity against a genotypic and phenotypic variety of contemporary clinical isolates of particularly Enterobacteriales. Apramycin susceptibility was not compromised in clinical isolates resistant to gentamicin, tobramycin, amikacin, and plazomicin. For aminoglycoside susceptible isolates, the potency of apramycin with modal MICs between 2 and 8 mg/l depending on species was close to that of amikacin but lower than that of gentamicin or tobramycin with modal MICs between 0.5 and 2 mg/ml in broth microdilution assays. The safety profile of apramycin was favorable in comparison to other aminoglycosides and efficacy has been confirmed in in-vivo mouse infection models with diverse pathogens.

**Conclusion:**
The findings presented here provide profound proof of concept for the efficacy of apramycin in Gram-negative systemic infections and superior coverage. Combined with an intrinsically lower risk of adverse side effects, apramycin may provide for a comfortable therapeutic window in the treatment of UTI, sepsis and pneumonia, and be of particular high value to patients with critical bacterial infections that are resistant to gentamicin, tobramycin, amikacin, and plazomicin.

**51**

F. Meier-Abt[3, 4], W. Wolski[2], G. Tan[2], L. Gillet[3], S. Amon[3], A. Theocharides*[1, 4], R. Aebersold*[1, 3], M. Manz*[1, 4]

**Repression of CXCL4/PF4 and activation of NFκB signaling suggests promotion of stem cell hyperproliferation in polycythemia vera patients**

**These authors contributed equally to this work.[1], Functional Genomics Center Zurich[2], Institute of Molecular Systems Biology, ETHZ[3], University Hospital Zurich[4]*

**Introduction:**
Classic myeloproliferative neoplasms (MPNs) are characterized by activated JAK-STAT signaling. Thereby, the same underlying mutations are associated with different phenotypes. The phenotypic diversity associated with activation of JAK-STAT signaling in MPNs implies additional pathogenic mechanisms, which are poorly understood. This is especially true for the phenotype of polycythemia vera (PV) stem cells leading to trilineage hyperproliferation, as opposed to pathogenic megakaryocytes in other MPNs. PV stem cell functionality is determined to a large extent by protein expression. Until now, large scale unbiased studies of protein expression in hematopoietic stem cells isolated from PV patients were impossible due to requirements of cell numbers far beyond what can be obtained in a clinical setting.

**Methods:**
We first developed a new data-independent acquisition (DIA) mass spectrometry (MS) technology for rare human hematopoietic stem cells (*Amon S., Meier-Abt F. et al. MolCellProteomics 2019*). This technology was applied to FACS-isolated hematopoietic stem and progenitor cell (HSPC) subpopulations from 124 blood samples of 18 patients with chronic and progressed PV and 21 control subjects. RNAseq was performed for the same samples. Proteomics and transcriptomics results were analyzed bioinformatically, including gene set enrichment analyses for altered signaling pathways. Identified targets and markers were validated by FACS in 33 independent patient and control samples as well as by *in vitro* functional assays.

**Results:**
Comparing the proteomics analyses of different HSPC subpopulations isolated from PV patients and from controls identified specific signatures for PV stem and multipotent progenitor cells during chronic disease and during disease progression. Specifically, CXCL4/PF4 and CLU were significantly downregulated by 81% and 78%, respectively, whereas NFκB signaling was significantly upregulated 1.5-fold in stem and multipotent progenitor cells of PV patients. Upon progression to post-PV myelofibrosis (MF) and post-PV acute myeloid leukemia (AML), the markers LGALS9 and SOCS2 were seen to be significantly upregulated on the protein, and in case of SOCS2 also on the RNA level. Results were validated in separate patient and control samples, highlighting especially the potentially critical role of repressed CXCL4/PF4 in the hyperproliferative phenotype of PV stem and multipotent progenitor cells. *In vitro* functional assays demonstrating a causal relationship between downregulation of CXCL4/PF4 and PV stem cell hyperproliferation are ongoing.

**Conclusion:**
Unbiased broad spectrum proteomics and transcriptomics analyses in stem and multipotent progenitor cells of patients with PV, post-PV MF and post-PV AML identified repression of CXCL4/PF4 and CLU as well as activation of NFκB signaling as potentially critical factors for the hyperproliferative phenotype of this disease. In line with our findings, *CXCL4/PF4* knockout mice have been previously shown to exhibit increased numbers of hematopoietic stem cells and increased stem cell proliferation (*Bruns I. et al. Nat Med. 2014*). Also, CLU is known to suppress excessive NFκB activation, and loss of CLU expression can lead to tumor progression in cells that rely on NFκB signaling for proliferation (*Shannan B. et al. Cell Death and Differentiation 2006*). Our findings in stem and multipotent progenitor cells of PV patients broaden the understanding of the molecular pathophysiology underlying polycythemia vera and open the door for the development of new therapeutic agents. Furthermore, LGALS9 and SOCS2 were identified as markers for disease progression that could potentially serve as diagnostic tools for early detection of progressive disease.

**52**

E. Breuer[2], M. Schneider[2], J. Eden[3], B. Pache[4], T. Steffen[3], M. Hübner[4], R. Lilian[2], A. Gupta[2], V. Kepenekian[1], G. Passot[1], P. Gertsch[2], O. Glehen[1], K. Lehmann[2]

**Mutations of Ras/Raf-Proto-Oncogenes impair Survival after Cytoreductive Surgery & HIPEC: Tumor biology remains king**

*Department of Digestive Surgery & Surgical Oncology, Université Hospital Lyon[1], Department of Surgery & Transplantation, University Hospital of Zurich[2], Department of Surgery, Cantonal Hospital of St. Gallen[3], Department of Surgery, Lausanne University Hospital (CHUV)[4]*

**Introduction:**
Cytoreductive surgery and hyperthermic intraperitoneal chemotherapy (CRS/HIPEC) improve overall survival in selected patients with peritoneal metastasis (PM) from colorectal cancer. Disease recurrence is however frequent and can occur in the peritoneum or hematogenous (PUL, HEP). Currently, patterns of disease recurrence after CRS/HIPEC are unknown, and no data is available whether the localization of recurrent disease has an impact on patient survival.

**Methods:**
The present study is a multicentric retrospective cohort analysis from 4 tertiary center hospitals. Patients received standard perioperative chemotherapy. HIPEC was indicated after radical cytoreduction (CC-score 0, no visible tumor) and performed at 42°C for 90 minutes with mitomycin C/doxorubicin (≥15 mg/m$^2$) or 43°C for 30 minutes with oxaliplatin (300-400 mg/m$^2$). Follow-up included clinical exams, tumor markers and CT scans every six months. Statistical analyses were performed with IBM SPSS (version 22, Chicago, IL). Student's T-test and Mann-Whitney U-test were used for comparison of continuous and interval data, Pearson's Chi square test for categorical data. Kaplan-Meier tables, survival plots and Mantel-Cox Log Rank test were used to test for differences in CSS and DFS. Uni- and multivariate analysis of categorical data was performed by binary logistic regression, while survival data were analyzed by Cox regression. The study was approved by the responsible ethics committee in Zurich, Switzerland (Nr. 2017-01656).

**Results:**
A cohort of n=433 patients with colorectal PM between 2005 - 2017 from four European centers was analyzed after CRS/HIPEC with curative intent (CC-score 0). Median PCI was 6 (IQR 3-11) and 75% of patients had preoperative chemotherapy. Median overall and disease-free survival of the cohort was 46 months (CI 39.5-52.5) and 12 months (CI 11.0-13.0). After a median follow-up time of 22 months, disease recurrence was detected in n=304 (70.2%) of patients, presenting as solitary distant metastases in n=103 (38.0%), isolated locoregional disease in n=109 (40.2%) and mixed recurrence in n=59 (21.8%) patients. Recurrence involving the peritoneum was associated with a significantly worse outcome compared to patients with distant recurrence in liver or lung only (35 vs. 43 months, HR 1.50, p = 0.029). On multivariate regression analysis, PCI >7 (OR 2.44, p=0.028), positive nodal stage of the primary (OR 4.10, p=0.009) and *RAS* mutational status (OR 3.60, p=0.002) were identified as predictive factors for disease recurrence in the peritoneum.

**Conclusion:**
Disease recurrence in the peritoneum is associated with impaired outcomes. Together with the disease load (PCI), factors associated with tumor biology (nodal status, *RAS* mutational status) determine the localization of recurrent disease.

**53**

E. Cannizzaro[1], J. Lu[2], C. Boudesco[1], T. Zenz[1]

**Role of DDX3X in B cell lymphoma**

*Department of Experimental Haematology, University Hospital, Zürich, Switzerland[1], Genome Biology Unit, EMBL, Heidelberg, Germany[2]*

**Introduction:**
DDX3X is an RNA helicase belonging to the DEAD-box (DDX) RNA helicases family. DDX helicases unwind dsRNA molecules by using energy derived from ATP hydrolysis and so enabling essential processes such as splicing, export, and translation. Human DDX3 homologs are sex chromosome-linked genes. Whereas DDX3X is expressed in all tissues, DDX3Y is detected mainly in male tissues (i.e. testis and prostate). DDX3X gene is recurrently mutated in a number of lymphoma subtypes (22% NK/T-Cell Lymphoma; 3-10% CLL; 2% DLBCL) with Burkitt's Lymphoma (BL) being the tumour showing the highest incidence (20-40%). Mutations found in lymphoma patients mostly map to the catalytic site of the protein and affect residues engaged in the binding of ATP and RNA molecules. Moreover, 30% of these mutations are putative disrupting (frameshifts, splice site and stopgains) and predicted to affect the expression of the endogenous protein. These observations suggest a potential tumour suppressor role of DDX3X in these tumours. The pattern of DDX3X mutations in BL patients shows no co-occurrence with mutations in known driver genes as well as similar recurrence in the endemic and sporadic form of the disease (suggesting no exclusive association with EBV infection). We aim at identifying the role of DDX3X and the molecular mechanism through which mutations in this gene promote lymphoma.

**Methods:**
To investigate the effect of targeting DDX3X expression in BL cell lines we applied a CRISPR/Cas9 approach and compared our results with CRISPR/Cas9 screens data in the Depmap portal.
In order to derive functional hypothesis on the role of DDX3X in lymphoma we compared the gene expression profile of wt vs mutant DDX3X BL patients. We have produced a BL cell line model in which we will characterize the role of DDX3X and its mutations: we express wt and mutant DDX3X in male BL cell lines that lack expression of endogenous DDX3X protein due to disrupting mutations and concurrently deplete expression of the DDX3Y homolog. This model provides a tool to isolate DDX3X function, assess DDX3X-dependent gene expression and proteomic profiling of BL cells and explore protein interactions through a mass spectrometry approach.

**Results:**
We found that survival of BL cells is dependent on the expression of DDX3X, irrespective of the presence of missense mutations. Interestingly, targeting of the DDX3Y homolog was also lethal in male cell lines with disrupting mutations in DDX3X. Our results were consistent with CRISPR/Cas9 screens data that show dependency of most cancer cell lines on the expression of DDX3X, irrespective of the mutation state of the gene. By comparing gene expression profiles of wt vs mutant DDX3X BL patients, we found enrichment of inflammatory pathways driven by downregulated genes (such as TNFa signalling, interferon response and apoptotic signalling). These observations indicate DDX3X may regulate inflammatory response in these cells.

**Conclusion:**
We hypothesize that DDX3X may act as a tumour suppressor by mediating a pro-apoptotic inflammatory signaling. Interestingly, a function for DDX3X in inflammatory response has been previously reported: DDX3X was found to mediate TLR signalling cascade by interacting with different kinases (TBK1, IKBs) and facilitating NF-kB-dependent transcription. We will exploit our BL cell line model to test our hypothesis, uncover the pathways in which DDX3X is required and clarify the molecular mechanism through which its depletion/mutation benefits B cell lymphoma cells. Moreover, this tool will provide us with a way to interrogate DDX3X-dependent drug response in lymphoma cells.

**55**

D. Birrer[1], K. Horisberger[1], A. Rickenbacher[1], M. Turina[1]

**Kono-S anastomosis in Crohn's disease: Short-term results of a wide antimesenteric functional end-to-end anastomosis for ileocecal resection**

*Department of Surgery and Transplantation, University Hospital of Zurich, Switzerland[1]*

**Introduction:**
Crohn's disease (CD) is a chronic inflammatory disease that mostly affects the terminal ileum. The need for surgical intervention in Crohn's disease is caused in most cases by complications of the disease, intolerance of medical therapy or drug refractory courses [1, 2]. Medical therapy has profoundly improved the course of the disease and reduced the need for surgical interventions [3]; however, about 30% of patients still require surgery eventually.
In the further course of the disease, 30-50% of the patients develop a recurrence of the disease after ileocecal resection, and re-operation rates gradually increase over time [4, 5]. This leads to the question whether alterations in the surgical technique may make a difference and could be able to lower reoperation rates. One possible alteration is the radical resection of the mesentery of the affected segment as published in a retrospective cohort study by Coffey et al. [6], which is currently being challenged by a randomized controlled trial (NCT03769922). However, the most widely discussed topic in surgery for Crohn's disease in recent years is the technique of the anastomosis. The efficacy and safety of established types such as end-to-end, side-to-end and side-to-side has been shown; however, the comparison of stapled versus hand-sewn anastomosis referring to the need for re-surgery failed to show a superiority of one technique over the other [7, 8]. In 2003, Kono established a new technique in order to reduce the rate of anastomotic strictures by recurrent CD (Figure 1) [9]. In fact, first results showed an impressive low rate of recurrence requiring reoperation[10]. Up to date, there are few comparative cohort studies with side-to-end as well with end-to-end anastomoses [11, 12]. In both comparisons, Kono-S anastomosis led to fewer short-term complications as well as improved long-term results with respect to anastomotic patency.
We herewith present the first Swiss cohort of consecutive CD patients operated at a tertiary referral center for CD. The aim of our present study was reproduce earlier reports on the safety and efficacy of the Kono-S anastomosis with short-term morbidity and rates of anastomotic leakage being the primary study endpoints.

**Methods:**
This is a retrospective single-center cohort study of all consecutive patients with Crohn's Disease undergoing ileocecal resection; patients' characteristics as well as specific data for the surgical procedure and short-term outcome were evaluated.

**Results:**
30 patients were operated for Crohn's disease of the terminal ileum (n=24) or anastomotic recurrence (n=6). In 20 patients, the resection was performed laparoscopically. Postoperative complications with Clavien-Dindo Score ≥ IIIb were observed in three patients. One patient showed a hemorrhage and had to undergo surgical hemostasis. Two patients developed anastomotic leakage and had to undergo surgery; in both cases ileostomy were created after resection of the anastomosis. Median hospital stay was 9 days [IQR 7-12]. Follow-up is 7 months [median; IQR 3.5-10.8].

**Conclusion:**
First results show a favorable outcome that is comparable to other techniques. Longer operation times are observed but the few published data concerning long-term recurrence are promising. Kono-S anastomosis may evolve to become the preferred technique for ileocecal resection in affected patients.

**56**

D. Heuberger[1], D. Ardizzone[1], RA. Schüpbach[1]

**Co-factor-dependent activation of the platelet receptor protease-activated receptor 4**

*Institute of Intensive Care Medicine[1]*

**Introduction:**
Thrombin, the key clotting serine protease, acts on coagulation and inflammation via protease-activated receptors (PARs). PAR1 and PAR4 are major regulators of human platelet activation and of vascular barrier integrity. Thrombin directly binds PAR1 on the hirudin-like binding site and cleaves PAR1 efficiently at very low nanomolar concentrations while PAR4 lacks a thrombin-binding site and therefore, very high nanomolar concentrations of thrombin are needed to cleave PAR4. Thus, thrombin-activated PAR1 initiates platelet activation while the activation of PAR4 at high thrombin concentrations leads to sustained irreversible platelet activation. In contradiction to the well-known role of PAR4 on platelet activation, the role of thrombin-activated PAR4 on the vascular barrier and vascular inflammation remains unclear. We recently published that thrombomodulin, a co-factor expressed on endothelial cells as well as leukocytes, improves PAR2 activation by thrombin and leads in increased activation of inflammatory pathways. Co-factor-dependent PAR4 activation was not addressed so far. We hypothesize that thrombomodulin recruits thrombin to the cell surface resulting in more efficient cleavage and activation of membrane-bound PAR4 compared to soluble thrombin. Thus, PAR4 switches from a high-dose thrombin receptor to an additional low-dose thrombin receptor.

**Methods:**
To observe the cleavage and activation of PAR4 by various thrombin concentrations, pcDNA3.1 plasmids containing PAR4 tagged with an N-terminal alkaline phosphatase (AP) were transfected alone or together with a pcDNA3.1 thrombomodulin plasmid in HEK 293T cells. The cleavage of the AP-PAR4 construct was detected by an established alkaline phosphatase assay (SEAP) measuring activity of the cell bound and the released AP. To map the cleavage site of thrombomodulin-bound thrombin on PAR4, all predicted thrombin cleavage sites on the N-terminus of PAR4 were mutated to an uncleavable alanine by site-directed mutagenesis.

**Results:**
AP-PAR4 wild type or mutant constructs were overexpressed alone or together with the thrombomodulin and the cleavage efficiency of various thrombin concentrations was measured. We found that in absence of thrombomodulin PAR4 was cleaved only at high thrombin concentrations of 30 nM while in presence of thrombomodulin the cleavage was significant with low thrombin concentrations at 1 nM.

**Conclusion:**
For the first time, we showed that low concentrations of thrombomodulin-bound thrombin efficiently cleaved PAR4. Whether the enhanced efficiency of PAR4 cleavage by thrombin in presence of thrombomodulin results in increased PAR4 activation will be studied by an in vitro NF-kB luciferase reporter system. The clinical relevance of the PAR4 activation by low concentrations of thrombomodulin-bound thrombin will be tested on the vascular barrier integrity as well as platelet activation.

**57**

L. Roth[2], L. Russo[2], C. Pauli[1], E. Breuer[2], R. Graf[2], P. Clavien[2], A. Gupta[2], K. Lehmann[2]

**The impact of hyperthermic intraperitoneal chemotherapy (HIPEC) on the anticancer immune response**

*Department of Pathology, University Hospital Zurich[1], Department of Surgery and Transplantation, University Hospital Zurich[2]*

**Introduction:**
The combination of cytoreductive surgery (CRS) and hyperthermic intraperitoneal chemotherapy (HIPEC) has improved survival of selected patients with peritoneal metastasis from colorectal cancer. Nevertheless, peritoneal recurrence, presumably due to remnant cancer cells, is common and requires further optimization of this locoregional treatment. Therefore, it is important to understand mechanisms operating behind HIPEC. We hypothesize that the combination of chemotherapy and hyperthermia might not only be cytotoxic, but may also induce strong immunogenic changes on the tumor and its microenvironment. We therefore assessed effects of Mitomycin C/Doxorubicin (M/D) and Oxaliplatin (Oxa), widely used in clinical settings, on the immunogenicity of colorectal cancer cell-lines and patient derived organoids.

**Methods:**
Colorectal cancer cell-lines and organoids derived from two patients with colorectal cancer were treated with M/D or Oxa for 30 minutes with and without hyperthermia ($43^0$C). MHC-I expression on cancer cells was analyzed 48 h after treatment using FACS and cancer testis antigen (CTA) expression 72 hours after treatment, using qPCR and western blot. To assess Mo-DC maturation, we set up a co-culture between differentially treated colorectal cancer cells and Mo-DC`s from a healthy human donor. We analyzed surface markers such as HLA-DR and CD 83 to assess Mo-DC maturation using FACS. Further, Mo-DC`s that were pre-incubated with treated and untreated colorectal cancer cells were added to purified CD8+ T-cells to measure their activation via intracellular IFN-y staining. To examine antigen specificity mediated by the HIPEC treatment, murine colorectal cancer cells with ovalbumin (MC-38-Ova) expression were differentially treated and co-cultured with splenocytes from OT-I mice. Activated specific CD 8+ T-cells were measured using FACS by intracellular IFN-y staining.

**Results:**
HIPEC treatment induced the expression of MHC-I molecules and two CTAs, Cyclin A1 and SSX-4. Compared to controls (no drug, $37^0$C), M/D at hyperthermic conditions increased Cyclin A1 by 53 folds and SSX-4 by 30 folds in a dose-dependent manner, similar to Oxa treated tumor cells. This finding could be confirmed with HIPEC treated organoids. On protein level, Cyclin A1 was highly increased compared to control treatment ($p=0.004$). On Mo-DC`s, after co-culturing with HIPEC treated colorectal cancer cells, we noticed a significant expression of CD83 and HLA-DR, both DC maturation markers. Furthermore, Mo-DCs after activation by co-culture with HIPEC-treated cancer cells, were able to prime CD 8+ T-cells, leading to enhanced IFN-y production by CD8+ T cells. These results could be confirmed with the specific murine model, where HIPEC treatment lead to 8.54% activated Ova specific T-cells compared to 4.37% without treatment.

**Conclusion:**
HIPEC treatment induces immunogenic changes in colorectal cancer cells and organoids via upregulation of MHC-I molecules and CTAs. Furthermore, HIPEC treatment induces antigen-specific immune responses. These novel insights may explain observed long-term effects in selected patients, and represent a novel aspect of HIPEC, beyond cytotoxicity allowing fine tuning of this treatment approach.

**58**

K. Slankamenac[2], D. Müller[1], A. Herzog[2], H. Kupferschmidt[3], A. von Eckardstein[1], D. Keller[2]

**Spectrum of acute drug toxicity during the most popular house and techno party in the world**

*Institut für Klinische Chemie, Universitätsspital Zürich[1], Institut für Notfallmedizin, Universitätsspital Zürich[2], Tox Info Suisse, Universität Zürich[3]*

**Introduction:**
Since 1991, the Street Parade, world's most popular house and techno parade in Zurich, is still a mecca for ravers. One Saturday in every August, about one million visitors celebrate this initially peaceful event which stands for love, freedom and tolerance.
However, extensive drug abuse has also been commonly seen. The prevalence of acute drug toxicity (ADT) due to novel psychoactive substances (NPS) during the Street Parade is unknown. Therefore, the aim was to investigate the drug spectrum of acute intoxicated patients from the Street Parade presenting in the Emergency Department (ED).

**Methods:**
We investigated consecutively urine samples of acute intoxicated patients who participated at the Street Parade and presented in a Swiss tertiary care ED in 2017 and 2018. The endpoints were the analysis of the drug spectrum and assessment of the prevalence of ADT by NPS.
Samples were analyzed by a screening method using liquid chromatography coupled to high-resolution mass spectrometry. Substances were identified by their theoretical exact mass and by comparing acquired tandem mass spectrometry (MS/MS) to library spectra.

**Results:**
In total, we analyzed 47 urine samples. Ten patients presented with symptoms of ADT but only a wide spectrum of different medications was detected. In 20 patients (42.5%), alcohol without any other drug was identified. Finally, 17 intoxicated patients (36.2%) consumed drugs plus alcohol. The three leading drugs were cocaine (21.3%), 3,4-methylenedioxymethamphetamine (MDMA) (19.1%) and tetrahydrocannabinol (THC) (17.0%) followed by methamphetamine (8.5%), methylphenidate (6.4%) and 2.1% for each lysergic acid diethylamide and amphetamine. Furthermore, one patient (2.1%) showed an abuse of NPS (methylon) in combination with alcohol, cocaine and MDMA.
An overdose of methamphetamine occurred in five patients in 2018 whereas no overdose of methamphetamine was detected in 2017.

**Conclusion:**
Cocaine, MDMA and THC in combination with alcohol are the most prevalent drugs in Street Parade patients whereas NPS are still rare. Methamphetamine intoxications seem to increase. Thus, future preventive strategies need to sensitize the rave scene about the drug spectrum and possible health consequences.

**59**

A. Bentrup[2], M. Müller[1], A. Lakkaraju[2], E. Lemes[2], L. Pelkmans[1], A. Aguzzi[2]

**Mechanisms Leading to Cytoplasmic Vacuolation in Mammalian Cells**

*Institute of Molecular Life Sciences, University of Zürich, Zürich, Switzerland[1], Institute of Neuropathology, University Hospital Zürich, Zürich, Switzerland[2]*

**Introduction:**
Endosomal-lysosomal processes are essential to maintain cellular homeostasis. To ensure smooth functioning of these cellular pathways, many proteins and lipids need to be in orchestra. Several sequential regulatory events coordinate the maturation of endosomes to lysosomes and interruptions in these processes have been associated with enlarged cellular compartments termed vacuoles. Vacuoles of different sizes and shapes have been observed in response to pathogen infections, storage diseases and in several protein misfolding disorders. Besides causing the characteristic spongiform changes that can be found in prion disease, cytoplasmic vacuolation was also observed in some familial forms of Alzheimer's disease, amyotrophic lateral sclerosis and Charcot-Marie Tooth disease.

**Methods:**
To investigate this phenotype, involved pathways and their role in neurodegenerative diseases, we have performed an unbiased genome-wide RNAi high-content screen using an arrayed siRNA library. The cells were fixed and stained using Alexa flour-coupled succinimidylester before imaging on an InCell Analyzer microscope. The pixel classifier Ilastik was trained on example images for a later segmentation of vacuoles. The final image analysis to quantify and characterize cytosolic vacuoles, will be done using pipelines programmed with Python and R. Genes that are found to induce vacuolation upon knock down, will be validated in a secondary RNAi screen and subsequently with the CRISPR technology. Selected pathways and genes will then be further investigated in vitro and in vivo. The exact origins and consequences of vacuoles will be analysed by iterative indirect immunofluorescence imaging (4i) and fluorescence-tagged viruses in vitro before creating mouse models for the genes of interest.

**Results:**
Conditions have been optimized for the reverse transfection of HeLa cells with siRNA in 384 well plates and subsequent staining and imaging. By visual inspection of the obtained images, we could confirm that the knock down of proteins involved in the maturation of endosomes like rab5a, rab7a, PIKfyve or fig4 do cause the vacuolation of cells. However, we have also found genes that have not been associated to these processes yet to cause vacuolation if knocked down. In the manual evaluation of one test plate, around 10% of the knocked down genes induced a mild or pronounced vacuolation phenotype. The random forest algorithm trained in Ilastik has produced probability maps for the localization of vacuoles. Further processing of these maps and the original microscopy images in Tissue Maps allowed the automated detection of vacuoles. For the secondary screen, the neuronal cell line SK-N-SH was selected due to the flat morphology and successful induction of vacuoles by PIKfyve knock down.

**Conclusion:**
The screen setting is suitable to identify genes that cause the vacuolation of cells upon RNA-mediated knock-down. The primary screen has been performed successfully, while the analysis and validation of the dataset is ongoing. The next step is to perform a smaller secondary screen on the subset of genes that scored high in the primary screen. After validation, follow-up experiments aim to link these findings to clinically relevant diseases to advance the understanding of mechanisms central to neurodegeneration.

**60**

A. Hülsmeier[1], T. Hornemann[1]

**Association between lipid droplets and 1-deoxy-sphinglipid formation**

*Institute of Clinical Chemistry, University of Zurich, Switzerland[1]*

**Introduction:**
Non-alcoholic fatty liver disease (NAFLD) is the most frequent cause of chronic liver disease worldwide. NAFLD is associated with various complications, such as chronic kidney disease, cardio-vascular as well as heart diseases and type 2 diabetes (T2DM). NAFLD comprises a spectrum of liver pathologies including steatosis, steatohepatitis and liver fibrosis, which can finally progress into terminal hepatocellular carcinoma. Liver steatosis is characterized by the intracellular accumulation of lipid droplets in hepatocytes - often as a result of excessive lipid supply. This lipid accumulation is associated with increased levels in plasma 1-deoxy-sphingolipids (1-deoxySL) – a cytotoxic class of sphingolipids that contribute to beta cell failure and insulin resistance in T2DM. The reason why 1-deoxySL are elevated in steatosis is not clear, and might be related to either an increased formation or a reduced catabolism of these lipids.

**Methods:**
Fluorescence microscopy, long-chain base analyses and lipidomic profiling, using liquid chromatography coupled tandem mass spectrometry.

**Results:**
To investigate the molecular connections underlying lipid droplet formation and sphingolipid metabolism in more detail, we established a Huh7 hepatocyte based steatosis model. Supplementing Huh7 cells with free fatty acids such as palmitate or oleate, resulted in a robust induction of lipid droplets and increased 1-deoxy-sphingolipid levels similar to the clinical situation.

**Conclusion:**
Using this model, we will investigate the metabolic interplay between lipid droplet formation and 1-deoxySL metabolism in more detail.

**61**

L. Liberale[2], A. Akhmedov[2], N. Vlachogiannis[1], N. Bonetti[2], V. Nageswaran[3], M. Miranda[2], F. Montecucco[4], J. Beer[2], T. Lüscher[2], K. Stamatelopoulos[1], K. Stellos[1], G. Camici[2]

**Sirtuin 5 promotes arterial thrombosis through endothelial plasminogen activator inhibitor-1**

*Cardiovascular Disease Prevention Hub, Faculty of Medical Sciences, Newcastle University, Newcastle upon Tyne, UK;[1], Center for Molecular Cardiology, University of Zurich, Wagistrasse 12, 8952 Schlieren, Switzerland[2], Department of Cardiology, Charité-Universitätsmedizin Berlin, Campus Benjamin Franklin, Hindenburgdamm 30, 12203, Berlin, Germany;[3], IRCCS Ospedale Policlinico San Martino Genoa – Italian Cardiovascular Network, L.go R. Benzi 10, 16132 Genoa, Italy;[4]*

**Introduction:**
Arterial thrombosis as a result of plaque rupture or erosion is a key event in myocardial infarction and ischemic stroke. Sirtuin 5 (SIRT5) is a NAD+-dependent protein deacetylase, desuccinylase and demalonylase belonging to the sirtuin superfamily. Beside lifespan regulation, aging and longevity genes also modulate age-dependent cardiovascular diseases. As such, SIRT5 has been implicated in acute ischemic stroke and cardiac hypertrophy. To date, the role of SIRT5 as a putative mediator of arterial thrombosis has not been investigated.

**Methods:**
*Sirt5* transgenic (*Sirt5*$^{Tg/0}$) as well as *Sirt5* knock-out (*Sirt5*$^{-/-}$) mice underwent photochemically-induced carotid endothelial injury to trigger arterial thrombosis. Primary human aortic endothelial cells (HAECs) treated with SIRT5 silencing RNA (si-SIRT5) as well as peripheral blood mononuclear cells (PBMCs) from acute coronary syndrome (ACS) patients and non-ACS controls (total n=171) were employed to translate our experimental findings to humans.

**Results:**
Compared to WT controls, *Sirt5*$^{Tg/0}$ mice displayed accelerated arterial thrombus formation following endothelial-specific damage. Conversely, in *Sirt5*$^{-/-}$ mice thrombus formation was blunted. Platelet count, volume and function were unaltered, as assessed by ex vivo collagen-induced aggregometry. Furthermore, activation of the coagulation cascade as assessed by vascular tissue factor (TF) activity, plasma TF concentration or vascular and plasma expression of its inhibitor TF pathway inhibitor (TFPI) was unaltered. More frequent thrombus embolization episodes and increased circulating D-dimer levels suggested increased activation of the fibrinolytic system in *Sirt5*$^{-/-}$ mice. In line with this, *Sirt5*$^{-/-}$ mice also showed reduced plasma and vascular expression of the fibrinolysis inhibitor plasminogen activator inhibitor (PAI)-1. In HAECs, SIRT5-silencing inhibited PAI-1 gene and protein expression in response to TNF-α. This effect was mediated by increased AMPK activation and reduced phosphorylation of the MAP kinase ERK 1/2, but not JNK and p38 as shown both in vivo and in vitro. Lastly, PAI-1 was associated with SIRT5 gene expression and both genes were found to be increased in ACS patients compared to non-ACS controls after adjustment for age, sex, smoking, diabetes mellitus, arterial hypertension and hyperlipidemia.

**Conclusion:**
SIRT5 promotes arterial thrombosis by modulating fibrinolysis through endothelial PAI-1 expression. Hence, SIRT5 inhibition may be an interesting therapeutic target in the context of atherothrombotic events.

**62**

M. Benker[1], S. Obahor[1], R. Werner[1], C. Caviezel[1], S. Hillinger[1], D. Schneiter[1], I. Opitz[1], I. Inci[1]

**Impact of preoperative comorbidities on postoperative complication rate and outcome in surgically resected NSCLC patients**

*Department of Thoracic Surgery, University Hospital Zurich[1]*

**Introduction:**
Patient selection for surgical resection is important for improved outcomes in NSCLC. Due to the steady increase of older patients referred to surgery, the question of comorbidities became more pressing in recent years. This study aimed to analyse whether preoperative comorbidities had an impact on postoperative complications or survival after anatomical lung resection for NSCLC.

**Methods:**
In a retrospective analysis of 1225 patients who underwent anatomical lung resection for NSCLC between 2000 and 2015, preoperative comorbidities, such as pulmonary, cardiovascular, abdominal, renal and endocrine, were identified. Their effect as well as the influence of patient characteristics on postoperative complications and survival was analysed. The primary outcome was the postoperative complication rate and overall survival.

**Results:**
78.9% of patients showed preoperative comorbidities while 38.6% suffered at least one complication. Hypertension was the most prevalent comorbidity (34.1%, n=416) followed by COPD (26.4%, n=322), other malignancies (19%, n=232) and coronary artery disease (12.7%, n=155). Pulmonary complications were most common (26.4%, n=322) followed by cardiac (14.8%, n=181) and gastrointestinal (3%, n=36). While certain patient characteristics, i.e., increasing age, low BMI, and low FEV1, affected the overall complication rate ($p<0.001$, $p=0.008$, $p=0.008$, respectively) and survival ($p<0.001$ each), the impact of comorbidities varied. Hypertension (OR=1.492, $p=0.031$) and coronary artery disease (OR=1.523, $p=0.096$) lead to cardiac complications significantly more frequently. History of myocardial infarction was a protective prognostic factor (OR=0.283, $p=0.052$). COPD didn't influence the occurrence of pulmonary complications ($p=0.525$). However, history of heavy smoking (OR=1.008, $p=0.003$), low BMI (OR=0.932, $p<0.001$) and low FEV1 (OR=0.993, $p=0.065$) did.

**Conclusion:**
Various preoperative comorbidities didn't seem to affect the overall frequency of postoperative complications (Figure 1) and long-term survival in patients who underwent NSCLC surgery. While hypertension and coronary artery disease lead to increased cardiac complications, history of myocardial infarction was protective, possibly due to rigorous preoperative cardiac assessment.

**63**

E. Boran[1], T. Fedele[2], P. Hilfiker[3], L. Stieglitz[1], T. Grunwald[3], J. Sarnthein[1], P. Klaver[4]

**Neuronal firing in the medial temporal lobe reflects human working memory workload and capacity**

*Klinik für Neurochirurgie, UniversitätsSpital und Universität Zürich[1], National Research University Higher School of Economics, Moscow, Russian Federation[2], Schweizerisches Epilepsie-Zentrum, Zurich[3], University of Applied Sciences in Special Needs Education, Zurich[4]*

**Introduction:**
The involvement of the medial temporal lobe (MTL) in working memory (WM) is controversially discussed in neuroimaging, electrophysiology, neurodevelopmental and lesion studies. Critically, it is unclear if the MTL supports working memory to increase capacity.

**Methods:**
We tested visual working memory using a change detection task. The stimulus was an array of colored squares. The array size for a specific trial determined the workload (low workload: 1, 2, high workload: 4 or 6). The encoding period was temporally separated from the maintenance period. Our subjects were patients with epilepsy undergoing presurgical monitoring with implanted electrodes (13 subjects tested in 16 sessions, age 19-59 years, 8 male). We grouped subjects on memory capacity (low vs. high). We recorded single neuron firing in the MTL within and outside the seizure onset zone.

**Results:**
A subset of MTL neurons exhibited persistent firing during maintenance, at a higher rate than during fixation. We classified those as maintenance neurons. Entorhinal cortex had the highest percentage of maintenance neurons (10% of all neurons, permutation test against scrambled data, $P = 0.002$). Some of these neurons were in regions within the seizure onset zone and were subsequently resected. We used a neural decoder to predict workload on a trial-by-trial basis. Neural firing in the entorhinal cortex predicted workload with the highest accuracy for subjects with low memory capacity (73% accuracy, permutation test against scrambled data, $P = 0.005$). Neural trajectories in the component space distinguished set size early in trials.

**Conclusion:**
We showed that persistent neural firing reflects visual WM maintenance. Entorhinal cortex may relate to processing overload in working memory for subjects with low memory capacity. The resection area contained neurons that actively participated in cognitive processing.

**64**

S. Valizadeh[1, 3, 5], M. Cheetham[1, 5], L. Jancke[2, 3, 5], E. Battegay[1, 5], R. Renzel[4], E. Efthymiou[4], L. Imbach[4]

**Automated decision support for EEG-based classification of epilpesy after first unprovoked seizure. A new approach using neuronal indices of dynamic effective connectivity**

*Department of Internal Medicine, University Hospital Zurich, Zurich, Switzerland[1], Department of Special Education, King Abdulaziz University, Jeddah 21589, Saudi Arabia.[2], Division Neuropsychology, Institute of Psychology, University of Zurich, Switzerland[3], Division of Epileptology, Department of Neurology, Clinical Neuroscience Center, University Hospital Zurich, University of Zurich, Zurich, Switzerland[4], University Research Priority Program (URPP) "Dynamic of Healthy Aging", University of Zurich, Switzerland[5]*

**Introduction:**
Background: The initial 20-minute standard EEG after first ever unprovoked epileptic seizure has a poor diagnostic yield. The accurate diagnosis of epilepsy is time-consuming, often requiring repetitive standard EEGs or long-term EEG. A reliable and higher yielding screening method for automated epilepsy classification is needed.
Objective: We tested whether recently developed neural biomarkers based on the temporal dynamics of effective connectivity improve the diagnostic yield of initial EEG.

**Methods:**
We extracted Granger causality (GC)-based indices of effective connectivity from the interictal resting-state EEG data of N=67 adult patients (acquired after first unprovoked epileptic seizure and without interictal epileptiform discharges), used a feature selection method to identify sets of features that distinguish well between epilepsy and nonepilepsy, and tested a range of machine learning (ML) classifiers for optimal epileptic vs. nonepileptic discrimination. We used accuracy, sensitivity and specificity as evaluation criteria of ML-based classification performance compared with final epilepsy diagnosis.

**Results:**
Automated ML-based classification achieved 84% specificity, 42% sensitivity and 73% accuracy. Given the high specificity of the ML classifier, a negative result indicates that the first seizure is less likely to be an initial manifestation of epilepsy. The sensitivity was considerably better than that of early standard EEG alone, and the overall accuracy was superior to the diagnostic yield of the first and second long-term EEGs.

**Conclusion:**
While appropriate cut-off levels need to be determined, the high specificity of this automated method enhances assessment at first standard EEG of whether the first seizure amounts to an initial manifestation of epilepsy. The reported sensitivity could contribute to early risk assessment by helping the clinician to evaluate whether to lower the threshold for commencing AED treatment.

**65**

P. Nocchi[1], D. Canepa[1], S. Märsmann[1], B. Eggerschwiler[1], Y. Neldner[1], HC. Pape[1], P. Cinelli[1], E. Casanova[1]

**Dissecting the role of the ectonucleotidases CD39 and CD73 in fate decision of human adipose-derived stem cells**

*University Hospital Zurich[1]*

**Introduction:**
Mesenchymal stem cells (MSCs) are somatic multipotent stem cells, which possess self-renewal ability, multilineage differentiation potential, and immunomodulatory response. They play an important role in maintaining tissue homeostasis. Particularly, human fat tissue is a good source of multilineage adipose-derived stem cells (ASCs), which can be differentiated into osteoblasts. MSCs/ASCs exist as a heterogeneous mix of progenitors and lineage committed cells with differential potential and regenerative properties. Thus, despite their interesting therapeutical use, the real identity of ASCs is still largely unknown. By using the novel technology of mass cytometry (CyTOF) we were able to isolate a subpopulation of ASCs possessing enhanced bone differentiation ability. Analysis of 30 ASC lines confirmed that lines more prone to osteogenic differentiation exhibit high expression of ALP and low expression of CD73, whereas donors with less osteogenic differentiation ability express high levels of CD73 and no ALP. Two ectonucleotidases CD39 (ectonucleoside triphosphate phosphohydrolase) and CD73 (ecto-5'-nucleotidase) convert ATP into adenosine. Adenosine mediate then their physiologic actions via interactions with the purinergic P1 receptors: A1, A2A, A2B, A3. In this study, we investigated in six human ASC lines, with divergent osteogenic differentiation potential, the role of CD73 and CD39. By employing specific ectonucleotidase inhibitors or agonists, we could modulate the activity of these enzymes and investigate their role during osteogenesis.

**Methods:**
Expression levels CD39, CD73, and all P1 receptors were measured by qRT-PCR in three "good" and three "bad" osteogenic differentiating lines, in their undifferentiated state and during 21 days of osteogenic differentiation. Next, activity was measured and cells were stimulated with ATP (CD39) or AMP (CD73) and phosphate production was quantified with Malachite Green Phosphate Assay. Thereafter, cells were treated with several ectonucleotidase inhibitors (APCP, POM1) or agonists (ATP, AMP, NECA) in combination or alone during osteogenic differentiation and differentiation was quantified by qRT-PCR or Alizarin Red staining.

**Results:**
CD73 expression analysis during osteogenic differentiation revealed diminished expression in the "good" lines and constant expression in the "bad" lines. However, CD73 activity strongly diminished in the first 4 days of differentiation in the "good" lines whereas increased in the "bad" lines. Importantly, APCP-mediated CD73 inhibition converted "bad" osteogenic differentiating lines into "good" differentiating lines. On the other side, CD73 inhibition plus addition of NECA (adenosine agonist) reverted this effect.

**Conclusion:**
In the past years, there has been increasing appreciation of purinergic regulation of bone metabolism, but often the available studies reported contrasting results and are mainly performed in rodents and not human cells. There is therefore the need to fully elucidate the role of nucleotides and the involved enzymes in bone metabolism. In our study, we identified CD73 as a negative regulator of osteogenic differentiation of human ASCs. The availability of chemical compounds able to fine tuning the activity of purinergic receptors, as well as of other involved factors, renders the investigation of these signaling pathways very intriguing not only for dissecting the physiological mechanisms involved in bone formation and regeneration but also for a putative future clinical use.

**66**

Y. Puspitasari[1], C. Diaz-Canestro[1, 6], I. Sudano[2], A. Flammer[2], N. Bonetti[1], P. Wuest[1], L. Liberale[1, 4], S. Constantino[1], F. Paneni[1, 2], J. Beer[1, 3], F. Ruschitzka[2], M. Hermann[2], T. Luscher[1, 7], G. Camici[1, 2, 5]

**The Role of Matrix Metalloproteinase-2 on Age-dependent Arterial Stiffness**

*Center for Molecular Cardiology, University of Zurich, Schlieren, Switzerland[1], Department of Cardiology, University Heart Center, University Hospital Zurich, Zurich, Switzerland[2], Department of Internal Medicine, Cantonal Hospital Baden, Baden, Switzerland[3], Department of Internal Medicine, University of Genoa, Genoa, Italy[4], Department of Research and Education, University Hospital Zurich, Zurich, Switzerland[5], Faculty of Kinesiology, Libin Cardiovascular Institute of Alberta, University of Calgary, Calgary, AB, Canada[6], Royal Brompton & Harefield Hospitals, Imperial College, London, UK[7]*

**Introduction:**
Arterial stiffness is a well-characterized sign of vascular aging that precedes and strongly predicts the development of several cardiovascular diseases (CVD) including hypertension, stroke and heart failure. The age-dependent stiffening of large elastic arteries is primarily attributed to the loss of interlaminar elastic fibers and the increase of collagen fibers, which are regulated by matrix metalloproteases (MMPs), including MMP-2. Previous studies have described a strong correlation between MMP-2 levels and arterial stiffness. However, the causative link between age-dependent arterial stiffness and MMP-2 remains unclear. Hence, this study aimed to prospectively investigate the effect of MMP-2 gene silencing on the development of age-dependent carotid stiffness in WT mice.

**Methods:**
Pulse Wave Velocity (PWV), as the gold standard technique to assess arterial stiffness, was assessed in the right common carotid artery (RCCA) of C57BL/6 wild type (WT) mice of various ages ranging between 3 and 25 months. Plasma and vascular levels of MMP-2 on RCCA were also measured and correlate with PWV. Moreover, aged WT male mice (18-21-month-old) were treated for 4 weeks with either MMP-2 siRNA or Scr siRNA via tail vein injection every 4 days and PWV was assessed at baseline, 2 and 4 weeks.

**Results:**
Our in vivo longitudinal study demonstrates an age-dependent increase in carotid PWV. The levels of vascular and circulating MMP-2 were also found increase with age. MMP-2 knockdown by siRNA reduced vascular MMP-2 level which in turn attenuated age-dependent carotid stiffening. In addition, siMMP-2 treated mice showed an increased elastin to collagen ratio. Furthermore, enhanced phosphorylation of the activatory eNOS Ser1177 was also observed in siMMP-2 group without affecting level of total eNOS and Akt phosphorylation. Interestingly, co-immunoprecipitation experiments demonstrated that MMP-2 directly interacts with eNOS and this interaction is augmented with age.

**Conclusion:**
Silencing of MMP-2 attenuates age-dependent carotid stiffness by affecting elastin to collagen ratio and interfering with eNOS activation. Thus, MMP-2 may mediate ECM remodeling and endothelial-dependent vasorelaxation in the development of age-dependent vascular stiffness.

**67**

E. Casanova[3], L. Stähli[3], A. Rodriguez Palomo[1], S. Tiziani[3], O. Gröninger[2], S. Märsmann[3], D. Canepa[3], B. Eggerschwiler[3], Y. Neldner[3], HC. Pape[3], M. Liebi[1], P. Cinelli[3]

**Comparison of bioengineered PLGA/aCaP scaffolds with aligned and random fiber orientation for improved bone regeneration**

*Chalmers University of Technology[1], ETH Zürich[2], University Hospital Zurich[3]*

**Introduction:**
Bone is a highly organized and specialized organ, which regenerate and repair by itself. However, in case of “critical size bone defects”, where natural bone healing is compromised, bone grafting is required. Tissue engineering of artificial bone substitutes represents a promising alternative to autologous or allogenic bone grafts, for repairing structure and function of the damaged bone. The traditional bone tissue engineering approach combines the use of osteoconductive scaffold together with osteogenic cells and growth factors. As the highly organized structure is often not fully restored in the regenerated bone, we tested an aligned nanocomposite to mimic the native organized structure of bone extracellular matrix (ECM). In this study, we made use of human adipose-derived mesenchymal stem cells (ASCs) and we investigated in vitro and in vivo bone regeneration of ASCs and ASC-derived ECM on either aligned or randomly oriented electrospun PLGA/aCaP (Poly(lactic-co-glycolic) acid/ amorphous calcium phosphate) nanocomposites.

**Methods:**
Distribution, orientation, and alignment of seeded ASCs on both types of scaffolds was tested in vitro. Histological sections were stained with Haematoxylin-Eosin or Phalloidin and Hoechst. ASC seeded scaffolds were investigated with Scanning Electron Microscopy (SEM). For the generation of ECM, decellularization was assessed by a combination of chemical (three different chemical approaches were tested), mechanical, and enzymatic treatments. ECM quality was investigated by Collagen I, Hoechst, and Mason-Goldner-Trichrome histological staining and SEM images. Four categories were tested in vivo (10 mice per group) in a mouse model for femoral critical size bone defect: (1) RANDOM scaffold WITH ASCs, (2) ALIGNED scaffold with ASCs, (3) RANDOM scaffold with ECM, (4) ALIGNED scaffold with ECM. After 7 weeks, 5 mice per group were sacrificed, femurs were isolated, dehydrated and embedded into poly(methyl methacrylate) (PMMA). These samples were then analyzed with small-angle scattering tensor tomography (SAXS), which revealed the structure and the orientation of the collagen fibers in the four groups. All the other mice were sacrificed after 10 weeks, femurs were isolated, fixed in formalin, decalcified and sections were prepared for histological staining. All samples were analyzed also with mCT and bone regeneration were assessed.

**Results:**
In vitro data confirmed cells alignment along the scaffold fibers, resulting in the case of the aligned scaffolds into aligned collagen fibers and oriented ECM. For scaffold decellularization, Triton X-100 chemical treatment followed by the mechanical and enzymatic procedures, resulted into the best-conserved ECM. mCT of the bones revealed regeneration in all four categories. SAXS images highlighted highly oriented collagen fibers in the ALIGNED groups, which showed also higher bone regeneration with no gap between the scaffold-bone borders.

**Conclusion:**
The highly organized and hierarchical structure of bone over different length scales establishes its unique mechanical properties. Scaffolds used for bone tissue engineering should mimic the native structure and function of the bones. Here we demonstrated that an aligned scaffold guide cell spreading and migration, generating an oriented ECM and improving bone regeneration. This is a promising approach allowing organized bone regeneration with improved mechanical and regenerative functions.

**68**

P. Wawrzyniak[1], P. Srikanthan[1], I. Hartling[1], C. Gemperle[1], N. Noureddine[1], D. Mathis[1], M. Hersberger[1]

**Anti-inflammatory effect of omega-3 fatty acids on activated CD4+T cells**

*Division of Clinical Chemistry and Biochemistry, Children's Research Centre, University Children's Hospital Zurich, Switzerland[1]*

**Introduction:**
Triglyceride (TG)-based lipid emulsions form an integral part of life-saving total parenteral nutrition (TPN) and are provided to patients who are unable to orally ingest, digest or absorb the necessary daily amount of food. Currently available therapies often cause considerable side effects, with evidence that lipid emulsions containing high amounts of omega-3 polyunsaturated fatty acids, have less side effects.We compared the effect of a commercial fish oil based lipid emulsion (Omegaven) compared with omega-3 poor soybean oil lipid emulsion (Intralipid) on the activation of primary human T cells.

**Methods:**
CD4+T cells were isolated by magnetic cell sorting from primary human peripheral blood mononuclear cells and were stimulated with anti-CD2, anti-CD3 and anti-CD28 antibodies for 48 hours in the presence of lipid emulsions. Fatty acids composition was measured by triple quadrupole GC-MS/MS system. Production of cytokines: was analyzed using intracellular staining for flow cytometry following 6 hours stimulation with PMA, Ionomycin and brefeldin and culture supernatants were measured by magnetic multiplex immunoassay with a customized human premixed multi-analyte kit.

**Results:**
Treating human primary CD4+T cells with Omegaven led to a dose-dependent increase in cellular omega-3 fatty acids and to a reduced cytokine production of TNFa, IFNg and IL-4 as compared with CD4+T cells treated with Intralipid. Interestingly, cytokine measurement in culture supernatant showed also decreased production of TNFa and IFNg and IL-13 in opposite to IL-5, which was increased.

**Conclusion:**
Our results demonstrate that CD4+T cells treated with Omegaven incorporate the omega-3 polyunsaturated fatty acids, and this leads to reduced production of pro-inflammatory cytokines and the activation of CD4+T cells.

**69**

L. Russo[1], L. Roth[1], A. Gupta[1], K. Lehmann[1]

**Improving loco-regional treatment of peritoneal metastasis**

*Surgical Oncology Research Laboratory[1]*

**Introduction:**
Selected patients with peritoneal metastasis show survival benefits, when treated with the combination of cytoreductive surgery (CRS) and hyperthermic intraperitoneal chemotherapy (HIPEC). However, recurrence of the disease limits long-term survival requiring optimization of HIPEC treatment. Hence, it is important to understand biological mechanisms behind HIPEC. We could show that HIPEC treatment induced strong immunogenic changes in colorectal cancer cells in-vitro. After HIPEC treatment, increased expression of two CT-Antigens (Cyclin A1 and SSX-4) was observed. Moreover, HIPEC led to the activation of dendritic cells when co-cultured with treated colorectal cancer cells. Primed dendritic cells activated CD8+ T cells to produce IFN-g. As a next step, we want to establish a PM mouse model to study the induction of adaptive immune response after HIPEC treatment in-vivo.

**Methods:**
C57BL/6 and BALB/c mice were injected i.p with syngeneic murine colorectal cancer cell lines MC-38 and CT-26, respectively. To define the transition of microscopic to macroscopic tumor lesions and the tumor penetrance, mice were sacrificed 24h, 48h, 72h and 7 days post tumor cells injection. Microscopic lesions were analysed via histology. To test cytotoxicity of chemotherapeutic agents, mice were treated with 10mg/L Mitomycin C/Doxorubicin i.p. on 3rd or 7th day after tumor cells injection.

**Results:**
The tumor incidence using MC-38 cancer cells in the peritoneum of C57BL/6 mice was ca. 70%, whereas tumor penetrance using CT-26 cancer cells in BALB/c mice was 80%. During the first 72 hours, no macroscopic tumor was detected in both strains. Furthermore, mice treated early with M/D (3 days post tumor cells injection) presented a lower tumor load compared to mice, which were treated at a later time point with M/D (7 days post tumor cells injection). Interestingly, the late M/D treated mice had similar tumor load as the control group.

**Conclusion:**
We are developing two PM mouse models that are promising to test novel HIPEC treatments and subsequent immune responses. To further fine-tuning the model we plan to use the IVIS System in order to allow optical recognition of cancer cells prior and post HIPEC treatment.

**70**

M. Barbagallo[1], D. Naef[1], J. Beer[1], H. Hireche-Chikaoui[1]

**Right ventricular thrombi, a challenge in imaging diagnostics: a case series study.**

*Kantonsspital Baden[1]*

**Introduction:**
Presence of a Right Heart Thrombus (RHT) is an infrequent[MB1] and life-threatening condition, thus immediate diagnostic and therapy is mandatory. While current literature proposes a multimodal non-invasive imaging diagnostic, we suggest to perform cardiac magnetic resonance imaging (MRI) in patients with high risk for thrombotic events. Therefore, we reported results from an observational study, in which patients in younger age, with previous bleeding events, congestive heart failure, cancer, syncope, systolic blood pressure < 100 mmHg and arterial oxyhaemoglobin saturation <90% had a higher risk for RHT.

**Methods:**
We analyzed 2 patients presenting with Righ Heart Thrombus with echocardiography and cardiac magnetic resonance imaging.

**Results:**
We report two cases of intraventricular RHT in two male patients, which were missed during routine cardiac diagnostic by transthoracic echocardiography (TTE) and computer tomography (CT). For further clarification we performed cardiac MRI, which in both cases leaded to detection and simultaneously further characterisation of the masses. Therefore, reliable distinction from tumour masses was possible.

**Conclusion:**
In this case series, we discuss the role of cardiac MRI for the detection of intraventricular RHT. We consider the relatively expensive and time intensive imaging procedure and weight it up to its assumed high sensitivity and specificity and importance for differential diagnostics and therapeutic decision making. Additionally, we discuss in which condition a cardiac MRI might be indicated, aiming high pre-test probability.

**71**

Iv. Jelcic[2], C. Esposito[1], J. Sarabia del Castillo[1], N. Caduff[3], F. Al Nimer[2], J. Wang[2], Il. Jelcic[2], A. Lutterotti[2], C. Münz[3], M. Sospedra[2], L. Pelkmans[1], R. Martin[2]

**In depth characterization of the autoreactive B-T cell interactome in Multiple Sclerosis**

*Institute of Molecular Life Sciences, University of Zurich, 8057 Zurich, Switzerland[1], Neuroimmunology and MS Research Section (NIMS), Neurology Clinic, University of Zurich, University Hospital Zurich, 8091 Zurich, Switzerland[2], Viral Immunobiology, Institute of Experimental Immunology, University of Zurich, 8057 Zurich, Switzerland[3]*

**Introduction:**
Multiple sclerosis (MS) is an autoimmune disease of the central nervous system (CNS) in which autoreactive T cells are considered to be the major effector cells in orchestrating and promoting CNS injuries. However, B cells emerged as additional important player in MS immunopathogenesis since B cell depletion therapy very effectively reduces new relapses. Recently, we provided an important link between these two cell populations by demonstrating that memory B cells activate brain-homing autoreactive T cells in MS.

**Methods:**
Based on a simple in vitro assay, we have shown increased spontaneous proliferation or so-called “autoproliferation” of peripheral blood T cells in MS patients. Here, we evaluated also in detail the frequency, phenotype and signatures of autoproliferating B cells by using multiparametric flow cytometry and RNAseq analyses. Furthermore, we used iterative indirect immunoflurescence imaging (4i) to further elucidate the interaction, formation and subcompartmentalization of autoproliferating B and T cells. Finally, we dissected the interactome of autoproliferating B and T cells by analyzing the expression and activity of receptor-ligand pairs on transcriptional and protein level.

**Results:**
Autoproliferation involves besides effector memory T cells also a substantial fraction of B cells which were increased during inactive phases of the disease (remission) and even more under anti-VLA4 treatment (natalizumab). Among these B cells, we mainly detected class-switched memory B cells with strong upregulation of HLA-DR, which had a high capability of inducing T cell proliferation in an HLA-DR-dependent manner. Autoproliferation of B cells was independent of CD40 signaling, and we did not detect transcripts for EBV, a strong environmental risk factor of MS. However, among the essential factors we identified the kinase BTK. Transcriptional analyses of these B cells revealed a pro-inflammatory phenotype, in particular of IFN-gamma, and interestingly a number of genes that are involved in germinal center-like formation. Indeed, we could demonstrate by 4i-technology that autoproliferating cells form huge cell clusters of interacting B and T cells. Interestingly, BTK inhibitors were able to completely disrupt the formation of these lymphoid-like structures. By dissecting the B-T cell interactome we finally revealed a tight network of co-receptor-ligand pairs that contribute to this interaction.

**Conclusion:**
Collectively, our data provide novel insights in the activation signatures of autoproliferating B cells and their resulting interactome with autoreactive T cells in MS. Particularly, the identification of autoproliferating B-T cell-rich follicles are instrumental to approach numerous questions on the dynamics of pathogenic B-T cell interactions in MS. We now aim to use this promising in vitro approach as a drug screening platform for the identification of future therapeutic targeting.

**72**

A. Nasrallah[3], M. Kraljevic[2], A. Taheri[3, 4], V. Marzolla[3, 5], A. Jomard[3, 5], C. Wolfrum[5], A. von Eckardstein[3], F. Ruschitzka[1], T. Lutz[4], E. Osto[1, 3, 5]

**Decoding the vasodilatory effects of bile acid through TGR5 receptor**

*Department of Cardiology, University Heart Center, University Hospital Zurich[1], Department of General Surgery, University Hospital Basel[2], Institute of Clinical Chemistry, University Hospital Zurich[3], Institute of Veterinary Physiology, Vetsuisse Faculty, University of Zurich[4], Laboratory of Translational Nutrition Biology, Federal Institute of Technology, ETHZ[5]*

**Introduction:**
Bariatric surgery is the most effective body weight loss therapy against severe obesity leading to reduced cardiovascular morbidity and mortality. A metabolic hallmark of the gold-standard bariatric surgery, Roux-en-Y gastric bypass (RYGB), is a rise in circulating gut hormones, i.e. bile acids (BA). BA, previously considered as fat absorption mediators, have recently emerged as vital metabolic modulators, becoming attractive targets for the pharmacological treatment of numerous metabolic diseases. Among other pathways, BA activates the TGR5 membrane receptor and PKA-dependent signaling inducing endothelial nitric oxide (NO) synthase (eNOS) activation and NO production, which in turn leads to vasodilation. Thus, BA may contribute to the ameliorated endothelial function observed early after RYGB. We hypothesize that the lack of TGR5 in obese mice impairs the vaso-protective effects of RYGB.

**Methods:**
8-week old male wild type (WT) and systemic TGR5 knockout mice ($TGR5^{-/-}$) were put on CHOW or high-fat (60%) high-cholesterol (1.25%) diet (HFHCD) for 16 weeks. HFHCD-induced obese mice were separated into 4 groups (n=10), and respective surgeries performed: sham operation in WT and $TGR5^{-/-}$, and RYGB operation in WT and $TGR5^{-/-}$ mice. Mice were metabolically phenotyped pre and 1 month post-surgery. Upon sacrifice, cumulative relaxation responses of thoracic aortic rings were performed to insulin ($10^{-11}$-$10^{-6}$M) and GLP-$1^{(7–36)}$ amide ($10^{-12}$-$10^{-6}$M) after submaximal contraction with norepinephrine ($10^{-6}$M), repeated with pre-incubation of eNOS-inhibitor (L-NAME, $10^{-4}$M) to test NO-dependent relaxation. Total cholesterol, high density lipoprotein cholesterol (HDL-C), non-esterified fatty acids (NEFA) and total plasmatic BA were checked using commercially available kits.

**Results:**
$TGR5^{-/-}$ mice under CHOW have impaired vasodilation in response to GLP-1 or insulin, compared to WT. Pre-incubation with L-NAME abolished relaxation to GLP-1 and insulin in both groups compared to baseline suggesting a NO-dependent mechanism. Upon HFHCD, vasodilatation is impaired in $TGR5^{-/-}$ and WT compared to CHOW controls. Although RYGB induced significant bodyweight loss ($p=0.0002$), decreased food intake ($p=0.0278$), and better glucose tolerance ($p<0.0001$) in $TGR5^{-/-}$ and WT mice, vasodilation improved only in RYGB-WT, with an increase of 50% vasodilation in response to GLP-1 and a +70% insulin-mediated vasodilation compared to sham-operated controls. Total cholesterol levels were similar in all study groups. BA were significantly decreased in $TGR5^{-/-}$ lean mice ($p=0.0166$) as compared to WT. After RYGB in obese $TGR5^{-/-}$, BA tend to decrease, circulating HDL-C significantly decrease ($p=0.0392$), and NEFA significantly increase ($p=0.0395$).

**Conclusion:**
Under CHOW, in the absence of the TGR5 receptor, the NO-dependent vasodilatory effect of GLP-1 and insulin is blunted. Moreover, bariatric surgery performed in obese $TGR5^{-/-}$ mice is not able to improve obesity-induced endothelial dysfunction as it does in WT animals. Indeed, RYGB has TGR5-independet benefits on weight loss, food intake, and glucose tolerance similarly in $TGR5^{-/-}$ and WT mice. These novel findings unravel a pivotal role of BA and TGR5 receptor as gatekeeper of endothelial homeostasis contributing to the improvement of obesity-induced endothelial dysfunction after RYGB.

**73**

M. Generali[2], E. Casanova[1], D. Kehl[2], D. Wanner[2], S. Hoerstrup[2], P. Cinelli*[1], B. Weber*[2]

**Autologous endothelialized small-caliber vascular grafts engineered from blood-derived induced pluripotent stem cells**

*Division of Trauma Surgery, Center for Clinical Research, University Hospital Zurich, University of Zurich, Zurich, Switzerland[1], Institute for Regenerative Medicine (IREM), Center for Therapy Development and Good Manufacturing Practice, University of Zurich, Zurich, Switzerland[2]*

**Introduction:**
An ideal cell source for human therapeutic and disease modeling applications should be easily accessible and possess unlimited differentiation and expansion potential. Human induced pluripotent stem cells (hiPSCs) derived from peripheral blood mononuclear cells (PBMCs) represent a promising source given their ease of harvest and their pluripotent nature. Previous studies have demonstrated the feasibility of using PBMC-derived hiPSCs for vascular tissue engineering. However, so far, no endothelialization of hiPSC-derived tissue engineered vascular grafts (TEVGs) based on fully biodegradable polymers without xenogenic matrix components has been shown.

**Methods:**
In this study, we have generated hiPSCs from PBMCs and differentiated them into αSMA- and calponin-positive smooth muscle cells (SMCs) as well as endothelial cells (ECs) positive for CD31, vWF and eNOS. Both cell types were co-seeded on PGA-P4HB starter matrices and cultured under static or dynamic conditions to induce tissue formation in vitro.

**Results:**
The resulting small diameter vascular grafts showed abundant amounts of extracellular matrix, containing a thin luminal layer of vWF-positive cells and a subendothelial αSMA-positive layer approximating the architecture of native vessels. Our results demonstrate the successful generation of TEVGs based on SMCs and ECs differentiated from PBMC-derived hiPSC combined with a biodegradable polymer.

**Conclusion:**
Our findings improving the generation of autologous vascular replacements using blood as an easily accessible cell source. These results pave the way for developing autologous PBMC-derived hiPSC-based vascular constructs for therapeutic applications or disease modeling.

**74**

S. Hiltbrunner[1], S. Kasser[1], S. Freiberger[3], S. Kreutzer[2], N. Toussaint[4], L. Grob[4], M. Rechsteiner[3], A. Soltermann[3], A. Curioni-Fontecedro[1]

**Resistance mechanisms in non-small cell lung cancer patients upon anti-PD1 therapy**

*Department of Medical Oncology and Hematology, University Hospital Zurich[1], Functional Genomics Center Zurich, ETH and University of Zurich[2], Institute of Pathology and Molecular Pathology, University Hospital Zurich[3], NEXUS Personalized Health Technologies, ETH Zurich[4]*

**Introduction:**
The development and clinical success of immune checkpoint inhibitors (ICIs) targeting the PD-L1/PD-1 pathway has revolutionized the treatment and outcome of patients with metastatic non-small cell lung cancer (NSCLC). However, NSCLC tumors might be resistant to such immunotherapy “ab initio” or acquire resistance after initial response. Mechanisms related to acquired resistance to immunotherapy have been described for melanoma, involving the interferon-gamma pathway.

**Methods:**
We have collected the clinical data and tumor samples from 9 patients who initially responded to immunotherapy (Nivolumab) and developed acquired resistance afterwards. Tumor samples were collected before treatment and at resistance and were analysed for immune markers by immunohistochemistry. From 4 tumor samples (2 paired from before and at resistance) we performed whole exome and RNA sequencing in order to investigate the changes in single nucleotide variants and gene expression alterations between the primary and resistant samples.

**Results:**
One group of patients had reduced numbers of infiltrating CD8 T cells and reduced expression of PD-L1 at time of resistance, the other group showed high CD8 T cell infiltration and high expression of PD-L1 but markedly enhanced expression of other inhibitory ligands. Furthermore, we detected mutations in genes related to immune responses at time of resistance. Specifically, type I and II IFN pathways were downregulated at time of resistance, which could lead to an impaired anti-tumor immune response. Both patients had a stable HLA-ABC expression without any loss of the allele. However, both patients had stable or even increasing tumor mutational burden at the time of resistance. Resistance to ICI therapy was independent on tumor infiltrating CD8 T cells and also independent on PD-L1 expression.

**Conclusion:**
We have identified mechanisms of resistance to immunotherapy in NSCLC patients. Such discovery is of great importance for the development of new therapeutical strategies and improve the outcome of NSCLC patients.

**75**

B. Schmid[1], E. Bersuch[1], A. Künstner[2], A. Fähnrich[2], H. Busch[2], M. Glatz[1], P. Bosshard[1]

**Skin mycobiome sequencing reveals a high fungal diversity in patients with severe atopic dermatitis**

*Department of Dermatology, Universitity Hospital Zurich, University of Zurich, Gloriastrasse 31, Zurich, Switzerland[1], Institute of Experimental Dermatology, University of Luebeck, Ratzeburger Allee 160, 23538 Luebeck, Germany[2]*

**Introduction:**
Atopic dermatitis (AD) is a multifactorial, chronic relapsing inflammatory skin disease. Characteristics are an impaired skin barrier and an altered skin immune system, which often come along with predominant colonization by *Staphylococcus aureus*. The role of fungi, i.e. the mycobiome, remains poorly investigated although AD patients are frequently sensitized to *Malassezia*, the most abundant fungus on skin. We aim to improve the understanding of the skin mycobiome in AD.

**Methods:**
Skin swabs of 11 AD patients and 11 healthy controls (HC) were taken from 4 skin sites (antecubital crease, glabella, vertex, and dorsal neck). To assess temporal shifts in the mycobiome, AD patients were sampled at 3 time points (0, 2 and 4 weeks). HC were sampled at 2 time points (0, 4 weeks). We assessed relative abundance of fungal genera and species by amplicon-based next-generation sequencing (NGS) of the fungal ITS1 region.

**Results:**
The most abundant fungi at all skin sites were *Malassezia* spp. The species distribution was site-dependent with high abundances of *M. globosa* at the neck and *M. restricta* at the glabella and vertex, and overall lower abundance of *Malassezia* at the antecubital crease. Patients with severe AD tended to be more frequently colonized with non-*Malassezia* fungi such as *Candida*. In most HCs and patients with mild to moderate AD, the mycobiome was comparable between individuals and stable over time. In contrast, in severe AD the mycobiome was different between individuals and changed over time.

**Conclusion:**
Patients with severe AD had a high intra- and interpersonal species diversity. We speculate that the impaired skin barrier in severe AD allows colonization with more different fungi than healthy skin. Vice versa, the altered mycobiome may cause activation of the skin immune system leading to inflammation and eczema. In the next step, we will correlate these results with the bacterial microbiome in the same samples.

**76**

J. Jelisejevas[1], D. Hofer[1], A. Saguner[1], A. Breitenstein[1], J. Steffel[1]

**Retrospective analysis of left femoral access for leadless pacemaker implantations**

*University Hospital Zurich[1]*

**Introduction:**
Leadless pacing using the Medtronic Micra TPS pacemaker has become a standard approach in many centers for patients in need of a single chamber pacemaker. Conventionally, the Micra TPS pacemaker is implanted via a right femoral access. However, due to various reasons, a left sided femoral approach may be necessary. In the current analysis, we compare the efficacy and complication rate in our cohort of patients with left versus right sided femoral venous access.

**Methods:**
Retrospective, observational, single-centre study with a total of 101 consecutive patients from June 2015 to September 2019.

**Results:**
86 patients underwent Micra TPS implantation via a right and 15 (15%) patients via a left femoral access. In 13 patients (13%), a Micra TPS pacemaker was implanted after TAVI procedure. Left femoral access was used in 54% of cases (7 of 13) as compared to 7% (6 of 88) in the remaining patients. All patients were implanted successfully with a low total complication rate of 2 %.
All major complications occurred in patients in whom right femoral access was used. Mean duration of the procedure was 48.8 minutes using right femoral access and 50 minutes in patients with a left femoral access (P=NS). Mean fluoroscopy time was 7.57 minutes versus 8.12 minutes during right and left sided access, respectively (P=NS). Pacing thresholds were low at implantation for both approaches (right femoral access: 0.5V/0.24ms, left sided access: 0.63 V/0.24 ms). The final Micra TPS position within the right ventricle was mid-septal in 85% (p = 0.53) for right femoral access implantation but only 67 % in patients undergoing Micra TPS implantation via left femoral access (p=0.59).

**Conclusion:**
Left femoral access was safe with an excellent implantation success rate as an alternative to right femoral access without longer implantation and fluoroscopy time. Leading cause of choosing left femoral access was in patients post TAVI in need antibradycardia pacing.

**78**

A. La Greca Saint-Esteven[1, 2], J. van Timmeren[2], S. Tanadini-Lang[2], E. Konukoglu[1]

**HPV Status Prediction Using Deep Learning in Head-and-Neck Cancer Patients**

*ETH Zürich[1], UniversitätsSpital Zürich[2]*

**Introduction:**
Radiochemotherapy is the gold-standard treatment in head and neck squamous cell carcinoma (HNSCC). Treatment is currently leading to very heterogeneous clinical outcomes depending on patient- and tumor characteristics, including Human Papilloma Virus (HPV) infection, which is considered as an important prognostic factor. In the recent years, quantitative image analysis has significantly gained relevance in order to improve the diagnostic accuracy and prognosis prediction accuracy.
Hand-crafted image features, also known as radiomic features, have been linked to tumor histology and treatment outcome and, more recently, it was shown that a CT-based radiomic approach could accurately predict HPV status. Deep learning (DL) has proven to be superior to any other image analysis tool in many applications, ranging from disease classification to outcome prediction. Hence, in this study we aim to prove the feasibility of DL to predict HPV status in head and neck cancer positron emission tomography (PET) images, under the hypothesis that HPV affects lymph nodes and tumor activity, which will be better differentiated in functional imaging. In order to obtain a fully generalizable DL model, the first aim of this project is to collect data from different institutions.

**Methods:**
Head and neck 18F-fluorodeoxyglucose (18F-FDG) PET images from HNSCC patients were collected from the University Hospital of Zurich, in addition to two public datasets from The Cancer Imaging Archive (TCIA): the Head-Neck-PET-CT collection from four different institutions in Québec (Canada) and the Head and Neck Cancer Atlas from MD Anderson Cancer Center in Texas (US). Information about each scan acquisition and image reconstruction was extracted, along with scanner manufacturer, model and patient clinical data in order to devise a pipeline for data standardization and image normalization. The next steps of the project will be to develop a DL model for HPV status prediction that automatically extracts features and detects patterns in the collected data, but that is also capable of predicting HPV status in new, unseen PET data. Therefore, the aim the collection of additional datasets to further validate model performance.

**Results:**
A total of 447 PET scans were collected, out of which 65% were acquired at the University Hospital of Zurich. Approximately 87% of these scans were obtained using a GE Medical Systems scanner with ordered subsets expectation maximization (OSEM) being the most common reconstruction algorithm (around the 44%). Pixel spacing was greater than 5x5 mm for more than 50% of scans, and ranged from 2.34x2.34 mm to 5.46x5.46 mm. Regarding patient characteristics and clinical data, 84% of the patients were male, more than 90% of them were at least 60 years old and approximately 43% of them were HPV-positive. The most frequent primary tumor site was the oropharynx (around 40% of the cases), followed by the hypopharynx (14%).

**Conclusion:**
HPV status is known to be a relevant prognostic factor in head and neck cancer patients. Hence, its determination through image analysis by means of deep learning, which requires minimal manual work and has proven to be superior to other image analysis tools, is of great interest. In this study, we focus on PET imaging as it provides information about tumor and lymph nodes activities, which are supposedly altered by HPV infection. In order to build a powerful and accurate deep learning model, 447 PET scans of head and neck cancer patients were collected in this study, with 57% of them being HPV-negative and the 43% remaining HPV-positive. Future steps include data standardization and the design and implementation of the deep learning model to achieve HPV status prediction.

**79**

S. Balakrishna[4, 8], L. Salazar-Vizcaya[1], K. Kusejko[4, 8], V. Kachalov[4, 8], C. Thurnheer[1], J. Roth[3], A. Calmy[5], M. Cavassini[6], M. Battegay[3], P. Schmid[2], E. Bernasconi[7], F. Günthard[4, 8], A. Rauch[1], R. Kouyos[4, 8]

**Modelling the syphilis epidemic among HIV-positive and negative MSM in Switzerland**

*Department of Infectious Diseases, Bern University Hospital, University of Bern, Bern, Switzerland[1], Division of Infectious Diseases and Hospital Epidemiology, Cantonal Hospital St. Gallen, Switzerland[2], Division of Infectious Diseases and Hospital Epidemiology, University Hospital Basel, Basel, Switzerland[3], Division of Infectious Diseases and Hospital Epidemiology, University Hospital Zurich, Zurich, Switzerland[4], Division of Infectious Diseases, Geneva University Hospital, Geneva, Switzerland[5], Division of Infectious Diseases, Lausanne University Hospital, Lausanne, Switzerland[6], Division of Infectious Diseases, Regional Hospital Lugano, Lugano, Switzerland[7], Institute of Medical Virology, University of Zurich, Zurich, Switzerland[8]*

**Introduction:**
Over the last decade, syphilis incidence among HIV-positive and negative men who have sex with men (MSM) has strongly increased in Switzerland. Here we use a mathematical model that considers factors such as changing sexual behaviour to reproduce the syphilis epidemic.

**Methods:**
We set up a transmission model consisting of 36 coupled ordinary differential equations to model the syphilis epidemic in MSM in Switzerland between 2006 and 2017. We stratified the model by syphilis stage, cascade of care and sexual risk behaviour (MSM reporting occasional partners) to account for infectiousness, disease progression and exposure to transmission. Additional model layers include the episode of syphilis (first or recurrent) and HIV status. The model was parameterized and calibrated by fitting to the observed diagnosed cases from the Swiss HIV Cohort Study (SHCS) and the published data from the Federal Office of Public Health (FOPH), Switzerland.

**Results:**
We assessed the information of 5560 HIV-positive MSM registered in the SHCS between 2006 and 2017. 1272 (22.8%) HIV-positive MSM had at least one episode of syphilis and 521 (41.0%) of them had recurrent episode(s) of syphilis. The overall diagnosed cases of syphilis among MSM in Switzerland has increased from 113 in 2006 to 456 cases in 2017. Our mathematical model reproduced the strong increase in syphilis diagnoses from a mean of 124 episodes in 2006-2008 up to a mean of 438 episodes in 2015-2017, with an estimated additional 35 episodes every year. The model also reproduced about three-fold higher syphilis incidence in MSM reporting occasional partners compared to MSM reporting no occasional partners.

Model predictions and observed syphilis cases in HIV-infected and uninfected MSM

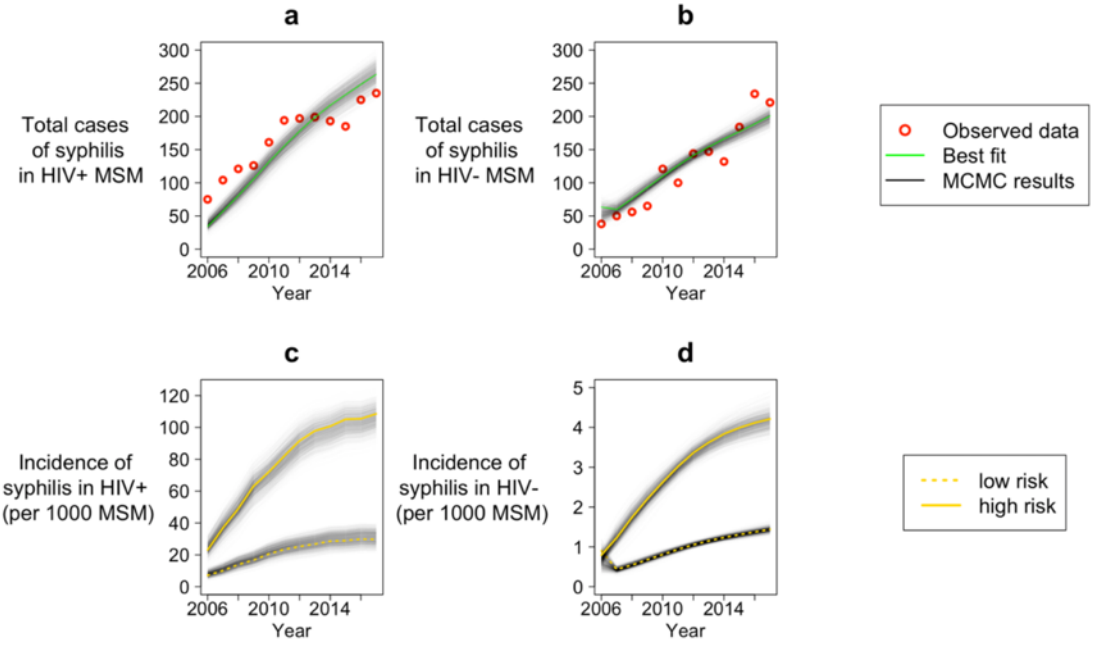


Panel a and b shows the optimized model fit; Panel c and d shows the model predictions;
Observed data – Data used to optimize model; Best fit – optimized model fit;
MCMC – Markov chain Monte Carlo;
low risk – MSM reporting no occasional partners; high risk – MSM reporting occasional partners;

**Conclusion:**
Our model accurately reconstructs the syphilis epidemic among MSM in Switzerland by capturing changes in sexual risk behaviour and interactions between HIV-positive and negative MSM. Syphilis incidence increased markedly in both HIV-positive and negative MSM and correlated with sexual risk behaviour.

**80**

I. Banik[2], M. Levesque[2], E. Busch[1], C. Dooley[1], E. Patton[3], T. Jana[3], P. Cheng[2]

**NRASQ61K melanoma is more aggresive than BRAFV600E melanoma in zebrafish models and can be rescued by p38 activation**

*Sanger Institute[1], Universitatspital Zurich[2], University of Edinburgh[3]*

**Introduction:**
It is widely accepted that melanoma results from the acquisition of several sequential oncogenic events. The two most frequently mutated oncogenes in melanoma are BRAF and NRAS, in which activating mutations lead to constitutive signaling of the MAPK pathway and thereby enhance tumor growth and promote disease progression. However, there have been only a few studies investigating these two oncogenes in parallel directly comparing their impact on tumor initiation and progression. Therefore, in this study we measured tumor growth kinetics in parallel using in vivo zebrafish melanoma models.. Melanoma models that express the activated human oncogenes $NRAS^{Q61K}$ or $BRAF^{V600E}$ under control of the MITF promoter in zebrafish melanocytes have proven to be powerful models to study the basic mechanisms of tumorigenesis. Previously zebrafish have been modelled to produce melanoma that are biologically equivalent of human naevi and melanoma.

**Methods:**
As the biology of NRAS and BRAF driven melanomas is somewhat different, we wanted to study the growth of melanoma driven by BRAF and NRAS mutations in parallel. To do this, we used the same cloning strategies and zebrafish backgrounds to standardize our results. The transgenic lines were made using minicoopR vector and Tol2 transgenesis system with the only difference being in the gene of interest. Both, $BRAF^{V600E}$ and $NRAS^{Q61K}$ genes were of human origin. In addition to, we used mitf mutant zebrafish (Nacre) with p53 loss throughout the study. We observed significantly faster tumorigenesis of $NRAS^{Q61K}$ driven melanoma compared to tumors driven by $BRAF^{V600E}$.Our analysis of The Cancer Genome Atlas revealed that P38-MAPK14 is often gained in human melanomas with NRAS oncogenic mutations and loss-of-function p53 who survive longer than their peers. P38α-MAPK14 over-expression *in vivo* significantly delayed the onset of $NRAS^{Q61K}$ driven melanoma, confirming its role of a tumor suppressor in this genetic background. These results could be reproduced in vitro showing that stable overexpressing p38α-MAPK14, or pharmacological activation of p38, had tumnor suppressive effects in $NRAS^{Q61K}$ mutant human primary melanoma cultures.

**Results:**
NRAS transgenic zebrafish had early tumor onset (35days) compared to BRAF transgenic fish (120days) and tumors derived from both lines showed histological similarity to human melanoma. TCGA analysis of NRAS mutant melanoma patients showed amplification of p38 in those that survived longer. Over-expression pf p38 in NRAS transgenic zebrafish delayed the tumor onset by 35 days. In 6 patient derived pruimary melanoma cell lines, stable transfection of pharmacological activation by anisomycin resulted in tumor suppressive effects such as reduced clonogenicity and cel viability. Furthermore, these tumor suppressive effects could be attributed to apotosis mediated cell death. Finally, anisoymcin as single agent is better than MEK inhibitor trametinib (IC50<0.02µM). Co-treatment of cells with anisomycin and trametinib resulted in snyergistic effect with low cytotoxic drug doses.

**Conclusion:**
In conclusion, we observed that NRAS transgenic zebrafish has more aggressive melanoma than BRAF and that zebrafish is a good model to study melanoma due to its histological and morphological similarity to human melanoma. We could observe that p38 MAPK14 is often amplified in patients with NRAS mutant melanoma who survive longer than their peers. In transgenic zebrafish with NRAS mutant melanoma, over-expression of p38 delayed tumor onset. In patient derived primary melanoma cells with NRAS mutation, stable over expression of p38 or pharmacological activation by anisoymcin resulted in tumor suppressive effects. More importantly, NRAS mutant melanoma cells resistant to MEk inhibitor could be re-sensitized by using low dose anisoymcin. Furthermore, combined treatment of NRAS mutant melanoma cells with anisomycin and trametinib resulted in synergistic effect with very low dose cytotoxic drug concentrations.

**81**

A. Potapenko[1], L. Rohrer[1], A. von Eckardstein[1]

**Scavenger receptor SR-BI splice variants 1 and 2 differ by cellular localization and interaction with HDL and LDL in endothelial cells**

*Institut für Klinische Chemie[1]*

**Introduction:**
Scavenger receptor SR-B1 limits the transendothelial transport of both HDL and LDL. Two different splice variants, SR-BIvar1 and SR-BIvar2, differ by their carboxyterminal amino acid residues. By the use of biochemical and microscopic techniques we compared the two for their cellular localization and interaction with lipoproteins.

**Methods:**
We generated isoform specific antibodies against the carboxyterminal regions as well as untagged, GFP- and mCherry-tagged constructs of the two SR-BI variants. The latter were used for transient transfection of HAECs as well as stable transfection of EA.hy926 cells. For colocalization we used confocal microscopy, stochastic optical reconstruction microscopy, structured illumination microscope, as well as life spinning disk confocal microscopy.

**Results:**
Few minutes after adding to the cells, fluorescent HDL is colocalised with SR-BIvar1 but not SR-BIvar2. Thereafter HDL shows no overlap with SR-BI. We also colocalized GFP-SR-BIvar1 but not mCherry-SR-BIvar2 with the plasma membrane and early endosomes (Rab5a) during early time points. In agreement with the colocalisation, only the overexpression of SR-BIvar1 enhanced the cell association of HDL at 37°C. Only in the presence of HDL both SR-BI variants are colocalized with late endosomes. In the presence of HDL or LDL, both SR-BI variants but no lipoprotein are. detected in lysosomes.

**Conclusion:**
The SR-BI splice variants 1 and 2 differ by cellular localization and interaction with HDL. Similar high resolution microscopic studies are initiated to investigate the interaction of the SR-BI variants with LDL and to further elucidate the endothelial trafficking of HDL, LDL and the SR-BI variants.

**82**

M. Paolucci[2], N. Wuillemin[1], C. Arena[1], Y. Wäckerle-Men[2], T. Kündig[2], D. Bieli[1], T. Sonati[1], P. Johansen[2]

**Allergen-blocking antibodies: a novel concept of peanut-allergy immunotherapy**

*Mabylon AG, Schlieren, Switzerland[1], University Hospital Zurich and University of Zurich, Zurich, Switzerland [2]*

**Introduction:**
Peanut allergy is an IgE-mediated disease with hypersensitivity to peanut (PN) proteins. At current, there is no immunotherapy available for these patients. The binding of PN allergens to IgE-FcεRI complexes, on the surface of mast cells and basophils, causes cellular degranulation that triggers symptoms of allergy. In the current project, we aim to develop and test a novel PN immunotherapy based on allergen-specific human monoclonal anti-PN antibodies (mAbs).

**Methods:**
Sera from PN allergic patients were screened for PN-specific IgE and IgG by ImmunoCAP and ELISA. From selected patients, B cells were isolated, and mAbs against PN allergens were molecularly cloned. The allergen specificity and binding affinity were tested by ELISA and surface plasmon resonance. The antibody function was tested in vitro with leucocytes from PN-allergic patients in basophil activation and in leukotriene release tests. Immunotherapeutic efficacy was performed in C3H mice sensitised with PN allergens by multiple low-dose intraperitoneal injection of peanut allergen extract. Mice received anti-peanut mAbs by intravenous injection at different time points before allergen-provocation by systemic injections of high-dose PN allergen extract. The anaphylaxis was monitored by clinical scoring and body temperature drop.

**Results:**
We identified patients with anti-PN IgGs and were able to recover B cells and to clone mAbs with high affinity for different PN proteins. The mAbs inhibited basophil activation and leukotriene secretion in vitro. When sensitised mice were challenged with a mixture of anti-PN mAbs and PN allergen extract, no clinical signs of anaphylaxis were observed, while a challenge with PN allergens extract caused strong anaphylactic reactions and temperature drops. When sensitised mice were treated by passive immunization with anti-pN mAbs 1-14 days before the challenge, the anaphylaxis could be fully abrogated.

**Conclusion:**
In closing, functional anti-PN IgG mAbs could be cloned from PN-allergic patients, and full protection against allergic anaphylaxis could be obtained by immunotherapy in PN-allergic mice. The results may pave the way for new clinical options for patients with difficult or untreatable allergies as well as for patients with seasonal allergies where allergen exposure is perennial.

**83**

J. Prange[1, 2], D. Mohr-Haralampieva[1, 2], R. Alves de Sousa[1, 2], N. Steinke[1, 2], F. Schmid[1], D. Eberli[1]

**Translational Medicine: From the lab bench to patient-ready GMP production**

*University Hospital Zurich[1], University of Zurich[2]*

**Introduction:**
The production of advanced therapy medical products (ATMP) represents new and endless possibilities in tissue and cell based personalised therapies. In order to guarantee patient safety ATMP production is regulated via Good Manufacturing Practice (GMP) guidelines. These guidelines help allow the safe translation of basic research data into the development of ATMPs. GMP production has strict quality control/management requirements that must be met at every step of production, with multiple quality checkpoints throughout the process. Verification and validation of personnel, processes and methods, materials and substances before clinical trials are vital to ensuring patient-risk is minimised.
Here, we aim to provide an overview of all GMP-related preparatory work for the manufacture of muscle precursor cells (MPCs) in a phase I clinical trial performed in Zurich.

**Methods:**
Translating lab research to a patient-ready production process took around 2 years and will be presented at a glance focussing on various verifications and validations required for the approval of the MPC-manufacturing.

**Results:**
Analytical methods, covering microbiological assessment as well as cell counting and characterization, were verified to provide reliable values during production. 7 study runs and 2 process verification runs were performed before the media fill process was carried out. All runs were resolved successfully and the media fill process qualified the production process and personnel for MPC manufacturing. The documentation process in preparation for phase I clinical trials was also finalised, with material specification, storage, risk assessments, transport, production, etc. being created and signed into effect.

**Conclusion:**
Cell and gene therapies have immense potential to treat a huge variety of illnesses, but their potential for contamination and misproduction must be curtailed via stringent supervision. GMP guidelines exist precisely for this: to ensure the safety of the therapy and reduce danger to the production system and the personnel involved in it. Setting up a GMP-compliant system is extremely costly and time consuming, however, given the potency of tomorrow's treatment, are becoming more and more necessary.

**84**

A. Reuss[1, 2], A. Crimi[2], L. Frick[2], P. Nilsson[1], A. Aguzzi[2]

**Establishing a 3D histological grading system for early and late amyloid beta (Aβ) and tau pathology in Alzheimer's disease (AD) patients**

*Department of Chemistry, Linköping University, Linköping,Sweden[1], Institute of Neuropathology, University Hospital Zurich, Zurich, Switzerland[2]*

**Introduction:**
The grading of disease stages of the NIA-AA classification system in Alzheimer's disease (AD) is based on plaques density (Mirra et al., 2002) as well as on amyloid beta (Aβ) and tau spread in distinct brain regions according to the Thal phases (Thal et al., 2002) and Braak & Braak stages (Braak & Braak, 1991). Neuropathological diagnoses are currently made via 2D histology, cutting tissue blocks into very thin sections and staining with distinct dyes and antibodies on different slices. However, topographical information may get lost and the evaluation of colocalization is often difficult. 3D histology preserves topographical information of the whole tissue block and allows distinguishing real colocalization from accidental overlap of morphological structures in distinct planes. Furthermore, it enables to display large structures like blood vessels and fiber tracts in a defined volume. In this project, we establish a 3D histological grading system for early and late Aβ and tau pathology in distinct brain regions of AD patients and compare it to the conventional 2D histological grading system.

**Methods:**
Formalin-fixed and paraffin-embedded tissue samples from distinct brain regions of human autopsy AD patients of different stages and age-matched controls are taken from the autopsy archive in a blinded and anonymized way. The tissue blocks of the regions of interest are cleared and stained for Aβ and tau as well as the surrounding neuronal structures. Data is acquired by lightsheet imaging via the custom-made mesoSPIM. Deep learning algorithms allow the automated analysis and quantification of Aβ and tau deposits in different brain regions as well as the segmentation of the vascular tree.

**Results:**
Formalin-fixed and paraffin-embedded human brain tissue blocks from autopsy cases have been successfully cleared and stained for different dyes and antibodies. The study is currently ongoing. The samples are stained for different blood vessel types in relation to Aβ plaques for the evaluation of cerebral amyloid angiopathy (CAA) and the changes of the vascular tree during Aβ spread. In addition, neurites are displayed together with tau pathology for the analysis of dystrophic neurites. Finally, astrocytes and microglia are shown in terms of gliosis and neuroinflammation. The algorithms for the quantification of Aβ and tau deposits have been established. The segmentation of the vessels via deep learning algorithms has also been established. Vessel efficiency calculation and cerebral blood flow simulation are still ongoing.

**Conclusion:**
The clearing and antibody staining of formalin-fixed and paraffin-embedded archival human brain tissue have been established and sample collection of AD patients and age-matched controls for staining, lightsheet imaging, and data analysis via deep learning algorithms has been started. Following the current NIA-AA classification system, we expect to establish a more accurate 3D histological grading for early and late Aβ and tau pathology compared to conventional 2D histology.

**85**

G. Ingoglia[1], A. Yalamanoglu[1], M. Pfefferlé[1], D. Schaer[1], F. Vallelian[1]

**Direct targeting of macrophages with an anti-CD40 antibody triggers a macrophage activation syndrome in mice**

*Department of Internal Medicine - University Hospital of Zurich[1]*

**Introduction:**
Macrophage activation syndrome (MAS) is a secondary Hemophagocytic Lymphocytic Histiocytosis, complicating the disease course of rheumatic disorders. MAS is an overwhelming systemic inflammation characterized by an uncontrolled immune activation and hyperinflammation. Macrophages are the main source of proinflammatory cytokines during MAS, but very little is known about their potential as primary drivers of the disease. The CD40-CD40 ligand (CD40L) interaction is a pivotal regulator of the immune system, mediating T-cell dependent antigen presenting cells activation. In vivo administration of an agonistic antibody against the CD40 receptor mimics the effects of CD40L, activating the macrophages and inducing systemic inflammation. In the present study, we aimed to dissect the role of macrophages as drivers of MAS by treating mice with anti-CD40 antibody.

**Methods:**
Mice were treated intraperitoneally (i.p.) with 200 µg of anti-CD40 or saline solution as control for 12 or 30 or 48 hours. A combined protocol with Colony Stimulating Factor 1 receptor (CSF1R) kinase inhibitor-enriched diet plus clodronate liposomes was used to deplete the macrophages. LysM-Cre CD40flox/flox mice were used to specifically knockout the expression of CD40 on macrophages surface. TNF receptor knockout mice (TNFRKO) and IFNγ knockout mice (GKO) were used to abrogate the signals induced by TNF and IFNγ.

**Results:**
Mice treated with anti-CD40 developed a macrophage-driven multiorgan and systemic inflammation. A massive release of transaminases into the plasma was observed 30 hours after the treatment, reflecting the pathogenic sequence of activation starting with macrophage and endothelial activation leading to disseminated intravascular coagulation (DIC), thrombosis and focal necrosis of the liver. CD40 ligation on macrophages recapitulated the typical biochemical features of MAS. Mice developed a cytopenia, the plasma ferritin and soluble CD25 levels were drastically increased. Macrophage depletion by clodronate- liposomes completely abrogated the disease pathology. To ultimately validate the role of macrophages as disease driver, we generated a macrophage-specific conditional CD40 knockout mouse and found that the knockout animals were protected against the disease process. Supporting the key role of macrophages, we showed that TNF and IFNγ were required for disease expression.

**Conclusion:**
In the present study, we discovered that anti-CD40 treatment induces a TNFα and IFNγ-driven disease resembling the most typical clinical and laboratory features of MAS. We dissected the role of macrophages as key driving cells in the pathogenesis of the disease and found that macrophage ablation abrogated the disease pathology. In clinical trials, the administration of agonistic anti-CD40 antibody to cancer patients has been associated to cytokine release syndrome, liver toxicity, thromboembolic complications, anemia and thrombocytopenia, mirroring the clinical and biochemical features we observed in our mice. Collectively, our study underlines the central role of macrophages and the potential threat of anti-CD40 cancer therapy as drivers of MAS.

**86**

L. Isenegger[1], P. Bode[2], C. Pauli[2], U. Camenisch[2], C. Matter[1], H. Moch[2], C. Britschgi[1]

**Phenotypic and Functional Validation of an in vitro Candidate Kinase Inhibitor Screen in Clear Cell Sarcoma**

*Department of Medical Oncology and Hematology, University Hospital of Zurich, Switzerland[1], Department of Pathology and Molecular Pathology, University Hospital of Zurich, Switzerland[2]*

**Introduction:**
Clear cell sarcoma (CCS) is a rare aggressive soft tissue sarcoma. When localized it can be cured by surgery, however, local relapses and distant metastases develop frequently. CCS is notoriously unresponsive to chemotherapy, targeted therapy or immune checkpoint inhibition and there is consequently a highly unmet medical need to develop novel therapies. Therefore, we have performed a high-throughput small molecule screen using a candidate kinase modulator library on cultured CCS cell lines to identify novel therapeutic approaches.

**Methods:**
The screen was performed in collaboration with NEXUS (ETH Zurich) using the ActiTarg-K library (960 candidate kinase modulators). Two CCS cell lines and one normal human fibroblast control cell line were plated on 384-well plates, cultured for 24 hrs, followed by robot-assisted addition of the library compounds in two concentrations. After 72 hrs of exposure, cell survival was assessed using a resazurin-based cell viability read-out. Methods for in vitro validation encompass IC50 determination (resazurin-based), long-term proliferation assays (colony formation), Western blot analyses for apoptosis and autophagy markers, and fluorescent-activated cell sorting (FACS)-based apoptosis assays. In vivo validation will be performed using the CCS xenograft models established in the laboratory (BALB/cAnNRj-Foxn1nu/nu mice). For target discovery, we are performing unbiased in vitro kinase screens using the KINOMEScan® assay (Eurofins DiscoverX).

**Results:**
Using 960 compounds at two concentrations, we have screened six 384-well plates per cell line. Positive (doxorubicin 10µM) and negative controls (DMSO) were included and the Z-score was calculated as a quality control measure. This was above 0.6 on all the plates indicating very good assay quality. We performed a differential activity analysis and assigned each well as significance and effect size. Next, a cluster analysis of wells showing a significant and strong reduction of cell survival was performed in order to identify the candidate drug compounds with the desired therapeutic window; i.e. reduction of survival of CCS cells, while sparing control cells. This stringent analysis workflow identified 14 compounds with the desired effect pattern, of which we have validated the 10 with the strongest effect using long-term proliferation assays. Those assays are complemented by IC50 determination and apoptosis assays. In parallel, we are currently performing the target discovery using the KINOMEScan® assay.

**Conclusion:**
We have successfully performed an unbiased high-throughput small molecule screen. We have validated the most promising compounds in vitro and are currently characterizing the reduction of cell survival in apoptosis and autophagy assays. Next, we will validate the two most promising candidate drugs in in vivo models. In parallel, we are using a kinase screen and potentially proteomics approaches to identify the molecular targets of the identified compounds. Those targets will then be validated on our collection of CCS specimens, as well as on a dedicated CCS tissue microarray constructed by our international collaboration partners (Prof. Schöffski, UK Leuven and EORTC).

**87**

P. Hejduk[1], C. Rossi[1], A. Ciritsis[1], K. Borkowski[1], A. Boss[1]

**Automatic and standardized quality assessment of digital mammography with deep convolutional neural networks**

*University Hospital of Zürich[1]*

**Introduction:**
Quality control of mammography examination is in Europe generally performed using the Perfect-Good-Moderate-Inadequate criteria. Even though the PGMI criteria are well defined, subjectivity of human jugement may result in incorrect rating. On top of that, each of those tasks is time consuming and tedious.
Quality assesment automatization with Artifical inteligence is thus a viable solution to those problems, minimizing errors in quality rating and increasing general productivity in the mammography unit. With standarized reports it may become a tool for institutions' screening program quality assessment.

**Methods:**
For each mammographic projection the adequate criteria have been selected. Using AI methods (dCNN), for each of the features of examinations, models has been trained to evaluate quality of feature presentation and overall quality of mammogram in PGMI scale. Each model has been trained on at least 2000 images aquired from institution's database.
Custom, standalone device with dedicated GUI has been developed for a comparison with human-readers and consensus of assesment of professional radiologists.

**Results:**
Models accuracy varied from 84% to 97%. The overall classification of single features resulted into a PGMI score. Initial comparison with human reader assessments showed good agreement on overall quality assessment.

**Conclusion:**
AI models show promising results in automation and standarization of quality assessment of mammographies. The presented technology may be integrated in the clinical routine and result in lean quality controls.

**88**

S. Santos[1, 2], M. Mennet[3], O. Potterat[2], U. von Mandach[1], M. Hamburger[2], AP. Simões-Wüst[1]

**Bryophyllum pinnatum compounds inhibit the oxytocin-induced rise of intracellular calcium concentration in human myometrial cells**

*Department of Obstetrics, University Hospital Zurich[1], Department of Pharmaceutical Sciences, University of Basel[2], Weleda AG, Arlesheim[3]*

**Introduction:**
*Bryophyllum pinnatum* (Lamarck) Oken (Crassulaceae) is a succulent perennial plant traditionally used in the treatment of premature labour, first in anthroposophic hospitals and, recently, in conventional settings as an add-on medication. Experimental evidence obtained with uterus strips supports this use and suggests that bufadienolides might be responsible for the tocolytic effect. Previous work with myometrial cells showed that *B. pinnatum* leaf press juice (BPJ) inhibits the increase of intracellular free calcium concentration ($[Ca^{2+}]_i$) induced by oxytocin (OT), a hormone known to trigger myometrium contractions. However, it is not known which compounds in BPJ contribute to this inhibition.
We here compare the inhibitory effects of BPJ, a bufadienolide-enriched fraction (BEF) prepared from *B. pinnatum* leaves, a flavonoid-enriched fraction (FEF), the corresponding flavonoid aglycon mixture (A-Mix), bersaldegenin-1,3,5-orthoacetate (BO), the combination of BEF plus FEF, the combination of BEF plus A-Mix, and the OT-receptor antagonist atosiban on the OT-induced increase of $[Ca^{2+}]_i$.

**Methods:**
Human myometrial hTERT-C3 and PHM1-41 cells that had been loaded with a calcium specific fluorescent probe (Fura-2-AM) were pre-incubated with test substances or vehicle controls. Then, cells were stimulated with OT to induce a rapid and transient increase in $[Ca^{2+}]_i$. Cells were incubated with digitonin to obtain maximal $[Ca^{2+}]_i$, and with Tris-EGTA for corresponding minimal values. $[Ca^{2+}]_i$ was measured by real-time fluorescence spectrophotometry. To characterise combined effects, the median-effect method (CompuSyn software) was used.

**Results:**
BPJ led to a concentration-dependent decrease of the OT-induced increase of $[Ca^{2+}]_i$ in both cell lines ($p<0.0001$), achieving ca. 70% inhibition at a 20 µg/mL concentration. The OT-receptor antagonist atosiban was used as a positive control and also promoted a concentration-dependent effect on $[Ca^{2+}]_i$ (in both cell lines, $p<0.0001$). BEF, FEF, BO, A-Mix, BEF plus FEF, and BEF plus A-Mix led to concentration-dependent decrease of the OT-induced increase of $[Ca^{2+}]_i$ in hTERT-C3 cells ($p<0.05$). BEF (2.2 µg/mL), FEF (17.4 µg/mL), BO (0.04 µg/mL), and A-Mix (0.7 µg/mL), at concentrations corresponding to 20 µg/mL BPJ, led to ca. 25% decrease of the OT-induced increase of $[Ca^{2+}]_i$. The combination of BEF plus FEF led to a decrease of 55.3% while BEF plus A-Mix promoted a decrease of 38.0%. Both combinations resulted in synergistic effects (combination indices ranging from 0.08 to 0.6).

**Conclusion:**
We have confirmed previous observations showing that BPJ promotes a specific and concentration-dependent inhibition of the OT signalling pathway. Although BEF, FEF, A-Mix, and BO alone have weaker effects than BPJ, the combined treatment BEF plus FEF has an effect comparable to that of BPJ. *B. pinnatum* leaf fractions BEF and FEF have a synergistic effect on the inhibition of the OT-induced increase of $[Ca^{2+}]_i$.

**89**

A. Hariharan[2], M. Ronner[2], M. Sculco[1], E. Felley-Bosco[2]

**RNA editing and interferon signalling in mesothelioma**

*Department of Health Sciences, University of Eastern Piedmont, Novara, Italy[1], Laboratory of Molecular Oncology, Department of Thoracic Surgery, University Hospital Zürich, Zürich, Switzerland[2]*

**Introduction:**
Mesothelioma is a rare, aggressive cancer caused by asbestos exposure. In a mouse model of mesothelioma development, asbestos (crocidolite) exposure increased A-to-G changes in RNA from pre-cancer lesions, which persist in tumours. These changes result from activity of adenosine deaminases acting on RNA (Adar1, Adar2). One isoform of Adar1 is type I interferon induced. High Adar2 and low interferon stimulated gene (ISG - *Ddx58, Ifitm1, Ifit2*) expression are associated with decreased overall survival in mesothelioma patients.

**Methods:**
Adar2 knockout cell lines were developed from mouse RN5 mesothelioma cell line using CRISPR/Cas9 system. Single clones were characterised for Adars using sequencing, qPCR, and western blotting. Changes in expression of ISGs were analysed by qPCR. In-vitro assays - colony forming and spheroid building assay - were performed to detect differences in cell growth. Spheroids were treated with pemetrexed (standard therapy for mesothelioma patients) and tested for cell viability using Cell Titer Glo.

**Results:**
Clones heterozygous for Adar2 were isolated, since Adar2 is an essential gene in mice. qPCR and western blotting confirmed reduced Adar2 expression in two clones selected for further characterisation. The clones had increased Adar1 expression as well as ISG expression including interferon β. Colony forming and spheroid building assays showed that the clones grow slower compared to RN5 cells. In addition, increased sensitivity to pemetrexed treatment was observed in the clones compared to RN5 cells. A mechanism of resistance to pemetrexed is upregulation of dihydrofolate reductase (Dhfr), due to increased RNA editing by Adars, and the clones had reduced *Dhfr* mRNA expression compared to the RN5 cells.

**Conclusion:**
Adar2 contributes to increased cancer cell growth in mesothelioma. Adar2 has an effect on type I interferon signalling in mesothelioma. Adar2 may also play a role in the development of resistance towards pemetrexed in mesothelioma via the editing of *Dhfr*.

**90**

A. Gomariz[1, 2], P. Helbling[2], S. Isringhausen[2], U. Suessbier[2], M. Manz[2], O. Goksel[1], C. Nombela-Arrieta[2]

## Deep Neural Networks for the Characterization of the BM Vasculature with Different Immunomarkers

*ETH Zurich[1], University Hospital of Zurich[2]*

**Introduction:**
Bone marrow (BM) cavities are the primary sites of blood cell production, which is sustained by a rare population of self-renewing and multipotent hematopoietic stem cells (HSC). Local cues deriving from non-hematopoietic BM stromal cells critically modulate hematopoiesis and HSC maintenance through cell-cell interactions. Thus, the study of spatial distributions of different BM components can reveal key information on cellular crosstalk and the molecular mechanisms underlying hematopoietic regulation. Among stromal components, endothelial cells lining sinusoidal BM microvessels (sinusoids) have been shown to fulfill prime roles in the orchestration of hematopoietic development. Understanding how cells interact with their microenvironment requires imaging the tridimensional spatial context surrounding them. For this, we have already established advanced tissue processing and clearing protocols for the generation of 3D microscopy reconstructions of entire BM cavities with subcellular detail, where the different structures are targeted with specific combinations of immunomarkers. Nevertheless, generating a high-throughput and unbiased analysis requires advanced image processing methods that can correctly handle this data.

**Methods:**
We have developed a deep learning pipeline for automatic detection of tissue landmarks which handles the complexities of deep tissue fluorescence microscopy, namely the size and heterogeneity of the images. Furthermore, we propose a novel neural network that can achieve the task of automatically segmenting different vasculature types under the presence of diverse combinations of immunomarkers. In combination with a set of spatial statistical methods, we employ these tools to quantify how these segmented structures constrain the available volume and interact with each other within the tissue boundaries.

**Results:**
Applied to our BM datasets, these methods are used to segment the 3D sinusoidal microvascular networks together with arteries with unprecedented speed and accuracy. We show which markers are preferred for achieving the best performance, and demonstrate that with our novel versatile network, it is possible to achieve good results even in cases in which suboptimal immunolabeling strategies need to be employed. Our methodologies reveal that in homeostatic conditions, the sinusoids occupy 20% of the total BM volume and leave little space for other cellular populations. We also detected the mesenchymal stromal cells and report their preferential location in perisinusoidal regions, with 60% of them being in direct contact with the abluminal side of endothelial cell walls.

**Conclusion:**
In the BM, the results suggest that the stromal components have been previously inaccurately characterized, and we have proposed rigorous descriptors of their spatial confinement and cell frequencies.Importantly, our analytical pipeline can be employed to uncovering novel spatial phenotypes of immunostained cellular components in multiple organs.

**93**

C. Wolf[1]

**Impact of posters and the role of leadership in improving professional appearance of staff in the hospital**

*University Hospital Zurich[1]*

**Introduction:**
Nosocomial Infections are a serious threat to a patient during his hospital stay. Reducing the transmission of germs is an important step to keep the patient safe. One way to reduce the transmission of germs are standard precautions, specifically professional appearance. This includes keeping the hair above the shoulders, professional clothing, keeping the sleeves above the elbow, wearing no jewelry and keeping the fingernail short without artificial nails or nail polish added. The aim of this study is to enhance the application of professional appearance through a passive intervention and an active intervention. Nosocomial Infections are a serious threat to a patient during his hospital stay. Reducing the transmission of germs is an important step to keep the patient safe. One way to reduce the transmission of germs are standard precautions, specifically professional appearance. This includes keeping the hair above the shoulders, professional clothing, keeping the sleeves above the elbow, wearing no jewelry and keeping the fingernail short without artificial nails or nail polish added. The aim of this study is to enhance the application of professional appearance through a passive intervention and an active intervention.

**Methods:**
A passive intervention and active intervention with a control group is used to improve the behavior of the healthcare workers. The interventions are based on behavioral change theory. The passive intervention includes using posters on every patient door that contains the information for a correct professional appearance. The active intervention uses middle managers (head nurses and attending physicians) as role models to improve behavior. In addition, they are giving frequent reminders during the week to adherence to professional appearance. Observations of professional appearance take place for 3 weeks for each intervention. They are conducted with an IPad Application.

**Results:**
Passive Intervention:
The baseline compliance rate was calculated to be 50%. After the passive intervention the compliance rate improved significantly to 74,46%. The control group had also a significant improvement of 8%. This might be due to the 5% initiative of the hospital (reducing the acquisition of health care associated infections <5%) which already focuses on improving horizontal precautions like professional appearance. Yet, the intervention had a significant impact compared to the control group.

Active Intervention:
The active intervention had no significant improvement compared with the passive intervention. The compliance rate changed to 73,00%. The active intervention was still significantly better than the control group which might be due to the already proven effectiveness of the posters.

**Conclusion:**
In conclusion, the passive intervention had beneficial effects in regards to compliance rate of professional appearance. The active intervention had neither beneficial nor detrimental effects on the compliance rate. Using posters as a primer is a good way to change behavior in regards to professional appearance. To further improve this behavior it is necessary to implement regulations, which rewards or punishes good/ wrong behavior in regards to professional appearance.

**94**

G. Karsai[3], M. Lone[3], Z. Kutalik[4], T. Brenna[1], H. Li[2], D. Pan[2], A. von Eckardstein[3], t. Hornemann[3]

**FADS3 is a delta14Z sphingoid base desaturase that ameliorates the 1-deoxy-dihydroceramide associated toxicity**

*Dell Pediatric Research Institute, Departments of Chemistry, Pediatrics, and Nutrition, University of Texas, 1400 Barbara Jordan Blvd, Austin, Texas 78723, USA[1], Department of Physiology, University of Texas Southwestern Medical Center, Dallas, TX 75390, USA[2], Institute for Clinical Chemistry, University Hospital and University Zurich, 8091 Zürich, Switzerland[3], University Center for primary care and public health, University of Lausanne, Switzerland[4]*

**Introduction:**
Sphingolipids (SLs) are a diverse class of lipids that share a long-chain base (LCB) backbone. Sphingosine (d18:1) is the most abundant LCB in mammalian SLs that contains a single trans delta-4 double bond (DB), whereas sphingadienine (d18:2) the second most abundant LCB contains two DBs a trans delta-4 and a cis delta-14. While the trans delta-4 DB is introduced by the sphingolipid delta-4 desaturase (DEGS1), the desaturase responsible for the second DB is unknown.

**Methods:**
Here, we analyzed the LCB plasma profile in a gender-, age-, and BMI-matched subgroup of the CoLaus cohort (n = 658) followed by a genome-wide association study (GWAS). Combined with in vitro and in vivo metabolic labelling assays of genetically modified cells.

**Results:**
Plasma LCB profiling showed significant association of Sphingadienine levels with gender, being in average ~30% higher in females. A genome-wide association study (GWAS) revealed variants in the fatty-acid desaturase 3 (FADS3) gene to be significantly associated with the plasma d18:2/d18:1 ratio (p=-log 7.9). Metabolic labeling and genetic manipulations of cells, as well as plasma LCB profiling of FADS3-deficient mice confirmed that FADS3 is a bona-fide LCB desaturase required for the introduction of the delta-14Z double bound. Moreover, we showed that FADS3 is also required for the desaturation of the atypical cytotoxic 1-deoxy-dihydro-ceramides to 1-deoxy-ceramides. HEK293 cells overexpressing FADS3, were significantly more resistant to 1-deoxySA toxicity than WT cells. Whereas the downstream product 1-deoxySO showed similar toxicity. In summary, using a combination of metabolic profiling and GWAS, we identified FADS3 to be essential for forming delta-14Z DB containing LCBs, such as d18:2 and m18:1.

**Conclusion:**
Our results unravel FADS3 as a delta-14Z LCB desaturase, thereby disclosing the last missing enzyme of the SL de novo synthesis pathway.

**95**

M. Meerang[1], J. Kreienbühl[1], V. Orlowski[1], S. Müller[1], M. Kirschner[1], W. Weder[1], I. Schmitt-Opitz[1]

**Importance of Cullin4 Ubiquitin Ligase in Malignant Pleural Mesothelioma**

*University Hospital Zurich, Department of Thoracic Surgery[1]*

**Introduction:**
Loss of the tumor suppressor NF2 is frequent in malignant pleural mesothelioma (MPM). NF2 suppresses tumorigenesis in part by inhibiting Cullin4 ubiquitin ligase (CUL4) complex. Here we evaluated an importance of CUL4 in MPM and tested the efficacy of the cullin inhibition by pevonedistat, a small molecule inhibiting cullin neddylation.

**Methods:**
We assessed the expression of CUL4A and CUL4B in tissues using immunohistochemistry and quantitative real time PCR. We tested the efficacy of pevonedistat in 13 MPM cell lines in 2D and 3D culture compared to non-malignant mesothelial cell lines. Four groups of severe combined immunodeficiency SCID mice (n=8/group) haboring intraperitoneal (ip.) pevonedistat sensitive (MSTO211H) or resistant (ACC-Meso1) cell lines were treated with pevonedistat (50 mg/kg; ip.) on a 5day on/5day off schedule for 3 cycles. Treatment efficacy was assessed by means of overall survival. To evaluate the mechanism of treatment, additional groups of mice (n=5/group) were treated for one cycle followed by tissue collection and analysis.

**Results:**
CUL4 paralogs (CUL4A and CUL4B) were upregulated in MPM tumor specimens compared to non-malignant pleural tissues. High gene and protein expression of CUL4B was associated with worst progression free survival of MPM patients. Five MPM cell lines (38%) were highly sensitive to pevonedistat (IC50<0.5 µM), while non-malignant mesothelial cell lines are relatively resistant to the treatment (IC50~2.5 µM). This remained true in 3D spheroid culture. The treatment induced S/G2 cell cycle arrest and accumulation of cells undergoing DNA rereplication (containing >4N DNA content) more predominantly in the sensitive cell lines. DNA rereplication is known to be mediated by CDT1 accumulation and indeed the accumulation of CDT1 was detected after the treatment. Nevertheless, there was no difference in the extent of CDT1 accumulation comparing between sensitive and resistant cell lines. In vivo, pevonedistat treatment significantly prolonged survival of mice bearing both sensitive and resistant MPM tumors. Pevonedistat treatment reduced growth (phosphorylated histoneH3 positive) in pevonedistat sensitive tumor but increased apoptosis (cleaved–caspase3 positive) in pevonedistat resistant tumor. Thus, we analyzed cells associated with tumor microenvironment including mouse macrophage (F4/80+) and vessel formation (CD31+) that may explain the efficacy of pevonedistat in the resistant model. The treatment significantly reduced numbers of tumor associated macrophage in the resisitant (ACC-Meso-1) tumors, while it showed no effect in pevonedistat sensitive (MSTO211H) tumors. There was no effect on blood vessel formation in both tumor models at this time point.

**Conclusion:**
High CUL4B expression may play a role in MPM progression. Inhibition of cullins by pevonedistat induced growth arrest and DNA re-replication strongly in a subset of MPM cell lines. Pevonedistat showed favorable effect for MPM treatment in vivo, even for a resistant tumor model. This effect may be mediated by reduced tumor-associated macrophage infiltration.

**97**

A. Jomard[3, 5], O. Chavez-Talavera[6], A. Tailleux[6], P. Doytcheva[4], M. Bueter[1], A. Othman[3], A. Taheri[4], C. Wolfrum[5], T. Lutz[4], A. Von Eckardstein[3], F. Ruschitzka[2], B. Staels[6], E. Osto[2, 3, 5]

**Endothelial protective properties of Bile Acids bound to High-Density Lipoproteins: a novel therapeutic approach against obesity induced endothelial dysfunction**

*Department of Surgery &Transplantation, University Hospital of Zurich, Zurich, Switzerland[1], Heart Center Zurich, University Hospital of Zurich, Zurich, Switzerland[2], Institute of Clinical Chemistry, University Hospital of Zurich, Zurich, Switzerland[3], Institute of Veterinary Physiology, University of Zurich and Zurich Center for Integrative Human Physiology (ZIHP), Zurich, Switzerland[4], Laboratory of Translational Nutrition Biology, IFNH, ETH Zurich, Zurich, Switzerland [5], Universite Lille, Inserm, CHU, Lille, France and Institut Pasteur de Lille, U1011-EGID, F-59000 Lille, France[6]*

**Introduction:**
Bariatric surgery, i.e. Roux-en-Y gastric bypass (RYGB) reduces cardiovascular morbidity and mortality. We showed that high density lipoproteins (HDL)-mediated vasoprotection is improved early after RYGB. Circulating bile acids (BA) increase upon RYGB and are intensively investigated as crucial drivers of pleiotropic metabolic improvements after surgery. BA are signaling molecules increasingly recognized as regulators of metabolic homeostasis. BAs circulate free or bound to albumin and HDL. Our hypothesis is that HDL may facilitate BA delivery directly to endothelial cells, where BA synergize with HDL to promote vaso-protection. Purpose: We studied how RYGB changes the composition of BA bound to HDL (HDL-BA) and whether HDL functional properties may be enhanced by different BA bound to HDL.

**Methods:**
HDL were isolated by ultracentrifugation from 25 morbidly obese patients before and 1 year after RYGB. HDL-BA and the composition of lipid subspecies constituting HDL was determined by liquid chromatography-mass spectrometry and HDL vasoprotective properties were evaluated ex-vivo in human aortic endothelial cells (HAEC). Size and abundance of HDL particles were determined by NMR spectroscopy. BA function on HAEC was determined after 24-hour stimulation.

**Results:**
The increase in total BA concentrations observed in plasma 1 year after RYGB also translated into higher concentrations (up to 25%) of HDL-BA. Obesity-induced HDL dysfunction was reversed postoperatively, as shown by improved HDL-mediated endothelial NO production, anti-apoptotic effects and cholesterol efflux capacity. The size-composition analysis showed a post-operative shift towards larger HDL and modified lipid composition, containing less pro-inflammatory ceramides and increased antioxidant plasmalogens. After RYGB, there was a remodeling of HDL-BA, which are either agonists of the endothelial nuclear farnesoid X receptor (FXR), e.g. chenodeoxy-CA (CDCA), cholic acid (CA) or for the membrane TGR5 receptor, e.g. deoxy-CA (DCA). The composition-function analysis revealed that among all BA subclasses present on HDL, the specific enrichment of CA and CDCA bound to HDL correlated with an improved endothelial anti-apoptotic capacity of HDL (R -0.52, p=0.006 for HDL-CA and R -0.35, p=0.07 for HDL-CDCA). Exogenous loading of CA on obese, dysfunctional, pro-apoptotic HDL, was able to restore HDL anti-apoptotic function. Stimulation of HAEC with free CA and CDCA significantly improves endothelial NO production, while decreasing NADPH oxidase activity and apoptosis, and ameliorate glycolysis and oxygen consumption, as determined by extracellular flux analysis.

**Conclusion:**
CA loading onto obese dysfunctional HDL restored its anti-apoptotic function, mimicking the beneficial remodeling of HDL-BA observed after RYGB. These results suggest a crucial interaction between endothelial cells and BA in the improvement of HDL's vasoprotective properties. BA are a novel endothelial signaling molecules, with potential therapeutic vascular benefits.

**98**

G. Hamvas[2], A. Hofmann[2], V. Sakalidis[1], B. Goodale[1], M. Shilaih[1], B. Leeners[2]

**Innovative trial design using digital approaches: an example from reproductive medicine**

*Ava AG[1], University Hospital Zurich[2]*

**Introduction:**
Loss to follow-up and missing data are two of the most common reasons for clinical studies failure. Implementing digital methods in clinical trials has the potential to increase participants retention and procedural compliance, while reducing participant burden and maintaining their satisfaction. We recently conducted an innovative trial utilizing only digital methods to assess the accuracy of a wearable medical device for fertility tracking, and therein we examined participants' retention, compliance, and satisfaction.

**Methods:**
We designed a prospective longitudinal study in women to assess the relative accuracy of a multi-parameter wearable fertility device to detect ovulation ("Ava Fertility Tracker", Ava AG). Participants (n=66) wore the device nightly for up to 6 cycles, syncing their bracelet, taking body-temperature measurements, and urinary luteinizing hormone tests to determine their ovulation-day each cycle. Participants were recruited remotely through social media, online registration platforms, and email invitations. We collected all patient-reported outcomes and data from the wearable via a mobile app, wherein the study coordinator could monitor daily participant activity and send procedures reminders when forgotten. Participants could contact an independent customer support team for technical support. Finally, we surveyed the participants' perception of the site-less study design.

**Results:**
Participants were Swiss-residing women with an average age of 27.5 years(SD=4.1, range=19-36). Overall, 92% of participants completed the minimum requirement of trial (3 cycles) and 48.5% completed 6 cycles. Women who responded to the satisfaction survey (n=56, 85%) rated their experience with the social media recruitment (83%), online registration (98%) and online invitations (98%) as good or very good. 61% of respondents considered the trial design easy or very easy to integrate into their everyday life, which might be correlated to the observed high compliance (87% of study days had all three procedures conducted). Two thirds of participants (64%) preferred some personal contact with research staff, particularly during the onboarding process. Furthermore 98% of respondents found the study coordinator's remote support very helpful and 78% of participants were highly satisfied with the remote technical support.

**Conclusion:**
In this report we demonstrated that using digital approaches for clinical studies leads to a high rate of completion (92%) and procedural compliance (87%), while maintaining participants' satisfaction (>90% good or very good). This suggests site-less design could help maximize clinical data collection while minimizing participants' burden. Future studies with longer follow-up time will be needed to confirm these findings and assess whether the sampled population is biased towards digital natives. Moreover, digital approaches raise data protection and privacy concerns given the sensitivity of collected data. Overall, we believe that increasing the utilization of digital approaches in reproductive health research could increase the quality and the quantity of the data collected in this underrepresented research field.

**100**

F. Capecchi[1], L. Imbach[1], M. Schubring-Giese[1]

**Stimulus induced repetitive periodic or ictal discharges (SIRPIDs) are associated with high prevalence of non-convulsive status epilepticus and high mortality.**

*University Hospital of Zurich[1]*

**Introduction:**
Stimulus induced repetitive periodic or ictal discharges (SIRPIDs) are a rare EEG pattern in critically ill patients and associated with poor prognosis. However, its clinical significance regarding epileptic risk and anticonvulsive treatment is yet unclear.

**Methods:**
In a retrospective analysis, we reviewed 32 patients with SIRPIDs according to the American Clinical Neurophysiological Society (ACNS) criteria. SIRPIDs occurred after standardized painful stimulus in the hand during a standard 20-minute EEG. These cases were investigated regarding seizures, non-convulsive status epilepticus (according to Salzburg consensus criteria) and mortality.

**Results:**
In 23/32 patients (71.9%), SIRPIDs were associated with either non-convulsive status epilepticus (20/32, 62.5%) or seizures (3/32, 9.4%). In 75% of the patients with concurrent status epilepticus, SIRPIDs occurred after status epilepticus (on average 6 days later), but in 4 patients (20%) they were observed before a later to come status epilepticus. One patient suffered from non-convulsive status epilepticus two days before and one day after the appearance of SIRPIDs. In 8 patients the status epilepticus was refractory or super-refractory and 3 patients died before resolution of the status epilepticus. The overall mortality in the cohort was 47%. Mortality after occurrence of SIRPIDs was independent from status epilepticus.

**Conclusion:**
These findings corroborate the hypothesis that SIRPIDs are epileptiform interictal phenomena, commonly co-occurring with non-convulsive status epilepticus. Furthermore, SIRPIDs are associated with therapy-refractory course of status epilepticus. These findings suggest that initiation of prophylactic anticonvulsive treatment for SIRPIDs might be beneficial.

**101**

J. Ehrsam[1], S. Hillinger[1], O. Lauk[1], D. Schneiter[1], I. Schmitt-Opitz[1], M. Schuurmans[2], I. Inci[1]

**Surgical management of bronchial stump complication in cadaveric lobar lung transplantation**

*University Hospital, Department of Thoracic Surgery, Zurich, Switzerland[1], University Hospital, Division of Pneumology, Zurich, Switzerland[2]*

**Introduction:**
Lobar lung transplantation (LLTx) allows the use of oversized grafts for small recipients. In this technically demanding and not widely adopted procedure, prolonged air leak, kinking of vascular anastomoses and remaining dead space are frequent complications. We describe our experience in treatening the rarely reported bronchial stump insufficency (BSI) after LLTx.

**Methods:**
Between 1993-2016 we performed 120 cases of LLTx in our center. Among these, 3 developed BSI with empyema. They underwent accelerated treatment, consisting of radical debridement of the pleural cavity, packing with wet dressings of diluted 10% povidoneiodine, closure of the bronchial fistula, repeated change of dressings every 2 to 3 days until the chest is macroscopically clean and finally reinforcement of the stump with omentoplasty.

**Results:**
Case details who developed BSI were:
A) 48 year old female with Langerhanscell histiocytosis and BSI of the resected left lower lobe;
B) 44 year old male with cystic fibrosis and BSI of the resected right lower lobe;
C) 62 year old male with idiopathic pulmonary fibrosis and BSI of the resected right lower lobe.
Occurrence of fistula was observed 78 days, 29 days and 39 days after LLTx in A, B and C, respectively. Four surgical steps were necessary in case A and C, two in case B. Case A and B recovered well within 6 and 3 days of ICU and had 22 and 39 days overall re-hospitalization, respectively. Case C died 10 days after successful fistula revision due colitis with sepsis in aplasia.

**Conclusion:**
Bronchus stump after lower lobectomy in LLTx may cause secretion congestion, focal inflammation that results in BSI. Bronchus stump may not be avoided in case of LLTx with right lower lobe resection. Insufficiency can be treated successfully utilizing a multiple stage procedure with suture of the bronchus and covering with omentum flap.

**102**

J. Ehrsam[1], D. Schneiter[1], S. Hillinger[1], C. Caviezel[1], I. Schmitt-Opitz[1], M. Schuurmans[2], I. Inci[1]

**Cause of death after lung transplantation – a single center analysis**

*University Hospital, Department of Thoracic Surgery, Zurich, Switzerland[1], University Hospital, Division of Pneumology, Zurich, Switzerland[2]*

**Introduction:**
Postoperative cause of death in lung transplantation and time to its occurrence is reported occasionally. All causes of deaths in our recipients who underwent lung transplantation were investigated.

**Methods:**
We retrospectively analyzed all recipients transplanted between 1992 and 2018, with follow-up of October 2019. Median (min-max) survival was calculated to compare tendencies of incidence between groups.

**Results:**
Among all 521 transplantations performed, 333 recipients (63.9%) died. Median time to death was 40 (0-278) months.
Deaths which occurred within 1 month after transplantation were predominantly due to primary graft dysfunction (N=15, 4.5%), followed by cytomegalovirus infection (N=9, 2.7%), major bleeding (N=6, 1.8%) and idiopathic hyperammonemia (N=4, 1.2%).
Among all non-cytomegalovirus-infections (N=63, 19.9%), pneumonia (N=36, 10.8%) was the major cause of death, followed by colon perforation (N=12, 3.6%) and cholangitis (N=4, 1.2%). Observation time was median 21(0-230), 11.5(1-278) and 55(28-122) months, respectively.
Among patients with malignomas, death due to lymphoma (N=10, 3.0%) occurred after a median of 29.5(12-67) months, death due to carcinoma (N=36, 10.8%) after 92(19-219) months.
Cerebrovascular insult/bleeding led to 13 deaths (3.9%) after a median of 9(0-181) months. Death due to acute rejection (N=4, 1.2%) was observed at a median of 9(0-45) months. Chronic lung allograft dysfunction (CLAD) was diagnosed in 129 cases (38.7%), being the largest group with CLAD only as cause of death in 77 patients at a median onset of 53(5-246) months; CLAD and additional infection (N=44, 13.2%) median onset 39(5-145) months; CLAD and additional multi organ dysfunction (N=8, 2.4%) median onset 78(18-198) months. Cardiac (N=19, 5.7%) and renal failures (N=5, 1.5%) occurred late: median 103(0-271) months and 84(17-150) months, respectively.

**Conclusion:**
There is a large variety of causes of death after lung transplantation with a dominant role of infection, CLAD and carcinoma. With increasing follow-up time, infection becomes less prevalent and CLAD and carcinoma are observed more frequently.

**103**

K. Kusejko[7, 8], K. Zens[8], K. Darling[6], N. Khanna[5], H. Furrer[1], P. Vetter[3], E. Bernasconi[4], P. Vernazza[2], H. Günthard[7, 8], R. Kouyos[7, 8], J. Nemeth[7]

**Potential impact of latent tuberculosis on reducing the frequency of opportunistic diseases in HIV-infected individuals**

*Bern University Hospital[1], Cantonal Hospital St Gallen[2], Geneva University Hospital[3], Regional Hospital Lugano[4], University Hospital Basel[5], University Hospital Lausanne[6], University Hospital Zurich[7], University of Zurich[8]*

**Introduction:**
Approximately 28% of the human population (1.2 billion people) harbour Mycobacterium tuberculosis (MTB), with the overwhelming majority of infected individuals (more than 90%) not developing disease. Recent findings in the animal model suggest that latent infection with MTB (LTBI) may have symbiotic effects by protecting against MTB-unrelated infections via activation of the innate immune system. So far, potential interactions of latent MTB infection in HIV-infected individuals have not been investigated.

**Methods:**
We included all participants of the Swiss HIV Cohort Study with at least one documented MTB test. LTBI was defined as either a positive skin reactivity test or a positive IGRA test; patients who developed active MTB were excluded. Logistic regression was used to analyse the frequency of the most common opportunistic infections and laboratory conditions in the SHCS between patients with and without LTBI. In addition, linear regression was used to detect differences in the set point viral load between patients with and without LTBI. In multivariable models we corrected for baseline demographic characteristics, i.e., year of HIV diagnosis, HIV transmission risk group and ethnicity. In the analysis of opportunistic diseases, we corrected as well for the CD4 nadir.

**Results:**
A total of 13,675 SHCS patients had at least one MTB test documented, of whom 1027 (7.68%) had a LTBI and 316 (2.31%) developed active MTB. Patients with LTBI had significantly lower odds of having oral candidiasis (unadjusted odds ratio (OR) = 0.31, $p < 0.0001$; adjusted OR = 0.61) and oral hairy leukoplakia (unadjusted OR = 0.36, $p < 0.0001$; adjusted OR = 0.72, $p = 0.028$) as compared to MTB uninfected patients. In the case of other opportunistic diseases, the significant interaction with LTBI disappeared after correcting for demographic confounders and CD4 nadir. LTBI was associated with a reduced set-point viral load 0.27 (95%-confidence interval = [0.35, 0.20] log-reduction in the univariable, and 0.24 [0.32, 0.18] in the adjusted model).

**Conclusion:**
The finding that LTBI is independently associated with a reduced risk for oral candidiasis and oral hairy leukoplakia points towards a yet not appreciated interaction between LTBI and other infections. In addition, a significant reduction of the setpoint viral load in asymptomatic HIV-infected individuals suggests a more complex interaction between MTB infections and HIV than previously assumed.

**104**

J. Ehrsam[1], S. Hillinger[1], I. Schmitt-Opitz[1], D. Schneiter[1], I. Inci[1]

**Risk of Malignancy after Lung Transplantation: A Single Center Experience**

*University Hospital, Department of Thoracic Surgery, Zurich, Switzerland[1]*

**Introduction:**
Although malignancy is considered a common complication alter lung transplantation, profound studies about incidence, characterization, risk assessment and morbidity and mortality are scarce. Therefore we analyze all recipients at our center.

**Methods:**
All 521 lung transplant recipients at our center between 1992 and 2018 were retrospectively assessed for pre-transplant history and post-transplant onset of malignoma (censor date 01.05.2019). The incidence of occurrence was analyzed using Kaplan-Meier survival. Risk factors to develop a malignoma were assessed by multiple Cox-regression.

**Results:**
During the observation period, 3.1 % (N = 16) recipients were transplanted with a history of a cured malignoma, not reoccurring within at least 5 years. After transplantation, 3.1% (N =1 6) recipient developed a lymphoma, 22.1% (N=115) developed skin cancer and 11.7% (N=63) a non-skin-malignoma. Within non-skin-malignomas, gastrointestinal carcinomas (41.3%, N=26) and lung carcinomas (15.9%, N=1 0) were the predominant groups. Of note, 6 out of 10 lung carcinomas originated from the donor lung. 6.9% (N = 36) of the recipients died of malignoma, accounting for 10.8% of all observed deaths (N=333). The incidence of non-skin-malignancies was alter 1 year 2.4%, alter 5 years 10.5% and alter 10 years 24.4%. The incidence of skin cancer was at 1 year 1.8%, at 5 years 16.3% and at 10 years 35.8%. Multiple Cox-regression revealed that age >50 years (HR2.8; 95%CI 1.7-4.6) and the underlying diseases of emphysema (HR2.9: 95%CI 1.7-4.9) and interstitial pulmonary fibrosis (HR2.5; 95%CI 1.4-4.6) were independent risk factors to develop a non-skin-maligonoma.

**Conclusion:**
Post-transplant malignancies are an important reason for morbidity and mortality in lung transplantation. Screening for malignancies during follow up is crucial, especially when considering the increasing risk by the current trend toward an older recipient population, underlying diseases with a smoking history as weil as extended donor lungs.

**105**

J. Ehrsam[1], S. Hillinger[1], I. Schmitt-Opitz[1], D. Schneiter[1], I. Inci[1]

**Charlson-Deyo-Comorbidity-Index Predicts Long-Term Survival in Lung Transplantation**

*University Hospital, Department of Thoracic Surgery, Zurich, Switzerland[1]*

**Introduction:**
The Charlson-Deyo-Comorbidity-Index is a popular age independent score to predict long term survival. It incorporates 17 weighted comorbidity conditions and is established in a variety of clinical fields. However, the feasibility for lung transplantation is not yet tested. We therefore validate this score for primary graft dysfunction (PGD), short- to long-term survival and onset of ch ronic allograft dysfunction (CLAD).

**Methods:**
The Charleston-Deyo-Comorbidity-Index was assessed in all 466 lung transplant recipients at our center between 1992-2015. Discriminative ability was calculated by the area under the ROC curve (AUC) for 30-day to 10-year survival, severe PGD (grade III) and onset of CLAD. An AUC of 0.5 was considered as non-predictive and 1.0 as maximally predictive. Multiple Cox-regression was used to detect independent risk factors for mortality in the score. All calculations were adjusted for unilateral transplantation, retransplantation, recipient age, idiomatic pulmonary fibrosis, preoperative intensive care unit stay and marginality of the donor (Oto-Donor-Score).

**Results:**
Median Charslon-Deyo-Comorbidity-Index was 1 (range 1-5). PGD had an AUC of 0.65 (95%CI 0.59-0.72). The predictability increased from 30-day AUC0.58 (95%CI 0.48-0.69) over 1-year AUC0.67 (95%CI 0.60-0.73) to 10-year survival AUC0.72 (95%CI 0.67-0.78). A trend of decreased predictability was observed for onset of CLAD at 1-year AUC0.64 (95%CI 0.55-0.76) to 10-years AUC0.60 (95%CI 0.55-0.66). Multiple Cox-regression revealed the following comorbidities of the index as independent risk factors for mortality: congestive heart failure HR1.40 (95%CI 1.01 -1.94), coronary disease needing intervention HR1.72 (95%CI 1.10-2.68), end-stage diabetes mellitus HR5.93 (2.12-19.58), moderate liver disease HR2.53 (95%CI 1.71-3.74) and peripheral vascular disease HR2.43 (95%CI 1.1 8-5.00).

**Conclusion:**
The Charlson-Deyo-Comorbidity-Index has a fair prediction for PGD, mid-term survival and onset of CLAD and a good prediction for long term survival after lung transplantation. This score might be used for further clinical decision making in lung allocation. A different weighing and sub-categorization may even improve its prediction.

**106**

F. Scholkmann[1], T. Restin[2], M. Reinehr[3]

**Indications for an additional and overlooked vascular system of the human placenta: Preliminary results from an ongoing study**

*Biomedical Optics Research Laboratory, Department of Neonatology, University Hospital Zurich, University of Zurich, Zurich, Switzerland[1], Department of Neonatology, University Hospital Zurich, University of Zurich, Zurich, Switzerland[2], Institute for Clinical Pathology, University Hospital Zurich, University of Zurich, Zurich, Switzerland[3]*

**Introduction:**
Reports have been published for many years by Asian research groups describing the discovery and investigation of an additional vascular system in mammals termed the “primo vascular system” (PVS). This system has been shown to consist of primo nodes (PNs) and primo vessels (PVs) which differ from the vascular and lymphatic system. Although the discovery could be of high significance, the PVS is largely unknown by Western scientists.

**Methods:**
We investigated several human placentas with the aid of optical, fluorescence and electron microscopy.

**Results:**
In the placentas, parts of the PVS could be identified and analyzed. The PVS was detected by locating PNs on the surface of the placenta and pulling with a tweeter on them until a thread (the PV) was visible connecting the PN. The diameter of the PVs was about 50-100 µm, in agreement with previous reports. Staining of the placental tissue with Trypan Blue revealed a complex network of PVs and PNs along the umbilical cord and the connection of the umbilical cord with the placenta. The microscopic analysis showed that the PVS samples extracted by us resembled those shown in publications by the Asian research groups.

**Conclusion:**
Our initial investigation revealed that there are indeed vascular structures present on the surface of the placenta never before reported in medical textbooks and by Western scientists. In the next step, we plan to prove that these vascular structures are indeed a novel type of the vascular system which is distinct from the vascular and lymphatic system. We also aim to investigate the three-dimensional network structure of the PVS of the human placenta in detail.

**107**

H. Meister[2], M. Weller[2], S. Pascolo[1], P. Roth[2], T. Weiss[2]

**Engineered mRNA-based multifunctional chimeric antigen receptor (CAR) T cells show anti-tumor activity in glioblastoma**

*Department of Dermatology, University Hospital Zurich, Zurich, Switzerland[1], Department of Neurology and Brain Tumor Center, University Hospital Zurich, Zurich, Switzerland[2]*

**Introduction:**
CAR T cell therapy is a rapidly evolving immunotherapeutic anti-cancer strategy, which has shown impressive responses in extracranial malignancies and is currently also being explored for the treatment of glioblastoma. However, CAR T cell exhaustion caused by the immunosuppressive brain tumor microenvironment is a major challenge limiting the therapeutic efficacy. One strategy to overcome this problem is arming CAR T cells with pro-inflammatory cytokines. However, the administration of virally transduced stable cytokine expressing multifunctional CAR T cells comes with a higher risk of toxicity impeding clinical translation.

**Methods:**
Multifunctional CAR T cells were generated by co-transfection of in-vitro-transcribed mRNAs encoding for a Natural-killer receptor group 2 member D (NKG2D) based chimeric antigen receptor and the pro-inflammatory cytokines interleukin (IL) 12 and interferon (IFN) α2. Their anti-tumor activity was subsequently studied in vitro using co-culture assays and in vivo in an orthotopic immunocompetent glioma mouse model. Furthermore, we investigated mRNA electroporation as a transient strategy to improve the anti-tumor activity of virally transduced stably CAR-expressing T cells.

**Results:**
mRNA-based NKG2D CAR T cells efficiently lysed glioma cells in vitro. Cytolytic activity as well as effector cytokine expression were enhanced upon transfection of mRNAs encoding IL-12 and INF-α2. In vivo, repetitive intravenous administrations of NKG2D-based CAR T cells conferred a survival benefit in immunocompetent orthotopic glioma-bearing mice which was further improved upon co-electroporation of mRNAs encoding for IL-12 and INFα2. Treatment with viral transduced stable CAR expressing T-cells boosted by mRNA-based cytokine transfection was superior compared to treatment with fully mRNA-based multifunctional CAR T cells. Surviving mice were long-term protected against a tumor re-challenge. Systemic administration of mRNA-based multifunctional CAR T cells was tolerated without signs of toxicity.

**Conclusion:**
Engineering of IL-12 and IFNα2 expressing NKG2D based CAR T cells by means of mRNA transfection is feasible and a strategy to enhance the anti-glioma activity with low risk of toxicity.

**108**

B. Kovacs[13], S. Reek[3], C. Sticherling[12], A. Linka[9], P. Ammann[8], N. Krasniqi[2], A. Müller[11], R. Kobza[10], J. Schlaepfer[1], T. Reichlin[5], L. Haegeli[6], K. Mayer[7], H. Burri[4], A. Saguner[13], J. Steffel[13], F. Duru[13]

**Which patients are most likely to benefit from the wearable cardioverter-defibrillator? – findings from the Swiss WCD registry**

*Centre hospitalier universitaire vaudois, service de Cardiologie[1], GZO Spital Wetzikon, Abteilung für Kardiologie[2], Hirslanden Klinik Aarau[3], Hôpitaux Universitaires de Genève, service de cardiologie[4], Inselspital Bern, Klinik für Kardiologie[5], Kantonsspital Aarau, Klinik für Kardiologie[6], Kantonsspital Graubünden, Abteilung für Kardiologie[7], Kantonsspital St. Gallen, Klinik für Kardiologie[8], Kantonsspital Winterthur, Klinik für Kardiologie[9], Luzerner Kantonsspital, Klinik für Kardiologie[10], Stadtspital Triemli, Klinik für Kardiologie[11], Universitätsspital Basel, Klinik für Kardiologie[12], Universitätsspital Zürich, Klinik für Kardiologie[13]*

**Introduction:**
The wearable cardioverter-defibrillator (WCD) has established itself as a temporary protection from sudden arrhythmogenic death in selected patients at risk. However, it is still of debate which patients and for what duration benefit from its use. Therefore, appropriate patient selection is key. This study reports the results of the Swiss WCD registry with an emphasis on implantable cardioverter-defibrillator (ICD) implantation rate and ICD therapies.

**Methods:**
We retrospectively reviewed the indications, baseline characteristics and administered therapies in patients prescribed a WCD at 12 participating centers rom 2014 until 2018 in Switzerland. Further data on medical therapy, WCD therapy adherence, and ICD implantation rates were collected.

**Results:**
456 patients were included in our study comprising of 66% of all Swiss patients prescribed a WCD in the examined time period. The mean age was 57 ±14 years, 18% were female and the mean ejection fraction (EF) was 32% ± 13. Indications for WCD use and appropriate shock rate are shown in the figure. Patients wore the WCD over a median of 58 days (range 1-455) with a median daily average wear-time of 22.6 hours (range 0.6-23.8). 17 appropriate therapies were administered by the WCD to a total of 12 patients leading to a therapy rate of 2.6% over a median wear-time of 16 days (range 2-79) and to a therapy rate of 3.9% in patients with ischemic cardiomyopathy (ICM) with an EF ≤35%. ICM with an EF ≤35% and bridging to ICD-implantation or heart transplantation as indication for WCD prescription were significantly associated with an appropriate therapy ($p = 0.046$ and 0.003, respectively). One patient with non-ischemic cardiomyopathy (NICM) received an appropriate therapy (0.8%). The mean EF in patients receiving an appropriate therapy by the WCD was also significantly lower ($p = 0.04$). No patient with wearing the WCD for congenital/inherited heart disease or risk stratification with an EF >35% had a therapy administered by the WCD. There were no inappropriate therapies during the investigated time period. After cessation of WCD use EF improved to 38% ±13; ultimately, 212 patients (46%) were implanted with an ICD. During a follow-up of 476 days (range 7-2347) 22 (9.8%) patients received an appropriate therapy by their ICD. Four of the 22 had prior appropriate therapy by the WCD.

**Conclusion:**
ICM with severely reduced EF was the most common indication for WCD use leading to a high rate of appropriate therapy by the WCD. This, however, did not translate in a higher rate of appropriate ICD-therapies during follow-up in this subpopulation possibly due to significant improvements in their ejection fractions. Patients with NICM or congenital/inherited heart disease seldom had an appropriate therapy by the WCD.

**109**

R. Schweizer[3], A. Taddeo[1], M. Waldner[3], H. Klein[3], N. Fuchs[3], P. Kamat[3], S. Targosinski[3], A. Barth[3], M. Drach[2], V. Gorantla[4], P. Cinelli[5], J. Plock[3]

## Adipose-derived Stromal Cell Therapy Combined with a Short Course Non-Myeloablative Conditioning Promotes Long-term Graft Tolerance in Vascularized Composite Allotransplantation

*Department for BioMedical Research, University of Bern[1], Department of Dermatology, University Hospital Zurich (USZ), University of Zurich[2], Department of Plastic Surgery and Hand Surgery, Regenerative and Reconstructive Plastic Surgery Laboratory, University Hospital Zurich (USZ), University of Zurich[3], Department of Surgery, Wake Forest Baptist Medical Center, Institute for Regenerative Medicine, Winston-Salem, NC, USA[4], Department of Traumatology, Division of Surgical Research, University Hospital Zurich (USZ), University of Zurich[5]*

**Introduction:**
The risks of chronic immunosuppression limit the utility of vascularized composite allotransplantation (VCA) as reconstructive option in complex tissue defects. We evaluated a novel, clinically translatable, radiation-free conditioning protocol that combines anti-lymphocyte serum (ALS), tacrolimus and CTLA4-Ig with adipose-derived stromal cells (ASCs) to allow VCA survival without long-term systemic immunosuppression.

**Methods:**
Full-mismatched rat hind-limb transplant recipients received tacrolimus (0.5mg/kg) for 14 days and were assigned to four groups: CTRL received no conditioning; ASC-group received CTLA4-Ig (10mg/kg BW s.c. POD 2, 4, 7) and donor ASCs (1x10^6 iv, POD 2, 4, 7, 15, 28); ASC-CYP-group received CTLA4-Ig, ASC plus cyclophosphamide (50mg/kg i.p., POD 3); ASC-ALS-group received CTLA4-Ig, ASCs plus ALS (500µL i.p., POD 1, 5). Banff grade III or 120 days were endpoints. Blood samples were analyzed for chimerism and Tregs by flow cytometry and for cytokines by multiplex assays.

**Results:**
ASCs dose-dependently suppressed alloresponse in vitro. Median rejection-free VCA survival was 28 days in CTRL (n=7), 34 in ASC (n=6) and 27.5 in ASC-CYP (n=4). In contrast, ASC-ALS achieved significantly longer, rejection-free VCA survival to postoperative day 120 in 6/7 animals (86%). This correlated with persistent multi-lineage donor-cell chimerism up to 16 weeks, and elevated systemic and peripheral allograft skin Tregs, with no signs of acute cellular rejection in skin and muscle samples. Long-term VCA accepting animals were negative for donor-specific antibodies and vasculopathic changes at endpoint suggesting absence of chronic rejection. Cytokines such as IL-1β, IL-2, TNF-α, IP-10 and MCP-1 and MCP-3 were elevated in animals rejecting early and might serve as early markers for rejection.

**Conclusion:**
Taken together, a regimen comprised of short-course tacrolimus, repeated CTLA4-Ig and ASC administration, combined with cell-depletion with ALS, promotes long-term VCA survival without chronic immunosuppression promoting sustained donor-cell chimerism and elevated Treg levels.

**110**

R. Schweizer[2, 3, 5], M. Waldner[2, 3, 5], S. Oksuz[3, 4, 5], W. Zhang[3, 5], C. Komatsu[3], J. Plock[2], V. Gorantla[3, 5], M. Solari[3, 5], L. Kokai[3, 5], K. Marra[1, 3, 5], J. Rubin[1, 3, 5]

**Evaluation of Porcine versus Human Mesenchymal Stromal Cells from Three Distinct Donor Locations for Cytotherapy after Rapid Expansion with Endothelial Growth Medium**

*Department of Bioengineering, University of Pittsburgh, USA[1], Department of Plastic Surgery and Hand Surgery, Regenerative and Reconstructive Plastic Surgery Laboratory, University Hospital Zurich (USZ), University of Zurich[2], Department of Plastic Surgery, University of Pittsburgh Medical Center, USA[3], Department of Plastic, Reconstructive and Aesthetic Surgery, Gulhane Military Medical Academy, Turkey[4], McGowan Institute for Regenerative Medicine, University of Pittsburgh, USA[5]*

**Introduction:**
Mesenchymal stromal cell (MSC)-based cytotherapies fuel the hope for reduction of chronic systemic immunosuppression in allotransplantation. MSCs harvested from distinct anatomical locations may have different behavior and lead to different outcomes in preclinical research. Herein we compared human and porcine MSCs from omental fat (O-ASC), subcutaneous fat (SC-ASC) and bone marrow (BM-MSC) under rapid culture expansion with endothelial growth medium (EGM).

**Methods:**
MSCs isolated from pigs and deceased human organ donors were compared for yield, viability, cell size, population doubling times (PDT), surface marker expression and differentiation potential after rapid expansion with EGM. Immunosuppressant toxicity on MSCs was investigated in vitro for four different standard immunosuppressive drugs. Immunomodulatory function was compared in mixed lymphocyte reaction assays (MLR) with/without immunosuppressive drug influence.

**Results:**
Human and porcine omental fat yielded significantly higher cell numbers than subcutaneous fat. Initial PDT was significantly shorter in ASCs than BM-MSCs and similar thereafter. Viability was reduced in BM-MSCs. Porcine MSCs were positive for CD29, CD44, CD90, while human MSCs expressed CD73, CD90 and CD105. All confirmed adipogenic differentiation capacity. Cell sizes were comparable between groups and were slightly larger in human cells. Rapamycin revealed slight, mycophenolic acid strong and significant dose-dependent toxicity on viability/proliferation of almost all MSCs at therapeutic concentrations. No relevant toxicity was found for Tacrolimus and Cyclosporin A. Immunomodulatory function was dose-dependent and similar between groups. Immunosuppressants had no significant adverse effect on MSC immunomodulatory function.

**Conclusion:**
MSCs from different harvest locations and donor species differ in terms of isolation yields, viability, PDT, and size. However, we could not detect relevant differences regarding immunomodulatory function in presence of or without immunosuppressants after rapid expansion with EGM. Human and pig O-ASC, SC-ASC and BM-MSC share similar immunomodulatory function in vitro and warrant data extrapolation from large animal studies. These findings need consideration in preclinical and clinical MSC applications.

**111**

H. Klein[2], P. Niggemann[2], P. Buehler[3], F. Lehner[2], R. Schweizer[2], D. Rittirsch[2], N. Fuchs[2], M. Waldner[2], P. Steiger[3], P. Giovanoli[2], T. Reding[1], R. Graf[1], J. Plock[2]

## Pancreatic Stone Protein Predicts Sepsis in Severely Burned Patients Irrespective of Trauma Severity

*Pancreas Research Laboratory, Department of Visceral Surgery & Transplantation[1], UniversitätsSpital Zürich, Department of Plastic Surgery and Hand Surgery[2], Universitätsspital Zürich, Institute of Intensive Care Medicine[3]*

**Introduction:**
The burn victim's inherent state of hyperinflammation frequently camouflages septic events delaying the initiation of targeted intensive care therapy. Accurate biomarkers are urgently needed to support sepsis detection before patients' clinical deterioration.

**Methods:**
Analysis of biomarker kinetics (PSP, routine markers) was per- formed on 90 patients admitted to the Zurich Burn Center between May 2015 and October 2018 with burns □>15% total body surface area with regard to infection and sepsis (Sepsis-3) over a 14-day time course.

**Results:**
PSP differentiated between sepsis, infection and sterile inflamma- tion from day 3 onward with an area under the curve of up to 0.89 ($P < 0.001$); therefore, competing with procalcitonin (area under the curve = 0.86, $P < 0.001$). Compared to routine inflammatory biomarkers, only PSP demonstrated a significant interaction between time and presence of sepsis – signifying a steeper increase in PSP levels in septic patients as opposed to those exhibiting a nonseptic course (interaction $P < 0.001$). Event-related analysis demonstrated tripled PSP serum levels within 72 hours and doubled levels within 48 hours before a clinically apparent sepsis.

**Conclusion:**
PSP is able to differentiate between septic and nonseptic patients during acute burn care. Its steep rise up to 72 hours before clinically overt deterioration has the potential for physicians to timely initiate treatment with reduced mortality and costs.

**112**

G. Panteloglou[3], P. Zanoni[3], L. Rohrer[3], J. Kuivenhoven[2], A. Rimbert[2], A. Tybjaerg-Hansen[1], N. Dalila[1], W. März[4], A. von Eckardstein[3]

**The coatomer (COP I) complex limits the cell-surface abundance of the LDL receptor and cellular LDL uptake**

*Department of Clinical Biochemistry, Rigshospitalet, Copenhagen University Hospital, Copenhagen, Denmark[1], Department of Pediatrics, Section of Molecular Genetics, University Medical Centre Groningen, University of Groningen, Groningen, Netherlands[2], Institute of Clinical Chemistry, University and University Hospital of Zurich, Switzerland[3], Vth Department of Medicine, Medical Faculty Mannheim, University of Heidelberg, Mannheim, Germany; Clinical Institute of Medical and Chemical Laboratory Diagnostics, Medical University Graz, Graz, Austria; SYNLAB Academy, SYNLAB Holding Deutschland GmbH, Augsburg and Mannheim, Germany[4]*

**Introduction:**
The LDL receptor (LDLR) is the main regulator of LDL-c levels in plasma. For up to 40% of patients with familial hypercholesterolemia, the genetic origin is unknown. We here aimed at the discovery and validation of novel genes limiting the uptake of LDL into hepatocytes.

**Methods:**
We performed a genome wide genome-wide RNA interference screening in Huh7 hepatocarcinoma cells. We used other siRNAs to knock-down individual candidate genes in Huh7 cells to measure their effect on the uptake of LDL and the cell surface abundance of LDLR with FACS, on the mRNA expression of sterol-regulated genes by RT-PCR, and the glycosylation of LDLR by Western Blotting. We explored data banks for the association of mutations in candidate genes with LDL-c levels.

**Results:**
Three out of nine members of the COP I complex were among the top hits limiting LDL uptake into Huh7 cells. Knock down of the COP I subunits resulted in marked reduction of LDL uptake and LDLR cell surface abundance. Loss of COP I genes did not suppress LDLR gene expression but interfered with the normal glycosylation of LDLR. We found rare mutations in specific COP I genes associated with elevated levels of LDL-c in the general Danish population as well as in German coronary heart disease patients with very high LDL-c levels who are not affected by mutations in the canonical FH genes.

**Conclusion:**
Our findings suggest that the COP I genes regulates the trafficking of LDLR and hence LDL-c plasma levels.

**113**

L. Roth[5], X. Muller[5], R. Graf[5], Y. Tian[5], B. Imthurn[4], P. Imesch[1], F. Taran[1], N. Ochsenbein[2], M. Choschzick[3], P. Clavien[5], P. Dutkowski[5], O. De Rougemont[5]

**Ischemia Reperfusion Injury in Uterus Transplantation**

*Department of Gynecology, University Hospital Zurich[1], Department of Obstetrics, University Hospital Zurich[2], Department of Pathology, University Hospital Zurich[3], Department of Reproductive Endocrinology, University Hospital Zurich [4], Department of Surgery and Transplantation, University Hospital Zurich[5]*

**Introduction:**
Uterus transplantation is a novel treatment for patients with absolute uterine infertility (AUFI). The main indication is the Mayer-Rokintansky-Küster-Hauser-Syndrome, characterized by a congenital absence of the uterus. The birth of a healthy baby boy 2015 in Sweden two years after live donor uterus transplantation, was a breakthrough. Although most programs worldwide actually use live donor grafts, some, e.g. Belgium, Czech Republic and Brazil opted for a deceased donation program. Given that, the uterus is not a vital organ, the risk for healthy donors might not be justified for a non-lifesaving procedure. In 2017, the first baby was born from a deceased graft in Brazil. Deceased donor grafts are inherently exposed to ischemia. Knowledge on the impact of ischemia reperfusion injury (IRI) on organ viability, pregnancy and birthrates is scarce. We therefore aim to investigate the role of ischemia reperfusion injury on short-term graft viability in an isolated ex-vivo uterus perfusion model. We then established a novel rodent uterus transplant model to study long-term graft viability, pregnancy and live birth.

**Methods:**
Uterus grafts were procured from brain-dead donor pigs and cold stored on ice for either 2h (control) or 24h (cold storage). The grafts were perfused ex-vivo with autologous blood during 3h to simulate the early phase of transplantation. IRI was quantified by macroscopic changes of the organ during reperfusion and by analyzing tissue and perfusate samples at different time points during perfusion. The right uterine horn was procured from female Brown Norway (BN) and Lewis rats. After donor surgery, uterus transplantation was perfomed orthotopically. After 4 weeks of graft stabilization, the transplanted animals were ready to mate.

**Results:**
In the control group (n=4), tissue reperfusion was homogenous resulting in rhythmic muscle contractions. In contrast, 24 hours of cold storage (n=4) resulted in in-homogenous reperfusion leading to rapid tissue swelling without visible contractions and disrupted endometrium. Hypoxanthine, a marker of ischemia, accumulated 2.89-times more during the prolonged ischemia phase and increased during the first 60 minutes of reperfusion up to 3.59-times higher compared to the control group.
In total, 8 rats were successfully transplanted (n=4 BN, n=4 Lewis rats). BN rats presented a 100% pregnancy rate with a live birth rate of 75%. 1 rat had a miscarriage. In comparison, the Lewis rat strain showed a pregnancy rate of 50% (n=2). Both pregnant rats delivered healthy babies.

**Conclusion:**
The first part of our preliminary results clearly show that cold storage affects the viability of uterus grafts. This may have significant impact on patient safety and possibly pregnancy rate as well. Therefore, the second part with the successful establishment of a rodent uterus transplantation and mating procedure provide a unique experimental setting to investigate the impact of ischemia reperfusion injury on live birth. Both will allow us to understand mechanisms of ischemia reperfusion injury in uterus transplantation, a prerequisite for the implementation of a deceased donor program.

**114**

I. Condado Morales[1], R. Moos[1], A. Aguzzi[1], S. Hornemann[1]

**Microfluidic Approaches for the Sensitive Detection and Characterisation of Prion Aggregates**

*Institute of Neuropathology, University Hospital Zurich[1]*

**Introduction:**
Prion diseases (PD) are a group of fatal neurodegenerative disorders associated to the self-assembly of the prion protein (PrP). PrP exists as PrPC in non-infected hosts and as PrPSc (Scrapie) as the main infectious agent. PD share common characteristics to other neurodegenerative disorders such as Parkinson's and Alzheimer's disease, like the aggregation of PrP into large amyloid plaques. The main difference of PD's to other protein misfolding diseases is that they have the unique characteristic of being highly infectious. The infectious agent, PrPSc, has been challenging to study due to its low abundance as well as polydisperse nature. As such, microfluidics may provide an alternative to the classical biophysical techniques, due to their sensitivity enhancement and unique fluid control that allows purely diffusional mixing. Here we propose to apply the diffusional sizing technique in combination with immunoassay detection for the size analysis of prion aggregates in mouse brain homogenates. Furthermore, we propose the development of a prion amplification assay by combining real-time quaking-induced conversion (RT-QuIC) that exploits the self-replication nature of prions, with droplet-based microfluidics.

**Methods:**
In particular, we use Microfluidic Diffusional Sizing technique in combination with the specificity of immunoassays, termed the Immuno Diffusional Sizing (IDS) to characterise the size of PrP native and aggregates in solution. We exploit the purely diffusive mixing in microchannels where the protein of interest moves into a co-flowing auxiliary stream. The diffused and non-diffused fractions are quantified with an immunoassay such as TR-FRET or ELISA, which confers specificity to the method and makes it suitable for complex mixtures.
In order to enhance the sensitivity of RT-QuIC, it could be developed in a microdroplet format. The low volume of the order of nano- to picolitres of the microdroplets allows avoiding false positives caused by spontaneous primary nucleation of the proteins, thus increasing its limit of detection. With enhanced sensitivity over bulk RT-QuIC, it could be applied to an earlier detection of PD, to detect aggregates in CSF or other body fluids. The development of such assay can provide information on the stochasticity of primary nucleation, which is normally difficult to study with bulk techniques.

**Results:**
The IDS method has been used to the size analysis of recombinant PrPC, as well as ex vivo PrPC and prion aggregates found in brain homogenates from tg20 non-infected and RML6-infected mice. A microdroplet-based amplification assay has been previously applied to the detection of insulin aggregates (Pfammatter et al 2017). We aim to apply such technology to other proteins associated to PDs, such as PrP or alpha-Synuclein, related to Parkinson's disease.

**Conclusion:**
In conclusion, this approach will enable the implementation and optimisation of a microfluidic platform for prion characterisation and amplification, with potential use in high throughput screening of aggregation inhibitors and as a potential tool for prion strain discrimination. By further theoretical modelling of the seeded reactions, a deeper understanding of the aggregation mechanism will be acquired and could potentially lead to the development of early diagnosis and therapeutic strategies for prion diseases. The final piece of work will give a general overview of the in vitro aggregation process of PrP, as well as an established diagnostics assay that could be applicable to use with patients of CJD or Parkinson's disease.

**115**

S. Hussung[3], B. Pfefferle[3], F. Nollmann[3], R. Klar[3], A. Devisme[1], M. Boerries[1], U. Wittel[2], R. Fritsch[4]

**Ex vivo Drug Testing in Patient-Derived Pancreatic Cancer Organoids**
**Challenges and Potential Applications**

*Department für Biometrie, Epidemiologie und Medizinische Bioinformatik, Universitätsklinikum Freiburg, Medizinische Fakultät, Universität Freiburg[1], Uniklinik Freiburg, Klinik für Allgemein- und Viszeralchirurgie[2], Uniklinik Freiburg, Klinik für Innere Medizin I (Hämatologie, Onkologie und Stammzelltransplantation)[3], Universitätsspital Zürich, Klinik für Medizinische Onkologie und Hämatologie[4]*

**Introduction:**
The identification of individual therapeutic vulnerabilities in pancreatic cancer (PDAC) based on tumor molecular profiling is extremely challenging. 92%-95% of PDACs harbor oncogenic KRAS mutations and there is currently no successful targeting strategy for KRAS-driven tumors. Patient-derived pancreatic cancer organoids (PDOs) preserve genotype and phenotype of individual tumors and therefore uniquely allow for testing drug sensitivities ex vivo in a co-clinical setting.

**Methods:**
For this project, we generated a large living biobank of PDOs derived from patients undergoing resection or surgical biopsy of pancreatic adenocarcinoma at the University of Freiburg Pancreatic Cancer Center. Organoid cultures undergo a standardized work-up including histology and quantitative KRAS mutational analysis by digital droplet PCR (ddPCR), followed by NGS panel or whole exome sequencing.

**Results:**
For drug testing, we have been optimizing an ex vivo drug screening protocol for individual drugs and rational drug combinations. We present and discuss findings from drug testing in 2D vs. 3D culture as well as in the presence and absence of stroma cells. Drug testing results are aligned with individual tumor's molecular profiles. We discuss challenges and further optimization with a future co-clinical trial in mind.

**Conclusion:**
Ex vivo drug testing of patient-derived organoids holds great potential as a novel tool for pancreatic cancer precision oncology.

**116**

S. Saeedi Saravi[2, 4], G. Camici[1], T. Lüscher[1], T. Michel[3], J. Beer[2, 4]

**Age-dependent changes of aquaporin-1 modulate platelet/endothelial dysfunction in atherothrombosis**

*Center for Molecular Cardiology, University of Zurich, Schlieren[1], Department of Internal Medicine, Cantonal Hospital Baden[2], Division of Cardiovascular Medicine, Department of Medicine, Brigham and Women's Hospital, Harvard Medical School, Boston, USA[3], Laboratory for Platelet Research, Center for Molecular Cardiology, University of Zurich, Schlieren[4]*

**Introduction:**
Background: Aging is a condition which favors the development of cardiovascular diseases (CVD), including atherothrombosis. Aquaporins are a family of transmembrane water channels, and some isoforms such as aquaporin-1 (AQP1) may be permeable to hydrogen peroxide (H2O2), a major reactive oxygen species (ROS). Since increased ROS and oxidative stress are known as a major pathophysiology of age-associated atherothrombosis, exploration of the effects of aging on aquaporin-1 (AQP1) expression and its role in platelet/endothelial function is relevant. Therefore, we hypothesized that aging induces AQP1 expression in both platelets and endothelial cells that will result in H2O2-regulated platelet hyperactivity and endothelial dysfunction and a subsequent increased risk of atherothrombosis.

**Methods:**
Methods: Human aortic endothelial cells (HAEC) from passages 4 (young) to 15 (senescent in aging) were lyzed and subjected to immunoblotting to probe AQP1 abundance and the signaling phospho/total proteins (AMPK, acetyl-coA-carboxylase (ACC), caveolin-1 and eNOS). Endothelial cells were transfected with constructs containing H2O2 biosensor, HyPer, targeted either to cell nucleus or cytosol for further fluorescence live cell imaging. Human blood samples were taken and divided into 2 groups of AQP1 inhibitor (Bacopaside II, 10 µM)-treated and non-treated to examine the platelet binding to vWF and rolling on vWF-coated microchannels under high-shear flow conditions (100 dyn/cm2) in order to mimic blood flow in stenosed arteries. Platelet impedance aggregation in response to low concentrations of collagen (2 µM), ADP (1 µM) and TRAP (1 µM) were recorded for 5 min followed by pre-treatment with Bacopaside II, and analyzed by AGGRO/LINK® software (Chrono-Log).

**Results:**
Results: Immunoblot analyses demonstrated that aging leads to significant increases in AQP1 protein abundance and phosphorylation of caveolin-1 and ACC (Ser79), along with decreases in phosphorylation of eNOS (Ser1177) and AMPK (Thr172) compared to young control (for each, $P<0.01$, $n>6$). Fluorescence imaging documented a robust H2O2 production in the senescent endothelial cell cytosol, but not nucleus, and activated "atherogenic" NF-κB-regulated genes, whereas an increase in the transcription of Nrf2-modulated "atheroprotective" genes was seen in the young cells ($P<0.05$). On the other hand, AQP1 inhibition reduced platelet binding on vWF and thrombus formation, whereas platelet rolling velocity and distance traveled on vWF under high-shear flow increased compared to control group ($P<0.01$). Also, a decrease was found in platelet response to collagen, ADP and TRAP following 5 min of induction ($P<0.05$).

**Conclusion:**
Conclusion: These studies, for the first time, demonstrate that aging induces AQP1 expression in endothelial cells and platelets, and subsequently modulates the dephosphorylation of AMPK/eNOS. These may increase the risk of endothelial dysfunction and elevated platelet aggregation/thrombus formation under shear stress. Additionally, age-dependent activation of ACC may lead to enhanced production of pro-coagulant and pro-inflammatory cytokines. Therefore, pharmacologic inhibition of AQP1 could potentially be exploited as a therapeutic strategy for attenuation/prevention of age-related atherothrombosis.

Keywords: Aging; Aquaporin-1; Platelet/endothelial dysfunction; Atherothrombosis

**117**

Z. Kotkowska[1, 2], P. Johansen[2], C. Halin Winter[1], P. Schineis[1], E. Varypataki[2], I. Kolm-Djamei[2], T. Kündig[2]

**Photochemical internalization (PCI): a novel method for induction of cytotoxic CD8 T-cell responses with cancer vaccines**

*ETH Zurich, Department of Chemistry and Applied Biosciences, Zurich, Switzerland[1], University Hospital Zurich, Department of Dermatology & University of Zurich, Zurich, Switzerland[2]*

**Introduction:**
**Background:** Cancer is a public health matter and one of the leading causes of death worldwide. Currently, cancer vaccination approaches aim at enhancing the patient's immune response against the tumor. Cytotoxic T lymphocytes (CTLs) are the most potent anti-tumor immune cells, capable of recognizing tumor antigen presented by antigen presenting cell (APC) in complex with major histocompatibility complex class I molecule (MHC I). Nowadays, the main problem of cancer vaccines is the inefficacious delivery of antigens to the cytosol of APC, which results in not efficient stimulation of CTLs. Photochemical internalization (PCI) may bypass this problem based on the topical co-delivery of antigens with a photosensitizer. Upon their endocytosis by APC, the photosensitizer localizes in the endosomal membranes. When the skin is subsequently treated with light, activation of the photosensitizer leads to the membrane disruption and release of the endosomal content into the cytosol.

**Objectives:** The primary objective is to develop PCI-based vaccination as a method for the stimulation of anti-cancer CTLs. As a secondary objective, treatment-associated innate immune reactions in the skin are studied.

**Methods:**
Mice received intradermal injections of photosensitizer and antigen. Eighteen hours later, light was administered, and at various time points thereafter, skin and lymph nodes were harvested for analysis of innate immune responses by histology, fluorescence microscopy, and flow cytometry. Antigen-specific CD8 T-cell responses were measured in blood and spleens by flow cytometry. Finally, the effect of PCI-based immunization was tested in mouse-model of melanoma.

**Results:**
Histological and microscopic analysis of the skin revealed light- and photosensitizer-dose-dependent innate inflammatory responses in the skin. The symptoms of inflammation observed in the treated skin included acanthosis, edema and infiltration of immune cells. PCI improved proliferation of antigen-specific CD8 T cells and their cytokine production as compared with PCI-free vaccination. Proliferation was independent on CD4 T-helper cells as observed using MHC class II-deficient mice. Finally, PCI facilitated anti-tumour responses and survival in mice with subcutaneous melanoma.

**Conclusion:**
The results demonstrate the PCI can facilitate stimulation of CTLs with tumor-suppressing capacity. The results further suggest that early innate immune responses may be an important part of the mechanism of action of PCI-based vaccines. Further studies will also focus on how these innate immune responses translate into effective anti-tumor CTL responses.

**118**

M. Mueller[1, 2], M. Heinzelmann[2], B. Roth Z'graggen[2], M. Schlaepfer[1, 2], B. Beck-Schimmer[1, 2]

**Sevoflurane's primary metabolite hexafluoroisopropanol attenuates the inflammatory response in human effector and target cells, mediated by inhibition of NF-κB p65 translocation**

*Institute of Anesthesiology, University and University Hospital Zurich, Zurich, Switzerland[1], Institute of Physiology, University of Zurich, Zurich, Switzerland[2]*

**Introduction:**
Hexafluoroisopropanol (HFIP), the primary sevoflurane metabolite, is detected in blood samples of patients after sevoflurane anesthesia. Sevoflurane-mediated protection has been described decades ago, recently an immunomodulatory effect of HFIP has been demonstrated in septic rodents, attenuating inflammation and improving survival. Immunomodulation was not yet confirmed in humans and the mode of action has to be investigated. This study aimed to determine the impact of HFIP on inflammation in human blood samples, representing the effector cell compartment and to evaluate the interference with the inflammatory NF-κB pathway in human pulmonary microvascular endothelial cells (HPMEC) as target cells.

**Methods:**
Blood samples from healthy volunteers were stimulated with LPS and treated with HFIP (4 and 8mM). Interleukine-6 (IL-6) as an important biomarker in the cascade of severe inflammation was determined. For NF-κB pathway analyses, HPMEC were stimulated with LPS and treated with 8mM HFIP. IL-6 was measured in cell supernatant. Cytoplasmic and nuclear proteins were harvested, and Western blots allowed quantifying phosphorylation of IKK-complex, degradation of IκBα, as well as nuclear transmigration of NF-κB. Results are expressed as relative values of the LPS treated samples. Means and standard deviation were calculated and one-way ANOVA and Dunnet post-hoc test were used to compare groups. Statistical significance was set at $p<0.05$.

**Results:**
HFIP dose-dependently attenuated the LPS-induced inflammatory response in human blood samples (LPS vs. LPS+HFIP 4mM: 100±0 vs. 63±16%, $p<0.001$; LPS vs. LPS+HFIP 8mM: 100±0 vs. 17±9%, $p<0.001$). Likewise, the LPS-induced IL-6 expression was attenuated in HPMEC representing the vascular compartment (LPS vs. LPS+HFIP 8mM: 100±0 vs. 54±12%, $p<0.001$). HFIP accentuated the LPS-mediated phosphorylation of the IKK complex and degradation of IkBα, but impaired nuclear transmigration of the p65 subunit (LPS vs. LPS+HFIP 8mM: 100±0 vs. 44±17%, $p<0.001$).

**Conclusion:**
This study shows a dose-dependent attenuation of a LPS-induced inflammatory reaction in human effector and target cells using HFIP. Moreover, our data reveal, that inhibition of NF-κB p65 transmigration might be the molecular mechanism responsible for HFIP-mediated protection.

**119**

A. Moncsek[2], C. Wu[2], S. Benke[1], E. Friebel[3], B. Becher[3], B. Müllhaupt[2], J. Mertens[2]

**Understanding the contribution of immune cells to fibrosis progression in NASH**

*Cytometry Facility, University of Zurich, Zurich, Switzerland[1], Department of Gastroenterology and Hepatology, University Hospital Zurich, Zurich, Switzerland[2], Institute of Experimental Immunology, University of Zurich, Zurich, Switzerland[3]*

**Introduction:**
Non-alcoholic steatohepatitis (NASH) is a chronic liver disease with strongly increasing prevalence worldwide. NASH is histologically characterized by the presence of hepatic inflammation and hepatocyte injury (ballooning) due to accumulation of liver fat (steatosis). NASH has been shown to correlate with an increased risk of liver fibrosis, cirrhosis and hepatocellular carcinoma (HCC). The key predictor of NASH-related progression to cirrhosis is fibrosis. Activated resident and infiltrating immune cells play a crucial role in perpetuating chronic liver injury and fibrosis progression as they induce activation of stromal fibroblasts. In NASH, the detailed composition and interactions of hepatic immune cells are not well understood.
To examine the mechanisms that drive the progression from hepatic fat deposition to fibrosis and eventually HCC, we investigate immune cell-related mechanisms of fibrosis development in NASH. More in detail, we will identify and characterize immune cell subpopulations in NASH, which are the drivers of fibroblast activation and fibrosis progression.

**Methods:**
Multiplex flow cytometry was employed to characterize the immune landscape of human liver biopsies from NASH patients and liver samples from a diet-induced murine NASHmodel. In addition, immunofluorescence was performed to investigate immune cell and fibroblast localization.
Furthermore, immune cell subpopulations from mice receiving standard chow or western diet were isolated and characterized regarding their secretion of pro-fibrotic factors using in situhybridization, mRNA expression and immune assays. In addition, supernatant transfer assays were performed to study and modulate the impact of soluble immune cell-mediated pro-fibrotic factors on fibroblasts activation *in vitro*.

**Results:**
Multiplex flow cytometry and immunofluorescence analysis of human and mice liver tissue suggest that a dynamic immune cell infiltration into the liver contributes to the progression of NASH. In addition, immune cells locate in direct proximity to stromal cells allowing for direct cell-cell interaction. Preliminary *in vitro* experiments showed the ability of different murine immune cell subpopulations to secrete pro-fibrotic factors and to activate fibroblasts. In addition, this immune cell-mediated fibroblast activation was more pronounced when immune cells where derived from NASH mice.

**Conclusion:**
NASH-related activation and infiltration of immune cells drives the progression of fibrosis via immune cell-secreted pro-fibrotic factors. Inhibition of these factors could be a new approach to ameliorate liver fibrosis and could represent a NASH and HCC preventive strategy.

**120**

M. Valletti[1], D. Eshmuminov[1], C. Gutschow[1], K. Lehmann

**Survival benefit in gastric cancer patients with chemotherapy-responsive peritoneal disease: a plea for a better local control**

*Visceral and Transplant Surgery, University Hospital Zurich, 8091 Zurich, Switzerland[1]*

**Introduction:**
The optimal treatment in patients with gastric cancer and peritoneal disease remains controversial. Some guidelines indicate palliative treatment only, while others consider surgical treatment, in case of positive lavage cytology or limited peritoneal disease. Here we analyzed the role of peritoneal disease in patients with gastric cancer, and the prognostic relevance of response to neoadjuvant therapy.

**Methods:**
Patients with adenocarcinoma of the stomach or esophago-gastric junction from a single center operated between 2011 and 2019 were analyzed. According to histology and lavage cytology patients were classified into four groups: A) negative peritoneal cytology, B) positive cytology, converted to negative after neoadjuvant chemotherapy, C) no conversion after chemotherapy, and D) patients with visible peritoneal metastasis.

**Results:**
Overall, n=204 patients were included. The majority of n=151 (74%) patients had no peritoneal disease, n=14 (7%) had positive lavage cytology which converted to negative after chemotherapy, no conversion was observed in n=6 (3%), and peritoneal metastasis was detected in n=33 (16%). Median overall survival was not reached in patients without metastasis and was 22 months (95% CI:17.2-27.5) after conversion, resulting in three-year survival rates of 61% and 40%. Median overall survival was reduced to 15 months (95% CI: 10.7-19.3) in patients without conversion or visible peritoneal metastasis, without difference between the two groups. The conversion rate to negative lavage cytology depends on the perioperative chemotherapy regimen and was significantly higher with FLOT compared to ECF (p=0.018).

**Conclusion:**
Patients with positive lavage cytology who convert after neoadjuvant chemotherapy have a better overall survival compared to non-converted patients, and surgical treatment should therefore be considered. However, peritoneal recurrence remains frequent after conversion and therefore urges for better local control.

**121**

M. Schmidt[4], M. Studer[7], A. Kunz[7], S. Studer[1], J. Bonvini[4], M. Bueter[6], L. Kook[3], S. Haile[3], B. Beck-Schimmer[2, 4, 5], M. Schläpfer[4, 5]

**Does oxycarbon improve cerebral oxygenation during apnea? A mono-center randomized cross-over trial inspired by aviation-research.**

*Clinical Trials Center, University Hospital Zurich, Zurich, Switzerland[1], Department of Anesthesiology, University of Illinois at Chicago, Chicago, USA[2], Epidemiology, Biostatistics and Prevention Institute, University Zurich, Zurich, Switzerland[3], Institute of Anesthesiology, University Hospital Zurich, Zurich, Switzerland[4], Institute of Physiology, University Zurich Irchel, Zurich, Switzerland[5], Institute of Surgery, University Hospital Zurich, Zurich, Switzerland[6], Swiss Air Force, Bern, Switzerland[7]*

**Introduction:**
Several projects in aviation and high-altitude research have demonstrated improved cerebral perfusion, performance, and oxygenation by adding CO2 in hypobaric hypoxia [1]. Hypoxia is of concern also in anesthesia, especially in patients with a decreased oxygen reserve.
This study aimed to test whether 5% CO2 in O2 increases the time until significant cerebral hypoxia was detected by near-infrared spectroscopy (NIRS) in bariatric patients under normobaric conditions.

**Methods:**
After ethical approval, patients (18-65 years), BMI >35kg/m2 requiring anesthesia for bariatric surgery at the University Hospital Zurich were included in this mono-centric, single-blinded, controlled, crossover proof-of-concept study.
According to the randomization, patients received first oxycarbon (5%CO2, 95%O2) or the comparator (95%O2). After a wash in of 10 minutes, apnea was performed by disconnecting the ventilator from the endotracheal tube until NIRS value dropped by 20% from baseline, or until SpO2 decreased to 80% (as a safety termination criterion). Reventilation was then performed until parameters returned to baseline. With the crossover design, the procedure was repeated with the other substance (oxycarbon or comparator). During apnea, NIRS, vital signs, and bispectral index were recorded permanently, blood samples were drawn at the beginning and the end of the apnea.

**Results:**
Based on the power calculation, 30 patients were enrolled. Tissue oxygenation drop by 20% was not reached in this patient population, as the safety termination criterion was reached first. The time until oxygen saturation dropped to 80% was similar after both interventions (mean difference -6s [95%CI from -19 to 7] p=0.37), but both cerebral tissue oxygenation index and PaO2 were higher after oxycarbon administration (difference of 1.46% [95% CI: from 0,33 to 2.59], p=0.018, and 0.6 kPa [95 CI: 0.12 to 1.09], p=0.021, respectively).

**Conclusion:**
This study demonstrates improved blood and cerebral tissue oxygenation upon oxycarbon administration. The possible link to a clinical scenario for improvement of cerebral oxygenation has to be investigated in future trials.

References
1. Imray CH et al, Clin Sci (Lond) 2003

**123**

H. Gannon[2], T. Zoa[2], M. Kiessling[1], E. Levanon[3], W. Hahn[2], M. Meyerson[2]

**Dependency on the adenosine deaminase ADAR1**

*Department of Medical Oncology and Hematology, University Hospital Zurich, 8091 Zurich, Switzerland[1], Department of Medical Oncology, Dana-Farber Cancer Institute, Boston, MA 02215, USA[2], The Mina and Everard Goodman Faculty of Life Sciences, Bar-Ilan University, 52900 Ramat Gan, Israel[3]*

**Introduction:**
Systematic exploration of cancer cell vulnerabilities can inform the development of novel cancer therapeutics.

**Methods:**
Here, through analysis of genome-scale loss-of-function datasets, we identify adenosine deaminase acting on RNA (ADAR or ADAR1) as an essential gene for the survival of a subset of cancer cell lines.

**Results:**
ADAR1-dependent cell lines display increased expression of interferon-stimulated genes. Activation of type I interferon signaling in the context of ADAR1 deficiency can induce cell lethality in non-ADAR1-dependent cell lines. ADAR deletion causes activation of the double-stranded RNA sensor, protein kinase R (PKR). Disruption of PKR signaling, through inactivation of PKR or overexpression of either a wildtype or catalytically inactive mutant version of the p150 isoform of ADAR1, partially rescues cell lethality after ADAR1 loss, suggesting that both catalytic and non-enzymatic functions of ADAR1 may contribute to preventing PKR-mediated cell lethality.

**Conclusion:**
Together, these data nominate ADAR1 as a potential therapeutic target in a subset of cancers.

**125**

S. Hiltbrunner[4], C. Britschgi[4], C. Magnani[4], L. Bankel[4], T. Nguyen-Kim[5], P. Gulati[6], W. Weder[2], I. Schmitt-Opitz[2], O. Lauk[2], C. Caviezel[2], A. Tabor[1], P. Schröder[1], A. Knuth[4], C. Münz[6], C. Renner[4], R. Stahel[4], O. Boyman[3], U. Petrausch[7], A. Curioni-Fontecedro[4]

**A phase I clinical trial of malignant pleural mesothelioma treated with locally delivered autologous fibroblast activating protein (FAP)-targeting chimeric antigen receptor (CAR) T cells**

*Biontech, Mainz[1], Departement of Thoracic Surgery, University Hospital Zurich[2], Department of Immunology, University Hospital Zurich, and Faculty of Medicine, University of Zurich[3], Department of Medical Oncology and Hematology, University Hospital Zurich[4], Institute of Diagnostic and Interventional Radiology; University Hospital Zurich[5], Institute of Experimental Immunology, University of Zurich[6], Onkozentrum Zürich, Swiss Tumor Immunology Institute[7]*

**Introduction:**
Malignant pleural mesothelioma (MPM) is a cancer with an increasing incidence worldwide due to the use of asbestos. MPM is incurable despite the use of multimodal treatment. Tumor spread confined to the thoracic cavity is a hallmark of MPM, providing a rational for local treatment. We developed a chimeric antigen receptor (CAR) targeting fibroblast activating protein (FAP), a cell-surface antigen that we have shown to be highly expressed in epithelial cancers.

**Methods:**
Using a Δ-CD28-costimulated CAR, we initiated a phase I clinical trial (NCT01722149) to determine the safety and persistence of intra-pleurally administered anti-FAP-CAR T cells in the blood. A single dose of 1x $10^6$ re-directed T cells was administered through a pleural catheter. Patients were monitored on an intensive care unit for 48h. Clinical evaluations of on-target and off-tumor toxicity were assessed for 3 months. Laboratory analyses included cytokines, CRP and detection of CAR T cells in the pleural effusion and blood over time. Radiological evaluation with PET-CT scans was performed as standard of care.

**Results:**
Three patients with metastatic MPM were treated, with all patients receiving at least two cycles of chemotherapy prior to CAR T-cell administration. No CAR T-cell-related toxicities were observed. Intense monitoring for cytokine release syndrome showed significant changes on a subset of cytokines. CAR T cells were detected in the peripheral blood after treatment. Activity of the patients' redirected T cells was confirmed in vitro. With a median follow-up of 21 months, 1 out of 3 patient is alive as to date.

**Conclusion:**
This is the first clinical trial to be concluded using intra-pleural administration of anti-FAP CAR T cells in patients with pleural mesothelioma. The treatment was well tolerated without any evidence of treatment-related toxicity. Persistence of CAR T cells was documented in the periphery.

**126**

L. Imbach[1], R. Christian[1], M. Oertel[2], L. Stieglitz[2]

**A multimodal electrophysiological map of the anterior nucleus of the thalamus from intraoperative deep brain recordings in epilepsy patients**

*Department of Neurology, University Hospital and University of Zurich, Zurich, Switzerland [1], Department of Neurosurgery, University Hospital Zurich, Zurich, Switzerland[2]*

**Introduction:**
Deep brain stimulation (DBS) in the anterior nucleus of the thalamus (ANT) is an effective therapy for patients with pharmaco-resistant focal epilepsy. However, treatment response varies considerably between patients and previous studies showed that the anti-epileptic effect of anterior thalamic DBS may depend crucially on the stimulation site within the ANT.

**Methods:**
We aim to improve DBS efficacy in epilepsy patients by providing an electrophysiological map of the ANT based on intra-operative electrophysiological neuro-monitoring. To this end, we recorded intraoperatively 16-channel surface EEG, local field potentials (LFP), and micro-electrode recordings (MER) along the implantation trajectory in 7 patients (14 trajectories). Data post-processing included spike-frequency analysis, spectral analysis of local field potentials and cortico-subcortical coherence.

**Results:**
Along a superior-to-inferior trans-ventricular trajectory, LFP, MER and spectral coherence provided reproducible and complementary electrophysiological information: Theta band (4-8 Hz) LFP activity was maximal in the most superior part of the ANT with a decreasing gradient along the trajectory. MER spike frequency analysis revealed a bimodal distribution with two independent peaks 7mm and 10mm after the ventricular ANT border, respectively. Spectral coherence analysis revealed increased theta band coupling between the LFP and ipsilateral temporal EEG electrodes with maximal coherence towards frontal derivation in the upper ANT and towards temporal regions in the middle part of the ANT.

**Conclusion:**
These findings corroborate the feasibility to use intra-operative electrophysiological monitoring for delineating the ANT. The main oscillatory activity in the ANT is in the theta band and might serve as a biomarker to determine the most effective stimulation site within the ANT and to enhance treatment response after DBS implantation. Coherence analysis might provide a useful tool to optimize the stimulation site within the ANT on an individual level depending on the cortical seizure focus.

**127**

J. Wang[8], I. Jelcic[8], L. Mühlenbruch[3], V. Haunerdinger[11], N. Toussaint[9], Y. Zhao[2], C. Cruciani[8], W. Faigle[8], M. Foege[8], T. Binder[7], T. Eiermann[4], L. Opitz[6], L. Fuentes-Font[5], R. Reynolds[5], W. Kwok[1], J. Nguyen[10], J. Lee[10], A. Lutterotti[8], C. Münz[12], H. Rammensee[3], M. Hauri-Hohl[11], M. Sospedra[8], S. Stevanovic[3], R. Martin[8]

**Tightly Linked HLA-DR15 Alleles Cooperate in Shaping an Autoreactive T Cell Repertoire in Multiple Sclerosis**

*Benaroya Research Institute at Virginia Mason, Seattle, WA 98101, USA[1], Biometric Research Program, Division of Cancer Treatment and Diagnosis, NCI, NIH, Rockville, MD 20850, USA[2], Department of Immunology, Institute of Cell Biology, University of Tubingen, 72076 Tubingen, Germany[3], Department of Transfusion Medicine, University Medical Center Hamburg-Eppendorf, 20251 Hamburg, Germany[4], Division of Neuroscience, Department of Brain Sciences, Imperial College London, London, UK[5], Functional Genomics Center Zurich, Swiss Federal Institute of Technology and University of Zurich, 8057 Zurich, Switzerland[6], Institute for Clinical Transfusion Medicine, Hospital Braunschweig, 38114 Braunschweig, Germany[7], Neuroimmunology and MS Research Section (NIMS), Department of Neurology, University Hospital Zurich, University of Zurich, 8091 Zurich, Switzerland[8], NEXUS Personalized Health Technologies, ETH Zurich, 8093 Zurich, Switzerland[9], One Lambda, Inc., a part of Thermo Fisher Scientific, West Hills, CA, USA[10], Pediatric Stem Cell Transplantation, University Children's Hospital Zurich, 8032 Zurich, Switzerland[11], Viral Immunobiology, Institute of Experimental Immunology, University of Zurich, 8057 Zurich, Switzerland[12]*

**Introduction:**
Many autoimmune diseases show a strong association with certain HLA molecules. Multiple sclerosis (MS) is a prototypical example with the HLA-DR15 haplotype as its strongest genetic risk factor, which amplifies the effects of some of the environmental contributors, such as Epstein Barr virus (EBV) infection and smoking. The HLA-DR15 haplotype contains two HLA-DR alleles, which give rise to the molecules DRA1*01:01/DRB5*01:01 (referred to as DR2a) and DRA1*01:01/DRB1*15:01 (referred to as DR2b). Despite the longstanding knowledge of this genetic linkage, the functional mechanisms by which the HLA-DR15 haplotype affects MS pathogenesis are not clear.

**Methods:**
We analyzed DR2a- or DR2b-presented immunopeptidomes by isolation of DR2a- or DR2b-peptide complexes using the allele-specific antibodies and subsequent liquid chromatography/mass spectrometry (LC/MS). We then synthesized potential pathogenic self-peptides included in DR2a- or DR2b-presented immunopeptidomes and tested their immunogenicity in HLA-DR15$^+$ HD and MS patients by using PBMCs and CD4$^+$ T cell clones (TCCs) from MS patients as the test objects.

**Results:**
Autoreactive CD4$^+$ T cells but also proinflammatory B cells are central pathogenetic factors, and since HLA-DR molecules present antigenic peptides to CD4$^+$ T cells, we characterized here the peptidomes presented by the two HLA-DR15 allomorphs in blood B cells, blood monocytes, and thymic tissues. Self-peptides derived from the HLA-DR α- and β-chain themselves are abundantly presented by the HLA-DR15 allelic products not only on peripheral blood B cells but also in thymic tissues. HLA-DR-derived self-peptides (HLA-DR-SPs) likely select an autoreactive CD4$^+$ T cell repertoire that is cross-reactive with certain environmental pathogens and disease-associated, pathogenic self-peptides. We further identified autoreactive CD4$^+$ T cell clones which recognize HLA-DR-SPs with low avidity and peptides from the infectious agents EBV and *Akkermansia*, as well as the novel MS autoantigen RAS guanyl-releasing protein 2 (RASGRP2), with high avidity.

**Conclusion:**
Our data demonstrate that the two MS-associated HLA-DR15 allelic molecules exert double functions both as antigen-presenting structures and as a source of peptides. This is relevant during thymic selection, peripheral maintenance of autoreactive T cells, and full activation thereof by MS-associated pathogens and disease-related autoantigens.

Acknowledgements: The project is supported by ERC Advanced Grant N°340733–HLA-DR15 in MS and by the Clinical Research Priority Program MS of the University Zurich

**128**

E. Felley-Bosco[3], J. Fonteneau[2], W. Qi[1], M. Ronner[3], A. Hariharan[3], C. Blanquart[2], H. Rehrauer[1]

**Contribution of RNA editing to mesothelioma heterogeneity**

*Functional Genomics Center Zurich[1], INSERM UMR 1232[2], Laboratory of Molecular Oncology, Thoracic Surgery, USZ[3]*

**Introduction:**
Recent studies have shown heterogeneity of genetic alterations and transcription profile in mesothelioma. In an experimental model of mesothelioma development in *Nf2+/-* mice exposed to asbestos (crocidolite) we have observed increased levels of A -> G mutations of RNA in pre-cancer lesions which were maintained in tumors (Rehrauer, Wu, et al., Oncogene, 2018). These changes result from the activity of adenosine deaminases acting on dsRNA (Adar1 and Adar2). One isoform of Adar1 is induced by interferon type 1, which is generally associated to anti-viral response. Our aim was to investigate how RNA editing contributes to mesothelioma heterogeneity.

**Methods:**
RNA editing levels in human mesothelioma were determined with the Alu editing index (AEI) computational tool using Mesothelioma TCGA RNA-seq data. Additional data were obtained using either primary mesothelioma cells or mesothelioma cell lines. When RNA-seq data was not available, *AZIN1* editing levels using RNA editing site-specific qPCR (RESS-qPCR) was used as surrogate. Levels of RNA editing were correlated to *ADAR1* and *ADAR 2* expression levels. Basal type 1 interferon signalling was based on expression of interferon-induced genes (ISG).

**Results:**
ADAR activity is heterogenous in mesothelioma and editing of some regions depends on *BAP1*, a tumor suppressor gene frequently mutated in mesothelioma. This is relevant since activation of type 1 interferon signaling has been observed in tumors with *BAP1* inactivation (Hmeliak, Sanchez-vega et al, Cancer Discovery 2018). Levels of A-to-G mutations in RNA are correlated to the expression of ADAR1 in TCGA mesothelioma data, primary mesothelioma cultures and mesothelioma cell lines. We have also observed that primary mesothelioma cultures that are sensitive to Measle oncolytic viruses and which have an intact *IFNB1* gene show a basal activation of type 1 interferon pathway and have an increased ADAR activity.

**Conclusion:**
Overall, our analysis confirm that RNA mutations contribute to mesothelioma heterogeneity and suggest that ADAR activity is relevant in the context of immunotherapies.

**129**

S. Souzan Salemi[1], S. Sheryl Preda[1], T. Tullio Sulser[1], D. Daniel Eberli[1]

**Effect of myostatin inhibitor on smooth muscle regeneration**

*University Hospital Zürich[1]*

**Introduction:**
Smooth muscle cells (SMCs) are the main component of the bladder detrusor muscle. Tissue engineering therapies utilizing smooth muscle regeneration may provide alternative treatments for diseases such as bladder dysfunction, urinary incontinence and erectile dysfunction. A major problem so far has been finding a reliable source of healthy SMCs that can be used for tissue engineering purposes. Myostatin is a negative regulator of muscle growth and differentiation also known as secreted growth differentiation factor (GDF8). Myostatin inhibitors are used in clinical trials as a therapy for skeletal muscle diseases but the role and the expression pattern of myostatin has not been reported yet within bladder SMCs. Thus the goal of our research is to improve the SMCs quality and quantity by inhibiting myostatin with suramin, a polyanionic compound that prevents TFG-β1's from binding to their receptors. For this purpose, we investigated the expression pattern of myostatin gene and protein in human and rat bladder SMCs. Furthermore, we examined, if a combination of myostatin with its inhibitor suramine could further increase the cell proliferation and cell number.Smooth muscle cells (SMCs) are the main component of the bladder detrusor muscle. Tissue engineering therapies utilizing smooth muscle regeneration may provide alternative treatments for diseases such as bladder dysfunction, urinary incontinence and erectile dysfunction. A major problem so far has been finding a reliable source of healthy SMCs that can be used for tissue engineering purposes. Myostatin is a negative regulator of muscle growth and differentiation also known as secreted growth differentiation factor (GDF8). Myostatin inhibitors are used in clinical trials as a therapy for skeletal muscle diseases but the role and the expression pattern of myostatin has not been reported yet within bladder SMCs. Thus the goal of our research is to improve the SMCs quality and quantity by inhibiting myostatin with suramin, a polyanionic compound that prevents TFG-β1's from binding to their receptors. For this purpose, we investigated the expression pattern of myostatin gene and protein in human and rat bladder SMCs. Furthermore, we examined, if a combination of myostatin with its inhibitor suramine could further increase the cell proliferation and cell number.

**Methods:**
Human and rat bladder derived SMCs were characterized by immunofluorescence and flow cytometry (FACS). The changes in gene and protein expression level for SMC specific markers: calponin, smoothelin, α-SMA, MyH11; and myostatin related proteins: Myostatin, Activin receptor IIB, Smad 2 and 3 and phospho Smad were investigated by immunostaining (WES). SMCs were cultured in the presence and absence of suramin, a pharmacological inhibitor of myostatin and myostatin protein. Cells proliferation was evaluated by WST-1 assay.

**Results:**
Expression was detected in SMCs at RNA level by real time PCR and at protein levels by WES and FACS analysis. The myostatin expressing cells showed the expression of Smad 2 and 3, calponin, smoothelin and MYH11. Treatment with suramin led to dose dependent increase in cell proliferation with 10, 20 and 30 mg/ml and decrease upon 100 mg/ml after 1, 2, 5 and 8 days compared to untreated controls. In suramin treated SMCs (20 mg/ml), myostatin expression was reduced on day 5 compared to day 1 and untreated control which led to increase in cell number. SMCs treatment with myostatin protein (100 ng/ml) resulted in reduced cell proliferation.

**Conclusion:**
Our study demonstrates for the first time that myostatin is expressed in bladder derived smooth muscle cells and may play an important role in cell proliferation and contraction. Inhibition of myostatin might lead to novel supporting strategies for improvement of smooth muscle cells for future tissue engineering applications.

**130**

M. Hilty[4], H. Hayward-Koennecke[4], C. Kaiser[2], F. von Kaenel[2], C. Esteban[1], S. Napolitano[3], F. Luchs[4], O. Mujkic[2], R. Iseli[2], S. Iseli[2], S. Broicher[5], O. Geisseler[5], G. Raetsch[1], E. Hafen[3], R. Martin[4], S. Bignens[2, 3], A. Lutterotti[4]

**MitrendS –an app-based hand function test for multiple sclerosis**

*Department of Computer Science, ETH Zurich, Switzerland[1], Institute for Medical Informatics, Berne University of Applied Sciences, Berne, Switzerland[2], MIDATA Cooperative, Zurich, Switzerland[3], Neuroimmunology and MS Research, Neurology Clinic, University Hospital Zurich, Zurich, Switzerland[4], Neuropsychology, Neurology Clinic, University Hospital Zurich, Zurich, Switzerland[5]*

**Introduction:**
Monitoring symptom progression in multiple sclerosis (MS) patients is challenging, because of the heterogeneity in clinical presentation. Generally accepted disability rating scales, such as the Expanded Disability Status Scale (EDSS) neglect upper limb- and other functions, especially at moderate and higher disability levels. Specifically designed mHealth tools provide the opportunity to investigate symptoms of MS more in depth than any prior method. This study investigates a newly developed tool to measure hand function on a tablet app called MitrendS and compares it with current clinical methods.

**Methods:**
This monocentric clinical study compares the gold standard for manual dexterity, the nine-hole peg test (NHPT), with two digital tests on a tablet app in 74 MS patients and 45 healthy controls. Participants with incomplete data were excluded. Healthy controls were compared with MS patients and within group comparisons between the gold-standard and app tests were performed. All participants completed the NHPT and two MitrendS specific hand dexterity tests called Line-Test and Points-Test with both hands.

**Results:**
A positive correlation (dominant: r=0.52, non-dominant: r=0.60) between the Points Test and the NHPT was demonstrated in MS patients. The Line Test did not correlate with the NHPT or the Points Test. When comparing controls to patients, the NHPT showed significant group differences. The NHPT strongly correlated with the EDSS score. All tests showed an age dependency, which is more pronounced in the NHPT than the app-based tests.

**Conclusion:**
Our data show that the comparison between analog methods and new digital measurements poses unique challenges. The Points-Test shows an excellent correlation with the NHPT. Together with the Line-Test, it has the potential to create an individual symptom profile for hand functions. Although further studies are needed to collect the necessary contextual information, it can be shown that the high individual differences, which can only be captured by digital tools, provide the opportunity to discriminate between symptoms in a ubiquitously available hand-function testing suite.

**131**

L. Jörimann[1, 2, 3], A. Inderbitzin[1, 2, 3], C. Schenkel[1], D. Braun[1, 2], C. Grube[1], H. Kuster[1], K. Metzner[1, 2], H. Günthard[1, 2]

**Characterization of the HIV-1 latent reservoir in early treated individuals**

*Division of Infectious Diseases and Hospital Epidemiology, University Hospital Zurich, Zurich, Switzerland[1], Institute of Medical Virology, University of Zurich, Zurich, Switzerland[2], Life Sciences Zurich Graduate School, University of Zurich, Zurich, Switzerland[3]*

**Introduction:**
The main barrier to cure HIV-1 infection in patients is the latent reservoir, a pool of latently infected CD4+ T cells containing replication-competent but transcriptionally silent provirus. The latent reservoir is established early during infection and persists even during suppressive antiretroviral treatment (ART). The latent reservoir is maintained through the longevity of latently, HIV-1 infected resting T cells, potential clonal expansion of those cells, and possibly, due to low-level virus replication followed by infection of new target cells, however, the mechanisms of persistence are not completely understood.

**Methods:**
The persistence of the latent reservoir through these mechanisms will be studied in patients who started ART in less than 180 days after primary HIV-1 infection. Viral diversity is low at this time point enabling the investigation of virus evolution, which is a marker for ongoing replication. Near full-length HIV-1 genome PCR and next generation sequencing will be applied to longitudinal patients' blood samples to assess virus evolution in latently HIV-1 infected T cells and potential emergence of drug-resistant viruses. Together with HIV-1 reservoir size estimates, viral load data and other clinical parameters, this study will allow us to estimate the impact of low-level replication on the maintenance of the latent reservoir in early treated individuals.

**Results:**
The near full-length PCR protocol was established using a nested hemi-length approach and shows good coverage in 62.5% for the first 24 patients' samples. Single cell capture of reactivated env expressing CD4+ T cells for later sequencing works with latent cell lines and CD4+ T cells harboring HIV vector.

**Conclusion:**
We were able to establish a protocol to amplify and sequence near full-length HIV-1 provirus from patients' samples. However, not all samples can be amplified, which could be due to possible deletions at the primer binding site and generally a small number of intact provirus. Furthermore, single cell capture assay can be used later on for single cell characterization of interesting patients' samples.

**132**

J. Schniering[1], H. Gabrys[2], M. Brunner[1], M. Maciukiewicz[1], C. Blüthgen[3], D. Kenkel[3], O. Distler[1], M. Guckenberger[2], M. Bogowicz[2], D. Vuong[2], K. Karava[2], T. Frauenfelder[3], S. Tanadini-Lang[2], B. Maurer[1]

**Computed tomography-based radiomics as novel diagnostic tool for detection and staging of interstitial lung disease in systemic sclerosis – transferability from experimental to human lung fibrosis**

*Center of Experimental Rheumatology, University Hospital Zurich, Switzerland[1], Department of Radiation Oncology, University Hospital Zurich, Switzerland[2], Institute of Diagnostic and Interventional Radiology, University Hospital Zurich, Switzerland[3]*

**Introduction:**
High resolution computed tomography (HRCT) is a cornerstone in the diagnosis and monitoring of interstitial lung disease (ILD) in systemic sclerosis (SSc). Radiomics is a promising research field, which automatically extracts mineable quantitative metadata from medical images, aiming to identify imaging biomarkers. In this study, we evaluated 1) the potential of CT-based radiomics features for diagnosis and staging of (experimental) ILD and 2) the transferability of radiomics signatures from mice to human ILD.

**Methods:**
Radiomics analysis was performed on micro-CT scans from bleomycin (BLM)-treated mice and NaCl-treated controls at days 3, 7, 14, 21, 28 and 35 after intratracheal BLM instillation (n=6-9/group), as well as on human HRCT scans from 98 SSc patients. In total, 154 radiomics features were extracted from segmented lungs using the in-house developed software Z-Rad (Python 2.7). Univariate analysis was performed to discriminate between healthy and diseased subjects as well as limited and extensive fibrosis (<20% and ≥20% disease extent on CT), and the transferability of radiomics signatures between mice and humans was quantified.

**Results:**
Radiomics features with good predictive performance (area under the receiver operating characteristic curve (AUC) >0.7 and p-value<0.05) were considered as candidate discriminators. Under this criterion, we identified 105/154 radiomics features, describing image intensity and texture that differentiated NaCl controls from BLM-treated mice and 56/154 features that discriminated limited (<20%) from extensive (>20%) BLM-induced ILD. In human SSc-ILD, 124/154 features differentiated ILD from non-ILD and 121/154 features discriminated limited from extensive fibrosis. Notably, for diagnosis 89 and for staging 46 features overlapped between mice and humans, resulting in 85% or 82% transferability, respectively.

**Conclusion:**
The results of this proof-of-concept study suggest that 1) the well-established mouse model of BLM-induced ILD is a valuable model system to test defined hypotheses in radiomics research and 2) that radiomics features show great potential as quantitative imaging biomarkers for diagnosis and staging of SSc-ILD.

**133**

C. Millan[1], L. Prause[1], N. Hensky[1], T. Sulser[1], D. Eberli[1]

**Culture of Cancer Cells in 3D Hydrogels Induces Secretion of EVs that Promote Invasion and Chemoresistance**

*USZ Urology Clinic[1]*

**Introduction:**
In cancer, extracellular vesicles (EVs) have been implicated as key mediators of metastasis owing to their ability to delivery molecular cargo from the primary tumor to distal pre-metastatic sites. Identifying the EV-specific proteins and RNAs that are involved could shed light on novel therapeutic targets and/or biomarkers for early-stage diagnosis. The source of EVs used for such studies is critical, but the vast majority majority of in vitro studies involving cancer EVs have been conducted using cells cultured on standard 2D plastic surfaces that may not reflect physiological gene/protein expression. Previously, we have shown that cancer cells cultured in a novel 3D hydrogel display enhanced expression of tumor-associated antigens in addition to chemoresistance, indicative of advanced-stage clinically relevant phenotypes, compared to the same cells cultured in 2D. Here, we demonstrate the striking effect that this 3D culture model can have on both the secretion behavior and the molecular cargo found in EVs with a focus on prostate cancer.

**Methods:**
Cells were cultured in a previously characterized 3D biopolymer scaffold composed of modified polysaccharides chitosan and alginate to simulate the tumor. For a range in comparisons we focused on 4 cell types: PC3 (aggressive prostate cancer cells), LNCaP (less aggressive prostate cancer cells), PNT1 (benign prostate epithelial cells), and adipose-derived stem cells (ADSCs; non-prostate cells included as controls). EVs secreted by cells in 3D were compared to those secreted by the same cells cultured in 2D (tissue culture plastic). Characterization of EVs was done by transmission electron microscopy (TEM), nanoparticle tracking analysis (NTA), and western blot for known EV markers. Molecular cargo of EVs was assessed via proteomics and RNA sequencing. Functional comparisons were performed on invading cancer cells treated with EVs, as well as response to chemotherapeutic treatment with or without EV stimulation.

**Results:**
All cell types showed heightened EV production when cultured in 3D, ranging from 2-5x increased EV-protein per cell depending on cell type. The size distributions in terms of EV-diameters did not vary across cell types or culture conditions as measured by nanoparticle tracking analysis, DLS, and TEM. Next generation sequencing (NGS) and proteomics analyses revealed dramatic alterations in EV content as a result of 3D culture. Principle component analysis performed on NGS data of the 500 genes of highest variance exhibited the highest magnitude of expression changes for the PC-3 cells and the ASCs. Gene ontology enrichment indicated ubiquitous down-regulation of genes involved in directing intracellular protein traffic for all cell types. Differences seen in proteomics were equally stark – an average of 400 extra proteins were detected in proteomics of 3D-EVs that were not found in 2D-EVs of the same cell type. EVs from cancer cells cultured in 3D resulted in nearly double the number of invading cancer cells in a matrigel invasion assay. In addition, 3D-EVs conferred nearly 15% higher survival to cancer cells treated with Doxorubicin compared to samples without EVs or with EVs from 2D cultured cells.

**Conclusion:**
The in vitro culture conditions of cancer cells has a profound effect on the cargo of secreted EVs. 3D culture of cancer cells elicits higher EV production, EVs with heightened functional effects related to metastatic cancer, and may be ideally suited for identification of novel therapeutic targets and/or liquid biopsy biomarkers for diagnostic applications.

**134**

S. Sun[2], M. Ronner[2], F. Frontini[2, 3], W. Qi[1], H. Rehrauer[1], A. Hariharan[2], M. Wipplinger[2], E. Felley-Bosco[2]

**Endogenous Retrovirus expression and activation of type-I interferons signaling in an experimental mouse model of mesothelioma development**

*Functional Genomic Center Zürich, ETH Zürich/University of Zürich, Zürich, Switzerland[1], Laboratory of Molecular Oncology, Department of Thoracic Surgery, University Hospital Zürich, Zürich, Switzerland[2], Section of Cell Biology and Molecular Genetics, University of Ferrara, Ferrara, Italy[3]*

**Introduction:**
Malignant pleural mesothelioma (MPM) is a rapidly progressive tumor. Recently, The Cancer Genome Atlas consortium revealed that type-I interferons (IFNs) signaling is associated with a better overall survival for MPM patients. Type-I IFNs are secreted by infected cells particularly viral pathogens, however, there is no viral infection in MPM. We made the hypothesis that it originates from activation of endogenous retrovirus (ERV) and double stranded RNA (dsRNA).

**Methods:**
ERV expression was analyzed in RNA-seq data from tissue in three groups of mice: sham, asbestos exposed mice without and with tumor. ERV and interferon stimulated genes (ISGs) expression was determined by qPCR. To assess the role of methylation, genomic DNA was submitted to sodium bisulfite treatment followed by quantitative methylation specific PCR. As positive control, DNA demethylation was induced in mouse mesothelioma derived primary RN5 cells by 5-Aza-2'-deoxycytidine (5-AzaC) treatment. dsRNA was quantified by flow-cytometry. To block the type-I IFN signaling, RN5 cells were treated with Ruxolitinib, a JAK1/2 inhibitor.

**Results:**
Total ERV levels were significantly higher in tumor samples compared to non-tumor samples. Expression of tumor specific "Meso-ERV1-12" was verified by qPCR in mouse tissues. Basal "Meso-ERV1-12" expression was significantly higher in RN5 cells compared to mouse embryonic fibroblast (MEF) and was significantly increased by 5-AzaC treatment. This was accompanied by increased levels of dsRNA, and ISGs (*Ifit2, Ddx58*). "Meso-ERV7" promoter was significantly demethylated in tissue from asbestos exposed mice compared to sham mice and in RN5 cells upon 5-AzaC treatment. Basal ISGs expression was higher in RN5 cells compared to MEF and was significantly decreased upon Ruxolitinib treatment.

**Conclusion:**
These observations indicate that ERV expression increases upon mesothelioma development, likely due to promoter demethylation, and is paralleled by increased levels of dsRNA and activation of type-I IFN signaling.

**135**

N. Karavasiloglou[1, 2], K. Matthes[1, 2], M. Limam[1, 2], D. Korol[1], M. Wanner[1, 2], S. Rohrmann[1, 2]

**Risk of subsequent invasive cancers in women diagnosed with breast cancer in situ: Results from the Cancer registry of Zurich, Zug, Schaffhausen and Schwyz**

*Cancer Registry Zurich, Zug, Schaffhausen and Schwyz, University Hospital Zurich, Zurich, Switzerland[1], Division of Chronic Disease Epidemiology, Institute for Epidemiology, Biostatistics and Prevention, University of Zurich, Zurich, Switzerland[2]*

**Introduction:**
Even though breast cancer in situ incidence has been increasing in the past decades, the prognosis of women diagnosed with breast cancer in situ has not been extensively investigated. Based on the existing literature, women with breast cancer in situ have a higher risk of developing a subsequent invasive breast cancer, but the magnitude of the risk varies considerably; conflicting information has been reported regarding their potential risk for developing a subsequent invasive non-breast cancer.

**Methods:**
Data from more than 1,000 women living in the Canton of Zurich and diagnosed with a primary breast cancer in situ between 2003 and 2015 were used in our analyses. Standardized incidence ratios (SIRs) were calculated to compare the risk of an invasive breast or non-breast tumor among women with a primary breast cancer in situ with the corresponding risk of a primary invasive breast or non-breast tumor in the female population of the Canton of Zurich. To investigate which factors are associated with the risk of being subsequently diagnosed with invasive breast or non-breast cancer we used Cox proportional hazards regression models.

**Results:**
Breast cancer in situ patients had higher risk of being diagnosed with invasive breast cancer and non-breast cancer (i.e. invasive cancer in all sites except breast and non-melanoma skin cancer combined) compared to the general population. The SIRs differed slightly by age at breast cancer in situ diagnosis. Older age at breast cancer in situ diagnosis was statistically significantly associated with a subsequent invasive non-breast cancer diagnosis.

**Conclusion:**
Breast cancer in situ patients in Zurich had higher risk of being diagnosed with invasive breast or invasive cancer in sites other than the breast compared to the general population. Of all the potential risk factors for a subsequent invasive (breast or non-breast) cancer tested, only age at breast cancer in situ diagnosis was statistically significantly associated with a subsequent invasive cancer diagnosis in sites other than the breast.

**136**

S. Hiltbrunner[1], R. Wechsler[3], A. Friedlaender[2], D. Akhoundova[1], L. Bankel[1], S. Kasser[1], S. Bihr[1], C. Britschgi[1], A. Addeo[2], M. Maathuis[3], A. Curioni-Fontecedro[1]

**Biomarkers for immunotherapy in non-small cell lung cancer patients based on retrospective data from USZ and HUG**

*Department of Medical Oncology and Hematology, University Hospital Zurich[1], Oncology Department, University Hospital of Geneva[2], Seminar for Statistics, ETH Zurich[3]*

**Introduction:**
The development of checkpoint inhibitors has revolutionized current cancer treatment. Metastatic non-small cell lung cancer patients are treated with anti-PD-L1/PD-1 checkpoint inhibitors. Some patients do response well to the treatment, however, there is a group of patients without significant response to therapy.

**Methods:**
Here, we have analysed retrospective data acquired from 138 patients treated at the University Hospital Zurich (USZ) from 2015 to 2018. Our aim was to find markers of response in data collected during normal routine treatment.
We performed univariable und multivariable survival analysis (Kaplan-Meister Estimator and Cox Proportional Hazard Regression Models) on this dataset. The primary outcome was overall survival (OS). The p-values of the test from the data set from USZ were not adjusted. Four hypotheses were defined and thereafter validated with a verification data set from Hôpitaux Universitaires de Genève (HUG) consisted of 28 patients treated with immunotherapy from 2017 to 2019. To verify the hypothesis multiple testing correction was applied.

**Results:**
The univariable analysis showed positive effects of high eosinophils (above 0.135 G/l), high lymphocytes (above 1.29 G/l) and high PD-L1 expression on tumor cells (above 50%) on overall survival. Patients with squamous cell carcinoma have a significant lower survival time compared to patients with adenocarcinoma as previously shown. Patients who had first line chemotherapy have a significant higher risk to die at a certain time point compared to patients who had immunotherapy/chemotherapy combined or immunotherapy alone as a first line treatment. Our hypotheses aim to confirm the beneficial effect of lymphocyte numbers, PD-L1 expression, histology and first line treatment. Verification analysis with the data set from HUG showed no significance any longer on a 5% level.
The resulting cox model of the multivariable analysis showed that patients with different histologies have significantly non-proportional hazards. Therefore, the model was stratified by histology and the variables with an effect were: lymphocyte and eosinophil numbers, PD-L1 expression on tumor cells and first line treatment. The data from HUG could not confirm the stratified Cox model.

**Conclusion:**
The study pointed out that the first line treatment affects heavily the survival time of the patients. Other biomarkers like lymphocyte count and PD-L1 expression should be prospectively investigated since no significance after multiple testing correction with the verification set was found.

**137**

D. Karademir[1], V. Todorova[1], C. Grimm[1]

**CRISPR activation of an essential endogenous neuroprotective pathway in the mouse retina**

*Lab for Retinal Cell Biology, Department of Ophthalmology, University of Zurich, Schlieren, Switzerland[1]*

**Introduction:**
Müller cells are the principal macroglia of the retina that not only provide crucial homeostatic and metabolic support to retinal neurons, but also promote their survival upon damage through endogenous neuroprotective signalling pathways. We and others have shown that leukemia inhibitory factor (LIF) is key to Müller glia-based neuroprotection. LIF is expressed by a subset of Müller glia in the damaged retina, and is necessary and sufficient to activate a signalling pathway that supports photoreceptor survival in mouse models of both light-induced and inherited retinal degeneration. Despite its striking neuroprotective effects, high levels of LIF are deleterious to retinal function, preventing its usage in human patients so far.

**Methods:**
Here we propose a novel, broadly applicable, CRISPR-based neuroprotective strategy, wherein we will utilise adeno-associated viral delivery to upregulate endogenous LIF transcripts using a CRISPR activation system. Evidence for the regulation of Lif at the RNA level through its 3'UTR suggests that the increased levels of Lif mRNA will be degraded unless damage conditions in the retina stabilise the transcript, allowing for a need-based supply of extra LIF to the retina. We will test our system in both light-induced and inherited models of photoreceptor degeneration, which mimic different human disorders.

**Results:**
In silico design, cloning and the in vitro testing of the system has been completed. We have achieved in vitro activation of LIF up to 70-fold with our CRISPR system. AAV packaging for viral transduction of Müller glia *in vivo* is ongoing.

**Conclusion:**
CRISPR activation of Lif is currently possible in vitro. Upon testing in vivo, we expect to observe higher levels of LIF only upon damage conditions, supporting the neuroprotection of the retina without deleterious effects of constant high levels of LIF. By using a non-mutating approach, we hope also to contribute to the development of a novel therapeutic approach with potential applications for human patients.

**138**

O. Lauk[1], V. Orlowski[1], T. Neuer[1], B. Battilana[1], I. Schmitt-Opitz[1], M. Kirschner[1]

**Association between microRNAs and clinical, inflammatory factors in patients with malignant pleural mesothelioma undergoing multimodality therapy**

*Department of Thoracic Surgery, University Hospital Zurich[1]*

**Introduction:**
Some clinical factors and molecular markers seem to have a prognostic impact in patients with malignant pleural mesothelioma (MPM), but aren`t fully clarified yet. Low platelet counts, hypoalbuminemia among others and microRNAs (miRNAs), small non-coding RNA molecules that regulate gene expression, may predict longer survival in patients with MPM, as previously published by Kirschner et al., 2014 (1). miRNAs may play a role in controlling inflammation and in the prevention of uncontrolled inflammation.
The aim of this analysis was to investigate possible correlations between tumor microRNA expression and clinical markers of inflammation, as well as to further evaluate their prognostic value prior to surgery.

**Methods:**
Of 140 patients from our prospective database, who had undergone induction chemotherapy followed by extrapleural pneumonectomy (EPP) between 1999-2014, 67 patients had matching tissue samples available. The following blood parameters available after induction chemotherapy were analysed: white blood cells (wbc), platelets and C-reactive protein (CRP).
Biopsies from diagnosis (before chemotherapy), as well as intraoperative tissue samples were collected for all patients and analyzed for 6 miRNAs (miR-21-5p, -23-3p, -30e-5p, 221-3p, -222-3p). WBC, platelets, CRP and the 6 miRNAs were correlated using Kendall`s tau_b correlation test for continuous variables. Overall survival (OS) was calculated with Kaplan Meier analysis and tested with long rank test.

**Results:**
The majority of patients were male (n=59) and of epithelioid histotype (n=55).
The analysis revealed weak, but significant correlations between preoperative platelets and miR-221 (r=0.19, p=0.03), as well as preoperative CRP and miR-21 (r=0.18, p=0.03), -23a (r=0.24, p=0.01), -221 (r=0.28, p=0.001) and -222 (r=0.17, p=0.05) (intraoperative tissue samples) and miR-21(r=0.17, p=0.04) and -23a (r=0.17, p=0.04) (tissue samples from diagnosis). The following molecular markers showed a positive influence on OS, if expressed lower: miR-23a (32months vs 18 months; p=0.004), miR-221 (32 months vs 19 months; p=0.01) at time of diagnosis and miR-23a at time of surgery (29 months vs 19 months; p=0.04).

**Conclusion:**
We identified several statistically significant correlations between preoperative inflammatory and blood parameters (CRP and platelets) and intratumoral microRNA expression at EPP, suggesting a link between inflammation and microRNA expression. In addition, in line with previous data, the analysis revealed a statistically significant improvement of OS for 2 miRNAs available at time of diagnosis. More in-depth studies of the observed correlations are ongoing, also investigating the potential of combined inflammatory/microRNA markers as prognosticators, which could be used for selection of patients undergoing multimodality therapy.

**139**

Y. Zhang[1], F. Schläpfer[2], V. Orlowski[2], I. Schmitt-Opitz[2], M. Kirschner[2]

**MicroRNAs in chemotherapy response in malignant pleural mesothelioma**

*Department of Thoracic Surgery, the 2nd Hospital of Jilin University, China[1], Department of Thoracic Surgery, University Hospital Zurich[2]*

**Introduction:**
Identification of malignant pleural mesothelioma (MPM) patients responding to platinum-based chemotherapy, the current gold-standard for MPM, remains a challenge as no reliable predictive marker has been identified thus far. In a previous profiling study, we identified microRNAs with differential abundance in tumour tissue of responders and non-responders to induction chemotherapy before extrapleural pneumonectomy. Candidates from this profiling are now investigated in vitro for their potential to alter the response of MPM cell lines to cisplatin and/or pemetrexed.

**Methods:**
Commercially available MPM cell lines MSTO-211H, H28, Meso-1, Mero-82 and ONE58, as well as the transformed non-malignant mesothelial cell line MeT-5A are reverse transfected with mimics of microRNAs that showed differential expression in responders and non-responders to cisplatin-pemetrexed chemotherapy. 24h post transfection, cells are treated with increasing concentrations of cisplatin and/or pemetrexed for 72h or 120h, at which point the effect on cell growth is being assessed.

**Results:**
Initial analyses, were performed on cells overexpressing miR-221-3p, miR-380-5p and miR-30e-5p. For all three microRNAs, increased expression resulted in an increase in sensitivity towards cisplatin, in at least 3/6 MPM cell lines, while the sensitivity of non-malignant MeT-5A was not affected. The strongest increase in sensitivity was observed for miR-221, which reduced the observed IC50 for 5 days cisplatin from 17.59uM to 2.65uM ($p<0.0001$) in MSTO and from 21.59uM to 5.54uM ($p<0.0001$) in Meso-1 cells. So far, no changes in sensitivity to pemetrexed could be observed when cells were transfected with miR-221-3p, miR-380-5p or miR-30e-5p. Overexpression of additional microRNAs (e.g. miR-145, miR-625-3p and miR-30a) is currently underway as well as investigation of the effect of microRNA overexpression on the sensitivity of cells to the combined cisplatin-pemetrexed treatment.

**Conclusion:**
First in vitro investigations of the effect of altered expression of microRNAs previously linked to response to cisplatin-pemetrexed chemotherapy, suggest that overexpression of these microRNAs has the potential to increase the sensitivity to cisplatin. In further steps, using tumour samples, possible links between microRNA expression and response to bevacizumab as well as immunotherapy approaches will be in investigated.

**140**

M. Kirschner[2], M. Meerang[2], O. Lauk[2], K. Furrer[2], I. Grgic[1], V. Orlowski[2], F. Tschanz[1], M. Guckenberger[1], M. Pruschy[1], W. Weder[2], I. Schmitt-Opitz[2]

**Efficacy of irradiation combined with intracavitary cisplatin-fibrin after lung-sparing surgery in an orthotopic rat model of mesothelioma**

*Department of Radiation Oncology, University Hospital Zurich[1], Department of Thoracic Surgery, University Hospital Zurich[2]*

**Introduction:**
Localized treatment after tumor resection in malignant pleural mesothelioma (MPM) is aiming for better local tumor control. Here we tested the safety and efficacy of combination treatment with intracavitary cisplatin-fibrin (cis-fib) plus hemithoracic irradiation (IR), applied after lung sparing surgery, in an orthotopic immunocompetent rat model.

**Methods:**
We randomized male F344 rats into five groups (cis-fib (n=9), 10Gy IR (n=6), 20Gy IR (n=9), cis-fib+10Gy IR (n=6), cis-fib+20Gy IR (n=9)). Sub-pleural (parietal) tumor implantation was performed on day 0 with 1 million syngeneic rat mesothelioma cells (IL45-luciferase). We detected tumor nodule formation in all animals by bioluminescence imaging (BLI) on day 8. Tumors were resected on day 9 followed by treatment with intracavitary cis-fib or NaCl-fib. On day 12, CT guided local irradiation in a single high dose (dose rate: 3Gy/min) of the former tumor region, resembling IMRT in human patients, was applied. We monitored animal's health status daily and tumor growth every 3 days by BLI.

**Results:**
None of the animals, whether with radiotherapy alone or in combination with cis-fib, showed any signs of pulmonary side effects. None had reduced pulmonary functions, measured by increased breathing or the appearance of blue or white colored ears/extremities/eyes assuming desaturation. No weight loss was observed after 10Gy IR, either alone or in combination with cis-fib. Treatment with a single dose of 20Gy IR or cis-fib+20Gy IR caused weight loss on the day after treatment but all animals regained weight 2 days thereafter. No deterioration of body conditioning or activity score were observed in the immediate post-interventional phase. Regarding efficacy, we detected comparable tumor growth in animals treated with 10Gy IR compared to no IR (cis-fib) group. Thus, we decided to escalate to 20Gy after treating 6 animals/group. Three days after treatment with 20Gy IR (day 15), we detected a significant difference in tumor growth in IR alone compared to cis-fib+IR group (mean tumor growth (%) 539 vs 252; p=0.04). On day 21, there was a significant difference in tumor growth between cis-fib vs cis-fib+IR treated tumors (mean tumor growth (%) 2295 vs 660; p=0.01).

**Conclusion:**
Irradiation alone and in combination with local intracavitary cis-fib application in rats is safe up to a dosage of 20Gy. The administration of local 20Gy radiotherapy in combination with cis-fib enhances tumor control while only minimally (and short term) affecting animal's well-being. These data suggest a promising effect of combined local treatment with cis-fib+IR for MPM.

**141**

M. Lone[1], T. Hornemann[1]

**Tango to promiscuity: Role of SPTLC3 in generating sphingolipid diversity in Human cells**

*Institute for Clinical Chemistry[1]*

**Introduction:**
Sphingolipids (SLs) are a diverse and essential class of structural and signalling lipids. The first rate limiting step in the de-novo synthesis of SLs is the formation of amino hydroxy alkanes or long chain base (LCB). Typically, LCB's such as sphingosine (SO) are formed through conjugation of L-serine and palmitoyl-CoA, catalyzed by pyridoxal 5' phosphate (PLP) dependent serine palmitoyltransferase (SPT). Besides, SPT can use a variety of other acyl-CoA's and amino acids as substrates, which results in a broad spectrum of putative reaction products. Mammalian SPT consists of three core subunits SPTLC1, SPTLC2 and SPTLC3 of which only SPTLC2 and 3 bear a PLP binding motiff. At protein sequence level, SPTLC3 subunit is most similar to SPTLC2 (68% identity and 84% similarity) than SPTLC1 (21% identity and 45%). SLs in human plasma and tissues contain a large variety of LCBs. However, the role of each individual subunit on enzyme activity and contribution towards the SL product spectrum is not known. In present work, we aim to decipher the function of each of the core subunits and influence on the SL variability in human cells.

**Methods:**
Using CRISPR/Cas9 generated SPTLC1, 2 and 3 deficient cell models, we investigated the role of each subunit on enzyme activity and SL product spectrum. To look for the influence of each subunit on SL synthesis, we determine the incorporation of stable isotope labelled L-serine in de novo produced SLs in KO and transgenic cells expressing SPT subunits. Lipids were identified and quantified using high resolution mass spectrometry coupled to liquid chromatography (LC-MS). Co-immunoprecipitation, fluorescence and immuno-fluorescence assays were used to determine the interaction and stoichiometry of these proteins within the SPT complex.

**Results:**
We show that SPTLC1 is the essential component of the complex, which forms a functional SPT enzyme with either SPTLC2 or SPTLC3. While SPTLC1 in combination with SPTLC2 primarily synthesized C18 and minor amounts of C19 and C20 LCB's, SPTLC1 and SPTLC3 produces a broader product spectrum ranging from C16 to C20 LCBs. Among the products formed by SPTLC3 we identified a unique branched LCB's. This ante-iso methyl-branched C18 LCB is formed by the SPTLC3 specific conjugation of a branched chain fatty acyl-CoA. The branched LCB could be metabolically labelled by amino acid, isoleucine therefore providing a novel link between SL synthesis and branched chain amino acid metabolism. Lipidomics revealed that branched LCB is incorporated into ceramides and sphingomyelins showing a unique *N*-acylation pattern. Branched chain LCBs are specifically present in human plasma but absent from plasma of rodents such as mice and in the former are part of the low and high density lipoprotein particles (LDL and HDL).

**Conclusion:**
We report on a novel SPT function and elucidate the synthesis of a novel class of SL in human cells. In spite of sequence similarity to SPTLC2, SPTLC3 activity commences formation of a wide range of SLs, most importantly, the synthesis of odd chain and monomethylated SLs. The precursor substrates channel to SPT from amino acid catabolism. At the cross roads of amino acid and fatty acid metabolism, SPTLC3 therefore further widens the perimeter of SPT function.

**142**

P. Knobel[1], V. Waller[1], M. Pruschy[1]

**Exploring ADAM17 as an immune checkpoint modulator**

*Clinic for Radiation Oncology[1]*

**Introduction:**
Lung cancer is one of the most frequent cancer types. Treatment of patients consists of either surgery with or without (radio-)chemotherapy or the combination of radiotherapy (RT) with concurrent chemotherapy and more recently immunotherapy. So far, no satisfying combined treatment modality exists to control lung cancer. Therefore, novel molecular targets for anticancer agents alone and in combination with radiotherapy/immunotherapy are of high demand. Our Laboratory for Applied Radiobiology, Department of Radiotherapy, University Hospital Zurich is interested in how the RT-induced secretome of lung tumors affects the tumor microenvironment. Therefore, we performed an exhaustive large-scale secretome analysis from irradiated tumors. Analysis of the most pronounced secreted factors points towards a common upstream metalloproteinase called ADAM17.
ADAM17 is an extracellular metalloproteinase that sheds and releases target proteins and therefore modulates the signaling in the tumor microenvironment.

**Methods:**
Orthotopic lung and allograft tumor mouse models in immune competent mice. Small animal image guided radiotherapy device.

**Results:**
We have discovered in orthotopic lung and allograft tumor mouse model in immune competent mice that the combined treatment of RT and an ADAM17-directed inhibitory antibody (MEDI3622) leads to significant tumor growth delay and 1.5 time-prolonged survival comparing to the single treatment modalities. We further discovered that ADAM17 inhibition strongly decreases extracellular PD-L1 but not MHC-I or MICA/B levels in human and murine lung cancer cell lines and therefore affects PD-L1-dependent immune cells such as Natural killer cells, CD8+ and regulatory T-cells. We hypothesize with these previous results that ADAM17 acts as a PD-L1 immune checkpoint modulator that improves RT-induced immunogenic cell death.

**Conclusion:**
It is known that that RT induces immunogenic cell death by triggering the immune system via upregulation of activating stimuli such as MHC-I or neoantigens but also inhibitory proteins such as PD-L1. We postulate with our results that the combined treatment with RT and ADAM17 inhibition improves the treatment outcome through RT-induced immunogenic cell death and downregulation of inhibitory PD-L1 levels. Eventually this will render the tumor " hot" again and improves recruitment of tumor killing immune cells.
Refining these investigations are essential for the successful launch of a clinical study. We will identify and validate 1) the mechanistic role of ADAM17 on the tumor-immuno-microenvironment after RT and 2) additional druggable immune checkpoint targets in clinically relevant tumor models and patient-derived material. Patients in clinical trials could receive the most effective treatment combinations with RT in order to improve tumor control.

**143**

E. Lemes[1], A. Lakkaraju[1], A. Bentrup[1], J. Sarabia del Castillo[2], M. Losa[1], L. Pelkmans[2], A. Aguzzi[1]

**Determinants of the toxicity of PIKfyve depletion**

*University Hospital Zürich, Institute of Neuropathoplogy[1], University Zürich, Institute of Molecular Life Sciences [2]*

**Introduction:**
Prion diseases are protein misfolding disorders mainly defined by the deposition of abnormal aggregates (PrPSc) of the cellular prion protein (PrPC). A characteristic feature of prion disease is the accumulation of enlarged intracellular vacuoles. Research from our lab showed that degradation of PIKfyve, a lipid kinase on late endosomal membranes, is depleted in prion-infected mouse brains and in Creutzfeldt-Jakob disease resulting in vacuolation. Ablation of PIKfyve in an in vitro model system leads to vacuolation and subsequent cell death, suggesting that PIKfyve depletion drives toxicity in prion infection. In the first part we propose to carry out a synthetic viability screen (SVS) using a genome-wide pooled CRISPR/Cas9 library, to identify modulators of vacuolation. We aim to identify genes which when deleted rescue the lethality induced by PIKfyve downregulation. In the second part we aim to ascertain the biochemical composition of the vacuoles using Iterative Indirect Immunofluorescence Imaging (4i).

**Methods:**
We will be using GT1-7 cells (immortalized mouse hypothalamic neurons). The mouse Brie lentiviral pooled CRISPR library containing 19,674 sgRNAs was obtained from Addgene. Amplification of the CRISPR library and packaging into lentivirus will be performed for SVS. Genomic DNA from the viable cells will be extracted and the inserted sgRNA portion will be amplified by PCR followed by next-generation sequencing. For 4i, GT1-7 cells were ablated of PIKfyve (siRNA; 72h) in 384-well plates, stained and imaged iteratively using 19 antibodies and the IN Cell Analyzer microscope. Images are computationally processed for morphological analysis using the software TissueMAPS and Ilastik.

**Results:**
In the first paradigm, we have established the pipeline to carry out the SVS. GT1-7 cells were transfected with plasmid containing gRNA targeting PIKfyve and inducible Cas9 (CRISPRKO-PIK). Time course analysis revealed vacuolation within 8 hours of doxycycline treatment followed by complete cell death after 7 days. The process of amplifying the pooled CRISPR library and packaging into the lentiviral expression system is currently underway. In a second paradigm, we performed 4i cytochemistry on GT1-7 cells depleted of PIKfyve using 19 antibodies. The microscopy dataset yielded three proteins that show alterations in vacuolated cells; GM130 (cis-Golgi associated protein) shows fragmentation and abnormal aggregation suggesting a general disruption of the Golgi complex, a phenomenon previously reported in neurodegeneration. SARA (localized in early endosomes), shows aggregated, punctate accumulation between vacuoles suggesting altered endosomal functioning. Lastly, HSP60, a mitochondrial chaperone previously reported to bind to prion protein showed an increased expression. These hits were further validated in prion infected GT1-7 cells, and perturbations similar to PIKfyve downregulation were observed.

**Conclusion:**
We have generated an inducible system to ablate PIKfyve using CRISPR/Cas9 and further set up the cell line and conditions required to implement a genome wide synthetic viability screen. Using 4i, we have identified three proteins that are perturbed upon PIKfyve depletion and in prion infection. The role of these proteins in manifestation of vacuoles and toxicity in prion infection is being currently ascertained. Using the above two paradigms, we hope to identify the determinants of vacuolation and downstream toxic modules associated with prion mediated neurotoxicity, and ultimately test whether these can be novel therapeutic targets.

**144**

D. Vuong[3], M. Bogowicz[3], J. Unkelbach[3], S. Hillinger[4], S. Thierstein[5], E. Eboulet[5], S. Peters[2], M. Pless[1], M. Guckenberger[3], S. Tanadini-Lang[3]

**Quantitative image analysis to compare anatomical primary tumor location for surgical and non-surgical treatment regimens for locally advanced NSCLC (SAKK 16/00)**

*Department of Medical Oncology, Kantonsspital Winterthur, Winterthur, Switzerland[1], Department of Oncology, Centre Hospitalier Universitaire Vaudois (CHUV), Lausanne, Switzerland[2], Department of Radiation Oncology, University Hospital Zürich and University of Zurich, Zurich, Switzerland[3], Department of Thoracic Surgery, University Hospital Zürich and University of Zurich, Zurich, Switzerland[4], Swiss Group for Clinical Cancer Research (SAKK) Coordinating Center, Bern, Switzerland[5]*

**Introduction:**
Locally advanced non-small cell lung cancer (NSCLC) carries a poor prognosis despite multi-modal therapy. The anatomical location and extension of the primary lung tumor (PT) have shown prognostic value for outcome prediction, however was often assessed manually. Using a quantitative voxel-based approach, PT spatial distribution of surgical and non-surgical treated patient cohorts were compared upon treatment location and relation to overall survival (OS).

**Methods:**
Two NSCLC patient cohorts (IIIA/IIIB/N2, 6th ed.) were included: (a) LUNG1 (n = 107) treated with definitive radiochemotherapy (single-institution, retrospective) and (b) SAKK (n = 135) treated with neoadj. chemo- or radiochemotherapy prior to surgery (SAKK-16/00). Pre-treatment CT scans were registered to a reference patient CT (contour-only based deformable image registration, MIMVista, 6.9.2.). Each PT was transferred to the reference patient lung while its original shape was isotropically scaled to maintain the patient tumor to lung volume ratio. Two maps were created: (1) Frequency map with PT occurrences and (2) frequency weighted cumulative status (fwCS) map where PT locations were uni-labeled with 2-yr OS patient status (control:-1/no control:1). An anatomical atlas was created to define risk areas (2 cm from bronchi, heart, mediastinum, 1 cm from the chest wall, peripheral divided in RL, AP). PT location prevalence was studied using a normalized frequency difference map. Risk areas were compared using mean fwCS values.

**Results:**
The difference map showed that LUNG1 patient PTs covered more frequently the right region proximal to the main bronchus, whereas SAKK patient PTs were located more at the mediastinum in superior location. In terms of OS, mean fwCS values were larger in all risk areas for LUNG1 compared to SAKK cohort (median increase: 0.67 (0.17-1.8)), which is also reflected in the cohort median OS difference.

**Conclusion:**
In this feasibility study, differences in anatomical tumor location between patients receiving non-surgical therapy compared to multi-modal therapy with surgery were identified. Further analysis is needed to study on clinical confounding bias on general treatment outcome.

**145**

A. Kelley[1, 2], H. Kuster[1], K. Neumann[1], C. Leemann[1], P. Rindler[1], K. Kusejko[1, 2], D. Braun[1, 2], R. Kouyos[1, 2], K. Metzner[1, 2], H. Günthard[1, 2]

**Time Trends of Replication Capacities of Transmitted Founder Viruses in Zurich**

*Division of infectious Diseases, University Hospital Zurich, Zurich, Switzerland[1], Medical Virology, University of Zurich, Zurich, Switzerland[2]*

**Introduction:**
Evolution of HIV-1 towards higher virulence could potentially be of public health concern and so far, controversial data has been published on this topic. To address this issue, we measured the replication capacities (RC) of 308 transmitted founder (T/F) viruses obtained from patients enrolled in the Zurich Primary HIV-1 Infection (ZPHI) study over a 15-year period (2002-2017).

**Methods:**
The ZPHI is comprised of patients with documented acute (<90 days) or recent (90-180 days) HIV-1 infection, with the estimated date of infection (EDI) determined based on unambiguous risk behavior, clinical, and laboratory data. Primary HIV-1 isolates of T/F viruses were derived from acute/recent phase CD4+ T cells or plasma by co-culturing with stimulated peripheral blood mononuclear cells (PBMCs). In a well-controlled, large-scale replication capacity assay, all 308 T/F viruses were, in parallel, used to infect $2*10^5$ CD8 depleted PBMCs from 3 donors with 200 $TCID_{50}$ of virus in quadruplicates and cultured for 7 days. Viral supernatant was transferred daily onto TZM-bl luciferase reporter cells to measure the kinetics of virus infectivity. RC was determined as the area under curve (AUC) for the median of the replicates.

**Results:**
308 patients were included, with the EDI ranging between 12 and 180 days (mean = 58 days) at the day of sampling. The majority of the patients were male (89.2%), of white ethnicity (77.5%), infected with HIV-1 subtype B (70.8%), and the major HIV-1 transmission group was men who have sex with men (70.1%). From 2002-2017, between 13 and 34 individuals with acute/recent HIV-1 infection were enrolled per year (mean = 22). The RC of the 308 T/F viruses did not change significantly in the years 2002-2017 (slope = 0.0106, p = 0.225), when all viruses were included in the analysis. When the analysis was restricted to subtype B isolates (n=218), there was a significant increase in RC in a univariable analysis (slope = 0.0299, p = 0.0076).

**Conclusion:**
In the univariable analysis, a significant increase in RC was found for HIV-1 subtype B T/F viruses, but not for all subtypes combined. Potentially, this finding could illustrate that by increasing the proportion of ART treated and suppressed patients in the population over time - as happened in Switzerland during this period - this could select for viruses with increased virulence in the diminishing pool of remaining transmitters.

**146**

T. Schweizer[2], F. Andreoni[2], E. Marques Maggio[3], S. Dudli[1, 4], A. Zinkernagel[1, 2]

**Staphylococcus aureus – host interactions in a porcine ex vivo spondylodiscitis model**

*Center for applied Biotechnology and Molecular Medicine (CABMM), University of Zurich, Zurich, Switzerland[1], Department of Infectious Diseases and Hospital Epidemiology, University Hospital Zurich, University of Zurich, Zurich, Switzerland [2], Department of Pathology and Molecular Pathology, University Hospital Zurich, University of Zurich, Zurich, Switzerland[3], Department of Rheumatology, University Hospital Zurich, University of Zurich, Zurich, Switzerland [4]*

**Introduction:**
The incidence of vertebral bone and disc infection, termed spondylodiscitis, has doubled over the last two decades, in particular in the elderly. *Staphylococcus aureus* is the most frequent pathogen isolated in spondylodiscitis. In order to achieve cure, patients receive long-term antibiotics as well as surgical debridement, when indicated. Still little is known about the pathophysiology of this disease. Hence, we aimed at establishing a novel high-throughput *ex vivo* model, which would recapitulate key clinical aspects of spondylodiscitis. As model host we selected pigs since they share many physiological and immunological similarities to humans. Pig material is readily available as a waste byproduct of the food industry and, given the size, material coming from one animal can be used to address several questions.

**Methods:**
Intervertebral discs including adjacent vertebral bodies were purchased and punch biopsies prepared. After *S. aureus* infection over a period of two days, bacterial load, location, growth dynamics and histological appearance were analyzed. Furthermore, transmission electron and confocal laser scanning microscopy were performed to analyze bacterial migration within the lacunae-canalicular network. Additionally, host response was assessed by flow cytometry and quantitative RT-PCR.

**Results:**
Porcine spines were validated as a suitable spondylodiscitis model. Clear histopathological similarities to human spondylodiscitis were found. Bacteria were recovered in high numbers from the vertebral bodies and intervertebral discs even two days after infection. *S. aureus* was found to invade host cells, with increasing numbers of intracellular bacteria observed over time. Furthermore, recovered bacteria displayed an increased time to regrowth on agar plates, the typical feature of adaptation to a stress situation within the host. Microscopical analysis revealed bacterial migration within the dense cortical bone, as well as alongside collagen fibrils in the annulus fibrosus. *S. aureus* was found to invade host cells-occupied lacunae in the bone as well as disc and to reside within empty lacunae. Host cells underwent apoptosis upon challenge with *S. aureus*, resulting in empty lacunae and slight upregulation of IL-1β and RANKL cytokines expression.

**Conclusion:**
We successfully established a reproducible, high-throughput *ex vivo* porcine *S. aureus*-infection spondylodiscitis model, which accurately mirrors the histopathological appearance of human cases. We show that *S. aureus* migrates within the osteocyte-lacunae-canalicular network of cortical vertebral bone and alongside collagen fibrils as well as within lacunae of chondrocytes in the intervertebral disc. When reaching the lacunae, *S. aureus* was found to efficiently invade these cells and also induce apoptosis. As a next step, we aim to identify *S. aureus* mechanisms triggering apoptosis in lacunae-occupying cells by looking at the possible involvement of toll-like-receptors as well as candidate toxins released by *S. aureus*.

**147**

H. Gabrys[3], L. Basler[3], S. Hogan[1], M. Pavic[3], M. Bogowicz[3], D. Vuong[3], S. Tanadini-Lang[3], R. Förster[3], M. Huellner[2], R. Dummer[1], M. Guckenberger[3], M. Levesque[1]

**Radiomics for prediction of metastatic melanoma patient survival after immunotherapy**

*University Hospital Zurich, Department of Dermatology, Zurich, Switzerland[1], University Hospital Zurich, Department of Nuclear Medicine, Zurich, Switzerland[2], University Hospital Zurich, Department of Radiation Oncology, Zurich, Switzerland[3]*

**Introduction:**
Immune checkpoint inhibition has achieved substantial improvements in survival of metastatic melanoma patients; however, reliable biomarkers for patient selection are lacking. This study aims to assess the predictive potential of PET/CT-based radiomics for modeling patient overall survival (OS) in metastatic melanoma patients receiving checkpoint inhibitors.

**Methods:**
A retrospective single-institution cohort of 112 patients with metastatic melanoma was the basis of this study. Patients were treated with either single-checkpoint-inhibition using anti-PD-1-antibodies or dual-checkpoint-inhibition in combination with anti-CTLA-4-antibodies. PET/CT imaging was done before the treatment (TP0) and at 3 months after the treatment initiation (TP1). All individual metastases (n=716 over all patients) were segmented on all images for calculation of radiomic features (n=172) describing shape, intensity, and texture of the metastases. To perform the analysis on a patient level, radiomic features extracted from multiple lesions were aggregated via weighted arithmetic mean, where the weight corresponded to a lesion volume. Logistic regression models were built using the data available at TP0 and delta-radiomic features calculated between TP0 and TP1. The performance metric was the area under the receiver operating characteristic curve (AUC). The generalization performance of the models was estimated with a nested cross-validation (inner loop: 10 times repeated 10-fold cross-validation, outer loop: 10 times repeated 5-fold cross-validation). Model calibration has been evaluated with calibration curves and the Brier score. The radiomic models were benchmarked against models based only on metastases volume.

**Results:**
The OS at 12 and 36 months was 84% and 55%, respectively. Prognostic models based on radiomic features achieved AUCs of 0.87 +/- 0.08 and 0.74 +/- 0.13 at 12 and 36 months, respectively. Volume-based models performed slightly worse with AUCs of 0.83 +/- 0.15 and 0.71 +/- 0.13, at 12 and 36 months, respectively. Nevertheless, the radiomics models were more stable and better calibrated than the volume-based models. Inclusion of PET-based radiomic features did not improve performance of radiomic models in either of the investigated scenarios. Considering only the largest lesion instead of the weighted mean of all lesions resulted in AUC scores smaller by 0.16 on average.

**Conclusion:**
Radiomic features, considering all metastases in one patient from baseline imaging and follow-up imaging at 3 months, allow for accurate prediction of survival in metastatic melanoma patients at 12 and 36 months after treatment with immune checkpoint-inhibitors.

**148**

N. Schneider[4], F. Bernays[4], M. Ferster[3], C. Lustenberger[3], W. Karlen[3], R. Huber[1, 2], C. Baumann[4], A. Maric[4]

**Acoustic stimulation may reduce impairments in vigilance induced by chronic sleep restriction**

*Child Development Center, University Children's Hospital Zurich[1], Department of Child and Adolescent Psychiatry, University of Zurich[2], Department of Health Science and Technology, ETH Zurich[3], Department of Neurology, University Hospital Zurich, University of Zurich[4]*

**Introduction:**
Sufficient sleep is necessary to maintain normal performance in everyday life. An insufficient habitual sleep duration, namely chronic sleep restriction (cSR) interferes with restorative processes linked to sleep as their time for action is reduced. Vigilance is amongst the most sensitive neurobehavioral domains for sleep restriction induced impairments as can be quantified by a decrease in response speed after multiple days of sleep restriction in the psychomotor vigilance task (PVT). Electrophysiologically, the restorative function of sleep is reflected by slow waves (SWs) during deep sleep. Acoustic stimulation during sleep enables modulating SWs, potentially allowing to intensify the restorative function. This might mitigate the observed behavioral impairments after sleep restriction.

**Methods:**
Young male subjects undergo 2 x 7 consecutive nights of cSR, preceded by 7 nights of regular sleep. In one week, SWs are enhanced using acoustic stimulation (stim week), in the other week tones are muted (sham week). The tones are presented in the up-phase of SWs in a 6 second ON window followed by a 6 second OFF window in which no tone is presented. Subjects perform a 10 minute laptop PVT every night 1 hour before their habitual bed time. On the day preceding the first cSR night and the day following the last cSR night PVTs are performed 5 times each, adjusted to the individual sleep-wake schedule throughout the day. We performed a preliminary analysis of PVT performance including data of 6 subjects. Reaction times below 100 ms and above 500 ms were excluded due to being classified as false starts and lapses (inability to respond within a reasonable time range), respectively. Speed (1/reaction times) was assessed as a measure of performance. Slow wave activity (SWA), the spectral power in the slow wave frequency range 0.5 – 4Hz, was calculated for all artifact free 6 second windows. We then compared the grand mean of both window types (ON vs. OFF) across all nights of a subject.

**Results:**
Preliminary comparisons show that during the stim compared to the sham week there is a significant SWA increase in ON- relative to OFF-windows (repeated measurements ANOVA, $p < 0.05$). First insights into behavior suggest significantly reduced speed on the last two cSR days compared to the first in both conditions (linear mixed model, $p=0.006$ and $p=0.002$). Although this demonstrates, that subjects show the expected cSR related performance decrease at the end of both cSR weeks, the responses were faster in the stim compared to the sham week (linear mixed model, $p=0.006$).

**Conclusion:**
First indications show that SWA can be enhanced in young healthy adults using acoustic stimulation. Furthermore, our results indicate that the decrease in speed induced by cSR might be counteracted by acoustic stimulation. This preliminary analysis focused on reaction times in the normal range. Future analysis will reveal if acoustic stimulation is able to reduce the number of lapses (i.e. failures to respond), which are of higher importance for everyday life.

**149**

I. Heggli[2], S. Epprecht[2], A. Juengel[2], B. Betz[1], S. Spirig[1], F. Wanivenhaus[1], F. Brunner[1], M. Farshad[1], O. Distler[2], S. Dudli[2]

**Dysregulated Adhesion of Modic Type I Change Bone Marrow Stromal Cells**

*Balgrist University Hospital[1], Center of Experimental Rheumatology[2]*

**Introduction:**
Modic type 1 changes (MC1) are vertebral bone marrow lesions associated with non-specific low back pain (LBP). The pathophysiology of MC1 includes inflammation, fibrosis, and high bone turnover. Bone marrow stromal cells (BMSCs) are key regulators of these processes: BMSCs contribute to inflammation by regulating myelopoiesis/osteoclastogenesis; BMSC can differentiate into osteoblasts contributing to high bone turnover, and BMSC can differentiate into pro-fibrotic myofibroblasts.
The aim was to identify dysregulated biological processes in MC1 BMSCs contributing to the pathobiology of MC1.

**Methods:**
Bone marrow aspirates were obtained from LBP patients with MC1 undergoing lumbar spinal fusion. Aspirates were taken prior to screw insertion. From each patient, a MC1 and a healthy control (HC) aspirate from the adjacent vertebral body were collected (n=8+8). BMSCs were isolated by plastic adherence and expanded. RNA from BMSCs passage 3 were sequenced (n=3+3) (Illumina Novaseq) and gene ontology of significantly dysregulated genes ($p<0.05$) was analyzed. Specificity and rate of BMSC matrix adhesion were quantified: BMSCs (n=8+8) were seeded on fibronectin-coated, collagen I-coated, and non-coated plastic dishes in six technical replicates. Fibronectin- and collagen-coated dishes were blocked with 1% BSA. Non-adherent cells were removed after 15min, 30min, and 4h. Adherent cells were stained with Hoechst and counted. Percentage of attached cells after 15min and 30min were measured and normalized to the 4h time-point (100% of live cells attached). From 0 min to 15 min BMSCs settle. Therefore, BMSC adhesion was evaluated from 15 min to 30 min. Percentage of adherent cells of MC1 and HC BMSC were compared with paired t-test.
In order to identify integrins responsible for dysregulated cell-matrix adhesion, gene expression of 15 relevant integrins were measured by quantitative real-time PCR (qPCR). Normalized expressions were compared between MC1 and HC BMSC (n=8+8) with paired t-test.

**Results:**
By RNA sequencing, 154 genes were differentially expressed between MC1 and HC BMSCs ($p\leq0.01$; log2-ratio$\geq0.5$). Gene ontology enrichment analysis revealed an overrepresentation of the biological process “cell-matrix adhesion” among all significantly regulated genes ($p<9.3e-13$). A change in cell adhesion was corroborated with adhesion assay: while there was no difference in binding to collagen I (73% MC1, 72% HC, p=0.87), fibronectin (78% MC1, 80% Ctrl, p=0.35) and non-coated (31% MC1, 40% HC, p=0.15) surface after 15min, binding occurring between 15min and 30min to collagen I (MC1 +16%, HC +10%, p=0.10), fibronectin (MC1 +17%, HC +6%, p=0.03), and non-coated surface (MC1 +46%, HC +35%, p=0.05) was increased in MC1. Integrin gene expression analysis revealed significant upregulation of ITGB1 in MC1 vs. HC (fold change = 1.24, p=0.047), whereas there was no significant difference between the other integrins tested.

**Conclusion:**
Adhesion of BMSCs to matrix and integrin β1 expression are increased in MC1. Integrin β1 is essential for cell-matrix adhesion and an important contributor to the initiation and progression of tissue fibrosis, a hallmark of MC1. Therefore, BMSCs and integrin β1 might be relevant novel targets for the treatment of MC1.

**150**

T. Mlambo[1], M. Alessandrini[3], R. Myburgh[2], L. Baroncini[1], S. Bredl[1], M. Manz[2], P. Salmon[3], R. Speck[1], K. Krause[3]

**A novel combinatorial approach combining CAR T cell therapy, PD1 knockdown and CCR5 disruption as a once-off treatment for HIV**

*Department of Infectious Diseases & Hospital Epidemiology, University Hospital Zürich[1], Department of Medical Oncology and Hematology, University Hospital Zurich[2], Department of Pathology and Immunology, Faculty of Medicine, University of Geneva[3]*

**Introduction:**
The human immunodeficiency virus (HIV) type-1 is a major global health burden, which has claimed over 25 million lives in the past 30 years. While effective, combined anti-retroviral treatment (cART) is associated with adverse events, viral resistance in the case of non-adherence and the inability to target the latent viral reservoirs. Novel once-off treatment for the cure of HIV is highly needed. In this study, we propose to introduce a chimeric antigen receptor (CAR) targeting HIV-infected cells and a microRNA down-regulating the check-point PD1 (programmed cell death 1) into the CCR5 genomic locus of T-cells. The CAR encodes for the CD4 cell surface molecule, which selectively binds the HIV envelope (env) surface protein expressed on productively infected cells and thus kills these cells in a highly specific manner. Furthermore, the PD1 microRNA will prevent or reverse HIV-associated T cell exhaustion and disruption of CCR5 will render these cells resistant to the predominant HIV strains. The efficacy of this approach will be evaluated in vitro and in vivo using 'humanized' mice.

**Methods:**
To assess the functionality of the CD4 CAR construct, transduction of peripheral blood mononuclear cells (PBMCs) was carried out using a lentiviral vector encoding the CD4 CAR. Next, a cytotoxicity assay was carried out using Hela243 cells which express HIV env. The Hela243 cells were stained with the PKH-26 membrane dye prior to incubation with the CAR T cells at different effector to target (E:T) ratios. Target cell death was assessed by the addition of the viability probe TO-PRO-3 iodide (TP3), followed by flow cytometry analysis.

**Results:**
After 72 hours, 95% specific lysis of target cells was observed at an E:T ratio of 1:1, whereas 67% cell death was observed with untransduced PBMCs, and only 5% with the target cells alone. To assess the ability of the CAR T cells to control HIV replication, autologous T cells were infected with the NL4.3 HIV strain and incubations carried out at different E:T ratios. ELISA for the HIV p24 antigen in the supernatant was carried out after 6 days. Compared to the control sample, CAR T cells resulted in a significant reduction in p24 antigen, with the greatest effect being observed with the 1:1 E.T ratio.

**Conclusion:**
As next steps, the effects of PD1 silencing and CCR5 knockdown will be assessed, and ultimately the efficacy of the CAR T cells in the context of in vivo prevention and treatment models will be determined. This combinatorial approach, which targets crucial elements involved in HIV pathogenesis in a way not previously explored, may be a significant step forward in the cure of HIV.

**152**

C. Meier[1], K. Freiburghaus[2], C. Bovet[2], J. Schniering[1], O. Distler[1], C. Nakas[2, 3], B. Maurer[1]

**Serum Branched-Chain Amino Acids as Biomarkers for Progressive Systemic Sclerosis-Associated Interstitial Lung Disease**

*Center of Experimental Rheumatology, Department of Rheumatology, University Hospital Zurich, Switzerland[1], Center of Laboratory Medicine, University Institute of Clinical Chemistry, University Hospital Bern, Switzerland[2], Laboratory of Biometry, Department of Agriculture, Crop Production and Rural Environment, School of Agricultural Sciences, University of Thessaly, Greece[3]*

**Introduction:**
In fibrotic diseases such as systemic sclerosis (SSc), local metabolic processes are altered with a tendency towards an anabolic state, which is at least partially reflected in serum. Circulating biomarkers for progressive interstitial lung disease (ILD) associated with SSc, the leading cause of death in SSc patients, are still sparse and not established in routine care. Metabolites as potential serum biomarkers in the context of SSc-ILD have not yet been investigated. Therefore, the objective of this study was to assess the potential of serum metabolites as biomarkers for progression of SSc-ILD.

**Methods:**
Age and sex matched serum samples of SSc patients from the Zurich SSc cohort and of healthy volunteers were analyzed. Progressive SSc-ILD was defined as either a relative decrease in forced vital capacity (FVC) of > 10%, a decrease in FVC of 5-9% and a concomitant decrease of carbon dioxide diffusion of > 15%, or an increase of the extent of lung fibrosis on computed tomography from < 20% to ≥ 20% compared to the previous logged visit. Sera of healthy controls, non-ILD SSc as well as stable and progressive SSc-ILD patients (n = 12 per group; total n = 48) were analyzed by semi-quantitative targeted liquid chromatography tandem mass spectrometry using positive and negative electrospray ionization (+/–ESI, respectively). The resulting peak areas were analyzed with R 3.6. For univariate analysis, FDR-corrected one-way ANOVA was used with the significance level set to 0.1. Changes between groups were analyzed using Tukey's post test. In multivariate group-wise partial least squares discriminant analysis (PLS-DA), variable importance in the projection (VIP) scores ≥ 2 were considered being statistically significant. For validation of the measurement of branched-chain amino acids (BCAAs) in SSc-ILD patient serum (n = 12 and 11 for progressive and stable SSc-ILD, respectively), a commercial enzyme-based colorimetric assay was used and data was analyzed using Student's t-test.

**Results:**
In total 85 metabolites (56 +ESI, 24 –ESI, 5 both) were detected. Univariate analysis of all groups revealed significant changes in 1-methyladenosine, L-tryptophan (+ and –ESI), L-tyrosine, L-leucine, and xanthosine (p = 0.077, 0.028, 0.028, 0.077, 0.028 and 0.032, respectively), with significant differences in xanthosine between stable and progressive SSc-ILD (p = 0.021). In PLS-DA, adenosine monophosphate and xanthosine, as well as the BCAAs L-isoleucine and L-leucine showed significant influence on x-variate component 1 (VIP = 2.01, 2.14, 2.41, 2.75, respectively), and, in the case of L-leucine and xanthosine, on component 2 (VIP = 2.21 and 2.09). Receiver operating curve (ROC) analysis of significant metabolites from uni- and multivariate testing resulted in significant separation of progressive and stable SSc-ILD patients by their levels of L-isoleucine, L-leucine, adenosine monophosphate, and xanthosine (area under the curve = 0.83, 0.85, 0.79 and 0.77; confidence interval = 0.66 – 1.00, 0.70 – 1.00, 0.60 – 0.97 and 0.55 – 0.99, respectively). Upon validation with an enzyme-based assay, progressive SSc-ILD patients showed significantly higher BCAA levels than patients with stable disease (mean = 286.5 and 235.5 nM, respectively; p = 0.005).

**Conclusion:**
Our exploratory study in SSc(-ILD) patients showed alterations in serum levels of BCAAs and other metabolites, corresponding with their current state of disease, indicating the potential use of serum metabolites such as BCAAs as diagnostic or prognostic biomarkers upon further confirmation in larger multicenter studies.

**153**

S. Anwer[1], P. S. Heiniger[1], S. Rogler[1], D. Cassani[1], J. Kebernik[1], N. Kuzo[1], L. Rebellius[1], G. Alexander[1], D. Schmid[1], M. Schuermann[1], A. P Pazhenkottil[1], M. Meyer[1], R. Schoenenberger-Berzins[1], C. Gruner[1], F. C. Tanner[1]

**Circumferential deformation for diagnosis and risk assessment in left ventricular non-compaction**

*Department of Cardiology, University Heart Center, University Hospital Zurich. Switzerland.[1]*

**Introduction:**
Echocardiography-based deformation analysis is used for studying left ventricular (LV) mechanics and has an emerging role in the diagnosis of cardiomyopathies. Left ventricular non-compaction (LVNC) is a rare cardiomyopathy characterised by a two-layered LV myocardium with prominent trabeculae separated by deep recesses perfused from the LV cavity. Left ventricular hypertrabeculation (LVHT) may be difficult to differentiate from LVNC. In this study, we aim a) to develop a diagnostic algorithm based on the deformation of LVNC in comparison with LVHT and controls, and b) to determine the associations of diagnostic parameters with outcomes.

**Methods:**
We analysed 45 LVNC patients, 45 LVHT individuals, and 45 controls matched for age, gender, and cardiovascular risk factors. Two experts confirmed and validated LVNC diagnosis according to the current echocardiographic criteria. LVHT was defined as presence of three or more trabeculae in the LV apex visualised in both parasternal short axis and apical views. Controls had a normal echocardiographic examination and no evidence of cardiovascular disease. Strain analysis was performed using TomTec Image-Arena (version 4.6).

**Results:**
Receiver observer characteristics curve (ROC) analyses revealed that global circumferential strain (GCS) < 22.3% differentiated LVNC from control or LVHT. In individuals with global circumferential strain (GCS) < 22.3%, an apical peak circumferential strain (aPCS) of 18.4% differentiated LVNC [< 18.4%] and LVHT [≥ 18.4%] (fig. 1-A).
Validation was performed by an independent echocardiographer blinded for the diagnoses on 32 subjects from each group, and results are shown in figure 1-B. The combined endpoint of cardiovascular events (CVE) in LVNC is described in figure 1-C.
Multi-variate regression analyses (fig. 1-D) demonstrated that GCS was associated with 11-fold increased risk of CVE independent of LVEF and NC:C ratio, while global longitudinal strain (GLS) displayed only 2-fold increased risk and the conventional parameters (left ventricular ejection fraction (LVEF) and non-compacted:compacted ratio (NC:C ratio) were not associated with outcomes. Regional peak circumferential strain as well as the GCS-derived parameters of left ventricular twist and basal-apical rotation ratio displayed significant associations too.

**Conclusion:**
A diagnostic algorithm with GCS and aPCS differentiates LVNC from LVHT and control with very high sensitivity and specificity independent of additional echocardiographic or clinical information. Circumferential strain derived parameters exhibit a very strong association with outcomes independent of LVEF and NC:C ratio. Absence of CVE in LVHT provides further evidence on the distinct nature of LVNC and LVHT.

**154**

J. Müller[1], R. Myburgh[1], M. Manz[1]

**Combinatorial Chimeric Antigen Receptor T cells for the Treatment of Acute Myeloid Leukemia**

*Clinic of Medical Oncology and Hematology[1]*

**Introduction:**
Acute myeloid leukemia (AML) is a neoplastic disease characterized by rapidly proliferating very early hematopoietic progenitors of myeloid lineage. With current treatment regimens only <30% of all patients with newly diagnosed disease are alive 5 years after initial diagnosis mostly due to disease relapse. While B cell malignancies are already successfully treated with Chimeric Antigen Receptor (CAR) T cells targeting mostly CD19, in AML, approaches targeting a single antigen might be insufficient due to overlapping antigen profiles of AML blasts and healthy cells leading to unacceptable toxicities including aplasia and/or cytopenia. We therefore set out to develop a dual-targeting CAR using a split CAR system with a combination of c-Kit (CD117) and CLEC12A (CLL-1).

**Methods:**
To first test the functionality of a CLL-1 targeting CAR, we designed a transgene consisting of the human GM-CSF receptor signal peptide followed by a single-chain variable fragment (scFv), derived from a published anti-CLL-1 antibody (M26) sequence. This fragment was linked to the intracellular 2nd generation signalling unit, containing the 4-1BB co-stimulatory and CD3ζ stimulatory domains, via a CD8α-derived hinge and transmembrane domains and the selection and safety marker RQR8 separated by a T2A ribosomal skip sequence. Lentivirus containing the CAR plasmid was produced by transfecting HEK293T cells and healthy donor T cells from PBMCs were transduced with concentrated lentiviral particles. To test the functionality of CLL-1 directed CAR T cells a FACS-based killing assay with the myeloid cell lines K562 (CLL-1-) and HL-60 (CLL-1+) was performed. In a next step, a dual-CAR vector containing the CLL-1 targeting scFv linked with the CD3ζ stimulatory domain and the c-Kit targeting scFv already developed and characterized in CAR format in our lab was cloned in front of the intracellular costimulatory domain 4-1BB.

**Results:**
The transduction efficacy of naïve healthy donor T cells assessed by CD34-staining of the co-expressed minimal epitope RQR8 was around 70-80%. Subsequent expansion using stimulation with CD3/CD28 beads and IL-2 resulted in 200-300fold expansion of CAR T cells and control T cells after 6 days. A series of killing assays showed that anti-CLL-1 CAR T cells specifically eliminate CLL-1+ HL-60 cells and spare CLL-1- K562 cells. The specific killing efficiency was 70-80% at an effector-to-target ratio of 1:1 and decreased with decreasing ratios. Establishment of a series of double- and single-positive target cell line as well as dual-specific CAR T cells and their testing in vitro and vivo are currently ongoing.

**Conclusion:**
The aim of my project is to address the unresolved problem of finding the best possible target antigen for immunotherapy of AML. The several requirements for an ideal target antigen – namely surface expression in exclusively malignant cells in a high number of patients, immunogenicity and necessity for tumor cell proliferation – might not be met by a single antigen in AML. Therefore, we use a combinatorial approach allowing for more complex inputs to the effector T cell than recognition of a single surface antigen: Construction of split CARs with various antigen specificities allows the design of more complex effector cells, which are only activated if a combination of surface antigens is expressed on a target cell. By focusing on the combination of CD117 and CLL-1, both expressed on a majority of AML cases, but with an otherwise non-overlapping on-target off-tumor profile, we aim to develop a novel safe and effective approach for AML therapy.

**156**

S. Steiner[1], T. Reding[1], D. Lenggenhager[2], M. Stopic[1], M.E. Healy[2], A. Gupta[1], G. Wanner-Seleznik[1], R. Graf[1]

**Gastrokine 1 and 2 in pancreatic carcinogenesis: one family with two distinct roles?**

*Department of Surgery and Transplantation, University Hospital Zurich[1], Institute of Pathology and Molecular Pathology, University Hospital Zurich[2]*

**Introduction:**
Late detection of pancreatic ductal adenocarcinoma (PDAC) and limited treatment options lead to poor survival of PDAC patients. A better understanding of the pathomechanism of PDAC development will help identify new therapeutic approaches. An early event during tumorigenesis is the development of pre-malignant lesions such as pancreatic intraepithelial neoplasia (PanIN). While studying a K-Ras driven mouse model (KC mice) of PDAC, which recapitulates the stepwise progression of pancreatic cancer, we serendipitously identified Gastrokine 1 (GKN1) and Gastrokine 2 (GKN2) in early PanIN lesions. Importantly, we confirmed the presence of GKN1 and GKN2 in human pancreatic premalignant lesions. GKNs are proteins derived from gastric epithelium, where they maintain gastric homeostasis and act as tumor suppressors. Therefore, we aim to investigate the function of this PanIN-specific GKN1 and GKN2 expression, to understand the early events that underlie the development of premalignant lesions leading to pancreatic carcinogenesis.

**Methods:**
We intercrossed KC mice with GKN1-/- or GKN2-/- mice. GKN1-/- KC, GKN2-/- KC and GKN+/+ KC pups were analyzed at the age of 3- and 9 months to quantify PanIN lesions and assess tumor development via histology. Furthermore, qRT-PCR and western blots were used to analyze genes and proteins (relevant for apoptosis, EMT or tissue remodeling and stroma composition) involved in tumorigenic processes. For all compared groups we analyzed the proliferation index and measured differences in pancreatic cyst sizes. A lentiviral construct overexpressing mouse GKN1 or GKN2 was generated to transduce Panc02 mouse pancreatic cancer cells to confirm the results in-vitro.

**Results:**
Absence of GKN1 or GKN2 dramatically accelerated the development of PanIN lesions in KC mice. 3 months old GKN1-/-KC and GKN2-/-KC mice showed more extensive ADM and PanIN lesions compared to GKN+/+ KC mice, coinciding with significant upregulation of genes involved in PanIN development, cytokine and chemokine expression as well as tissue remodeling. Interestingly, the mRNA expression analysis also revealed a significant difference in apoptosis regulation in GKN1-/- KC mice. Analysis of cleaved Caspase-3, FAS protein and activated cleaved Caspase-8 point towards a decreased apoptosis in the absence of GKN1 and suggests a possible involvement of GKN1 in the activation of the extrinsic apoptotic pathway. The histological comparison at 9-months showed that GKN1-/- KC mice developed a collagen-rich dense stroma around the pancreatic lesions compared to sparse stroma in KC animals. GKN1-/- KC mice showed an increased tumor incidence when compared to KC (44% vs 21%) and a more differentiated tumor phenotype. On the other hand, the histological evaluation shows that 9 month old GKN2-/- KC mice display a change of pancreatic tissue architecture resulting in big cystic lesions and a increased proliferation rate, which might explain altered tumor incidence in this model (39% vs 21%).

**Conclusion:**
We conclude that the absence of GKN1 or GKN2 leads to accelerated PanIN development. Based on our results, we suggest that GKN1 influences apoptosis avoidance at an early age through the extrinsic apoptosis pathway. Apoptosis avoidance and development of a dense stromal reaction in later stages leads to an increased tumor incidence. GKN2 plays an important role in maintaining pancreatic architecture during PanIN formation, especially influencing the cyst size and proliferation.

**157**

M. Wipplinger[1], M. Ronner[1], A. Okonska[1], A. Hariharan[1], E. Felley-Bosco[1]

**Identifying the regulatory role of Adenosine deaminase acting on dsRNA editing on RNA Binding Motif 8 protein in mesothelioma**

*Laboratory of Molecular Oncology, Thoracic Surgery, University Hospital Zürich, Zürich, Switzerland[1]*

**Introduction:**
Malignant pleural mesothelioma (MPM) is an aggressive cancer mainly associated with chronic asbestos exposure. In a previous whole genome silencing study we observed that BRCA1-associated protein 1 (BAP1) proficient cells show an impaired survival upon RNA Binding Motif 8 protein (RBM8A) silencing. RBM8A is a part of the Exon Junction Complex involved in RNA processing. High levels of RBM8a are associated with worse overall survival in mesothelioma and in an experimental mesothelioma development mouse model, we observed that mice display A to I edited forms of RBM8A mRNA upon asbestos exposure compared to healthy animals.

**Methods:**
siRNA was used to silence Adenosine deaminase acting on dsRNA (ADAR) 1/2. RBM8A expression levels upon silencing ADAR 1/2 were determined by qPCR and Western Blot. 3'UTR fragment containing the A-I editing sites was cloned into the pmirGLO vector and Dual Luciferase assay was used to investigate change in RNA stability.

**Results:**
Silencing ADAR1/2 in four different MPM cell lines resulted in a significant increase in RBM8A protein levels. The dual luciferase assay, performed in two cell lines, revealed a significant elevation of luciferase intensity upon both, siADAR1 and siADAR2, for both tested MPM cell lines, indicating a possible mRNA destabilizing effect of RNA editing in those cell lines.

**Conclusion:**
Our study provides first insight in the regulatory role of A-I editing on RBM8A in MPM cells, as we demonstrated that loss of ADAR1/2 leads to an increased RBM8A expression.

**158**

S. Costa[2], A. Gasperetti[2], D. Akdis[2], G. Suna[2], A. Medeiros-Domingo[1], C. Brunckhorst[2], F. Duru[2], A. Saguner[2]

**Familial ARVC in light of new genetic evidence: a case report**

*Swiss Dnalysis[1], Universitätsspital Zürich[2]*

**Introduction:**
Arrhythmogenic Right Ventricular Cardiomyopathy (ARVC) is an inherited condition, characterized by a high incidence of ventricular arrhythmias in the young, sudden cardiac death (SCD) and progressive fibrofatty infiltration of the ventricles, most often affecting the right ventricle. Approximately 60% of patients carry a genetic mutation, with more than 50% of the mutations affecting desmosomal genes, including plakoglobin (JUP), PKP2, desmoplakin (DSP), desmoglein-2 (DSG2) and desmocollin-2 (DSC2). In addition, some non-desmosomal genes such as transmembrane protein 43, desmin, titin, phospholamban, and RYR2 are also involved.

**Methods:**
We present the case of a 54-year-old man with familial predisposition for ARVC, who presented at the ER with sustained VT of unknown origin. Following clinical and imaging investigations, we diagnosed ARVC by presence of 2 major criteria and proceeded with genetic cascade screening of the patient for the same heterozygous genetic variant (mutation in the TTN-gene, c.26542C>T, classified then as potentially pathogenic) we had found in his affected sister 6 years ago. Another heterozygous variant in the SCN5A gene (c.274-24C>T) that we had found in his sister and which was previously published to be potentially pathogenic, has already been reclassified as benign recently, and therefore we did not screen the patient for this SCN5A variant.

**Results:**
Genetic cascade screening for the TTN variant showed him to be unaffected, and of interest, current literature review also reclassified this variant as benign. This led us to re-screen the patient using a larger cardiomyopathy panel, in order to detect a disease-causing variant. We are currently waiting for these genetic test results.

**Conclusion:**
The growing knowledge and vast amount of data obtained in cardiogenetics in recent years has on the one hand shed more light on previously unknown etiologies of genetic cardiac disorders, but on the other hand emphasizes the need for a thorough and more stringent gene reclassification in ARVC, following the new available genetic evidence and American College of Medical Genetics criteria.

**159**

A. Gasperetti[8], S. Costa[8], D. Akdis[8], A. Breitenstein[8], D. Hofer[8], C. Brunckhorst[8], C. James[5], M. Casella[3], L. Chen[4], S. Kany[7], S. Schenker[2], H. Jensen[1], M. Shibu[2], P. Platonov[6], S. Willems[2], H. Calkins[5], C. Tondo[3], J. Steffel[8], F. Duru[8], A. Saguner[8]

**First-in-World Report of Outcomes of Catheter Ablation for Atrial Arrhythmias in Arrhythmogenic Right Ventricular Cardiomyopathy**

*Aarhus University[1], Asklepios Kliniken Hamburg[2], Centro Cardiologico Monzino[3], Fuwai Hospital[4], John's Hopkins School of Medicine[5], Lund University Arrhythmia Clinic[6], Universitätsklinikum Hamburg[7], USZ[8]*

**Introduction:**
Arrhyhtmogenic right ventricular cardiomyopathy (ARVC) is a genetically inherited disease characterized by fibro-fatty infiltrations. Fibro-fatty infiltration in ARVC patients usually originates in the ventricles and it has been strongly associated with vnetricular arrhythmias and sudden cardiac death, but recent imaging studies showed a fibro-fatty infiltration at atrial level as well and reports of atrial arryhthmias in ARVC patients have been published. Effectiveness of catheter ablation for atrial arrhythmias in this subset of patients is currently unknown.

**Methods:**
Seven large-scale ARVC cohorts (Swiss ARVC registry, Centro Cardiologico Monzino ARVC cohort, John's Hopkins Medical Center ARVC registry, Fuwai Medical Center ARVC registry, The Scandinavian ARVC registry, Asklepios Klinik Hamburg ARVC registry, Universitätsklinikum Hamburg ARVC registry) were retrospectively searched for ARVC patients undergoing catheter ablation for atrial arrhythmias (namely: atrial fibrillation (AF), atrial tachycardia (AT), and cavo-triscupidal dependent flutter (CTI-FL)). Included patients needed to reach a "Definitive diagnosis" level of ARVC diagnosis confidence according to the 2010 International Task Force Criteria; no limitations regarding genotype charachterization were given. Baseline, procedural, and long term outcome data were collected. Acute and long-term success rate of catheter ablation for atrial arrhythmias in ARVC patients represented the study outcomes.

**Results:**
A total of 32 patients (84% male, median CHA2DS2-VASc 1 [1 -2], HAS-BLED 1 [0 – 2], and EHRA scores 2 [2 - 3]) with a definite ARVC diagnosis were enrolled. Mean age at atrial arrhythmia catheter ablation was 47.8 ± 15.4 y.o. At baseline, 63% of patients were on oral anticoagulants (OAC) (n= 9 warfarin; n = 11 new OAC). A left atrial (LA) catheter ablation was performed in 25 (78%) patients (n = 16 AF; n = 9 AT), while a catheter ablation for CTI-FL in 7 (22%) patients, respectively. Sinus rhythm was obtained peri-procedurally in all patients, with 2 (7%) patients with AF requiring intra-procedural electrical cardioversion. Over a mean follow up time of 36 [16.5 – 70] months, 11 (34%) patients experienced an atrial arrhythmic recurrence (LA group: n = 6 AF recurrences, n = 3 AT recurrences; CTI-FL group: n = 1 CTI-FL recurrence; n = 1 new AF) and 66% patients resulted on OAC.

**Conclusion:**
Catheter ablation for atrial arrhythmias in ARVC patients is a safe and effective procedure. Long term catheter ablation outcomes for AF, AT, and CTI-FL in these patients result comparable to those reported in large trials.

**160**

L. Clack[1], A. Wolfensberger[1], M. Faes Hesse[1], M. Meier[1], H. Sax[1]

**Tailored implementation of non-ventilator-associated pneumonia (nvHAP) prevention bundle as part of a type 2 hybrid implementation-effectiveness study**

*University Hospital Zurich[1]*

**Introduction:**
Hospital-acquired, non-ventilator-associated pneumonia (nvHAP) represent a significant portion of all cases of hospital-acquired pneumonia and leads to substantial morbidity and mortality. Yet, current research and prevention efforts focus almost exclusively on ventilator-associated pneumonia. To address this gap, we undertook a hybrid type 2 implementation-effectiveness study to assess the implementation of a 5-measure nvHAP prevention bundle. To increase likelihood of implementation success, we employed a tailored implementation strategy in which specific implementation interventions are selected according to locally identified behavioural determinants (barriers and facilitators) to improve performance of the nvHAP prevention bundle. The following work reports on the development and ongoing assessment of the tailored implementation strategy.

**Methods:**
This study was conducted in nine departments of the University Hospital Zurich, a tertiary-care university hospital. The study authors formed a central coordinating team and three "nvHAP delegates" representing the involved professional groups were identified in each participating department. During baseline, potential barriers and facilitators to bundle adherence were identified through exploratory observations and semi-structured interviews with frontline staff and nvHAP delegates from each department. Observation notes and interview transcripts were coded deductively using the Theoretical Domains Framework, which allowed a theoretically informed interpretation of mentioned behavioural determinants and mapping to interventions. Selection of tailored interventions followed a participatory approach, in which the study team used a theory-based approach to propose potential interventions and the local nvHAP delegates ultimately selected and adapted interventions based on feasibility and expected improvement opportunity. Chosen implementation interventions were documented in local action plans for each department, which served as guides for the subsequent implementation process.

**Results:**
A total of 23 observations, 31 frontline interviews, and 9 interviews with nvHAP delegates were conducted to identify potential barriers and facilitators. These varied by department and included: knowledge (e.g. lack of awareness of guidelines), social/professional role (e.g. ambiguity about professional responsibilities), skills (e.g. lack of prior experience, technical skills), and environmental context and resources (e.g. lack of time, ease of access and visibility of materials and equipment). Specific implementation interventions to address these factors included: education (e.g. informational events to increase knowledge about nvHAP and preventative measures and to clarify professional responsibilities), training (e.g. practical skills training to identify patient dysphagia), and environmental restructuring (e.g. posting informational posters as reminders, oral-care sets). The nature of the interventions were also adapted to the local context. For example, education could take the form of informational events, bedside teaching, or e-mail information distribution – depending on local compatibility.

**Conclusion:**
The diversity of the barriers and facilitators observed across participating departments led to the use of distinct implementation interventions – further justifying the use of a tailored implementation approach. The effectiveness of specific implementation interventions will be assessed as part of the ongoing hybrid implementation-effectiveness study.

**161**

M. Bogowicz[2], M. Pavic[2], O. Riesterer[2], F. Finazzi[2], H. Garcia Schüler[2], E. Holz-Sapra[2], L. Rudofsky[2], S. Glatz[2], L. Basler[2], M. Spaniol[2], M. Hüllner[1], M. Guckenberger[2], S. Tanadini-Lang[2]

**CT radiomics differentiates levels of radiocurability in tumor subvolumes in head and neck cancer**

*Department of Nuclear Medicine, University Hospital Zurich and University of Zurich, Zurich, Switzerland.[1], Department of Radiation Oncology, University Hospital Zurich and University of Zurich, Zurich, Switzerland.[2]*

**Introduction:**
Radiomics was proposed as prognostic biomarker in head and neck cancer (HNC); however it is not clear what treatment could be offered to the patients with worse prognosis based on existing radiomic signatures. Here we investigated if radiomics can distinguish between tumor subvolumes with different levels of radiocurability, to potentially increase the dose to these parts.

**Methods:**
We have retrospectively collected data from 28 HNC patients treated with definitive radiochemotherapy fulfilling the following inclusion criteria: contrast-enhanced CT imaging prior to treatment, local in-field tumor recurrence confirmed by biopsy and FDG-PET/CT imaging at the time of recurrence. The recurrent tumor was contoured on the PET/CT image (g_rec) and the contours were rigidly transferred to the planning CT.
In a first step, two volumes were analyzed with radiomics: recurrence region (overlap between primary tumor (PT) and g_rec) and control region (PT minus recurrence). 162 intensity and texture features were extracted from the planning CT. Principal component analysis and multivariate logistic regression with backward selection were used to distinguish between control and recurrence regions. The final model was tested in a cohort of 12 patients from a phase II study selected based on the same inclusion criteria.
In a second step, we tested if radiomics allows, not only for differentiation of the levels of radiocurability, but also potentially for their detection. To that end the radiomics analysis was performed on 8 subvolumes of the primary tumor by splitting the tumor bounding box in 8 equal parts. If the subvolume consisted of more than 50% of voxels identified as g_rec it was classified as radioresistant subvolume. The model training and validation was performed analogous to the first step.

**Results:**
The final model, to distinguish the recurrent vs controlled tumor subvolumes in the pretreatment imaging, comprised two features, indicating that recurrence regions are more heterogeneous than control regions prior to any treatment. The model showed good performance in the validation cohort AUC=0.88 (95% CI: 0.72–1.00), sensitivity=0.75, specificity=0.83.
For the 8 subvolumes analysis, 3 features were selected in the training cohort. This model showed slightly inferior performance AUC=0.70 (95%CI: 0.53–0.86) in the validation cohort than the first model. However, for all 4 patients, who presented at least 1 out of 8 radioresistant subvolumes (more than 50% voxels identified as g_rec), at least one subvolume was identified correctly by the model.

**Conclusion:**
We have shown for the first time that pretreatment radiomics can differentiate levels of radiosensitivity in HNC. This is a potential first step towards radiomics-based dose painting.

**162**

N. Kuzo[1], B. Stähli[1], J. Kebernik[1], T. Nguyen-Kim[2], M. Eberhard[2], M. Schindler[1], F. Ruschitzka[1], F. Tanner[1]

## Normal Coronary Arteries as Negative Risk Marker in Patients with Severe Aortic Stenosis Undergoing Transcatheter Aortic Valve Replacement

*Department of Cardiology, University Heart Center, University Hospital Zurich, Zurich, Switzerland[1], Department of Diagnostic and Interventional Radiology, University Hospital Zurich, Zurich, Switzerland[2]*

**Introduction:**
Coronary artery disease and severe aortic stenosis (AS) frequently coexist. Data on the impact of coronary artery disease on outcomes after transcatheter aortic valve replacement (TAVR) are conflicting, and whether patients with normal coronary arteries are at lower risk remains uncertain.

**Methods:**
Consecutive patients with severe AS undergoing TAVR were included in the analysis and dichotomized according to the presence/absence of normal coronary arteries, defined as absence of epicardial coronary artery lesions with diameter stenosis ≥30% in vessels ≥1.5 mm in diameter on coronary angiogram in patients without prior coronary revascularization. The primary endpoint was mortality at 1 year.

**Results:**
Out of 1087 patients with severe AS undergoing TAVR, 268 (26.5%) patients had normal coronary arteries. These patients were younger, more likely women, and had lower EuroSCORE II and STS risk scores. While no significant difference in mortality between the normal coronary artery and the coronary atherosclerosis groups was observed at 30 days (3.4% versus 5.3%, Log rank p=0.21), corresponding rates at 1 year were 10.1% and 17.6% (Log rank p=0.004). In multivariable analysis, normal coronary arteries (adjusted HR 0.57, 95% CI 0.38-0.87, p=0.008), chronic obstructive pulmonary disease (adjusted HR 1.85, 95% CI 1.28-2.67, p=0.001), p=0.002) and glomerular filtration rate (adjusted HR 0.98, 95% CI 0.98-0.99, p<0.001) emerged as independent predictors of 1-year mortality.

**Conclusion:**
This study identified normal coronary arteries as negative risk marker in patients with severe AS undergoing TAVR. Hence, the presence of normal coronary arteries should be incorporated into the risk stratification of AS patients.

**163**

L. Krattiger[1, 3], B. Simona[2], M. Ehrbar[3]

**Establishment of a screening platform for the testing of pro- and antiangiogenic compounds**

*Department für Maschinenbau und Verfahrenstechnik ETH, Zürich, Schweiz[1], ECTICA Technologies, Zürich, Schweiz[2], Forschung Geburtshilfe, Universitätsspital Zürich, Schweiz[3]*

**Introduction:**
The aim of this project is to develop a platform that can be used for basic research, but also in a more clinical context to evaluate the effect of chemical, biological or cellular components added to microvascular networks. The platform should enable the study of cellular interactions in angiogenic and vasculogenic events and should furthermore be employable for the screening of pro- and anti-angiogenic factors. The challenges faced are the tailoring of culture conditions for the formation of reproducible vascular networks, which are sensitive to pharmacological manipulations, and making it suitable for high-throughput screening.

**Methods:**
The platform consists of co-cultures of human endothelial cells and stromal supporting cells embedded into a biomimetic poly(ethylene glycol) hydrogel matrix where they arrange into three-dimensional vessel-like structures within a well-plate format. Imaging-based techniques will are used to evaluate different culture conditions and the effect of various growth factors on the networks formed.

**Results:**
Various culture conditions and techniques have been tested and an overview of important parameters for microvascular network formation has been created. The most promising culture conditions will be further developed and finally applied to investigate open biological questions related to microvascular remodelling.

**Conclusion:**
This platform will have the potential to serve as an intermediate tool between simpler vascular-like in vitro cultures and animal models in microvascular research as well as pharmaceutical research.

**164**

P. Pagella[3], L. Jimenez-Rojo[3], S. Weber[2], P. Saftig[1], C. Cantu[4], T. Mitsiadis[3]

**ADAM10 acts as a modulator of notch signalling to regulate tooth enamel formation**

*Biochemisches Institut, Christian-Albrechts-Universität Kiel, Kiel, Germany[1], Department of Pharmacology and Toxicology, Carl Gustav Carus Faculty of Medicine, Technische Universität Dresden, Dresden, Germany[2], Orofacial Development and Regeneration, Institute of Oral Biology, University of Zurich, Zurich, Switzerland[3], Wallenberg Centre for Molecular Medicine (WCMM), Department of Clinical and Experimental Medicine (IKE), Linköping University, Linköping[4]*

**Introduction:**
Tissue homeostasis and regeneration are ensured by precise regulatory mechanisms that control stem cell proliferation, migration, and differentiation. The continuously erupting rodent incisor constitutes an optimal model to investigate these processes. Its continuous growth relies on spatially organized divisions and coordinated movements of stem cells and progenitors within dental epithelium and mesenchyme. We have previously shown that Notch signalling is essential for these processes, as well as cell fate specification within the epithelium of rodent incisors. Adam10 is a metalloproteinase that regulates Notch signalling and ensures epidermal integrity in many tissues. We here investigated the function of Adam10 and its in vivo relevance to Notch-mediated signaling in incisors epithelium.

**Methods:**
Epithelium-specific Adam10 conditional knock-out mouse model (K14:Cre;Adam10fl/fl); in vivo, in vitro lineage tracing (N1CreERT2;R26mT/mG); 3D imaging; immunohistochemistry/ immunofluorescence; scanning and transmission electron microscopy; organotypic cultures; RNA sequencing; mass spectrometry.

**Results:**
Teeth of K14:Cre;Adam10fl/fl mice exhibited severe malformations due to the lack of one of the four epithelial cell layers (Notch1+ stratum intermedium), which led to the disorganization and altered secretory activity of enamel-producing ameloblasts. These alterations led to the formation of defective enamel, a condition strikingly reminiscent of human enamel pathologies. Similarly, pharmacological inhibition of Adam10 led to stratum intermedium loss and severe enamel defects. We showed that the lack of stratum intermedium cells is not due to their death, but rather to their switch to another dental epithelial cell fate. This was demonstrated by lineage tracing analysis in N1CreERT2;R26mT/mG mice, where Adam10 inhibition resulted in the conversion of stratum intermedium cells into ameloblasts. We then characterized the interactome of Adam10 in the dental epithelium, and analysed in deep detail the transcriptome changes induced by Adam10 deletion in this tissue, and observed major deregulation of genes associated to the Notch signalling pathway.

**Conclusion:**
Overall, our data reveal that Adam10 is a major regulator of Notch signalling and essential for cell fate specification and differentiation events that are indispensable for unimpaired enamel formation.

**165**

L. Kovtonyuk[3], F. Caiado[3], E. Slack[1], E. Manz[3], H. Takizawa[2], M. Manz[3]

**Inflammageing of Hematopoietic Stem Cells is driven by IL-1**

*Institute of Food, Nutrition and Health, ETH Zürich[1], Kumamoto University[2], University Hospital Zurich[3]*

**Introduction:**
Lifelong continuous blood production is sustained through a stepwise differentiation program by a very limited number of self-renewing Hematopoietic Stem Cells (HSCs) in the bone marrow (BM).Hematopoietic cell development is tightly controlled by both cell intrinsic and extrinsic factors and dysregulation can lead to aplasia or neoplasia. During aging, HSCs undergo multiple changes, most notably they increase in numbers, reduce self-renewal capacity, their differentiation is skewed towards myelopoiesis, and their bone marrow (BM)–homing ability is reduced. We here evaluated how and to what extend HSC-extrinsic factors determine HSC behaviour during aging.

**Methods:**
To screen for aging-associated extrinsic factors, we performed antibody based protein arrays and transcriptome analysis with total BM of young (6-8 wk) versus aged (1 and 2y) wild type (WT) animals. Candidate factors were further confirmed by ELISA and qPCR. To test function of WT, germ free (GF), gnotobiotic (GB) or knock out (KO, i.e.IL-1r1KO, TrifKO, Myd88KO) HSCs, cells were transplanted into lethally irradiated mice which were bled monthly to follow long-term donor engraftment and lineage repopulation.

**Results:**
Antibody based protein arrays and transcriptome analysis with total BM of young versus aged animalsdemonstrated that RANTES, MIP-2, IL-1α and IL-1β are significantly upregulated in aged BM at both the protein as well as the RNA level. ELISA of peripheral blood (PB) serum and BM lysates indicated that IL-1α and IL-1β are locally increased and produced in BM, but are not significantly increased in PB serum. Further, various BM cell types of hematopoietic and non-hematopoietic origin upregulate Il1α andIl1β, with highest increase being derived from myeloid cells. This raised the possibility that elevated IL-1 is a result of an inflammatory response to circulating pathogen-derived compounds, possibly of bacterial origin. To prospectively test the role of IL-1-induced signalling and the microbiome during aging, we investigated the ageing-associated phenotype of HSCs in young and aged IL1RIKO mice and in young and aged GF and GB mice (mice with no or reduced microbial complexity). Both IL1RIKO and GF aged mice had lower counts of platelets and neutrophils in PB, and lower frequency of LT-HSCs (LKS Flt3-CD34-CD48-CD150+) in BM, compared to aged WT mice. Moreover, aged IL1RIKO LT-HSCs showed improved lymphoid lineage repopulation upon transplantation into lethally irradiated WT mice, compared to LT-HSCs of aged WT mice that demonstrated typical myeloid-biased lineage output. Interestingly, LT-HSCs from aged GF mice demonstrated lymphoid-biased lineage differentiation as observed from young mice. In line with this finding, no difference was observed in IL-1α and IL-1β protein concentrations in BM lysates from young and aged GF mice. On contrary HSCs from aged GB mice already demonstrated myeloid biased output. To test if IL-1 increase in aged steady-state mouse BM is indeed dependent on ligation of pattern recognition receptors and consecutive signalling, we analysed MyD88 and Trif KO mice, respectively. Both aged KO mice showed compared to WT mice reduced BM IL-1 levels and a reduced ageing-phenotype of HSCs. Similarly, antibiotic treated aged WT mice demonstrated lower levels of IL-1 in BM.

**Conclusion:**
Our data demonstrate that ageing associated phenotype and myeloid-biased differentiation of HSCs is a result of signals derived from the microbiome, that act through increased IL-1 signalling, locally in the BM.

**166**

M. Gruenbach[3], E. Schlaepfer[3], B. Escher[1], M. Schlapschy[1], A. Skerra[1], G. Schreiber[2], R. Speck[3], S. Bredl[3]

**Biological activity of different IFN-a subtypes - just an interplay between the dose and affinity?**

*Chair of Biological Chemistry, Technical University of Munich, MUNICH, Germany[1], Department of Biomolecular Sciences, Weizmann Institute of Science, REHOVOT, Israel[2], Department of Infectious Diseases, University Hospital Zurich, ZURICH, Switzerland[3]*

**Introduction:**
While there is an ongoing debate about the biological activity of IFN-α subtypes, we found only quantitative differences in their ability to block HIV ex vivo. Currently, we study PASylated (PAS) IFN subtypes with distinct IFNAR affinity in humanized mice for their biological effects and ability to block HIV. Notably, PASylation increases their half-lives 10x.

**Methods:**
First, we compared the activity of the PAS IFNs to the wild-type (WT) IFNs by using RPE-ISRE reporter cells. We then evaluated the PAS IFN's anti-HIV activities in ex vivo HIV-infected human PBMCs. We are currently determining the optimal dose/schedule for the PAS IFN treatment in humanized mice.

**Results:**
We found that PAS IFNs induce luciferase expression to a lesser extent than their WT counterparts. Similarly, PAS IFNs were less effective against HIV than the WT IFNs. The high affinity PAS IFN-α14 and YNS blocked HIV replication more efficiently than IFN-α2. In vivo data showed a dose-dependent stimulation of ISGs and a shift of the naïve T cell population towards an effector phenotype with IFN-α2 being equally potent as IFN-α14.

**Conclusion:**
High affinity IFNs are more potent at an equimolar dose in our ex vivo cellular assays. PASylation appears to decrease IFNs' potency, which we believe may be due to steric hindrance of the long tail. Strikingly, PAS IFN-α2 and IFN-α14 resulted in similar upregulation of ISGs in humanized mice treated three times a week. This dose schedule, however, appears to be too frequent as the ISGs prior to the next dose are still increased, which might result in immune exhaustion. We are currently working on refining the dosing schedule in vivo. We will then compare WT with PAS IFNs and explore their effects on HIV-infection in humanized mice.

**167**

M. Kahr[2], M. Rothenbühler[1], P. Silber[2], D. Perrouchoud[1], H. Györgyi[1], M. Shilaih[1], B. Leeners[2]

**Association of physiological and psychological stress and menstrual cycle disorders**

*AVA[1], University Hospital Zurich[2]*

**Introduction:**
Stress is a factor commonly associated with menstrual dysfunction, either as factor influencing cycle length or as inducing disturbances of hormonal regulatory patterns during the different cycle phases. Using the data of a longitudinal study, we assess the association of both psychological and physiological stress with cycle length.Stress is a factor commonly associated with menstrual dysfunction, either as factor influencing cycle length or as inducing disturbances of hormonal regulatory patterns during the different cycle phases. Using the data of a longitudinal study, we assess the association of both psychological and physiological stress with cycle length.

**Methods:**
We included women with cycle lengths of 21 to 50 days. Every participant had to wear the Ava bracelet at night measuring physiological parameters, and to sync the data using a mobile application. One of the parameters measured by the wearable device is heart rate variability, which is an indicator of physiological stress. Participants were asked to fill out a daily survey with health-related questions, including perceived stress level on a scale going from zero to 100. Follicular and luteal lengths were determined by home-based LH urine tests and the onset of the menstrual bleeding. We included all cycles for which data was available at least 80% of the cycle days. Participants were categorized as regular if their cycle length lay between 24 and 35 days. If more than one cycle out of six fell out of this cycle range or if a cycle deviated more than four days from the length of the others, participants were labeled as irregular. We investigated differences in cycle length across groups using the Mann-Whitney test and evaluated associations between both stress and cycle length using Pearson correlation. Additionally we evaluated the chance of ovulation by a multivariate regression model.

**Results:**
We included 89 women contributing a total of 312 cycles in the analysis. 62 women were categorized as having regular cycles and 27 with irregular cycles contributing to 211and 101 cycles, respectively. The luteal phase length did not vary across groups ($p=0.30$). The follicular length differs across groups ($p<0.001$), with 16 days (IQR 14-19) for regular cycling women and 19 days (IQR 16-23) for irregular cycles. Psychological and physiological stress were correlated ($p<0.001$). The correlation of both the mean and the peak psychological stress during follicular phase and the length of the follicular phase are statistically significant ($p<0.001$), whereas we could not find any association between physiological stress and follicular length ($p=0.64$).

**Conclusion:**
Using data of 312 cycles, we were able to show an association of between psychological but not physiological stress with follicular length. Further research is needed to shed light into the underlying mechanisms.

**168**

L. Barrios[1], P. Oldrati[1], D. Lindlbauer[1], M. Hilty[2], H. Hayward-Koennecke[2], C. Holz[1], A. Lutterotti[2]

**A Rapid Tapping Task on Commodity Smartphones to Assess Motor Fatigability**

*Department of Computer Science, ETH Zurich, Switzerland[1], University of Zurich & University Hospital Zurich, Switzerland[2]*

**Introduction:**
Fatigue is a common debilitating symptom of many autoimmune diseases, including multiple sclerosis. It negatively impacts patients' every-day life and productivity. Despite its prevalence, fatigue is still poorly understood. Its subjective nature makes quantification challenging and it is mainly assessed by questionnaires, which capture the magnitude of fatigue insufficiently. Motor fatigability, the objective decline of performance during a motor task, is an underrated aspect in this regard. Currently, motor fatigability is assessed using a handgrip dynamometer. This approach has been proven valid and accurate but requires special equipment and trained personnel.

**Methods:**
We propose a technique to objectively quantify motor fatigability using a commodity smartphone. The method comprises a simple exertion task requiring rapid alternating tapping. This new method was compared with a 30 second sustained maximum handgrip task measured with a hand dynamometer.

**Results:**
Our study with 20 multiple sclerosis patients and 35 healthy participants showed a Spearman's correlation of $\rho = 0.8$ ($p < .01$) with the baseline handgrip method. During the first 30 seconds, participants of the control group performed on average 249.1 taps ($\sigma = 56.6$ taps), while patients performed on average 170.6 taps ($\sigma = 60.3$ taps), leaving a large number of data points for analysis. A Bland-Altman analysis comparing the two methods shows a mean difference of almost zero (0.01) and all data within two standard deviations from the mean with limits of agreement between (LoA) [-0.08, 0.06] confirms the good agreement between both approaches.

**Conclusion:**
This smartphone-based approach is a first step towards ubiquitous, more frequent, and remote monitoring of fatigability and disease progression. We believe that our work is a first step towards measuring motor fatigability without having to rely on specialized equipment, which can be expensive and require professional supervision. We also think that our method may help quantify fatigue and complement the current use of subjective feedback through questionnaires, enabling patients to frequently and ubiquitously monitor their condition, and react to changes accordingly.

**169**

J. Jang[5], M. Haberecker[5], C. Curioni-Fontecedro[5], A. Soltermann[5], I. Gil-Bazo[1], F. Janker[5], H. Ilseon[3], K. Kwon[2], W. Weder[5], W. Jungraithmayr[4, 5]

**CD26/DPP4 a novel prognostic marker for lung adenocarcinoma**

*Clinica Universidad de Navarra, Spain[1], Dong-Gang Medical Center[2], Keimyung University Dongsan Medical Center[3], University Hospital Rostock[4], University Hospital Zürich[5]*

**Introduction:**
CD26/dipeptidyl peptidase 4 (CD26/DPP4) is an exopeptidase expressed on various malignancies associating with the activity of epithelial-mesenchymal transition (EMT). We found previously that the activity of CD26/DPP4 in human lung cancer is four times higher than in normal lung tissue and the inhibition of CD26/DPP4 decreased the growth of lung tumors in experimental models. These data encouraged us to analyze clinical samples for the expression of CD26/DPP4 and EMT markers in non-small cell lung cancers to unravel a function of CD26/DPP4 as a prognostic marker and potential therapeutic target for lung cancer.

**Methods:**
We employed multi-organ tissue micro array (TMA) of non-small cell lung cancer patient samples from two institutions, University Hospital Zurich and Dongsan Medical Center. To identify CD26/DPP4 and EMT markers (Ecadherin, Vimentin, beta-Catenin, Elastin, Periostin, and Versican), immunohistochemistry (IHC) on TMA was performed. Three pathologists scored the IHC intensity from zero to six in a blinded manner. The cohort consisted of 1126 patients (adenocarcinoma: 593; squamous carcinoma: 443; others (large cell carcinoma, adeno-squamous carcinoma): 90). The overall survival rate of patients was considered as a measure of prognosis. To identify a correlation between CD26/DPP4 and EMT related protein expression in lung cancer the Pearson correlation coefficient test was applied.

**Results:**
CD26/DPP4 IHC scores revealed that adenocarcinoma expresses significantly higher amount of the protein compared to normal lung or squamous carcinoma or others ($p=0.035$, $p<0.0001$, $p<0.0001$ respectively). In adenocarcinoma, patients with high CD26/DPP4 score (4-6) showed the worst overall survival compared to patients scoring low (1-3) or zero. The correlation analysis of CD26/DPP4 with EMT markers in adenocarcinoma showed that the epithelial marker Ecadherin was negatively correlated ($p=0.001$), while mesenchymal proteins Vimentin, beta-Catenin, Elastin were positively correlated with CD26/DPP4 ($p=0.03$, 0.01, and 0.001 respectively). Periostin and Versican showed no correlation with CD26/DPP4 expression.

**Conclusion:**
The expression of CD26/DPP4 was significantly higher in adenocarcinoma among non-small cell lung cancers and associated with worse survival of adenocarcinoma patients. Furthermore, the expression of CD26/DPP4 was significantly correlated with the EMT status. We therefore deem CD26/DPP4 to be a novel prognostic marker for lung adenocarcinoma. In consideration with CD26/DPP4 expression and patient survival of lung cancer, inhibition of CD26/DPP4 can potentially improve lung cancer patients' survival.

**170**

M. Lipiski[4], M. Eberhard[7], T. Fleischmann[4], S. Halvachizadeh[6], B. Kolb[7], F. Maisano[5], M. Kron[4], V. Falk[1, 2, 3], MY. Emmert[1, 2], H. Alkadhi[7], N. Cesarovic[3]

**Computed Tomography-based evaluation of porcine cardiac dimensions to assist in pre-study planning and optimized model selection for pre-clinical research**

*Department of Cardiothoracic and Vascular Surgery, German Heart Institute Berlin, Berlin, Germany [1], Department of Cardiovascular Surgery, Charité Universitätsmedizin Berlin, Berlin, Germany[2], Department of Health Sciences and Technology, ETH Zurich, Switzerland[3], University Hospital Zurich; Center of Surgical Research, Switzerland[4], University Hospital Zurich; Department of Cardiac Surgery, University Heart Center Zurich, Switzerland[5], University Hospital Zurich; Department of Trauma, Switzerland[6], University Hospital Zurich; Institute for Diagnostic and Interventional Radiology, Switzerland[7]*

**Introduction:**
The Domestic pig (*Sus Scrofa Domestica*) is an accepted animal model of cardiovascular research and in particular for the preclinical evaluation of prosthetic heart valves and trans-catheter implantation techniques. Pre-procedural planning with modern imaging modalities such as trans-esophageal echocardiography and three-dimensional computed tomography (CT) has become an integral part for the pre-selection of suitable animals for efficacy and safety studies of new medical devices in the cardiovascular field. A better understanding of porcine cardiac dimensions reduces post-implantation complications thereby enhancing preclinical study success, leading not only to higher cost efficiency but also to the observance of the ethical, legal and scientific obligation to the 3R principles by reducing the number of animals needed.

**Methods:**
Retrospective cardiac CT images of twenty-four domestic pigs (Swiss large white, intact females and castrated males) were segmented; structures of the aortic root, the mitral valve, the pulmonary trunk, the tricuspid valve, as well as the aortic-mitral angle and left atrial height were analyzed. Correlation coefficient (r) was calculated between the pig's body weight and all measured cardiac structures, a correlation matrix was created between all valve area sizes, left and right coronary height, coronary heights and length of ascending aorta.

**Results:**
Strong correlation was found between body weight and aortic valve area, and between body weight and length of ascending aorta; whereby the length from annulus to right and left coronary ostia does not correlate with the length of the ascending aorta. Strong correlation was furthermore found between body weight and trigone-trigone distance of the mitral valve, as well as between body weight and left atrial height. Right heart analysis only revealed strong correlation between body weight and length of pulmonary artery to bifurcation. Correlation between body weight and pulmonary valve is apparent but moderate. Aortic valve area and mitral valve area strongly correlate with each other.

**Conclusion:**
In Swiss large white pigs, valvular diameters and area sizes moderately to strongly correlate with pig's body weight. Length of the pulmonary artery to bifurcation, length of the ascending aorta and left atrial height can be well correlated with pig's body weight. Coronary ostia heights and aortic-mitral angle size can be neglected in animal size selection as no change was found for either of the two parameters with increasing body weight.

**171**

A. Saltari[1], A. Dzung[1], N. Tiso[3], M. Quadri[2], O. Eichhoff[1], A. Marconi[2], C. Pincelli[2], R. Dummer[1], M. Levesque[1]

## Activation of CD271 (NGFR) intracellular death domain induces apoptosis and overcomes targeted therapy resistance in melanoma ex-vivo and in vivo models

*Department of Dermatology, University Hospital Zurich Switzerland[1], Laboratory of Cutaneous Biology, Department of Surgical, Medical, Dental and Morphological Sciences, University of Modena and Reggio Emilia, Modena, Italy[2], Laboratory of Developmental Biology Lab, Department of Biology University of Padova, Padova, Italy[3]*

**Introduction:**
Overcoming targeted therapy resistance is a major challenge in cancer therapy. Since drug resistance often involves defects in cell death, the activation of apoptotic pathways are attractive targets for the development of new therapies. Several studies showed that CD271 (also known as p75NTR or NGFR) plays a critical role in melanoma progression by marking a population of slow cycling cells with increased invasive capacities. Moreover, CD271 is upregulated in melanoma patient-derived xenografts exposed to MAP-kinase pathway inhibitors and it is highly expressed in cells resistant to these drugs. CD271 is a transmembrane receptor, which belongs to the tumor necrosis factor receptor (TNFR) family and interacts with numerous ligands and receptors to modulate either survival or cell-death depending on the ligand. In addition, CD271 can signal alone or in association with other receptors (e.g., Trks, Nogo, sortilin, DR6) mediating a range of functions. This flexibility allows CD271 to play a fundamental role in the regulation of cell fate. The currently known ligands are mainly the neurotrophins (NTs). Unlike NTs, which bind CD271 with a low affinity and activate death or survival depending on the presence/absence of a co-receptor and on the intracellular interacting proteins, the β-amyloid (Aβ) has been shown to bind CD271 with a very high affinity and selectively activate its apoptotic pathway in the nervous system. The activation of the CD271 apoptotic pathway involves a double step proteolytic cleavage leading to the generation and consecutive activation of the intracellular domain (ICD).Given the relevance of CD271 in melanoma progression and drug response, this study aimed to activate the death-domain cell killing properties of CD271 to overcome targeted therapy resistance and prevent metastasis formation in melanoma. Unlike previous approaches that directly inhibited the receptor or blocked the pathways associated with its overexpression in resistant cells, we activated CD271's pro-apoptotic function resulting from its interaction with short β-amyloid peptides.

**Methods:**
Since the minimum sequence able to bind CD271 and containing the active motif was previously shown to be Aβ (amino acids 25-35), all experiments were performed using this short 10 amino acid peptide. The inverted sequence 35-25 was used as a control. 2D, 3D cultures, ex vivo (surplus patients biopsies) and in vivo (zebrafish) were used to evaluate melanoma cell death after treatment.

**Results:**
Targeting CD271 with a short peptide derived from the β-amyloid (Aβ) sequence overcomes melanoma drug resistance. Combining β-amyloid with chemo- or targeted-therapy is synergistic, resulting in a strong induction of apoptosis in 2D and 3D (8 cell lines) and ex vivo (3 patient-derived tumor samples). The treatment strongly reduces metastasis formation in vivo (1056 zebrafish larvae injected with five melanoma cell lines, with no observable toxicity). By studying its mechanism of action, we could demonstrate that β-amyloid is specific to CD271-expressing cells and induces CD271 cleavage and the subsequent phosphorylation of JNK (pJNK). The direct protein-protein interaction of pJNK with CD271 leads to PARP1 cleavage, p53 and caspase activation, and pJNK-dependent cell death. Finally, β-amyloid also mediated mitochondrial reactive oxygen species (ROS) accumulation, which can be reduced by CD271 overexpression, revealing the presence of a negative-feedback loop, in which CD271 plays an active role in rescuing cells from ROS-induced apopotosis.

**Conclusion:**
This study revealed a new potential treatment for acquired resistant melanoma. These results suggest that targeting CD271 can further activate cell death pathways and potentially improve the efficacy of standard targeted therapy strategies.

**172**

J. Jang[2], D. Linus[2], F. Janker[2], Y. Yamada[2], C. Opelz[2], W. Weder[2], W. Jungraithmayr[1, 2]

**The role of CD26 in fibrous formation in chronic lung allograft dysfunction**

*University Hospital Rostock[1], University Hospital Zürich[2]*

**Introduction:**
Chronic lung allograft rejection, termed chronic lung allograft dysfunction (CLAD), is the primary cause of death beyond the first year after transplantation (Tx). CLAD is a form of fibrous obliteration of small airways. The multifunctional protein CD26 is known to be a mediator of fibrous stroma formation. We here analyzed if CD26 is expressed in CLAD lesions in mouse lung Tx, and if the inhibition of CD26 attenuates fibrous formation.

**Methods:**
Allogeneic mouse lung Tx was performed using BALB/c (donor) and C57BL/6 (recipient) strains. CLAD related pro-fibrotic mediators were analyzed by RT-qPCR and western blotting, respectively. Protein levels of EMT-related genes (Vimentin, N-cadherin, E-cadherin, Slug, and Hif-1α) were determined by western blotting. CD26 co-expression with α-smooth muscle actin within transplants were assessed by immunofluorescence. By using primary lung fibroblasts from wild type and CD26-/- mouse strains and treatment of CD26 inhibitor (vildagliptin) ex vivo, EMT activity, and proliferation rate were assessed by western blotting and MTT assay, respectively.

**Results:**
CLAD lesions were developed in allografts eight weeks after Tx and could be confirmed by significantly higher expression levels of CLAD related pro-fibrotic genes (Tgfb1, Igf1, Mmp9, and Cxcl9) and α-smooth muscle actin compared to normal lungs ($p<0.05$). Along with the expression of CD26, EMT was confirmed to be active in CLAD lesions by a significantly higher protein expression of Vimentin, Slug, and Hif-1α vs. normal lungs ($p<0.05$). Also, CD26 was co-expressed with α-smooth muscle actin positive cells in CLAD lesions. The expression of EMT proteins were reduced in CD26-/- fibroblast as well as in wild type fibroblast that were treated with the CD26-inhibitor vildagliptin, but also the proliferation of CD26-/--fibroblasts, mediated by TGF-β1 and IFN-γ, was significantly diminished. Moreover, the inhibition of CD26 by vildagliptin resulted in a reduction of α-smooth muscle actin and N-cadherin from primary lung fibroblast.

**Conclusion:**
CD26 is expressed in CLAD lesions of lung allografts and its inhibition downregulates fibrosis-forming mediators. These data suggest that CD26 is a potential target to attenuate the development of CLAD lesions.

**173**

K. Klein[2, 6], T. Schweizer[2, 4], K. Siwy[6], B. Lechmann[5], P. Kronen[1, 6], A. Karol[6], A. Zinkernagel[1, 4], B. Von Rechenberg[1, 6], Y. Achermann[1, 3, 4], S. Darwiche[1, 3, 6]

**Establishment of an acute implant-associated Staphylococcus aureus bone infection model in sheep designed to evaluate novel osteomyelitis treatments**

Center for applied Biotechnology and Molecular Medicine (CABMM), University of Zurich, Zurich, *Switzerland[1], Contributed equally to this work (co-first authors)[2], Contributed equally to this work (co-senior authors)[3], Department of Infectious Diseases and Hospital Epidemiology, University Hospital Zurich, University of Zurich, Zurich, Switzerland [4], Johnson & Johnson Family of Companies[5], Muscoskeletal Research Unit, Vetsuisse Faculty, University of Zurich, Zurich, Switzerland[6]*

**Introduction:**
Orthopedic implant-associated infections pose a considerable socio-economic burden worldwide. They are mostly caused by *Staphylococcus aureus* and challenging to treat due to the formation of a biofilm, contributing to persistent or recurring infections. The infected bone area and affected adjacent implants have to be removed and antibiotic treatment installed to cure the infection. However, implants can rarely be removed in implant-associated osteosynthesis infections, due to stability reasons. These cases require innovative, specifically tailored treatment approaches. An innovative approach to tackle such implant-associated infections is the application of low frequency electromagnetic fields. Standard inert orthopedic implants used to stabilize a bone during the active osteosynthesis process could then be transformed into an active device delivering pulsed electromagnetic field (PEMF) therapy locally at the area of interest. The current study aimed to establish a novel sheep model in the acute phase of an implant associated bone infection in the proximal tibia, mimicking the clinical presentation of such infections in humans. Additionally, as a proof of concept, the potential benefit from PEMF therapy in curbing the progression of an acute bone infection was investigated.

**Methods:**
All animal experiments were conducted according to the Swiss laws of animal protection and welfare (license ZH046/18). A bone block was freed from the metaphyseal area of the proximal tibia of four adult female Swiss alpine sheep. *S. aureus* was then delivered into the defect and the bone block placed back and fixed with a metal plate and two adjacent screws, which were connected to an implanted transducer. Two animals received PEMF treatment twice daily. The sheep were sacrificed 21 days post-operatively. A layer-by layer dissection was performed to evaluate signs of inflammation, infection and necrosis. Tissue samples and implants were harvested for microbiological quantification and tissue samples were also harvested for histology analysis.

**Results:**
The animals of the control group displayed symptoms of discomfort, lameness, redness, swelling and local heat at the wound area as well as reduced load bearing of the operated hind limb until sacrifice, consistent with a localized acute infection. These symptoms resolved after maximally eleven days. Blood cultures and blood analyses throughout the 21-day post-operative period showed no signs of systemic infection or sepsis. Overall, the clinical signs pointed to an acute infection peak between three and nine days post-operatively. Deeper tissue layers revealed the formation of a localized abscess above the plate and osteolytic bone in the defect cavity in all animals. Histology showed advanced osteolysis and accumulation of acute inflammatory components of severe grade, characterized by infiltration of immune cells. The bacteria were mostly localized in the infected bone defect, with lower concentrations found on the implants and in the surrounding soft tissue in all animals. Bacterial counts did not show a significant difference or an appreciable trend between the control and PEMF-treated sheep.

**Conclusion:**
A sheep model of a localized acute orthopedic implant-associated infection caused by *S. aureus* using a large implant was established. As a proof of concept, the use of PEMF therapy as an alternative to antibacterial treatment was not compatible with an acute infection model. Since the model nicely mimicked an acute infection, it could be further used to evaluate novel treatment option for acute implant-associated infections with osteomyelitis.

**174**

C. Gonçalves Moreira[1], A. Müllner[1], P. Hofmann[1], V. Ginde[1], S. Erdogan[1], M. Scandella[1], M. Morawska[1], S. Masneuf[1], D. Noain[1], C. Baumann[1]

**Exploring CLASSOS as a potential therapeutic tool in TBI rats**

*Animal Sleep Laboratory, Neurology Department, University Hospital Zurich, Zurich, Switzerland[1]*

**Introduction:**
High slow wave activity (SWA), a feature of deep sleep, is believed to be essential for efficient intracellular and extracellular protein clearance in the rodent brain. Our past work showed that both sleep induction and sleep restriction in TBI rats promoted enhanced SWA, that is, deeper sleep. In association, we found preserved cognition after TBI and reduced up to 90% of posttraumatic diffuse axonal injury (DAI). However, our work lacked the specificity needed to undoubtedly point out to SWA as the major mechanistic player behind the observed ameliorated recovery. One non-pharmacologic and non-invasive way to specifically modulate SWA is to target slow oscillations (SOs) in a timely fashion using closed-loop acoustic stimulation. We have established that targeting auditory pulses to SOs' up-phase constitutes a privileged time window for boosting SWA without changing sleep amount, whereas intervening SOs' down-phase disrupts slow oscillatory patterns and, ultimately, diminish depth of sleep. We hypothesize that up-phase acoustic stimulation in TBI rats will increase SWA, translating into reduced posttraumatic DAIwhile down-phase stimulation will offer the opposite effect.

**Methods:**
We use a rat model of closed-head TBI compatible with electroencephalography/electromyography (EEG/EMG) measurements and simultaneous sleep-staging and closed-loop acoustic stimulation of slow oscillations (CLASSOs). We examined posttraumatic i) sleep depth and architecture, ii) histopathology by immunohistochemistry and stereology on chronic axonal accumulation of APP, and iii) cognition by novel object recognition test (NORT). Following, we aimed at evaluating the effect of sleep modulation immediately after trauma on TBI outcomes. Sleep modulation consisted of 5 days of different treatment combinations: up-phase vs. down-phase CLASSOs combined with control (Ctr; placebo) or sleep enhacement (SE; Sodium Oxybate, ~400mg/kg, i.p.), or sleep restriction (SR; gentle handling).

**Results:**
We expect to observe similar SWA changes in TBI animals as we previously saw in healthy individuals, i.e. up-phase stimulation increases SWA up to 14% whereas downstate stimulation decreases it down to -10%, both without altering total amount of sleep per 24h. More in-depth look into EEG data as well as detailed results regarding cognition and DAI will be shown in the poster.

**Conclusion:**
Improving SWA in a precise and uniform manner by CLASSOs might constitute a novel neuroprotective approach for treating TBI sequelae. Our results will shed light on the pathways linking deep sleep and recovery mechanism during NREM, and hopefully provide important hints paving the way to future non-pharmacologic sleep modulation therapies for TBI subjects.

**175**

M. Pfefferlé[3, 4], G. Ingoglia[3, 4], C. Schaer[2, 4], A. Yalamanoglu[3, 4], I. Dubach[3, 4], R. Buzzi[3], G. Tan[1], N. Schulthess[3, 4], K. Hansen[3, 4], R. Humar[3, 4], D. Schaer[3, 4], F. Vallelian[3, 4]

## Phenotypic and functional characterization of anti-inflammatory erythrophagocytes in the liver of hemolytic mice

*Functional Genomics Center Zurich, ETH Zurich/University of Zurich, Switzerland[1], Institut für Anästhesiologie[2], Klinik und Poliklinik für Innere Medizin[3], Universitätsspitals Zürich (USZ) [4]*

**Introduction:**
Many pathological processes are linked to red blood cell (RBC) stress and damage leading to their ingestion by macrophages. Erythrophagocytosis prevents the release of RBC toxins into the extracellular environment by allowing controlled degradation of the heme and iron-recycling. While the red pulp macrophages (RPMs) of the spleen are responsible for the majority of damaged RBCs clearance under homeostatic conditions, a specialized population of liver macrophages take over that role in the context of a generalised hemolytic stress. Previous in vitro studies have demonstrated that this process supports differentiation of macrophages with high antioxidative and iron metabolizing capacities. However, the impact of erythrophagocytosis on macrophage phenotype differentiation and immune functions have not yet been explored, largely due to the lack of appropriate animal models. In this study, we aimed to define the phenotype and immunomodulatory function of the specialized population of RBC degrading liver macrophages - termed by us erythrophagocytes.

**Methods:**
To characterize the phenotype and function of erythrophagocytes in vivo, we used the $Spta^{sph/sph}$ genetic mouse model of spherocytosis. These mice have a point mutation in the alpha-spectrin gene causing an erythrocyte membrane defect and accelerated clearance of RBCs by liver macrophages. To study the specific phenotype of erythrophagocytes, we performed in situ liver digestion to obtain non-parenchymal liver cell suspensions that were enriched for macrophages using F4/80 coated magnetic Dynabeads. Erythrophagocytosis was visualised by imaging fluorescent activated cell sorting (FACS) and the transcriptomic signature was studied using droplet-based single cell RNA-sequencing (10x Genomics). To study the inflammatory function of liver macrophages in vivo, we used an agonistic anti-CD40 antibody-induced necrotizing hepatitis model. Outcomes were liver enzymes (Reflotron), plasma cytokine levels (Bioplex), liver histology and liver macrophage proinflammatory genes expression (RT-qPCR and bulk RNA-sequencing).

**Results:**
We show that enhanced erythrolytic stress in spherocytic mice triggers expansion of a large population of erythrophagocytes in the liver. Using single cell RNA-sequencing, we found that this population had a phenotype that could be defined as $Marco^{high}$/$Hmox^{high}$/MHC-class $II^{low}$. Erythophagocytes expressed an anti-oxidative and anti-inflammatory transcriptional signature. A small population of Marco positive erythrophagocytes could also be observed in the wild-type mouse suggesting that erythrophagocytes comprise a physiological macrophage population with an enormous capacity to functionally expand during erythrolytic stress. Treatment of mice with anti-CD40 antibody induced an inflammatory syndrome with cytokine storm, focal liver cell necrosis, and disseminated intravascular coagulation. This pathology is highly dependent on a primary macrophage response as mice with a macrophage-specific CD40 knockout did not develop signs of disease. Intriguingly, the anti-CD40-induced disease was dramatically attenuated in hemolytic $Spta^{sph/sph}$ mice, suggesting that a functional shift of macrophage responses accompanies the phenotype transition from inflammatory liver macrophage to anti-inflammatory erythrophagocytes.

**Conclusion:**
Taken together, our results indicate that erythrophagocytosis skews liver macrophages into a hypo-inflammatory functional state expressing a typical transcriptional signature and providing protection from macrophage-driven liver inflammatory disease.

**176**

N. Häffner[1], J. Bär[1], V. Dengler Haunreiter[1], S. Mairpady Shambat[1], A. Zinkernagel[1]

**Colony heterogeneity of S. aureus agr knock out strains is independent of intracellular pH**

*Infectious Diseases and Hospital Epidemiology[1]*

**Introduction:**
Staphylococcus aureus causes chronic and relapsing infections, which are difficult to treat. So-called small colony variants (SCVs) have been associated with chronic infections and have been shown to increase under antibiotic pressure, low pH and intracellular localization. Clinically, S. aureus strains isolated from an infection often show a dysfunction in the accessory gene regulator (agr), a major virulence regulatory system in S. aureus. The role of agr deficiency together with the exposure to intracellular pH on SCV formation has not been elucidated yet.

**Methods:**
To assess the interplay of intracellular environment and agr function on SCV formation, we established a lung epithelial cell infection model. This allowed analyzing intracellular survival and localization of a panel of S. aureus wild type and isogenic agr knock out mutants as well as a natural dysfunctional agr strain by confocal laser scanning microscopy (CLSM). To monitor changes of the intracellular environment, quenching of FITC-labeled bacteria was used as an indirect readout for intracellular pH. Furthermore, we quantified bacterial colonies after one, three and five days of intracellular survival by time-lapse analysis to determine kinetics of colony appearance and SCV formation.

**Results:**
We found that S. aureus agr knock out mutants predominantly resided in a neutral environment, whereas wild type strains resided in an acidic environment. Despite their localization in a neutral intracellular milieu, S. aureus agr knock out mutants have an increased colony size heterogeneity and higher SCV numbers as compared to their corresponding wild type strains. Neutralizing the acidic compartments with chloroquine resulted in an up to seven-fold reduction of SCVs in S. aureus wild type strains, but not in S. aureus agr knock out mutants.

**Conclusion:**
We conclude that the formation of SCVs in S. aureus agr knock out mutants is independent from intracellular pH, whereas S. aureus wild type strains require an acidic intracellular environment to form SCVs. The in-depth understanding of the interplay between intracellular persistence, agr function and pH will help to identify new therapeutic options facilitating the treatment of chronic S. aureus infections in the future.

**177**

H. Hayward-Koennecke[2], C. Selles Moreno[2], M. Docampo[2], M. Morax[2], T. Ludersdorfer[2], V. Weichselbaumer[1], V. Treyer[1], M. Huellner[1], T. Mueller[2], C. Blumer[2], M. Sospedra Ramos[2], R. Martin[2], A. Lutterotti[2]

**First insights into biodistribution of a new tolerization approach using peptide-coupled autologous cells (ETIMSred study) in humans**

*Clinic for Nuclearmedcine, University Hospital Zurich, Zurich, Switzerland[1], Neuroimmunology and MS Research, Neurology Clinic, University Hospital Zurich[2]*

**Introduction:**
Multiple Sclerosis (MS) is a debilitating inflammatory disease of the central nervous system. Falsely directed T cells induce and perpetuate the disease. Tolerization approaches aim at silencing the pathologic immune response by specifically targeting these T cells without hampering the general immune system as many currently used immune treatments in MS do. A newly developed tolerization strategy employs intravenous autologous red blood cells (RBCs) chemically coupled with myelin peptides. The recently conducted ETIMSred phase I study showed excellent safety and tolerability of this promising approach. As shown in animals, peptide coupled RBCs undergo eryptosis shortly after re-infusion and their remains are taken-up by professional phagocytes in liver in spleen. These antigen-presenting cells (APCs) process and re-present the remnants in a tolerogenic manner. Animal studies using whole body imaging 90 minutes after injection of RBCs reveal their accumulation in liver and spleen. This was further confirmed by ex-vivo imaging of organs showing increased recruitment of RBCs in liver, spleen, kidney and lungs of these animals. However, the exact biodistribution in humans remained unclear. We therefore performed radioactive labelling of autologous peptide coupled RBCs before re-infusion in order to gain first evidence of biodistribution in humans in the currently ongoing ETIMSred extension study.

**Methods:**
To determine the distribution and sequestrating of peptide-coupled RBCs, 5ml of treated erythrocytes (taken from the blood bag) were labelled with the commonly employed 99mTechnetium (99mT) by UltraTag RBC kit. After the injection of 99mTc-RBCs the distribution was visualized by rapid and dynamic imaging acquisition via gamma scintigraphy and CT-Single Photon Emission Tomography (SPECT) at different time points (30min, 2h and 17h post-injection).

**Results:**
Labelling of antigen-coupled RBCs with 300Mbq 99Tc-Ultratag (99Tc binding: 30%) in patient ETIMS_01 showed a clear signal in in the spleen 2h post-injection as acquired by gamma scintigraphy, which was further supported by a clear signal in the spleen 3h post-injection as detected by SPECT. While in patient ETIMS_03 99Tc-binding did not reach sufficient levels in order to detect a clear signal. Two more patients have opted for this procedure in the currently ongoing study.

**Conclusion:**
This is the first study assessing the biodistribution of a tolerization approach using peptide-coupled autologous cells in humans. Radioactively labelling with 99Technetium of the autologous peptide-coupled RBCs showed an increased signal in the spleen 2h and 3h post-injection as seen in gamma scintigraphy and SPECT. This indicates a depletion of the antigen-couples RBCs in the spleen and further supports assumptions that opine the concept of APC being a main player for tolerance induction.

**178**

E. Randecker[1], G. Gantner[1], D. Spiess[1], A.P. Simões-Wüst[1]

**Health status, use of medication and recreational drugs during pregnancy: a cross-sectional survey in the Canton of Zurich**

*Department of Obstetrics, University Hospital Zurich[1]*

**Introduction:**
Use of medication and consumption of recreational drugs during pregnancy may have lasting effects on the development of the embryo/foetus. Therefore, pregnant women should be aware of those effects and receive adequate support from knowledgeable health professionals. These should be well informed - not only about the evidence level of the various treatments during pregnancy - but also about the needs and habits of pregnant women. Objectives of this analysis were to obtain an overview of the prevalence of different diseases and symptoms during pregnancy, characterise current medication use, and consumption of recreational drugs among pregnant women in the Canton of Zurich, often taken as a representation of the Swiss population.

**Methods:**
A questionnaire for pregnant women was created and distributed to participating obstetric clinics and birthing centres in the Canton of Zurich. Data collection took place between August 2018 and March 2019. Thereafter, data sets were manually digitalised and the - mainly descriptive - statistical analysis was performed using IBM® SPSS® Statistics.

**Results:**
In the analysis, 398 questionnaires were included (24.1% of distributed). The most common chronic diseases among the participating women were allergies (7.8%), thyroid disease (5.6%) and headache/migraine (5.4%), whereas heartburn disease (18.6%), iron deficiency/anaemia (16.7%) and morning sickness (14.3%) were the most frequently mentioned acute diseases. Some women reported mental diseases (chronic, 4.0%; acute, 13.2%). Most women reported at least one typical pregnancy symptom such as fatigue, nausea and gastroesophageal reflux. Almost half of the women took at least one medication during pregnancy. Painkillers (paracetamol, 37.5%; ibuprofen, 9.3%; diclofenac, 1.8%; others, 1.9%), anti-reflux medicines (aluminium hydroxide, 9.4%; pantoprazole, 7.1%; esomeprazole, 3.2%; others, 12.4%), and antibiotics (co-amoxicillin/amoxicillin, 11.7%; others, 5.2%) were frequently consumed during pregnancy. A few pregnant women consumed psychotropic medications (2.0%). More than 90% of the participants refrained from taking any recreational drug during pregnancy, 3 out of 4 women who were consuming tobacco before pregnancy quit after conception. Nevertheless, at least 1 in 27 pregnant women was smoking and 1 in 25 women was drinking alcohol during pregnancy (in most cases low amounts only).

**Conclusion:**
In addition to typical pregnancy symptoms, chronic and acute diseases were frequent among the participating pregnant women, showing how important knowledge on the safety - for both mother and child - of the various effective treatments is. Most commonly used medications are known to be safe for mother and child and are therefore recommended for use during pregnancy. That not always the most adequate medications were chosen suggests that more should be done to increase the acquaintance level of the present recommendations. The number of women reporting acute and chronic mental diseases was higher that of those taking psychotropic medications, indicating that some pregnant women might be undertreated. Most pregnant women were refraining from consuming alcohol, tobacco and illicit drugs, revealing a high health-awareness. However, since several women mentioned drinking alcohol and/or consuming tobacco, further preventive work is needed.

**179**

R. Buzzi[1], D. Schaer[1], R. Humar[1]

**Tracing the biodistribution of exogenously administered proteins in vivo using the TCO-tetrazine bioorthogonal reaction: A demonstration using cell-free hemoglobin**

*Division of Internal Medicine, University Hospital of Zurich[1]*

**Introduction:**
The preclinical development of protein therapeutics – biologics – requires the ability to track and identify them within their physiologic habitat without changing their properties. Here we applied an innovative bio-orthogonal chemistry-based technique for an inert protein tagging. This minimal chemical tag enables a fast covalent reaction with a functionalized fluorochrome after exogenous administration in a mouse model. We chose cell-free hemoglobin (Hb) as the protein to be evaluated because of its illustrative ability to distribute differentially through barriers into tissues and cell types on its own and after binding to its scavenger plasma protein haptoglobin in the circulation.

**Methods:**
We have functionalized purified mouse hemoglobin with a trans-cyclooctene (TCO) group using a N-hydroxysuccinimide (NHS) ester, which reacts with primary amines of the protein and forms a stable amid bond. The remaining NHS was removed by column filtration. A part of the functionalized TCO-Hb was complexed with an equimolar concentration of haptoglobin in vitro. Complex formation was confirmed by HPLC. TCO-Hb and TCO-Hb:haptoglobin complexes were then covalently bound to a tetrazine (Tz)-functionalized fluorochrome by the inverse electron demand Diels-Alder (IEDDA) reaction in vitro. Labeling efficiency determined by photo-spectrometric deconvolution revealed two bound fluorochromes for one Hb-subunit on average.

**Results:**
We have injected a high dose of TCO-Hb i.p. into the mouse to mimic an acute hemolysis. Alternatively, we have co-injected a saturating amount of haptoglobin i.v. to induce Hb:haptoglobin complex formation in the living animal. We have collected and analyzed plasma and organs were two hours after injection for biodistribution-studies across the blood-urine barrier, the blood-brain barrier, and the fenestrated liver sinusoid. Confocal Imaging of the kidney after Tz-labeling in situ revealed a strong and specific fluorescent signal of TCO-Hb inside the proximal tubule penetrating brush border cells, while TCO-Hb was not detected in plasma consistent with rapid passage of Hb through the blood-urine barrier. Co-injected haptoglobin formed complexes with TCO-Hb while in the animal's circulation in vivo, as spectroscopic plasma analysis demonstrated, and only trace amounts of TCO-Hb were detected in the kidney tubules. This observation confirms the increased molecular size of the complex disabled translocation into the urine. TCO-Hb alone or in the Hb:haptoglobin complex was not detected in the brain parenchyma, thus unable to penetrate the blood-brain barrier. In the liver, we found TCO-Hb:haptoglobin complexes inside Iba1-positive macrophages, which is consistent with a receptor-mediated clearance of Hb-haptoglobin complexes by liver-macrophages. Surprisingly, we found a wide-spread TCO-Hb signal in absence of Hp complexation by CD31-positive sinusoidal endothelium specifically in the liver.

**Conclusion:**
Strong and specific Tz-functionalized fluorochrome bonding was achieved within 40 min in situ at high dilutions, enabling high spatial resolution microscopy. TCO-functionalization of Hb preserved its native biodistribution in vivo, retaining haptoglobin complex formation ability and complex recognition/endocytosis by liver macrophages. Beyond, we have detected a potential Hb clearance pathway by liver sinusoids. As primary amino groups are present in every protein, this tracing procedure may be applied for preclinical absorption, distribution, metabolism, and excretion (ADME) data acquisition supporting the preclinical development of protein therapeutics.

**180**

R. Buzzi[5], M. Hugelshofer[4], K. Akeret[4], C. Schaer[5], H. Richter[2], R. Vaccani[5], V. Anagnostakou[3], P. Kronen[1, 7], Z. Kulcsar[3], M. Dennler[2], R. Humar[5], E. Keller[6], P. Kircher[2], D. Schaer[5]

**Targeting cell-free hemoglobin-toxicity in the subarachnoid space after aneurysmal subarachnoid hemorrhage**

*Center for Applied Biotechnology and Molecular Medicine (CABMM), University of Zurich[1], Clinic for Diagnostic Imaging, Department of Clinical Diagnostics and Services, Vetsuisse Faculty, University of Zurich[2], Department of Neuroradiology, Clinical Neuroscience Center, University Hospital and University of Zurich[3], Department of Neurosurgery, Clinical Neuroscience Center, University Hospital and University of Zurich[4], Division of Internal Medicine, University Hospital of Zurich[5], Neurointensive Care Unit, University Hospital of Zurich[6], Veterinary Anaesthesia Services – International[7]*

**Introduction:**
Secondary neurological damage, occurring between day 4 and 14 after the initial bleeding, is a major contributor to poor outcomes after aneurysmal subarachnoid hemorrhage (aSAH). Cerebral vasospasm, endothelial dysfunction, inflammation, and oxidative stress are known mechanisms of secondary neurological injuries after aSAH. However, up to date, there is no effective therapy to prevent secondary neurological damage and it remains the largest modifiable in-hospital risk factor. Several days after the initial bleeding, breakdown of erythrocytes within the subarachnoid space hematoma results in the accumulation of cell-free oxy-hemoglobin (Hb) in the cerebrospinal fluid (CSF) compartment. High cumulative concentrations of Hb in the CSF are associated with an increased incidence of delayed ischemic neurological deficits (DIND) and we have shown that cell-free Hb in CSF from patients after aSAH inhibits the NO-mediated vascular relaxation in isolated porcine cerebral arteries ex vivo. Here we investigated the toxic effects of Hb in the subarachnoid space sheep and provide proof-of-concept for a novel therapeutic approach using the natural Hb scavenger protein haptoglobin to neutralize Hb toxicity after aSAH.

**Methods:**
We established an acute in vivo sheep model with infusion of Hb and Hb:haptoglobin complexes into the CSF space. Digital subtraction angiography (DSA) and MRI were used to detect vasospasms and brain perfusion. At the end of the experiment, the brains were harvested for histological studies.

**Results:**
Dynamic MR imaging showed a rapid distribution of the infused Hb from the lateral ventricle to the basal subarachnoid space (n = 4). Infusion of Hb lead to cerebral radiographic vasoconstriction with a maximum after 60 min (n = 5). Overall, the diameter of large cerebral arteries decreased by 15%. In contrast, infusion of Hb:haptoglobin complexes did not lead to cerebral vasoconstriction (n = 5). Additionally, histological studies revealed constriction of small penetrating arteries surrounding the 4th ventricle in sheep infused with Hb, but not after infusion of Hb:haptoglobin complexes. As a mechanism we identified the delocalization of cell-free Hb from the CSF across tissue-barriers into the NO-sensitive smooth muscle cell layer of cerebral arteries. This delocalization was completely interrupted when the small Hb protein dimers were sequestered in the large Hb-haptoglobin complex. Additionally, we observed the delocalization of uncomplexed Hb into the brain parenchyma, which could lead to direct neuronal toxicity and triggering of inflammatory processes by Hb and it's breakdown toxins.

**Conclusion:**
Cell-free Hb is the most abundant red blood cell toxin in the CSF during the high-risk period for secondary neurological damage after aSAH. We identified Hb delocalization from the CSF into the vessel walls and brain parenchyma as the critical initial step of cerebral Hb-toxicity. Delocalized Hb interferes with the NO-signaling in cerebral arteries in vivo and leads to vasoconstriction of cerebral arteries. We provide proof-of-concept that Hp administration into the CSF compartmentalizes cell-free Hb within the CSF and restores vasodilatory NO-signaling in the cerebral vasculature. In conclusion, intraventricular Hp administration may represent a causal therapeutic approach to reduce the toxicity of cell-free Hb in patients with hemorrhages into CSF compartment.

**181**

D. Vdovenko[1], W. Wijnen[1], M. Zarak Crnkovic[1], P. Blyszczuk[1], M. Bachmann[1, 2], S. Costantino[1], C. Diaz-Canestro[1], F. Paneni[1], G. Camici[1], T. Lüscher[1, 3], U. Eriksson[1, 2]

**Controversial role of IL-23 in cardiac autoimmunity**

*Center for Molecular Cardiology, University of Zurich, Zurich, Switzerland[1], Department of Medicine, GZO – Zurich Regional Health Center, Wetzikon, Switzerland[2], Royal Brompton and Harefield Hospitals and Imperial College, London, United Kingdom[3]*

**Introduction:**
Autoimmunity is a dangerous risk factor in patients with cardiac inflammation. Manifestation of cardiac inflammation caused by different sources vary widely and, in some cases, progress to autoimmune myocarditis and further inflammatory dilated cardiomyopathy (iDCM) and heart failure. Heart-reactive CD4Th17 cells were claimed critical for pathogenesis of autoimmune myocarditis. IL-23 is a pro-inflammatory cytokine, predominantly produced by dendritic cells as specialized antigen presenting cells, promoting T cell differentiation towards Th17 effector cells. However, literature reports excessiveness of IL-23 in Th17-derived IL-17 production, and the specific role of IL-23 in pathogenesis of the disease is unclear.

**Methods:**
To explore the particular role of IL-23 in myocarditis progression we use dendritic cell model of experimental autoimmune myocarditis (EAM) in wild-type (wt) and IL-23-deficient mice. We inject mice with bone marrow-derived in vitro activated and loaded with cardiac-specific peptide dendritic cells (DC). This model mimics natural processes taking place during heart inflammation and provides a unique method to address the role of DCs-derived cytokines.

**Results:**
Surprisingly, all immunized mice were able to develop myocarditis, though wt receiving IL-23-/-bmDCs showed a twofold decrease in heart-infiltrating T cells and lower numbers of Th17 population both in heart and in the periphery comparing to those received wt bmDCs. Even further decrease in numbers of heart-infiltrating T cells appeared upon IL-23-/-bmDCs injections into IL-23-deficient mice. In comparison to IL-12, the other important pro-inflammatory cytokine of the same family, directly inducing differentiation of Th1 IFN-gamma–producing cells from naïves, IL-23 by itself cannot induce Th17 differentiation. None of the two cytokines affect proliferation, though, IL-23 activates T cell migratory potential and increases T cell migration by twofold. At the same time, deficiency of IL-23-production by bmDCs leads to lower migration of T cells. We also hypothesize the importance of IL-23-dependent T cell trafficking in the resolution of the acute stage of autoimmune myocarditis.

**Conclusion:**
Therapeutic approaches involving inflammatory cytokine targeting are a promising clinical perspective. Our observations underline IL-23 as not only a cytokine repolarizing Th17 maturation but also responsible for T cell trafficking in autoimmune myocarditis, which helps to understand the regulation of myocarditis development and improve a long-term prognosis on progression of myocarditis to heart fibrosis and iDCM.

**182**

V. Garcia[4, 5], S. Hiltbrunner[1], P. Tallon de Lara[3], M. Messerli[2], D. Akhoundova[1], L. Bankel[1], C. Britschgi[1], S. Bihr[1], D. Pizzuto[2], M. Anisimova[4, 5], I. Burger[2], A. Curioni-Fontecedro[1]

**An analysis of the effectiveness of immunotherapy in non-small cell lung cancer patients by tracking SUV lesion intensity**

*Department of Medical Oncology and Hematology, University Hospital Zurich[1], Department of Nuclear Medicine, University Hospital Zurich[2], Institute of Experimental Immunology, University of Zurich[3], Swiss Institute of Bioinformatics, Lausanne[4], Zurich University of Applied Sciences, Wädenswil[5]*

**Introduction:**
Non-small cell lung cancer (NSCLC) is frequently identified in a late stage resulting in an overall unfavourable prognosis and rapidly metastasizes into other organs. The paucity of curable approaches has recently advanced cancer immunotherapy as a novel therapeutic option. Therapeutic outcomes may be assessed by changes in standardized uptake values (SUVs) measured by PET/CT. For lung tumors, SUV measurements taken prior to immunotherapy application are compared to SUVs after application. Their change over time is used to assess the therapy's effectiveness. However, a meaningful estimate of the effectiveness of the therapy would require to know the SUVs of tumors at the time of immunotherapy application --the reference SUVs-- and to monitor the change in SUV over the time period following immunotherapy. Substituting these reference values by values measured substantially before immunotherapy is applied, can severely bias effectiveness estimates towards underestimates.

**Methods:**
In this study, we present two methods to correct for the bias of true reference SUV and to estimate effectiveness of immunotherapy within a patient from SUVs and metabolic tumor volumes (MTVs). These methods rely on a system of differential equations that describe the dynamics of within-patient colony size distributions of metastases. Fitting these distributions to patient data provides estimates on growth and decline rates of tumors before and after immunotherapy application, respectively.

**Results:**
We applied both methods to a set of data from 43 patients, with a total of ca. 500 lesion measurements. We observed that the within-patient distribution of SUV intensities prior to immunotherapy is well approximated by an exponential density. Our first method, relying on fitting the theoretical cumulative distributions to all metastases found in patients, leads to less satisfying results than the second method, where fits are performed on pairs of measurements taken before and after treatment. The tumor killing efficacies by the immunotherapy derived from these fits significantly correlate with treatment outcome as measured by overall survival.

**Conclusion:**
The here presented methods present a simple approach to make use of the heterogeneity of metastases within a patient. The heterogeneity is interpreted from the perspective of a mathematical model of cancer growth dynamics and broken down into a few meaningful and informative process parameters. These parameters offer a mathematically sound way to remove biases contained in contemporary effectiveness estimation approaches and may ideally translate into more precise therapy and improved clinical outcome.

**183**

I. Martinez Lopez[2], T. Papasotiropoulos[2], F. Schläpfer[2], S. Ulrich[1], M. Kirschner[2], I. Schmitt-Opitz[2]

**Biomarker identification for chronic thromboembolic pulmonary hypertension**

*Department of Pulmonology[1], Department of Thoracic Surgery[2]*

**Introduction:**
Chronic Thromboembolic Pulmonary Hypertension (CTEPH) is a rare, chronic, debilitating disease characterized by pathological changes that obstruct both sides of the pulmonary arteries. Pulmonary endarterectomy (PEA) can cure the disease, but not all patients qualify for this operation. Some genetic and molecular alterations have been associated but not uniquely characterized to CTEPH. In the present analysis, we wanted to assess the expression of microRNA in the resected tissue – short non-coding RNAs that act as posttranscriptional regulators of gene expression – with the aim to identify biomarkers for treatment allocation and give insight towards underlying pathological mechanisms behind this disease, which until now remain unclear.

**Methods:**
As a first strategy, tests from over 40 CTEPH RNA-later preserved tissues were performed using a microRNA-specific RT-qPCR approach. As initial candidates, we selected two microRNAs: miR-939 and miR-942. In order to assess possible associations between microRNA expression and CTEPH, we performed Spearman correlation between microRNAs and patient´s clinical factors, such as Jamieson and New York Heart Association Classifications, mean pulmonary artery pressure (mPAP), pulmonary vascular resistance (PVR), 6-minute walking distance test (6MWD) and oxygen saturation (SpO2).

**Results:**
Our findings show that miRNAs are differentially expressed between different patients and also between left- and right-sided disease. The reason behind the variation between both sides requires further investigation. Nonetheless, our preliminary analysis of 35 left-side patient tissues, found a trend towards positive correlation between mPAP levels and miR-939 ($R = 0.4286$, $p=0.01$). The SpO2 levels after 6MWD of 31 patients showed a negative correlation with the left miR-939 results ($R=-0.5402$, $p=0.002$).

**Conclusion:**
These early results demonstrate that miRNAs are not only detectable in PEA material but also, that its dysregulation might be involved in CTEPH pathophysiological mechanisms, associated to endothelial and inflammatory processes encouraging us to investigate further.

**184**

E. Boran[1], V. Scharding[1], K. Niklaus[1], G. Ramantani[2], J. Sarnthein[1]

**High frequency oscillations are more specific biomarkers of epileptogenic tissue than interictal spikes in the intraoperative ECoG.**

*Klinik für Neurochirurgie, UniversitätsSpital und Universität Zürich[1], Neuropädiatrie, Universitäts-Kinderspital Zürich, Zürich[2]*

**Introduction:**
Residual fast ripples (FR) in the intraoperative ECoG have recently been established as highly specific predictors of postsurgical seizure recurrence. However, in everyday practice, surgical decision is routinely based on the presence of interictal spikes. We investigated if FR indeed have the potential to outperform interictal spikes as a valid biomarker of epileptogenic tissue in the clinical setting.

**Methods:**
We analyzed the intraoperative ECoG recordings of two patients that underwent successful resective epilepsy surgery. The ECoG was performed by high-density grid electrodes with 5 mm spacing (hd-ECoG) in both cases. Interictal spikes were marked by two independent reviewers. FR were detected by a previously validated automatic detector. The location and rates of these two biomarkers were compared with the extent of resection that led to seizure freedom in both cases.

**Results:**
Across all 47 bipolar channels in pre-resection ECoG recordings, interictal spikes were detected in 18 channels, whereas FR were identified only in 9 channels. In both cases, the FR area was more restricted than the interictal spike area. All electrode contacts with FR were resected, i.e. there were no residual FR but several contacts with interictal spikes were left unresected, i.e. there were residual interictal spikes. FR guided a more limited resection than the one detected by interictal spikes. Moreover, the full resection of the FR area sufficed to achieve seizure freedom and residual interictal spikes did not predict postsurgical seizure recurrence.

**Conclusion:**
High frequency oscillations, particularly FR, are more specific biomarkers of the epileptogenic tissue than interictal spikes in the intraoperative ECoG. The detection of FR may improve postsurgical seizure outcomes and facilitate seizure freedom, while sparing healthy tissue.

**185**

E. Boran[1], J. Sarnthein[1], N. Krayenbühl[1], T. Fedele[2], G. Ramantani[3]

**High frequency oscillations in scalp EEG decrease after successful epilepsy surgery.**

*Klinik für Neurochirurgie, UniversitätsSpital und Universität Zürich[1], National Research University Higher School of Economics, Moscow, Russian Federation[2], Neuropädiatrie, Universitäts-Kinderspital Zürich, Zürich[3]*

**Introduction:**
High-frequency oscillations (HFO) are reliable EEG biomarkers of epileptogenicity, as has mainly been demonstrated in invasive recordings. Recently, these observations were extended to HFO recorded in the widely accessible scalp EEG. In a longitudinal approach, we investigated the clinical relevance of scalp HFO for therapy monitoring in focal epilepsies, particularly for the assessment of epilepsy surgery outcomes.

**Methods:**
In eight children with drug-resistant focal epilepsy that underwent epilepsy surgery, we prospectively recorded pre- and postsurgical scalp EEG. To detect clinically relevant HFO, we applied a previously validated automated detector.

**Results:**
Scalp HFO rates decreased following the full or partial resection of the epileptogenic zone in six patients, regardless of the lobar localization of the epileptogenic zone. Postsurgical scalp HFO rates were particularly low in the 4 patients that achieved seizure freedom and particularly high in the 2 patients that had postsurgical seizure recurrence.

**Conclusion:**
We thereby demonstrate that non-invasively recorded scalp HFO can be utilized as an outcome biomarker in epilepsy surgery. This is the first step towards implementing scalp HFO as a marker of disease severity and treatment response, particularly in the pediatric population.

**186**

S. Dudli[2], D. Haenni[3], I. Heggli[2], A. Juengel[2], U. Ziegler[3], M. Betz[1], J. Spirig[1], F. Wanivenhaus[1], F. Brunner[1], M. Farshad[1], O. Distler[2]

## Histomorphometry of Modic changes

*Balgrist University Hospital[1], Center of Experimental Rheumatology[2], Light Microscopy Center[3]*

**Introduction:**
Modic changes (MC) are specific for chronic low back pain. Despite the high prevalence of MC, the histopathology of MC remains poorly understood. The only published histological data from clinical MC biopsies are from Michael Modic's original paper. He analyzed three MC type 1 (MC1) and three MC type 2 (MC2) specimens with hematoxylin/eosin. He described MC1 as vascularized fibrous tissue and MC2 as yellow marrow replacement. No histomorphometric data is available that would help to understand the pathophysiology of MC. The aim of this study was to characterize MC histomorphometry with multiphoton excitation microscopy (MPE), histology, and immunohistochemistry (IHC) in order to better understand MC pathophysiology.

**Methods:**
From patients undergoing lumbar spondylodesis, bone marrow biopsies (n=2 MC1, n=5 MC2, n=5 control; based on T1- and T2-weighted MRI) were taken through pedicle screw trajectory before screw insertion. Fixed biopsies were analyzed en-bloc with MPE (n=2 MC1, 3 MC2, 2 control) and as paraffin sections with histology, IHC, and MPE (n=2 MC1, 4 MC2, 5 control). MPE: second-harmonics-generation (SHG) of collagen and tissue autofluorescence were recorded of large volumes. Fluorescence-life-time-imaging-microscopy (FLIM) of the auto-fluorescence signal was performed in key areas of en-bloc biopsies (n=1 MC1, 3 MC2, 1 control). Sections were stained histologically (eosin/hematoxylin, masson trichrome) and analyzed with IHC for alpha smooth muscle actin (aSMA), collagen-1, collagen-3, cellular fibronectin, and CD68 (macrophages).

**Results:**
MPE revealed a large spatial tissue heterogeneity in MC. Hematopoietic marrow was interdispersed with hypocellular MC elements. In MC1, fibrotic tissue replaced hematopoietic elements and colocalized with increased numbers of adipocytes and collagen-3 positive blood vessels. In MC2, hematopoietic marrow was replaced by adipocytes with little marrow fibrosis.Collagen-1 was exclusively found in fibrotic marrow. Collagen-3 and fibronectin fibers were present in fibrotic areas but were also found in control marrow. Adipocyte were surrounded by collagen-3. Alpha-SMA positive myofibroblasts were scarce in MC1 and almost absent in MC2 and control biopsies. Alpha-SMA positive vascular smooth muscle cells were more abundant in MC1. Macrophages were not increased in MC1 and MC2. Fibrotic marrow was best identified and visualized with MPE using SHG. MPE-FLIM was even more sensitive than MPE to detect collagen fibers and allowed stain-free identification of different cell types also in deep tissue layers based on auto-fluorescence life-time: adipocytes ($\tau$~2.1ns), leukocytes ($\tau$~0.5ns), erythrocytes ($\tau$~0.3ns), SHG of collagen ($\tau$<0.15ns) (Fig.d).

**Conclusion:**
Marrow fibrosis is best identified with SHG in MPE. MPE-FLIM of en-bloc biopsies in combination with IHC and histology allows unprecedented insight into the complex pathology of MC. MC1 bone marrow fibrosis is mainly a collagenous fibrosis with presence of collagen-3 (reticulin fibrosis). Adipocytes seem to play an important role in MC, because they colocalize with fibrotic tissue. Increased number of adipocytes have previously only been associated with MC2. Their abundance in MC1 along with spatial tissue heterogeneity suggest phases of MC1 flare-ups and MC2 remissions and questions the T1- and T2-weighted MRI-based MC classification.

**187**

C. Mamie[3], R. Bruckner[2], S. Lang[3], N. Shpigel[5], M. Turina[4], A. Rickenbacher[4], Y. Chvatchko[1], G. Rogler[3], M. Scharl[3]

## Expression of MMP-9 in resected intestinal fistula from patients with fistulizing Crohn's disease and from human xenograft mouse model for intestinal fistula

*Calypso Biotech SA, Plan-les-Ouates, Geneva, Switzerland[1], Department of Gastroenterology and Hepatology, Leiden University Medical Centre, Leiden, Netherlands[2], Department of Gastroenterology and Hepatology, University Hospital Zurich, University of Zurich, Zurich, Switzerland[3], Department of Visceral and Transplantation Surgery, University Hospital Zurich, University of Zurich, Zurich, Switzerland[4], Koret School of Veterinary Medicine, Hebrew University of Jerusalem, 76100 Rehovot, Israel[5]*

**Introduction:**
Fistulas treatment represent a major unmet medical need in the therapy of Crohn's disease (CD) patients. Current medical therapies, even anti-TNF antibodies, are often insufficient and do not achieve permanent fistula closure. Previous data point towards a critical role for metalloproteinase-9 (MMP-9) / gelatinase B in fistula pathogenesis. The aim of this project is to investigate whether MMP-9 might be a potential target for fistula therapy in CD patients.

**Methods:**
To study whether MMP-9 might represent a possible target for fistula therapy, we performed immunohistochemistry for total and active MMP-9, Cytokeratin 8 (CK-8) as well as active MMP-9/CK-8 co-staining in fistula specimen from perianal fistulas, entero-enteric fistulas, fistulas from non-responding patients under anti-TNF therapy as well as fistulas from the xenograft mouse model.

**Results:**
Our data show a possible role for MMP-9 in fistula pathogenesis and suggest MMP-9 as a possible therapeutic target for fistula therapy. As key findings, total and active MMP-9 are present in perianal as well as in entero-enteric fistulas. Of note, total and active MMP-9 are also expressed in CD fistulas in patients under anti-TNF treatment. Interestingly, we detected a clear co-staining of active MMP-9 and CK-8 in particular in cells lining the fistula tract as well as in transitional cells (TC) around the fistulas. Further, total and active MMP-9 are detectable in xenograft fistulas.

**Conclusion:**
Taken together, MMP-9 might play an important role for fistula pathogenesis in CD patients and our novel xenograft fistula model might be suitable for *in vivo* studies investigating a possible therapeutic role for targeting MMP-9 as fistula therapy.

**188**

B. Schmid[2], O. Hausmann[4], Y. Achermann[2], K. Wuertz-Kozak[1, 3, 5]

**The role of Cutibacterium acnes in intervertebral disc inflammation**

*Department of Biomedical Engineering, Rochester Institute of Technology, 106 Lomb Memorial Dr., Rochester, NY, USA[1], Department of Dermatology, Universitity Hospital Zurich, University of Zurich, Gloriastrasse 31, Zurich, Switzerland[2], Institute for Biomechanics, ETH Zurich, Hönggerbergring 64, Zurich, Switzerland[3], Klinik St. Anna, St. Anna Strasse 32, Lucerne, Switzerland[4], Spine Center, Schön Clinic Munich Harlaching, Harlachrngerstrasse 51, Munich, Germany[5]*

**Introduction:**
Low back pain is the primary cause of disability worldwide and one of its main sources is the degenerating intervertebral disc (IVD). Apart from innervation and chronic inflammation as contributors to discogenic back pain, the role of infection of the IVD with *Cutibacterium acnes (C. acnes)* as a pain inducer has become of interest. Thus, the aim of this study was to investigate whether and how *C. acnes* contributes to the inflammatory processes during disc degeneration.

**Methods:**
Primary human IVD cells (n = 4) were infected with a reference (ATCC11827) and a clinical *C. acnes* strain and incubated for 24 hours. Cells and supernatants were collected to analyze pro-inflammatory markers on the gene (qPCR) and protein (ELISA) level. In a subsequent experiment, the involvement of the toll-like receptor (TLR) pathway was investigated by co-treatment with Sparstolonin B, a TLR 2 and 4 inhibitor (n = 6). In addition, the prevalence of *C. acnes* infection in human IVD tissue (n = 30) was determined by 7 days of aerobic and anaerobic culture at 37 °C on Brucella agar plates and in thioglycolate broth. Statistics were done by testing continuous variables for normality using Kolmogorov-Smirnov tests. Further, one sample Wilcoxon Signed Rank tests (one-sided) were used to test whether medians were larger than 1 and corresponding paired tests were performed two-sided.

**Results:**
We detected *C. acnes* in 10% of surgically removed IVD biopsies, all of which were from IVD herniations. Stimulating IVD cells with two different *C. acnes* strains, gene expression of IL-1b (mean fold change ATCC strain (A): 2068, clinical strain (C): 694; $p = 0.03$), IL-6 (A: 713; C: 207; $p = 0.03$), IL-8 (A: 30275; C: 3676; $p = 0.03$), and iNOS (A: 2970; C: 1863; $p = 0.03$) was strongly upregulated compared to untreated controls. The increase could be confirmed on the protein level, with a good correlation to gene expression. IL-6 and (albeit less) IL-8 expression was reduced upon TLR2/4 inhibition in selected donors (mean expression IL-6: 54.7 ± 6.8% (48 - 64%); IL-8: 88.7 ± 18.5% (63 - 106%)), whereby responders and non-responders could not be differentiated by their basal expression levels of TLR2 or TLR4.

**Conclusion:**
Results of this study clearly demonstrate that exposure of IVD cells to *C. acnes* induces an inflammatory response that may ultimately contribute to pain development, hence providing a molecular link between *C. acnes* infection and discogenic back pain that involves TLR2/4 activation, yet only in a subgroup of patients. Whether the same response will be observed *in vivo*, where lower inoculums are present, remains to be proven in future studies.

**189**

R. Buzzi[2], K. Akeret[1], J. Klohs[3], R. Humar[2], M. Hugelshofer[1], D. Schaer[2]

**The red blood cell toxin heme as a therapeutic target after intracranial bleeding**

*Department of Neurosurgery, Clinical Neuroscience Center, University Hospital and University of Zurich[1], Division of Internal Medicine, University Hospital of Zurich[2], Institute for Biomedical Engineering, University of Zurich, ETH Zurich [3]*

**Introduction:**
Erythrolysis in a hematoma liberates a massive amount of cell-free hemoglobin (Hb) into the brain parenchyma or into the cerebrospinal fluid after intracranial or aneurysmal subarachnoid hemorrhage (aSAH), respectively. Outside of the reducing environment of the red blood cell, Hb can degrade and transfer its highly reactive heme groups to lipophilic tissue components, promoting lipid-oxidative tissue damage. Therefore, cell-free Hb and heme are thought to be involved in pathophysiological processes leading to secondary neurological damage after intracranial bleeding. Here we present a series of studies focusing on the distribution and the toxic effects of Hb and heme in the brain and we test the effect of the scavenger protein hemopexin as a potential therapeutic compound.

**Methods:**
To reduce complexity and study the isolated effect of cell-free Hb and heme after intracranial bleeding, we have established a mouse model with stereotaxic striatal injection of 10 µL purified hemoglobin (5 mM) or heme (1-2 mM). Heme distribution on histological sections was assessed using Zinc(II) Protoporphyrin IX (ZnPP) as fluorescent analog. Hb was coupled to a small trans-cyclooctene (TCO) tag for post mortem click-chemistry labeling combined with classical immune-fluorescence microscopy. Neurobehavioral deficits were determined using rotarod, beam walk and open-field testing. Additionally, brain edema and brain perfusion, as clinical correlates of neuronal damage, were measured with in vivo MR imaging.

**Results:**
We observed a rapid distribution of labeled Hb across the whole ipsilateral hemisphere already 2 hours after injection, but interestingly no specific uptake in microglia cells, which until now have been considered the brain-intrinsic Hb clearance and detoxification compartment. However, we found a specific signal in neuronal cells around the injection site and in the hippocampus. The heme analog ZnPP demonstrated a much more restricted regional distribution around the injection site. Hb injection did not cause detectable toxicity in any of the studied readouts. In contrast, heme-injection induced dose-dependent severe neurological deficits accompanied by localized edema, diffusion restriction and compromised perfusion in MR imaging. Post mortem histology revealed widespread activation of microglia and loss of GFAP positive astrocytes in the regions corresponding to the edema. Co-injection of heme with its endogenous scavenger protein hemopexin (Hx) completely rescued the observed phenotype.

**Conclusion:**
The rapid and widespread distribution of water-soluble Hb represents the high turnover and substantial flow of the interstitial fluid in the brain and highlights the possibility that Hb released from a localized site of damage could cause distant-site secondary injury. However, the rapid dilution in the large distribution volume after single-shot injection apparently limited the toxicity of cell-free Hb in our model. In contrast, the lipophilic heme remained immobilized around the injection site providing prolonged exposures of neuronal structures to toxic heme concentrations. These experiments emphasize the key function of Hb degradation and heme-transfer in the pathophysiological framework of erythrolysis-driven disease. Complexation of heme with hemopexin prevents lipophilic immobilization of heme and adverse oxidative tissue reactions. In conclusion, a reduction of the Hb/heme load or blocking their oxidative capabilities might decrease secondary neurological damage after intracranial bleeding.

**190**

S. Shim[1], J. Unkelbach[1], N. Saltybaeva[1], N. Berger[1], M. Marcon[1], H. Alkadhi[1], A. Boss[1]

**Evaluation of image quality, lesion detection and radiation dose in spiral breast CT equipped with a photon-counting detector.**

*University Hospital Zurich[1]*

**Introduction:**
Detecting submillimeter microcalcifications and small soft tissue masses is important for early-stage breast cancer detection. This study aims to evaluate the lesion detectability of a dedicated spiral breast CT equipped with a photon-counting detector, to propose optimal scan parameter settings to achieve low patient's radiation dose and high image quality based on measurements employing a dedicated breast phantom, to verify the lesion detectability in a patient image.

**Methods:**
A breast phantom with inserts (microcalcifications of 196/290/400µm diameters; masses of 1.8/3.18/4.76/6.32mm) underwent breast CT systematically varying X-ray tube currents between 5-125mA using two slabs of 100/160mm to assess the effect of the breast size. Signal-to-noise ratio (SNR) and contras-to-noise ratio (CNR) were calculated by region-of-interest analysis. Two experienced radiologists assessed the detectability of the inserts. Average absorbed dose was calculated by a validated Monte Carlo simulation. In a patient case who underwent breast CT and biopsy, the size of detected microcalcifications were evaluated.

**Results:**
SNR and CNR of inserts in the phantom showed logarithmic increases as a function of radiation dose independent to the size of breasts. Microcalcifications of 196µm dimeter were detected by applying optimal exposure settings associated with low dose, X-ray tube currents of 25/40mA, dose 4.3±0.1/5.7±0.1mGy for the small/large breasts, respectively. Every insert in other sizes was detected when the exposure setting is equal to or more than tube current 10/25mA with equivalent dose 1.7±0.0/3.6±0.1mGy. Inter-reader agreement in the phantom study was perfect ($\kappa$=1). In the patient's breast CT image, microcalcifications verified to be smaller than 290µm in the stereotactic biopsy image were detected.

**Conclusion:**
Breast CT provides an excellent image quality by administering a radiation dose, which is significantly lower than in cone-beam breast CT and comparable to conventional mammography.

**191**

A. Yalamanoglu[1], M. Pfefferlé[1], G. Ingoglia[1], I. Dubach[1], R. Buzzi[1], N. Schulthess[1], K. Hansen[1], D. Schaer[1], F. Vallelian[1]

**Antibody-induced CD40 signaling stimulates acute liver crisis in a mouse model of sickle cell disease**

*Klinik und Poliklinik für Innere Medizin - UniversitätsSpital Zürich[1]*

**Introduction:**
Sickle cell disease (SCD) affects millions of people worldwide with the highest frequency in Sub-Saharan Africa. The disease is defined by a point mutation in the beta hemoglobin chain rendering red blood cells (RBC) to sickle and hemolyze under stress conditions. Hemolytic anemia, pulmonary hypertension, acute kidney injury, stroke, and acute sickle hepatic crisis are some clinical complications of SCD. Eliciting factors for vaso-occlusive crises are inflammatory stress, hypoxia, and endothelial activation. Several models for SCD crisis in murine models have been proposed but all have inconsistent and weakly defined primary outcomes with overall poor experimental reproducibility. To study the main pathophysiological drivers of adverse events and explore novel therapeutics for SCD we aimed to establish a new inflammation-triggered SCD crisis model by using agonistic anti-CD40 antibody as a stimulus.

**Methods:**
We characterized sickle mice (HbS) and control littermates at baseline and after anti-CD40 injection. End-organ damage was assessed by histology, LDH and liver enzymes levels in plasma. The extent of hemolysis was quantified by the amount of kidney iron deposition and increase in bilirubin in plasma. Systemic inflammation, macrophage activation as well endothelial activation were assessed by cytokines and endothelial activation markers in plasma as well by VCAM1 upregulation in isolated liver endothelial cells by flow cytometry.

**Results:**
At baseline, HbS mice demonstrated higher levels of endothelial activation markers, bilirubin, iron deposition in the kidney and small liver infarcts compared to control mice. After anti-CD40 injection, sickle mice showed in comparison to control greater liver damage by higher level of liver enzymes, LDH and more extensive necrotic damage. Furthermore, levels of bilirubin and amount of iron deposition in the kidney increased in sickle mice in response to anti-CD40 treatment, suggesting acute intravascular hemolysis. After anti-CD40 challenge, HbS mice developed systemic inflammation with cytokine storm and disseminated intravascular coagulation with marked endothelial cell activation and extensive thrombus formation.

**Conclusion:**
After anti-CD40 treatment in sickle mice we found a systemic inflammatory response with accelerated hemolysis, extensive vaso-occlusion and ischemic end-organ damage in the liver. Overall the response towards anti-CD40 antibody stimulation was greater in sickle mice over control. Pre-existing vasculopathy in sickle mice might potentiate the adverse outcome. Based on our findings, anti-CD40 treatment might offer a new approach to study acute liver crisis in SCD. It might provide further insight to different co-players emerging during episodes of sickle crisis and help with the development of new therapeutics.

**192**

I. Dubach[1], R. Buzzi[1], A. Yalamanoglu[1], F. Vallelian[1], D. Schaer[1]

**Comparative phenotype characterization of three hemolytic genes in the mouse**

*Klinik und Poliklinik für Innere Medizin[1]*

**Introduction:**
Hemolysis is characterized by structural or functional red blood cell (RBC) damage leading to premature intravascular degradation or extravascular clearance of RBCs. Depending on the cause and severity of hemolysis, its sequelae are defined by anemia, hemoglobin-toxicity induced tissue injury or chronic iron overload. Genetic hemolytic diseases can be classified into three pathophysiological categories: mutations affecting red blood cell membrane components and cytoskeleton proteins, enzyme deficiencies, and hemoglobinopathies. In the past, different genetic mouse models of hemolysis have often been used interchangeably without consideration of gene-specific phenotypic characteristics. In this study, we systematically compared three existing genetic hemolytic mouse models. The Sptasph/sph mouse mimics a severe form of the human spherocytosis disease, the Berkley mouse HbS is a model of sickle cell disease (SCD), and the HbaTh3 mouse represents an intermediate severity type of beta-thalassemia. Our goal was to characterize the hemolytic phenotype of the three mouse models regarding the primary site and severity of RBC destruction, the extent of Hb-induced tissue injury, as well as secondary adaptive responses of erythropoiesis and iron metabolism.

**Methods:**
All mice were analyzed at age 8 - 10 weeks. The intensity of intravascular hemolysis was quantified with a novel haptoglobin capture assay. Molecular markers of compensatory adaptation of erythropoiesis and iron metabolism were measured by tissue bulk RNA-sequencing and shotgun mass-spectrometry (LC-MS/MS) of liver, spleen, and kidney. Hepcidin-25 was measured by a targeted mass-spectrometry method (SRM). Hematologic parameters, tissue iron accumulation, and markers of organ injury were determined by standard assays.

**Results:**
The Sptasph/sph mouse is characterized by a high intensity of intravascular hemolysis, a very strong erythropoietic compensatory response with massive iron overload in multiple organs, totally suppressed plasma hepcidin-25, and hemoglobinuria-induced kidney-injury. In contrast, the HbS SCD mouse and the beta-thalassemia HbaTh3 mouse have an almost exclusively extravascular hemolysis phenotype with more moderate anemia and variable compensatory responses. Apparently, the widespread tissue injuries in HbS SCD mice cannot be explained by hemolysis alone.

**Conclusion:**
Genetic mouse models of hemolysis demonstrate extensive phenotypic differences in terms of the site and intensity of RBC destruction and anemia, adaptive responses of erythropoiesis and iron metabolism, as well as hemolysis-induced organ injury. Our comparative study provides a comprehensive framework guiding future studies of hemolytic genes.

**193**

K. Burelo[1, 2], M. Sharifshazileh[1, 2], G. Indiveri[1], J. Sarnthein[2]

**A spiking neural network algorithm detects high-frequency oscillations in intracranial EEG**

*Institute of Neuroinformatics, UZH[1], Klinik für Neurochirurgie, USZ[2]*

**Introduction:**
High Frequency Oscillations (HFO) in the intracranial EEG (iEEG) are promising bio-markers for epileptogenic zone (EZ). Automated HFO detection ensures a prospective definition of a clinically relevant HFO. Conventional HFO detectors require high quality amplified signals, which necessitates large power consumption. Furthermore, the detection is off-line with algorithms implemented on conventional digital computers. However, the surgeon desires real-time detection of HFO to provide intraoperative feedback when delineating the EZ.

**Methods:**
We designed a spiking neural network (SNN) algorithm that can ultimately be implemented on a dedicated neuromorphic device with low power consumption (6.2 µW/channel) for online HFO recording and detection. We analyzed a dataset that is publicly available and contains iEEG of 20 patients with HFO markings. The SNN transforms iEEG data into spike events that are processed in an artificial neuronal network. Resection of the area with high HFO rate is taken to predict postoperative seizure freedom.

**Results:**
The SNN was optimized for recordings in patients with temporal lobe epilepsy (TLE) and stereotactic electrodes, where average HFO amplitude is 59 µV and HFO detection rate is 1.3 HFO/min. Still, HFO were also detected in patients with extra temporal epilepsy (ETE) and grid electrodes, with average HFO amplitude of 15 µV, albeit at a lower rate (0.4 HFO/min). Resection of the HFO area predicted seizure freedom in 6 out of 9 TLE patients (specificity 100%, sensitivity 67%). Conversely, resection of the HFO area predicted seizure freedom in 3 out of 11 ETE patients (specificity 43%, sensitivity 100%).

**Conclusion:**
The performance of the SSN is comparable to conventional HFO detection in TLE patients. Parameters still have to be optimized for recordings from extra temporal grid electrodes. Ultimately, an analog neuromorphic device might be able to provide user-friendly information to the medical team during epilepsy surgery.

**194**

M. Emmenegger[2], K. Frauenknecht[2], E. Capodaglio[2], P. Kumari[1], S. Grathwohl[3], J. Grimm[3], S. Hornemann[2], R. Riek[1], A. Aguzzi[2]

**Autoantibodies against major genetic risk factors for Alzheimer's Disease in unselected hospital-wide patient cohort**

*Department of Chemistry and Applied Biosciences, ETH Zurich, CH-8093 Zurich, Switzerland[1], Institute of Neuropathology, University Hospital of Zurich, CH-8091, Zurich, Switzerland[2], Neurimmune Holding AG, CH-8952, Schlieren, Switzerland[3]*

**Introduction:**
Alzheimer's Disease (AD) is the most common form of dementia affecting around 30% of people over the age of 80 and the fourth leading cause of death in developed countries. Genome-wide association studies (GWAS) have unequivocally pointed to the apolipoprotein E (APOE) as the most important susceptibility gene for late-onset AD (LOAD), followed by triggering receptor expressed on myeloid cells 2 (TREM2) with whom it interacts. The ApoE-ε4 isotype has been shown to facilitate amyloid beta aggregation, to impair its clearance, and to foster the formation of neurofibrillary tau tangles. Hence, ApoE-ε4 could be an important therapeutic target. Meanwhile, growing evidence suggests that the ApoE lipidation status is crucial in the modulation of the ApoE-TREM2 axis.

**Methods:**
Using an automated microELISA, we have interrogated an unselected patient cohort of minmally 22,272 patient samples for the presence of autoantibodies against the ε3, ε4, and a lipidated form of the ε4 isotypes of ApoE, aiming to identify patients harbouring anti-ApoE-ε4-specific autoantibodies. Alongside, we have tested patient samples against the TREM2 ectodomain (amino acids 19-174) and the cleavage site (amino acids 135-174). The reactivity spectrum was then correlated with medical data (ICD-10 codes, medications, free text diagnoses) and visualised using software packages in Python and R. Cellular material of patients of interest was isolated using Ficoll gradients. We then selected all samples with supra-threshold reactivity for a secondary screen. 102 samples (in two independent runs, in duplicates each) were tested against recombinant PrP (amino acids 23-230), alpha-synuclein nanodisc, recombinant ApoE-ε3, recombinant ApoE-ε4, ApoE-ε4 nanodisc, and recombinant TREM2aa19-174 and TREM2aa135-174.

**Results:**
Data from the primary screen did not reveal an association of anti-ApoE or anti-TREM2 autoantibodies with disease, with a generally low prevalence of positives (0.07% for ε3, 0.02% for ε4, and 0.07% for the lipidated form of ε4, 0.09% for TREM2aa19-74, 0.04% for TREM2aa135-174). Having identified the few potential samples of interest, the standardised re-validation of patient samples in the secondary screen showed that all samples with antibodies against the ε4 isotype also reacted against ε3, while there was no overlap with the lipidated form of ε4 (nanodisc). Several patients reacted against both forms of TREM2, with few patients selectively reacting against either the extracellular domain or the cleavage site. These results indicate, for the first time, the presence of ApoE lipidation-specific antibodies and antibodies against the ectodomain of TREM2 in human repertoires.

**Conclusion:**
Starting from an unselected collection of plasma samples, we have been able to identify few patients with antibodies against ApoE or TREM2. Amongst them, several samples seemed to contain antibodies directed specifically against lipidated forms of ApoE, with two samples stemming from the same patient (phlebotomy seven months apart). Currently, the most interesting candidates are further characterised for their binding properties and cloning of antibodies is attempted. Antibodies with the potential to modulate the ApoE-TREM2 signalling axis may bear a far-reaching potential in both understanding lipid metabolism and microglial phagocytosis as well as in therapy. Finally, antibodies targeting specific subforms of ApoE may help prevent the development of AD in susceptible patient groups at an early presymptomatic stage.

**195**

D. Gramatzki[2], A. Eisele[2], P. Roth[2], E. Le Rhun[2], E. Rushing[3], R. Stahel[1], M. Weller[2]

**Venous thromboembolic events in glioblastoma patients: an epidemiological study in the Canton of Zurich**

*University Hospital Zurich, Comprehensive Cancer Center[1], University Hospital Zurich, Department of Neurology[2], University Hospital Zurich, Department of Neuropathology[3]*

**Introduction:**
Venous thromboembolic events (VTE) are a common complication in cancer patients. Anticoagulant use is the appropriate treatment for acute VTE in cancer, although assumed to be associated with increased risk for bleeding. The population-based relationship of VTE and anticoagulant therapy to survival in glioblastoma patients remains unclear.

**Methods:**
Frequency, risk factors, treatment and complications of VTE were assessed in a glioblastoma cohort in the Canton of Zurich, Switzerland (2010 to 2014). Survival data were retrospectively analyzed using the log rank test.

**Results:**
248 glioblastoma patients with known isocitrate dehydrogenase (IDH) wildtype status were identified in a 5-year time-frame. Median overall survival (OS) was 12.8 months (95% CI 11.0-14.6), with a median follow up of 60.7 months (95% CI 51.4-70.0). VTE were diagnosed in 35 patients (14.4%; 5 out of 248 patients with no follow-up data on VTE). Median time from diagnosis to VTE was 2.23 months (95% CI 0.6-3.9); 3 patients (8.6%) had a history of VTE. Most patients were on steroids at time of diagnosis of VTE (68.6%), and a Karnofsky Performance Score of less than 70% was documented in 21 patients (60%). Most patients with VTE (88.6%) received therapeutic anticoagulation. Complications, resulting in the cessation of therapeutic anticoagulation, occurred in 11 patients (35.5%), mainly (9 patients, 81.8%) due to intracranial hemorrhage. OS did not differ between patients diagnosed with VTE and those without VTE (p=0.103). Tumor progression was the major cause of death (91.3%); 1.4% of patients died from VTE; 1.9% of the patients suffered unexpected sudden death.

**Conclusion:**
Although VTE were identified in 14.4% of glioblastoma patients, VTE was not the major reason for death. These data do not support the implementation of primary thromboprophylaxis in glioblastoma patients. Prospective clinical trials are needed to examine the association of anticoagulant use with survival in glioblastoma patients.

**196**

M. Emmenegger[2], A. Chincisan[2], Ch. Zografou[2], N. Wuillemin[3], D. Bieli[3], L. Saleh[1], A. Von Eckardstein[1], A. Aguzzi[2]

## Identification and mechanistic elucidation of IgG antibodies against a major peanut allergen in Cystic Fibrosis patients

*Institute of Clinical Chemistry, University Hospital of Zurich, CH-8091, Zurich, Switzerland[1], Institute of Neuropathology, University Hospital of Zurich, CH-8091, Zurich, Switzerland[2], Mabylon AG, CH-8092, Schlieren, Switzerland[3]*

**Introduction:**
Food allergies are disabling diseases that affect around 4% of children and 1% of adults. The most common food allergen associated with fatal or near-fatal anaphylaxis stem from peanuts. Peanut allergy remains a potentially life-threatening condition for which no cure exists. While many modern interventions attempt to desensitise patients at risk, an unexploited alternative could be to use fully human IgG antibodies with extremely high affinities for the peanut allergens. To detect such antibodies, we have been screening over 20,000 unselected hospital patients for the presence of IgGs against Arachis hypogaea 2 (Ara h 2), a major peanut allergen. Following the exploratory high-throughput screen, we have set up a pipeline to mechanistically investigate the incidental findings.

**Methods:**
High-throughput antibody profiling for IgG antibodies directed against the natural Ara h 2 was carried out using residual heparin plasma samples of unselected hospital patients. The reactivity spectrum was correlated with medical data (ICD-10 codes, medication, free text diagnoses) in a big data approach. Mononuclear cells of reactive patients were isolated using Ficoll gradients. The secondary screening was done with a panel of exogenous and endogenous antigens, using the same methodology as for the high-throughput screen.

**Results:**
In 22,199 individuals screened, 110 (or 0.5%) patients were identified to be distinctly reactive against natural (n) Ara h 2. We then correlated the medical record with the reactivity spectrum and found a strong association between anti-nAra h 2 IgGs and Cystic Fibrosis (CF), at statistical significance ($p = 4 \times 10^{-241}$). Unlike in peanut allergy patients, the presence of IgGs was not shown to be complemented by IgEs, in line with the absence of evidence of a clinically manifest peanut allergy in CF patients. Data mining has not evidenced an association of IgGs against Ara h 2 with CF subgroups.

**Conclusion:**
An exploratory analysis revealed that a large and statistically significant proportion of patients presenting with specific antibodies against the allergen suffer from CF but not from peanut allergy. Importantly, in multiple other campaigns where screens of similar dimensions were carried out using different antigens, no correlation with CF could be made, substantiating the specificity of our finding. Current efforts are directed towards understanding the link between those IgGs and the CF phenotype. Such approaches include the sequencing of the CFTR gene in peanut allergy patients, the B cell receptor repertoire analysis in patients with CF, the assessment of the CFTR in antigen processing and presentation, and the elucidation of the potential of the CF patient-derived anti-Ara h 2 IgGs to prevent peanut allergy. While this study shows both the potential of an unbiased screening approach and its usage in discovering patients of interest, fully human antibodies from these patients can be cloned and be employed as safe therapeutics to treat patients with peanut allergy.

**197**

I. Jelcic[2, 3], A. Müller[1], P. Stathopoulos[2, 3], N. Wolfensberger[1], J. Ruder[2, 3], A. Thesenvitz[2, 3], K. Ritter[1], A. Bachofner[1], M. Foege[2, 3], A. Lutterotti[2, 3], U. Schanz[1], R. Martin[2, 3]

## The Zurich Experience in Autologous Hematopoietic Stem Cell Transplantation for the Treatment of Multiple Sclerosis (aHSCT-in-MS) 18 Months after Approval

*Department of Medical Oncology and Hematology, University Hospital Zurich, Switzerland[1], Neuroimmunology and Multiple Sclerosis Research Section, Neurology Clinic, University Hospital Zurich, Switzerland[2], supported by the Clinical Research Priority Program (CRPP) Project "Precision MS", University of Zurich, Switzerland[3]*

**Introduction:**
Multiple sclerosis (MS) is a chronic demyelinating inflammatory disease of the central nervous system (CNS) and the most common cause of non-traumatic neurological disability in young adults. Autologous hematopoietic stem cell transplantation (aHSCT) is used for highly active relapsing-remitting or progressive forms of multiple sclerosis (MS) since 1995. Based on increasing evidence regarding efficacy and improved safety of aHSCT in MS, the Swiss Federal Office of Public Health (FOPH) granted approval in June 2018. To receive reimbursement and to be eligible for aHSCT, (a) the patient must show inflammatory breakthrough activity of MS despite conventional highly effective disease-modifying treatment; (b) the interdisciplinary hemato-neuroimmunological board at the University Hospital Zurich must confirm the indication for aHSCT; and (c) the patient has to agree to be enrolled in a prospective registry study ("aHSCT-in-MS") for 5 years after transplantation.

**Methods:**
Hematopoietic stem cells are mobilized with 2 days of cyclophosphamide 2g/m$^2$/d and Filgrastim (granulocyte-colony stimulating factor), collected via leukapheresis from the peripheral blood and frozen. Conditioning high-dose chemotherapy comprises BEAM-ATG, i.e. BCNU (d-6: 300mg/m$^2$), etoposide (d-5 to -2: 200mg/m$^2$/d), cytarabine (d-5 to -2: 200mg/m$^2$/d), melphalan (d-1: 140mg/m$^2$) and ATG (d+1 and +2: 3.75 mg/kg/d) after stem cell re-transfusion (d0). Within the registry study, we collect systematically clinical, radiological, laboratory, immunological and safety measures using RedCap as approved by the Cantonal Ethics Committee of Zurich (BASEC-Nr. 2018-01854).

**Results:**
Until now, 22 patients (11 females, 11 males) with a mean age of 41.3 ± 7.7 years, mean disease duration of 8.6 ± 4.9 years and a mean expanded disease status scale (EDSS) score of 5.0 ± 1.2 have been treated with aHSCT for MS. 7/22 (32%) patients had relapsing-remitting MS (RRMS), 8/22 (36%) secondary-progressive MS (SPMS) and 7/22 (32%) primary-progressive MS (PPMS). aHSCT was indicated because 5/22 (23%) patients had clinical activity (i.e. relapses), 7/22 (32%) had radiological activity (i.e. new or contrast-enhancing CNS lesions) and 14/22 (64%) had clinical progression – despite conventional highly effective immunomodulatory therapy. We observed infectious adverse events (AEs) in the majority of patients, i.e. mucositis, pharyngitis and/or enteritis (20/22), upper airway (4/22) and urinary (4/22) infection, CMV reactivation (2/22), HSV reactivation (3/22), herpes zoster (1/22) and BKV cystitis (2/22). Other AEs included Uhthoff's phenomenon (8/22), hypotension (3/22), epistaxis and cholecystolithiasis (each 1/22). Severe AEs included 2 additional, symptomatic CMV reactivations, each 1 hemorrhagic cystitis, gastroenteritis with ileus, laryngitis, cervical abscess, pulmonary embolism, gastrointestinal bleeding, manic episode. Although a substantial proportion of patients reported improvements of neurological functions and less fatigue, follow-up is too short to comment on long-term outcomes.

**Conclusion:**
The safety profile of aHSCT-in-MS is acceptable, but requires vigilant monitoring and optimized antibacterial and antiviral prophylactic care. Regarding the increased risk of CMV reactivation (4/22) and herpes zoster (1/22), we decided to establish prophylaxis with the CMV inhibitor letermovir in CMV-seropositive patients and to vaccinate all patients with Shingrix® after transplantation.

**198**

S. Erdogan[1], C. Gonçalves Moreira[1], D. Bimbiryte[1], A. Sethi[1], C. Baumann[1], D. Noain[1]

**Role of slow-wave sleep delta power on amyloid beta accumulation in a mouse model of Alzheimer's Disease**

*University Hospital Zurich[1]*

**Introduction:**
Recent evidence from murine models of Alzheimer's disease (AD) suggests that chronic sleep induction significantly decreases amyloid beta (Aß) accumulation in the mouse brain, whereas chronic sleep restriction has an opposite effect. In a recent study, our group showed that delta-rich slow-wave sleep (SWS) induction after TBI in rats reduces the accumulation of amyloid precursor protein (APP) in injured brains and alpha-synuclein (α-syn) in a mouse model of Parkinson's disease. Therefore, we propose that the mechanism behind such beneficial effect is the increased clearance of extracellular proteins during delta-rich SWS.

**Methods:**
We use the well-established tg2576 mutant mice as a model of AD and their wild type (wt) siblings as a control. We implanted electroencephalography/electromyography (EEG/EMG) headsets (Figure 2a) in adult Tg2576 mice (early: 5.5 months of age; late: 10.5 months of age) for periodic electrophysiological monitoring of vigilance states. After 14 days of recovery, we examined cognitive performance of the mice to determine baseline. After the behavioral tests, we administer animals with pharmacological SWS enhancer (Xyrem®, 300mg/kg, p.o.) or placebo twice daily for 2 or 10 weeks. We record 24 hours sleep/wake activity of mice before (baseline) and during the treatment. We use Congo red staining for the visual detection of amyloid plaques in the brains of both transgenic and wild type mice.

**Results:**
SLEEP: Our preliminary findings add new information to the phenotype of this Tg murine model. We show that their wake and NREM proportions, as well as their delta power density are significantly different from their wild-type littermates. The difference is driven mainly by changes during 12 h dark cycle.
BEHAVIOR: Their cognitive performance improved after 2 weeks of treatment with Xyrem® compared to their baseline, and this difference was a trend with a large effect in early and with a medium to large effect in late intervention groups.
AMYLOID BURDEN: Pharmacological enhancement of SWS was preliminary associated with a reduced Aβ plaque burden effect in 11.5 months of age tg2576 mice after 2 weeks of oral administration with Xyrem®, although no statistical significance was yet found.

**Conclusion:**
We will perform ELISA to analyze amount of soluble and insoluble Aβ and to assess whether there is a difference in beta-secretase-1 (BACE-1) expression in frozen brain tissue of wt and tg2576 mice after early interventions of SWS enhancement. We will complete the number of animals for pharmacological SWS enhancement groups and initiate pilots with acoustical SWS enhancement group. We will co-stain the brains from wt and tg2576 mice with immunohistochemistry and Congo red for Aβ plaque visualization. We will utilize two-photon microscopy (in collaboration with Prof. Helmchen) to explore the mechanism behind reduction of Aβ by using an Aβ tracker during SWS enhancement.

**199**

C. Meisel[1], C. Porcheri[1], T. Mitsiadis[1]

## The Role of Notch Signaling in Oral Cancers

*Institute of Oral Biology[1]*

**Introduction:**
Head and neck squamous cell carcinoma (HNSCC) defines a group of solid tumors originating from the mucosa of the upper aerodigestive tract, pharynx, larynx, mouth and nasal cavity. It is the sixth most common cancer in the world, with 600 000 new cases reported every year, with a metastatic evolution and poor prognosis. HNSCC heterogeneity and complexity reflects in a multistep progression, involving crosstalk of several molecular pathways. The Notch pathway is associated with major events supporting cancerogenic evolution: being crucial in regulating cell proliferation, maintenance of undifferentiation, angiogenesis and preservation of a pro-oncogenic microenvironment. Notch signaling is highly conserved and encompasses four transmembrane receptors in mammals, Notch1-4. Notch positive cells can therefore receive signals from neighboring cells expressing Notch ligands Delta-like ligands 1,3,4 and ligands Jagged1,2. The Notch signaling pathway is central in tumor development and is proposed to play a dual role acting as both oncogene and tumor suppressor. However, it remains to be elucidated how and in which stages, the Notch pathway is involved in the pathogenesis of oral squamous cell carcinoma, especially in the most affected tissue of the oral cavity, the tongue. In order to investigate the role of Notch signaling in the development and progression of oral cancer, a Notch1:creERT-mT/mG mouse tracer line is used as well as the 4-NQO model, representing a chemically inducible cancer mouse model. Exploiting this model, we investigate the role of Notch signaling in cancer formation and progression. Additionally, transcriptomic changes will be analyzed in late stages of the developed tumor of the 4-NQO model to get a deeper understanding of the underlying changes.

**Methods:**
Applied techniques include qRT-PCR, western blot, immunohistochemical and immunofluorescence approaches.

**Results:**
So far, we were able to show that the 4-NQO model induces histological changes to the tongue epithelium, resulting in an epithelial outgrowth (tumor). The arising outgrowth appears to be of an undifferentiated character due to high CK14 and CK5 expression. Additionally, we were able to determine that the receptor Notch1 is highly expressed and active in the developed tumor, as well as its ligand DLL4 which together drive down-stream gene transcription. Furthermore, it appears that the number of progenitor cells is increased within the tumor outgrowth.

**Conclusion:**
Therefore, we can conclude that Notch1 plays a significant role in the tumor tissue, maintaining its undifferentiated state and possibly influencing progenitor cell number and proliferation in the basal layer of the tongue epithelium.

**200**

P. Helbling[1], A. Gomariz[1], K. Loosli[1], S. Isringhausen[1], T. Yokomizo[2], M. Manz[1], C. Nombela-Arrieta[1]

**Tissue-Scale Spatial Analysis of Hematopoietic Stem Cells and Stromal Niche Subtypes in the Fetal Liver Microenvironment**

*Department of Medical Oncology and Hematology, University Hospital Zurich, Switzerland[1], International Research Center for Medical Sciences, Kumamoto University, Japan[2]*

**Introduction:**
During embryonic development, hematopoiesis migrates through different tissues in a sequential and finely timed manner. Hematopoietic stem cells (HSCs) are generated from endothelial walls of large blood vessels, subsequently colonize the fetal liver (FL), where they undergo proliferative expansion, before definitely settling in the bone marrow (BM). While adult BM niches have been extensively studied, the cellular and molecular makeup of FL niches that promote continuous self-renewing proliferation of embryonic HSCs, remain much less well characterized.

**Methods:**
We employed a customized pipeline for 3-dimensional quantitative microscopy (3D-QM) to visualize distribution patterns of HSCs in the FL, reveal the identity of putative stromal niche components, and investigate their spatial relationships.

**Results:**
Unexpectedly, organ-wide mapping of HSCs in reporter mice (Hlf-tdTomato/Evi-GFP) revealed no significant spatial association of HSCs (tdTomato+GFP+) or progenitor cells (tdTomato+GFP-) with liver sinusoids or portal vessels. Instead, HSCs displayed a widespread distribution throughout entire FL lobes. We next employed Cxcl12-GFP and Scf-GFP reporter mice to identify and visualize potential niche cell types. Abundant expression of CXCL12 and SCF was detected in two non-hematopoietic cell types, which were unequivocally characterized as DLK1+ hepatoblasts and CD140b+CD51+ mesenchymal cells. At E13.5, both densely populate the entire FL, restricting available space, and closely associate with HSCs. Interestingly, by E17.5 the strong downregulation of pro-hematopoietic gene expression in hepatoblasts and their differentiation into mature hepatocytes lead to a rapid decrease in SCF levels, which temporally coincide with declining liver hematopoiesis.

**Conclusion:**
Our results are therefore consistent with a model in which hepatoblasts and mesenchymal cells create a hematopoietic-supporting niche that transiently promotes the expansion of HSCs and that is dismantled in a developmentally timed manner as HSCs migrate out of this organ towards the developing BM.

**201**

S. Brugger[3, 5, 6], S. Eslami[3], M. Pettigrew[2], I. Fernandez Escapa[3], M. Henke[1], Y. Kong[4], K. Lemon[3, 7]

**Dolosigranulum pigrum picks sides in nasal microbiota via cooperation and competition**

*Department of Biological Chemistry and Molecular Pharmacology, Harvard Medical School, Boston, MA, USA[1], Department of Epidemiology of Microbial Diseases, Yale School of Public Health, New Haven, CT, USA[2], Department of Microbiology, The Forsyth Institute, Cambridge, MA, USA[3], Department of Molecular Biophysics and Biochemistry and W.M. Keck Foundation Biotechnology Resource Laboratory, Yale University, New Haven, CT, USA[4], Department of Oral Medicine, Infection and Immunity, Harvard School of Dental Medicine, Boston, MA, USA [5], Division of Infectious Diseases and Hospital Epidemiology, University Hospital Zurich, University of Zurich, Zurich, Switzerland[6], Division of Infectious Diseases, Boston, Children's Hospital, Harvard Medical School, Boston, USA [7]*

**Introduction:**
Multiple epidemiologic nasal passage microbiota studies identify the generally harmless bacterium *Dolosigranulum pigrum* as a candidate beneficial bacterium based on its positive association with health, including negative associations with colonization by pathobionts *Staphylococcus aureus* and *Streptococcus pneumoniae*.

**Methods:**
We used a multi-pronged strategy (Analysis of composition of microbiota (ANCOM) on species-level bacterial microbiota datasets from children and adults, in vitro co-culture assays, lactic-acid determination and whole genome sequencing with comparative genomics of 10 *D. pigrum* isolates) to gain new insights into *D. pigrum*'s functions and interactions in the nasal microbiota.

**Results:**
We detected in vivo systems-level and in vitro phenotypic cooperation with commensal *Corynebacterium* species. *D. pigrum*'s average genome size of 1.86 Mb and predicted auxotrophies indicate it must rely on its human host and co-colonizing bacteria bacterial neighbors for key nutrients. In in vitro interaction assays, *D. pigrum* alone inhibited *S. aureus* growth; however, *D. pigrum* plus a nasal *Corynebacterium* were needed to inhibit *S. pneumoniae* growth. D. pigrum produced L-lactic-acid but at levels insufficient to inhibit either *S. aureus* or *S. pneumoniae*. However, the genomes of 11 *D. pigrum* strains revealed a diversity of biosynthetic gene clusters including bacteriocins, microcins and lanthipeptides.

**Conclusion:**
Here, we validated in vivo correlations from human bacterial microbiota studies with functional assays and demonstrated positive association between the commensals *D. pigrum* and *Corynebacterium* spp. and antagonism against the pathobionts *S. aureus* and *S. pneumoniae* pointing to previously unrecognized means of niche competition. Our results increase the understanding of *D. pigrum*'s physiology and the mechanisms underlying the positive associations between *D. pigrum* and a healthy nasal microbiota.

**202**

T. Weiss[2], E. Puca[1], M. Weller[2], D. Neri[1], P. Roth[2]

**Immunocytokines are a novel immunotherapeutic approach against glioblastoma**

*Department of Chemistry and Applied Biosciences, Swiss Federal Institute of Technology (ETH Zürich), Zurich, Switzerland.[1], Department of Neurology and Brain Tumor Center, University Hospital Zurich and University of Zurich, Zurich, Switzerland[2]*

**Introduction:**
Glioblastoma is the most common and most aggressive primary brain tumor in adults with an urgent need for novel treatment options. The administration of pro-inflammatory cytokines could be a potent immunotherapeutic approach to shift the balance between tumor-associated immunosuppression and immune activation. However, the systemic administration of therapeutically active doses of pro-inflammatory cytokines is not feasible due to toxic side effects and there is a need for strategies that enable a targeted delivery of pro-inflammatory cytokines to the tumor site.

**Methods:**
We investigated different antibody-cytokine fusion products that enable a targeted delivery of interleukin (IL)-2, IL-12 or tumor-necrosis factor (TNF) to the tumor site by binding to a tumor-specific epitope of fibronectin. We investigated the expression of this tumor-specific epitope ex vivo in tumor-bearing mouse brains and human glioblastoma samples. For systematic characterization of the distribution of fibronectin-targeting antibodies, we used in vivo imaging upon administration of fluorescently labeled antibodies. Subsequently, we investigated the anti-tumor activity of IL-2, IL-12 or TNF fused to an antibody targeting this tumor-specific epitope in orthotopic immunocompetent mouse glioma models. Finally, we translated this immunotherapeutic strategy to patients with recurrent glioblastoma.

**Results:**
The tumor-specfic extra domain B of fibronectin is widely expressed in murine glioma models and human glioblastoma samples and a fluorochrome-labeled antibody targeting this tumor-specific epitope accumulated at the tumor site in the brain in vivo upon systemic administration. IL-2, IL-12 or TNF fused to this antibody conferred a survival benefit in orthotopic tumor-bearing mice and cured a fraction of tumor-bearing mice with long-lasting anti-tumor immunity. Mechanistically, antibody-fused TNFa induced necrosis in the tumor and increased the activation of tumor-infiltrating NK cells, whereas antibody-fused IL-12 mainly boosted an anti-tumor immune response mediated by NK cells and T cells. The first clinical translation of this approach using antibody-fused TNF for the treatment of patients with glioblastoma was tolerated without dose-limiting toxicities and in a patients with another surgery upon treatment with antibody-fused TNF, we demonstrate an increase of tumor-infiltrating immune cells.

**Conclusion:**
Our study demonstrates potent anti-tumor activity of this immunotherapeutic approach in orthotopic, syngneic glioma mouse models and we were able to characterize the mode of action for the different immunocytokines. First clinical experience with targeted delivery of TNF demonstrates feasibility and points toward direct cytotoxic and immune-mediated anti-tumor effects. This work builds a basis for future studies with immunocytokines as a promising treatment strategy for central nervous system tumors.

**203**

P. Frey[3], J. Bär[3], J. Bergada[3], K. Lemon[1, 4], A. Zinkernagel[3], S. Brugger[1, 2, 3]

**Quantifying variations in cellular fitness of bacteria with and without antimicrobial resistance: a high-throughput method**

*Department of Microbiology, The Forsyth Institute, Cambridge, MA, USA[1], Department of Oral Medicine, Infection and Immunity, Harvard School of Dental Medicine, Boston, MA, USA [2], Division of Infectious Diseases and Hospital Epidemiology, University Hospital Zurich, University of Zurich, Zurich, Switzerland[3], Division of Infectious Diseases, Boston, Children's Hospital, Harvard Medical School, Boston, USA [4]*

**Introduction:**
To evaluate changes in cellular fitness of bacteria, i.e., after acquisition of antimicrobial resistance, a scalable high-throughput method to analyze bacterial growth on agar is desirable. For this purpose we aimed to adapt a quantitative fitness analysis (QFA) method established for yeast cultures to bacterial use.

**Methods:**
In QFA, bacterial cultures are spotted in a predefined array on agar plates and photographed sequentially while growing in neighborly competition. These time-lapse images are analyzed using a purpose-built open source software to derive image density values for each culture spot. Subsequently, a Gompertz growth model is fitted to these optical density values of each culture spot and fitness is calculated from parameters of the model. For image segmentation validation we matched image density values to colony-forming unit (CFU) counts using linear regression. To represent a range of important pathogenic bacteria, we used different strains of *Enterococcus faecium*, *Escherichia coli* and *Staphylococcus aureus*, with and without antimicrobial resistances.

**Results:**
Overall, QFA permitted the construction of growth curves from semisolid agar plates and fitting of Gompertz models in all tested strains of *E. faecium*, *E. coli* and *S. aureus*. Image density values showed a strong correlation with the total CFU count per spotted culture ($p<0.001$) for all strains of the three species. Fitness was derived for XX culture spots and showed important differences between individual strains. QFA data suggested a substantial higher fitness of methicillin resistant *S. aureus* JE2 ($p = 0.002$) than Cowan.

**Conclusion:**
QFA is a viable method to analyze fitness of bacteria and detect substantial fitness differences between antimicrobial resistant strains of important bacterial pathogens. QFA is likely to be applicable to bacteria of other species and may help to estimate epidemiological antimicrobial persistence at a low cost.

**204**

S. Andresen[4, 8], S. Balakrishna[4, 8], D. Nicca[9], H. Günthard[4, 8], A. Schmidt[2, 10], A. Calmy[6], K. Darling[7], M. Stöckle[3], P. Schmid[2], E. Bernasconi[5], A. Rauch[1], R. Kouyos[4, 8], L. Salazar-Vizcaya[1]

**Behavioural patterns to identify key populations for syphilis prevention**

*Department of Infectious Diseases, Bern University Hospital Inselspital, University of Bern, Bern, Switzerland[1], Division of Infectious Diseases and Hospital Epidemiology, Cantonal Hospital St. Gallen, St. Gallen, Switzerland[2], Division of Infectious Diseases and Hospital Epidemiology, University Hospital Basel, Basel, Switzerland[3], Division of Infectious Diseases and Hospital Epidemiology, University Hospital Zurich, Zurich, Switzerland[4], Division of Infectious Diseases, Lugano Regional Hospital, Lugano, Switzerland[5], Division of Infectious Diseases, University Hospital Geneva, Geneva, Switzerland[6], Infectious Diseases Service, Department of Medicine, University Hospital of Lausanne (CHUV), Switzerland[7], Institute of Medical Virology, University of Zurich, Zurich, Switzerland[8], Institute of Nursing Science, University of Basel, Basel, Switzerland[9], Sigma Research, London School of Hygiene and Tropical Medicine, United Kingdom[10]*

**Introduction:**
Clustering HIV-positive men who have sex with men (MSM) by unsupervised machine learning based on their consistency of condom use revealed groups with dissimilar behaviour over time (Salazar-Vizcaya et al., CID 2019). However, the association between these behavioural clusters and sexual disease transmission is yet to be characterised. As syphilis transmission in MSM has sharply increased in Switzerland in the last decade, we assessed this association by analysing prevalence and incidence of syphilis among behavioural clusters in the Swiss HIV Cohort Study (SHCS) between 2005 and 2018.

**Methods:**
We included 2494 MSM enrolled in the SHCS reporting condomless anal intercourse with non-steady partners (nsCAI) at least once, with at least two years of follow-up and at least two syphilis tests between 2005 and 2018. We estimated the prevalence and incidence of syphilis infections (newly positive TPHA/TPPA or ≥4-fold VDRL increase) for each of the four previously inferred clusters and compared it to their respective proportions of men reporting nsCAI.

**Results:**
Incidence of syphilis increased from 0.08 infections per person-years in 2005 to 0.12 in 2018. Overall syphilis prevalence differed significantly between clusters. This finding was consistent with differences in average nsCAI proportion among clusters (OR:6.0, $p<0.0001$). Trajectories of syphilis incidence over time differed between clusters (Figure): Clusters with increasing nsCAI proportion also exhibited recent increases in syphilis incidence. However, increases in syphilis incidence were delayed compared to those in nsCAI proportion. The increase in syphilis incidence was particularly pronounced for clusters 3 and 4, two groups characterised by recent nsCAI increases. In 2018, these clusters contributed over half of the syphilis cases while making up less than one third of the population.

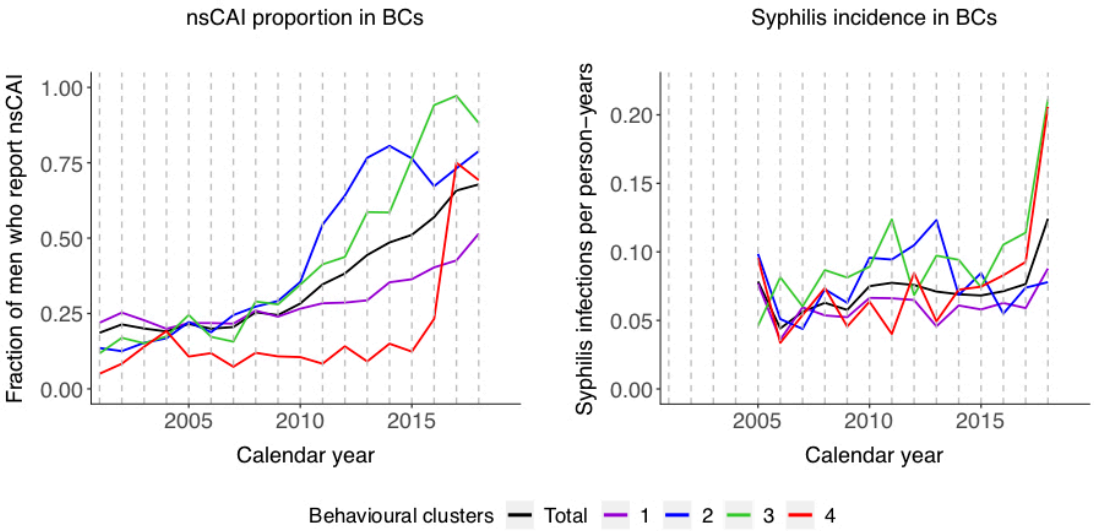


**Figure**. ***left*** Fraction of men who report nsCAI per behavioural cluster among MSM in the SHCS (recreated based entirely on Salazar-Vizcaya et al., CID 2019): 'Total' shows the development of the nsCAI fraction over all the included persons. The behavioural clusters labelled 1-4 represent groups of individuals who have previously been shown to display dissimilar nsCAI patterns over time. Cluster 1 represents 53% of the study population and shows the most stable nsCAI proportion. Cluster 2 makes up 20% of the population and shows an increase in nsCAI after 2010 and a decrease after 2014. Cluster 3, contributing 17% of the population, shows a steady increase in nsCAI until 2017. Cluster 4 make up 10% of the population and shows consistently lower nsCAI proportion from 2006 until its nsCAI fraction rapidly increases in 2017. ***right*** Syphilis incidence per behavioural cluster among MSM in the SHCS: number of syphilis infections (newly positive TPHA/TPPA or ≥4-fold increase in VDRL) per person-years at risk. 'Total' shows the development of syphilis incidence over all included persons. Abbreviations: nsCAI = condomless anal intercourse with non-steady partners, MSM = men who have sex with men, SHCS = Swiss HIV Cohort Study, TPHA/TPPA = Treponema pallidum particle agglutination/hemagglutination assay, VDRL = Venereal Disease Research Laboratory.

**Conclusion:**

Our preliminary results suggest that syphilis incidence over time differs between behavioural clusters and that specific clusters could be targets for potential interventions to prevent syphilis infections.

**205**

S. Hosseini[1], S. Anwer[1], P. Heiniger[1], F. Gustafierro[1], N. Kuzo[1], R. Hess[1], C. Brunckhorst[1], F. Dura[1], A. Saguner[1], F. Tanner[1]

**Novel echocardiographic methods for outcome prediction in patients with Arrhythmogenic Right Ventricular Cardiomyopathy**

*Department of Cardiology, University Heart Center, University Hospital Zurich[1]*

**Introduction:**
Echocardiography plays an important role in the diagnosis of Arrhythmogenic Right Ventricular Cardiomyopathy (ARVC). It is not known whether tissue Doppler imaging (TDI) alone or in combination with other echocardiographic parameters is useful for predicting outcome in ARVC. In this study, we aimed at understanding the association of different functional echocardiographic parameters including TDI with outcome in ARVC.

**Methods:**
We studied 63 ARVC patients, 54 patients (86%) with definite and 9 (14%) with borderline ARVC according to the 2010 Task Force Criteria. Clinical and echocardiographic parameters including TDI and speckle tracking derived deformation analysis were collected over a median follow-up time of 1976 days. The composite endpoints examined include cardiovascular mortality composite end-point (cardiovascular mortality and Heart transplantation; number:7; percentage: 11 %) and ventricular arrhythmia composite end-point (All sustained ventricular arrhythmias; number:21; percentage: 33 %).

**Results:**
Cardiovascular Mortality was significantly associated with changes in right-sided chamber morphology and function such as right ventricular (RV) end diastolic area (EDA) (β=1.14, p=0.002), right atrial (RA) diameters (β=4.17, p=0.001), and tricuspid annulus plan systolic excursion (TAPSE) (β=1.43, p=0.001). A decline in left ventricular (LV) ejection fraction was associated as well (β=1.08, p=0.004). Furthermore, cardiovascular mortality was significantly associated with systolic RV and LV TDI-derived parameters such as tricuspid S' (β=1.48, p=0.029), septal S' (β=2.13, p=0.037) and lateral S' (β=1.58, p=0.029). Endocardial RV global longitudinal strain also displayed association (β=1.58, p=0.001) with events.
Similarly, sustained ventricular arrhythmias were significantly associated with right-sided structure and function such as RV EDA (β=1.05, p=0.014), FAC (β=1.05, p=0.015), and TAPSE (β=1.119, p=0.011). Furthermore, ventricular arrhythmias were associated with RV and LV systolic TDI-derived parameters such as tricuspid S' (β=1.275, p=0.015) and septal S' (β=1.362, p=0.023). Endocardial RV global longitudinal strain (β=1.204, p=0.007) also was associated with events.

**Conclusion:**
TDI derived parameters were significantly associated with mortality and ventricular arrhythmias in ARVC patients. Hence, TDI is useful for outcome prediction in echocardiographic evaluation of ARVC. This is particularly interesting because TDI measurements are relatively easy to obtain, in particular in patients with difficult echocardiographic windows.

**206**

B. Eggerschwiler[1], E. Casanova Zimmermann[1], D. Canepa[1], H-C. Pape[1], P. Cinelli[1]

**Molecular properties and phenotypic outcomes of bone marrow-derived mesenchymal stem cells in patients with reduced bone mass density**

*Universitätsspital Zürich[1]*

**Introduction:**
Osteoporosis is a major health problem characterized by compromised bone mass density (BMD) and fat inclusions that predisposes patients to an increased risk of fracture. Osteoporotic patients differ from healthy subjects in bone mineral composition, bone mineral content, and crystallinity. About 40% of white postmenopausal women are affected by osteoporosis. Today, approximately 50% of women and 20% of men older than 50 years will experience an osteoporosis-related fragility fracture. According to the WHO, Osteoporosis is one of the top ten diseases regarding their economic and physiological burden.
We investigated the molecular properties and the corresponding phenotypic expressions of bone marrow-derived mesenchymal stem cells (BMMSC) regarding differentiation potential towards osteoblasts and bone formation capabilities. Since osteoporosis is caused by an imbalance of bone formation and bone resorption, we hypothezise that there are differences between BMMSCs of healthy patients and patients suffering from reduced BMD.

**Methods:**
Osteoporosis is a major health problem characterized by compromised bone mass density (BMD) and fat inclusions that predisposes patients to an increased risk of fracture. Osteoporotic patients differ from healthy subjects in bone mineral composition, bone mineral content, and crystallinity. About 40% of white postmenopausal women are affected by osteoporosis. Today, approximately 50% of women and 20% of men older than 50 years will experience an osteoporosis-related fragility fracture. According to the WHO, Osteoporosis is one of the top ten diseases regarding their economic and physiological burden.
We investigated the molecular properties and the corresponding phenotypic expressions of bone marrow-derived mesenchymal stem cells (BMMSC) regarding differentiation potential towards osteoblasts and bone formation capabilities. Since osteoporosis is caused by an imbalance of bone formation and bone resorption, we hypothezise that there are differences between BMMSCs of healthy patients and patients suffering from reduced BMD.

**Results:**
Quantitative analysis of the phenotypes revealed that there is only very poor correlation between osteogenic differentiation capability and bone heath status. Patients with reduced BMD showed, with a very high variability, decreased osteogenic differentiation compared to healthy individuals. Patients suffering from osteoporosis show lower osteogenic differentiation compared to patients suffering from osteoporosis.
Preliminary CyTOF data revealed that CD105 and SP7 are higher expressed in healthy individuals and SOX9 and STRO-1 are higher expressed in patients with reduced BMD.

**Conclusion:**
From our preliminary data, we currently conclude that the imbalance between bone formation and bone resorption may be caused by osteoclast hyperactivity. The differentiation potential of BMMSCs towards osteoblasts might have only a secondary role for the development of osteoporosis.

**207**

M. Schwyzer[1], K. Martini[1], S. Skawran[1], M. Messerli[1], T. Frauenfelder[1]

**Pneumonia detection in chest X-ray dose-equivalent CT: Impact of dose reduction on the detectability by Artificial Intelligence.**

*University Hospital Zurich[1]*

**Introduction:**
There has been a significant increase of immunocompromised patients in recent years due to new treatment modalities for previously fatal diseases. This comes at the cost of an elevated risk for infectious diseases, most notably pathogens affecting the respiratory tract. Early diagnosis and treatment of pneumonia can help reducing morbidity and mortality in those patients. In this study, we assessed the performance of a deep neural network in the detection of pulmonary infection in chest X-ray dose-equivalent CT.

**Methods:**
The 100 patients included in this retrospective study were referred to our department for suspicion of pulmonary infection and/or follow-up of known pulmonary nodules. Every patient was scanned with a standard dose and reduced dose CT protocol. Two readers annotated CT slices with pulmonary consolidations. We trained a deep neural network to perform binary classification whether pulmonary consolidation was present on a CT slice or not.

**Results:**
The AUC of the deep learning algorithm for the standard dose CT was 0.923 and significantly higher than the AUC (0.881) of the reduced dose CT. The sensitivity and specificity of the standard dose CT was 82.9% and 93.8% and the sensitivity and specificity of the reduced dose CT was 71.0% and 93.3%. The effective dose of reduced dose CT was 0.1 mSv and significantly smaller than of standard dose CT (1.5 mSv).

**Conclusion:**
Pneumonia detection with X-ray dose-equivalent CT using AI is feasible and can contribute to improved diagnostic performance compared to AI-based pneumonia detection with conventional chest X-ray.

**208**

F. Arnold[1], B. Sobottka-Brillout[1], C. Britschgi[1], H. Moch[1], M. Zoche[1], A. Kahraman[1]

**MTPpilot: An Interactive Software-Tool for NGS Result Analyses for Molecular Tumor Boards**

*University Hospital Zurich[1]*

**Introduction:**
Next-Generation Sequencing (NGS) cancer panels have become a key cornerstone for today's clinical decision making in oncology at the USZ. Results from these panels are at the core of the weekly molecular tumor board, where they support oncologists, pathologists, bioinformaticians, and geneticists in the search for the best treatment options for a patient. However, with the increasing size and complexity of NGS cancer panels, NGS results have become challenging to interpret, especially if presented merely in the form of a written report. Manual analysis of several mutations from a comprehensive NGS cancer panel is time-consuming and often incomplete.
To address these shortcomings, we developed the software Molecular Tumor Profiling Pilot (MTPpilot), which provides automated annotation, linking and interactive visualization to support the interpretation of NGS results at molecular tumor boards.

**Methods:**
MTPpilot is based on a Microsoft SQL database with a web-browser frontend implemented in PHP, HTML, and JavaScript. The SQL database holds tables for COSMIC, ClinVar, OnkoKB, ARUP and ExAC mutations to cross-check a patient's mutational profile against these databases. Metadata from UniProt, KEGG, Ensembl, PDB and the STRING database enrich the mutational profile with functional annotations. Target regions of most common gene panels are stored to check for concordance if multiple panels and gene tests have been run for the same patient. Optionally, MTPpilot can be connected to a local pathology database like PathoPro or a NGS lab database (e.g. MTPdb) to provide diagnostic pathology data and NGS history data for molecular tumor boards. To use MTPpilot, it is sufficient to upload a patient's mutational profile in VCF or tab-delimited format via a dedicated upload website.

**Results:**
An overview of a patient's mutational profile is given via an ideogram, which gives a first glance on the distribution and type of alterations on human chromosomes. If provided, the values of the clinical biomarkers Microsatellite-Instability (MSI), Tumor Mutational Burden (TMB), Loss-Of-Hydrozyogcity (LOH) and Large-Scale-Transitions (LST) are provided next to the ideogram. A patient's mutational profile is separated into distinct tables for short variants, copy-number-alterations, and rearrangements. All tables provide indications for the existence of mutations in databases such as COSMIC, OncoKB, ARUP, etc. Mutations can be interactively visualized either on a SMART protein domain representation or on protein 3D structures using the MTP 3D viewer. MTPpilot also supplies an interactive fusion viewer to display gene structure and breaking points of fusion partners. When integrated with the local NGS lab database called MTPdb, MTPpilot offers an interactive tissue slide viewer for haematoxylin and eosin (H&E) stained tissue slides and a PatientMatcher to identify patients with a similar mutational profile for diagnosis, therapy and physician matching.

**Conclusion:**
Taken together, these and many other functions included in the MTPpilot software provide a user-optimized environment that aids best-informed decision makings at the weekly molecular tumor board of the USZ. This is particularly important for large comprehensive genome panels where the interactive and graphical tools allow for a deeper understanding of the patient's tumor profile.

**209**

P. Schürch[1], A. Lakkaraju[3], L. Malinovska[2], T. Wildschut[1, 2], V. Lysenko[1], A. Aguzzi[3], P. Picotti[2], A. Theocharides[1]

**CALR mutations in myeloproliferative neoplasms affect chaperone function and differentially impact on client proteins**

*Department of Medical Oncology and Hematology, University Hospital Zurich[1], Institute of Molecular Systems Biology, ETH Zurich[2], Institute of Neuropathology, University Hospital Zurich[3]*

**Introduction:**
Calreticulin (CALR) is an endoplasmatic reticulum (ER)-resident chaperone that folds glycoproteins (GPs) such as the thrombopoietin receptor (TPOR), major histocompatibility complex I (MHC-I) and myeloperoxidase (MPO). CALR is frequently mutated in patients with myeloproliferative neoplasms (MPNs). The mutant variants are secreted from the ER due to the loss of the ER retention "KDEL" motif and pathologically activate the TPOR. Further, the mutation impairs the chaperone's ability to buffer calcium in the ER. Whether mutations in *CALR* affect its chaperone function quantitatively (low intracellular levels) or qualitatively (binding affinity to GP or chaperone function) is unknown. In addition, it is unclear whether mutant CALR affects the maturation of other GPs.

**Methods:**
To assess whether *CALR* mutations impact chaperone function, CALR mutants were expressed in CALR knockout (KO) HL-60 cells or murine CALR KO fibroblasts. MPO protein expression was used as a readout for CALR chaperone function. Binding of CALR to MPO was examined by coimmunoprecipitation assays in *CALR*-mutated MARIMO cell lines. To identify further unfolded proteins in MPN patients, primary neutrophils were subjected to limited proteolysis-coupled mass spectrometry (LiP-MS). This technology allows to detect structural changes in protein domains via structure-dependent cleavage patterns of "conformotypic" peptides.

**Results:**
Low intracellular concentration of secreted CALR mutants could cause glycoprotein deficiencies in homozygous *CALR*-mutated patients. In line with this assumption, the expression of MPO and MHC-I was reduced in HL-60 CALR KO cells. In homozygous patients however, MPO but not MHC-I expression was reduced showing that GPs react differently to reduced levels of CALR. Restoring intracellular levels of mutant CALR by either blocking its secretion or by expression of a "secretion-resistant" KDEL-positive mutant CALR did not rescue MPO expression indicating that decreased levels of *CALR* mutants are not responsible for the MPO deficiency. In line with previous reports, the LiP screen confirmed an upregulation of unfolded protein response (UPR) proteins indicative for ER stress in *CALR*-mutated cell lines. When comparing homozygous *CALR*-mutated patients to their *JAK2*-mutated MPN controls, we plotted significant structural changes against the expression levels of the underlying proteins thereby separating the proteins into different clusters. For instance, GPs consistently exhibited a reduction in abundance together with pronounced structural changes throughout multiple protein domains suggesting protein misfolding. Another cluster comprised mainly calcium-regulated proteins whose abundances remained unaltered. In contrast to the GPs, their structural changes exclusively mapped to calcium-binding domains (e.g. EF-hand domain) that most likely underwent a conformational shift caused by an altered calcium homeostasis that is typical for *CALR*-mutated MPN cells.

**Conclusion:**
Our data suggests that *CALR* mutations affect GPs in a client protein-specific manner. This seems not to be the sole consequence of CALR mislocalization, but rather due to a qualitative defect in chaperone function that we are currently investigating. Our screen identified further misfolded GPs in context of *CALR* mutations. We are currently validating whether these GPs are degraded like MPO via the canonical ER-associated protein degradation (ERAD) pathway or via alternative autophagy pathways. Furthermore, we aim to explore how increased protein misfolding and degradation in *CALR*-mutated cells could be therapeutically exploited.

**210**

O. Lauk[1], T. Neuer[1], R. Werner[1], S. Hillinger[1], I. Inci[1], K. Furrer[1], I. Schmitt-Opitz[1]

## Risk factors for the occurrence of postoperative empyema in malignant pleural mesothelioma patients undergoing macroscopic complete resection

*Department of Thoracic Surgery, University Hospital Zurich[1]*

**Introduction:**
Multimodal treatment as the best therapy option is recommended in selected cases for malignant pleural mesothelioma patients (MPM). Patient selection remains challenging especially in regards to postoperative morbidity and mortality. In a recent meta-analysis, postoperative empyema occurred with an incidence of 0.4% after extended pleurectomy/decortication (EPD) and 3.7% after extrapleural pneumonectomy (EPP). We conducted a retrospective study to detect risk factors leading to postoperative empyema after macroscopic complete resection (MCR).

**Methods:**
Of 362 consecutive MPM patients intended to be treated between September 1999 and December 2019, 179 patients were treated with induction chemotherapy followed by MCR, either with EPD (n=41) or EPP (n=138). Logistic regression analysis was performed. Assessment was done only in complete cases. Comorbidities, smoking status, surgery duration and kind of surgery were used as covariates to predict the appearance of empyema. Results are stated as odds ratio (OR) and 95% confidence interval.

**Results:**
Out of 179, 34 cases after EPP and 5 after EPD presented with postoperative early and late empyema, treated with repeated surgical interventions. Patient`s characteristics are shown in table. EPP patients have six times higher odds of empyema appearance than patients undergoing EPD (OR of 6.5, 95% CI: 1.4-36.7; p=0.02) and current smokers five times higher odds compared to former smokers/non-smokers with statistical significance (OR of 5.3, 95% CI: 1.6-18.6; p=0.01). Odds for empyema increase by 50% per hour of surgery (OR of 2, 95% CI: 1.1-2; p=0.01). Comorbidities lowers the odds of having an empyema by 55% (OR of 0.5, 95% CI: 0.2-1.2; p=0.1).

**Conclusion:**
Our data demonstrate that risk factors such as smoking status and surgery duration associated with the occurrence of postoperative empyema after MCR for patients with MPM. Careful patient selection and prevention of preoperative risk factors such as smoking cessation might further help to reduce the incidence of postoperative empyema.

**211**

M. Arnold[9], J. Schweizer[9], U. Fischer[7], L. Bonati[6], G. De Marchis[6], K. Nedeltchev[2], T. Kahles[2], C. Cereda[3], G. Kägi[1], J. Monataner[8], G. Ntaois[5], C. Förch[4], A. Luft[9], K. Spanaus[10], A. von Eckardstein[10], M. Katan Kahles[9]

**Lipoprotein(a) is associated with large artery atherosclerosis (LAA) stroke etiology and recurrent cerebrovascular events: Results from the BIOSIGNAL Study**

*Canton Hospital St.Gallen, Dept. Neurology[1], Cantonal Hospital of Aarau, Dept. Neurology[2], Cantonal Hospital, Lugano, Dept. Neurology[3], Universitiy Hospital of Frankfurt, Dept Neurology, Germany[4], Universitiy Hospital of Larissa, Dept. Internal Medicine, Greece[5], University Hospital of Basel, Dept. Neurology[6], University Hospital of Bern, Dept. Neurology[7], University Hospital of Seville, Dept. Neurology, Spain[8], University Hospital of Zurich, Dept. Neurology[9], University Hospital of Zurich, Dept. of Clinical Chemistry[10]*

**Introduction:**
Increased plasma levels of Lipoprotein(a) (Lp(a)) are associated with a history of acute ischemic stroke (AIS). However, its association with underlying stroke etiology and stroke recurrence in AIS patients is uncertain. We aimed to evaluate the association of Lp(a) with large artery atherosclerosis (LAA)-stroke etiology and recurrent cerebrovascular event risk.

**Methods:**
We measured Lp(a) within 24 hours of symptom onset in 1759 patients of the prospective multicenter BIOSIGNAL (Biomarker signature of stroke aetiology, NCT02274727) study. Co-primary outcomes were LAA-stroke etiology determined by the TOAST criteria (verified by the causative classification system (SSS-TOAST)) and recurrent cerebrovascular events within one year. Logistic regression and cox-proportional-hazards-regression models were used to estimate the association of Lp(a) with the outcome measures.

**Results:**
Lp(a) was associated with LAA stroke etiology adjusted for demographic and vascular risk factors (OR 1.39, 95%CI 1.1-1.75, p<0.01, per unit log10 Lp(a) increase). Interaction analysis for baseline risk factors revealed age as a potent effect modifier. The adjusted OR in patients aged ≤60 years was 3.69, (95%CI 1.89-7.18, p<0.001, per unit log10 Lp(a) increase), in patients aged >60 years the association was no longer significant. Moreover, Lp(a) levels >100 nmol/l (or 50mg/dl) were associated with an increased risk for recurrent cerebrovascular events among patients aged ≤60 years (adjusted HR 2.6, 95%CI 1.19-5.67, p=0.017).

**Conclusion:**
Individuals under 60 years with higher Lp(a) levels had a higher likelihood of LAA stroke etiology and a higher risk of recurrent cerebrovascular events. Therefore Lp(a) may be used to select patients for intensified monitoring by neurovascular imaging.

**212**

M. Arnold[3], C. Nakas[1], A. Luft[3], M. Christ-Crain[2], A. Leichtle[1], M. Katan Kahles[3]

**Independent prognostoc value of MRproANP levels in stroke patients is unaltered over time**

*Bern University Hospital, University Institute of Clinical Chemistry[1], University Hospital Basel, Dept. for Clinical Science[2], University Hospital of Zurich, Dept. Neurology[3]*

**Introduction:**
Midregional proatrial natriuretic peptide (MRproANP) is known to be independently associated with cardioembolic stroke etiology and to improve risk stratification for 90-day mortality when measured within 24-72 h after symptom onset in acute ischemic stroke (AIS). However, the optimal timepoint for assessment is unclear because the release kinetics in the acute phase after stroke has not been characterized. This study aimed to evaluate diagnostic and prognostic utility of MRproANP at different time-points during the first 5 days in patients with AIS.

**Methods:**
Samples for MRproANP measurements were collected at multiple time-points during the first 5 days of hospitalization in 348 consecutively enrolled AIS patients. The prognostic value for 90-day mortality, 90-day functional outcome and the association with cardioembolic stroke was assessed regarding the time of measurement and change over time was modeled using generalized estimating equations (GEE).

**Results:**
MRproANP levels were significantly higher in patients with cardioembolic stroke etiology (OR: 9.75 [95% CI: 3.2 – 29]; 10.62 [3.4 – 33.3]; 10.8 [3.1 – 37.1]; 19.4 [5.49 – 68.7] on admission, day 1, 3 and 5) and patients deceased within 90 days (OR 52.9 [7.3 – 384.1]; 60.4 [7.5 – 488.3]; 18.75 [2 – 174]; 25.38 [3.6 – 178.4] on admission, day 1, 3 and 5) during all measured time-points in the first 5 days of hospitalization. Change over time does not significantly modify the prognostic value of MRproANP.

**Conclusion:**
MRproANP remains highly predictive for mortality and cardioembolic stroke etiology in the acute phase of stroke; repeated measurements do not improve the prognostic value.

**213**

F. Meier-Abt[2, 3], J. Lu[1], M. Gwerder[3], M. Roiss[3], W. Huber[1], R. Aebersold[2], T. Zenz[3]

**Proteomics of Trisomy 12 Chronic Lymphocytic Leukemia (CLL) as Part of Multi-Omics CLL Profiling**

*EMBL Heidelberg[1], Institute of Molecular Systems Biology, ETHZ[2], University Hospital Zurich[3]*

**Introduction:**
Chronic lymphocytic leukemia (CLL), the most frequent leukemia in the Western world, is marked by genetic and epigenetic heterogeneity. The relationship of genetic and epigenetic changes in CLL cells to the evolutionary principles underlying CLL clone development is complex. Specifically, the functional consequences of gene mutations on tumor phenotype are poorly understood. In order to elucidate the complex relationship between (epi)genetic changes and tumor phenotype, we developed a multi-omics profiling platform of CLL patient samples with a special focus on the proteomic profiling of CLL.

**Methods:**
We acquired genetic, epigenetic (methylome), transcriptomic, functional (drug screen assays) and proteomics analyses in a total of 50 CLL patient samples. Data-independent acquisition mass spectrometry (DIA-MS) was performed for all samples. The resulting data were integrated with genetic, epigenetic, transcriptomic and functional data and analyzed bioinformatically. Furthermore, the proteomics data was assessed for changes in protein complex formations.

**Results:**
The unbiased proteomic analysis captured 4521 (Lumos) and 3942 (timsTOF) different proteins. For key molecular subgroups we identifies 87 (IGHV status, adj. p-value <0.01) and 535 (Tri12, adj. p-value <0.01) differentially regulated proteins. As an example, ZAP70 was found to be significantly upregulated in proteomics and transcriptomics data of IGHV unmutated patients. Furthermore, several genes located on chromosome 12 showed significantly increased RNA and protein expression in trisomy 12 CLL. Weaker associations were seen for individual gene mutations (SF3B1, p53, DDX3X) with differential protein expression. We performed gene set enrichment analyses and observed significant upregulations of several pathways such as interferon gamma, interferon alpha, MTORC1 and PI3K_AKT_MTOR signaling in trisomy 12 CLL (100 permutations, FDR <0.25). Integration with functional data from a drug screen assay showed 475 significant associations (p-value <0.01) with protein expression for unmutated IGHV CLL and 21 significant associations for mutated IGHV CLL. For example, downregulation of NFKB1 expression in unmutated IGHV CLL strongly correlated with viability after drug treatment.

**Conclusion:**
A unique multi-omics dataset was generated for CLL patient samples that allows to study the relationship between genetic, epigenetic, transcriptomic and proteomic alterations as well as corresponding changes in cell functionality as assessed by response to different drug panels. A special focus was placed on global protein expression of CLL patient cells, since it is protein expression that determines cell functionality. This integrated dataset opens the door for understanding the evolutionary principles underlying CLL clone formation. Furthermore, our studies will add to the general knowledge of how tumor cells integrate an additional chromosome on protein complex level.

**214**

F. Staubli[2], S. Dudli[2], I. Heggli[2], S. Fucentese[1], O. Distler[2], F. Brunner[1], A. Jüngel[2]

**Altered expression of neurotrophins and receptors in the skin of patient with Complex Regional Pain Syndrome (CRPS)**

*Balgrist Clinic, University Hospital, Zürich, Switzerland[1], Department of Rheumatology, Center of Experimental Rheumatology, University Hospital Zurich, Switzerland [2]*

**Introduction:**
Complex regional pain syndrome (CRPS) is a painful condition with clinical features including pain, sensory, sudomotor and vasomotor disturbances, trophic changes and impaired motor function. Symptoms usually appear after an initiating noxious event such as trauma and surgery. The incidence from CRPS varies from 5-26/100'000 affecting mainly women. The course varies from mild and self-limiting to chronic disease with a high impact on daily functioning and quality of life.
The pathophysiology includes an altered intercellular communication of sensory nerve fibers and resident cells thus preventing resolution of inflammatory processes. Neurotrophins and receptors are mediators in cell-to-cell communication and key mediators of pain signaling. The aim was to identify differential gene expression of neurotrophins and receptors in skin tissue and isolated skin fibroblasts contributing to the pathophysiology of CRPS.

**Methods:**
Skin biopsies from CRPS patients (affected and non-affected side, n= 4 each) and healthy subjects (HC, n= 4) were taken from upper and lower extremities from Balgrist Clinic to isolated total RNA. Skin fibroblast were isolated from additional skin biopsies of patients with CRPS affected side and healthy controls (n=4 each, passage 3-6). Cells were starved and subsequently stimulated with TNFa (10 ng/ml for 24 h) or TGFb (10 ng/ml for 24 h) to mimic the active disease. Total RNA was isolated from skin tissues by microRNeasy kit (Qiagen) and from isolated skin fibroblasts by miRNeasy kit (Qiagen) according to the manufactures instruction. Neurotrophin ligands (NGF, BDNF, NT3, NT4) and neurotrophin receptors (p75, TrkA, TrkB and TrkC) expression was measured by quantitative real time PCR (qPCR) using GAPDH as a reference gene.

**Results:**
The skin of patients with CRPS (affected versus the non-affected side) showed upregulated gene expression of BDNF (1.51+/- 0.44 fold), p75 (1.92+/-0.80 fold) and TrkB (1.38+/-0.47 fold).
Isolated skin fibroblasts from the affected side of patients with CRPS compared to healthy skin fibroblasts showed similar gene expression pattern. The basal expression of BDNF is increased (4.01+/-1.41 fold). Stimulation of the skin fibroblasts with TGFb induced BDNF gene expression in HC skin fibroblasts (1.4+/-0.57 fold), however not in skin fibroblasts of patients with CRPS (0.8+/-0.19 fold). Stimulation with TNFa downregulated BDNF in both, in HC skin fibroblasts (0.84+/-0.76 fold) and in skin fibroblasts of patients with CRPS (0.58+/-0.22 fold) compared to unstimulated cells.
The basal expression of p75 is increased in skin fibroblasts of patients with CRPS (4.55+/-3.29 fold). Stimulation of the skin fibroblasts with TNFa induced p75 gene expression in HC skin fibroblasts (2.4+/-1.22 fold) but not in skin fibroblasts of patients with CRPS (0.91+/-0.36 fold). TGFb induced the expression of p75 to the same extend in both HC (2.05+/-0.76 fold) and CRPS (2.17+/-1.44 fold).

**Conclusion:**
BDNF and the receptor p75 are both upregulated in CRPS skin tissue and isolated skin fibroblasts. TNFa and TGFb do not increase levels of BDNF further in CRPS. This might contribute to the dysregulated healing process and sustained pain. Therefore, targeting neurotrophins and receptors should be considered as novel therapeutic strategies in CRPS.

**215**

R. Chen[1], S. Saponara[1], T. Reding[1], R. Graf[1], S. Sonda[1]

**Peripheral serotonin-p21 axis contributes to metabolic changes during ageing**

*Swiss Hepato-Pancreatico-Biliary(HPB) Centre, Division of Surgical Research, Department of Visceral & Transplantation Surgery, University Hospital Zurich[1]*

**Introduction:**
Obesity, a worldwide epidemic, is associated with the development of numerous life-threatening comorbidities. The major medical complications of obesity are responsible for 70% of deaths worldwide. In this context, finding effective and safe approaches to prevent obesity are of paramount importance to improve life quality. A critical component associated with gain of body weight is ageing. One of the risk factors for ageing is abnormal lipid storage that leads to increased risks to develop obesity and associated disorders. Here we primarily investigated whether increased body weight and metabolic changes during ageing in the early phase of adulthood may predispose to the development of metabolic dysfunctions later in life. Secondly, we focused on molecular regulators of age-dependent weight gain, which may provide novel targets for preventive or therapeutic interventions to counteract obesity.

**Methods:**
In this study, we examined the regulation of body weight, metabolic parameters and adipose tissue histopathology in male C57BL/6 mice in early adulthood from two to six months of age. Genetically modified mice deficient for peripheral serotonin (Tph1 -/-), cyclin-dependent kinase inhibitor p21 (p21 -/-) or both were used to study the molecular regulators involved in age-related metabolic changes. The different parameters were evaluated by biochemical and immunohistochemical methods.

**Results:**
Our results revealed that the increased body weight during ageing in early adulthood is accompanied by increased levels of blood glucose and cholesterol. In addition, ageing was associated with hypertrophy of white adipose tissue. In addition, an increase of macrophage recruitment was observed. These are early indicator of adipocyte dysfunction. At the molecular level, aged adipose tissue had increased expression of the synthetic enzyme of serotonin (Tph), a regulator of hypertrophy and metabolic changes during diet-induced obesity. Ageing of genetically modified serotonin-p21 animals revealed that peripheral serotonin promotes age-associated metabolic changes in adipose tissue. Furthermore, glucose levels activated a p21-dependant signalling pathway.

**Conclusion:**
Accumulation of excessive body fat is a growing public health problem, which associates with leading causes of death. Even though, a better life style can prevent or reduce the complications, it is a complex and long process. Thus, elucidating molecular regulators of weight gain to prevent obesity are needed. Our results identify serotonin-p21 signalling pathways as a key metabolic regulator that supports early adulthood weight gain. Importantly, pharmacologic exploitation of this pathway may be beneficial for controlling excessive weight gain in a later stage of life.

**216**

C. Caiado[1], L. Kovtonyuk[1], M. Manz[1]

**Contribution of IL-1 Mediated Inflamm-ageing to Clonal Hematopoiesis Progression in Murine Models**

*UniversityHospital Zürich[1]*

**Introduction:**
Clonal Hematopoiesis of indeterminate Potential (CHiP) is defined as the presence of an expanded somatic blood cell clone carrying a mutation in genes that are drivers of hematologic malignancy including DNMT3A, TET2 (and others) at a variant allele frequency of at least 2% in the absence of other hematological abnormalities. CHiP has a prevalence of about 10% in the 70-80 year old population, further increases with ageing and associates with an increased risk of hematological malignancies, cardiovascular disease and all-cause mortality. Recent studies indicate that decades may elapse between acquisition of a mutation (DNMT3A, TET2) and CHiP development, suggesting that environmental factors contribute to clonal expansion. Thus, it is key to decipher CHiP pathobiology and drivers for progression. Here we hypothesize that hematological ageing and inflammation (inflamm-ageing) are drivers of CHiP and that therapeutic targeting of these processes can prevent progression to malignancy. We aim to test the effect of the IL-1 pathway - a key driver of hematopoietic stem and progenitor cells (HSPCs) inflamm-ageing (our unpublished data) - on the progression of Tet2 - driven CHiP.

**Methods:**
In vitro: To test the effect of IL-1 pathway activation on the self-renewal capacity of wild-type (WT) or Tet2+/- HSPCs (Lin-Sca-1+c-Kit+ cells) these were exposed to IL-1a or IL-1b and their colony forming unit (CFU) capacity over multiple plating was evaluated. In vivo: To test the effect of IL-1 pathway activation on Tet2+/- – driven CHiP progression we created bone marrow (BM) chimeras by transplanting total BM cells from CD45.2 WT or Tet2+/- animals with CD45.1 BM cells on a 1:9 ratio into lethally irradiated CD45.1xCD45.2 (F1) hosts. After 2 months, once homeostasis is re-established, chimeric animals were injected with IL-1a or b and peripheral chimerism of WT or Tet2+/- clones was longitudinally assessed. To gain some insight into the mechanism by which IL-1a leads to an increased Tet2+/- HSPCs fitness in vivo, we plan to expose WT and Tet2+/- animals to IL-1a and determined its effects on HSCPs population frequencies, cell cycle staging and survival. Further molecular characterization (RNA-Seq) of WT and Tet2+/- HSPCs exposed to IL-1a will allow us to clarify the gene network underlying the effect of IL-1a on Tet2 - driven CHiP.

**Results:**
Our preliminary in vitro data shows that in the absence of IL-1 ligands, Tet2+/- HSPCs show increased CFU capacity compared to WT. Interesting we observe that IL-1a, but not IL-1b, leads to a significant decrease of the self-renewal capacity of WT HSPCs, while this effect is mitigated in Tet2+/- HSPCs. In agreement, BM-chimerism experiments show that in vivo exposure to IL-1a, but not IL-1b, leads to a specific expansion of Tet2+/- derived hematopoietic populations in peripheral blood while shows no impact on WT cells. Characterization of the WT and Tet2+/- peripheral blood populations after IL-1a exposure indicates that the gain of fitness in the Tet2+/- clone results mostly from an increase of myeloid and b-cell differentiation.

**Conclusion:**
We show that IL-1a is a major pro-inflammatory cytokine regulating the expansion of Tet2+/- hematopoietic clones, further implicating inflamm-ageing as a key driver of CHiP progression and potential neoplastic transformation. Further dissection of the cellular and molecular networks underlying this effect will further clarify the impact of inflamm-ageing derived factor IL-1a on Tet2-derived CHiP opening potential avenues for preventive therapeutic interventions.

**217**

A. Vent[2], C. Surber[2], N. Graf[2], C. Buset[2], V. Figueiredo[1], G. Schönbächler[1], J. Hafner[2]

**Lidocaine 1%, epinephrine 1:100'000 with sodium hydrogen carbonate (bicarbonate) admixture in mixing ratio 3:1 is less painful than in mixing ratio 9:1: A double-blind, randomized, placebo-controlled, crossover trial**

*Kantonsapotheke Zürich[1], University hospital of Zurich[2]*

**Introduction:**
Uncountable surgeries are performed under local anesthesia. Our primary objective was to show that higher bicarbonate admixture to lidocaine at ratio 3:1 causes less burning sensation during injection than ratio 9:1. Secondary outcomes were to compare unbuffered lidocaine and placebo (saline), assess clinical relevance for the volunteersand to assess anesthetic effect and duration of local anesthesia.

**Methods:**
48 volunteers were included and divided into 2 groups. Group 1 received 4 subcutaneous injections: lidocaine 1% with epinephrine 1:100,000 buffered with bicarbonate 8.4% at ratio 3:1 versus lidocaine 1% with epinephrine 1:100,000 buffered at ratio 9:1 versus unbuffered lidocaine with epinephrine 1:100,000 versus sodium chloride 0.9% as control. Group 2 received the 2 buffered solutions at ratio 3:1 and 9:1 respectively. Injection pain was assessed using a Numerical Rating Scale from 0 to 10 and in view of clinical relevance, rated as desirable, acceptable, less acceptable or almost/totally unacceptable. Anesthesia was assessed with a standardized laser stimulus.

**Results:**
All volunteers completed the study, with no severe advents. Burning sensation the 9:1 mixture was rated significantly higher than the 3:1 mixture ($p=0.044$). Unbuffered lidocainewas rated significantly more painful than the 3:1 mixture ($p<0.001$) and the 9:1 mixture ($p=0.033$). Placebo was rated significantly more painful than the 3:1 mixture ($p<0.001$) and the 9:1 mixture ($p<0.001$).
The discomfort versus the comfort during injection was relevant for the majority of participants. In all volunteers, laser-induced pain was absent in the injection areas of the solutions containing lidocaine between 5 minutes and 3 hours after infiltration, and present in the injection areas of the placebo.

**Conclusion:**
Our study demonstrates that a bicarbonate admixture at ratio 3:1 causes even less discomfort. Also, the higher buffer admixture does not affect the anesthetic effect, which starts almost immediately after injection and lasts at least 3 hours.
Acidity has been assumed responsible for the burning sensation during infiltration. The detection of acid-sensing ion channel receptors or nociceptors supports this explanation. The causal link between pH and burning pain during infiltration is also supported by our trial with the unbuffered solution at pH 3.4 and with the pharmacologically inactive placebo at pH 6.2. The pain during infiltration with the neutralized solutions (solution 3:1: pH 7.5, solution 9:1: pH 7.3) was significantly reduced. The reason is that at neutral pH, lidocaine is predominantly present in its active form that is lipophilic, and in contrast to the inactive, hydrophilic form readily permeates the nerve membrane to bind from the cytosol to the acid-sensing ion channel receptors. We also demonstrated that saline is more painful thanunbuffered lidocaine because due to the absence of lidocaine, acidity causes a noticeably longer duration of burning sensation until the body itself neutralizes the injected solution. Our trial also supports the theory that $CO_2$ itself has analgesic effects. When bicarbonate is mixed with acidic lidocaine, water ($H_2O$) and carbon dioxide ($CO_2$) are formed. In the solution at ratio 3:1 more $CO_2$ is formed than in the one at ratio 9:1, which more effectively reduces the burning sensation of lidocaine.

## Conference Location

University Hospital Zurich
Grosser Hörsaal Ost
Rämistrasse 100
8091 Zürich

## Organizer / Contact Address

Gabriela Senti, Prof. MD
Director Research and Education
University Hospital Zurich
Rämistrasse 100
8091 Zürich
dfl@usz.ch

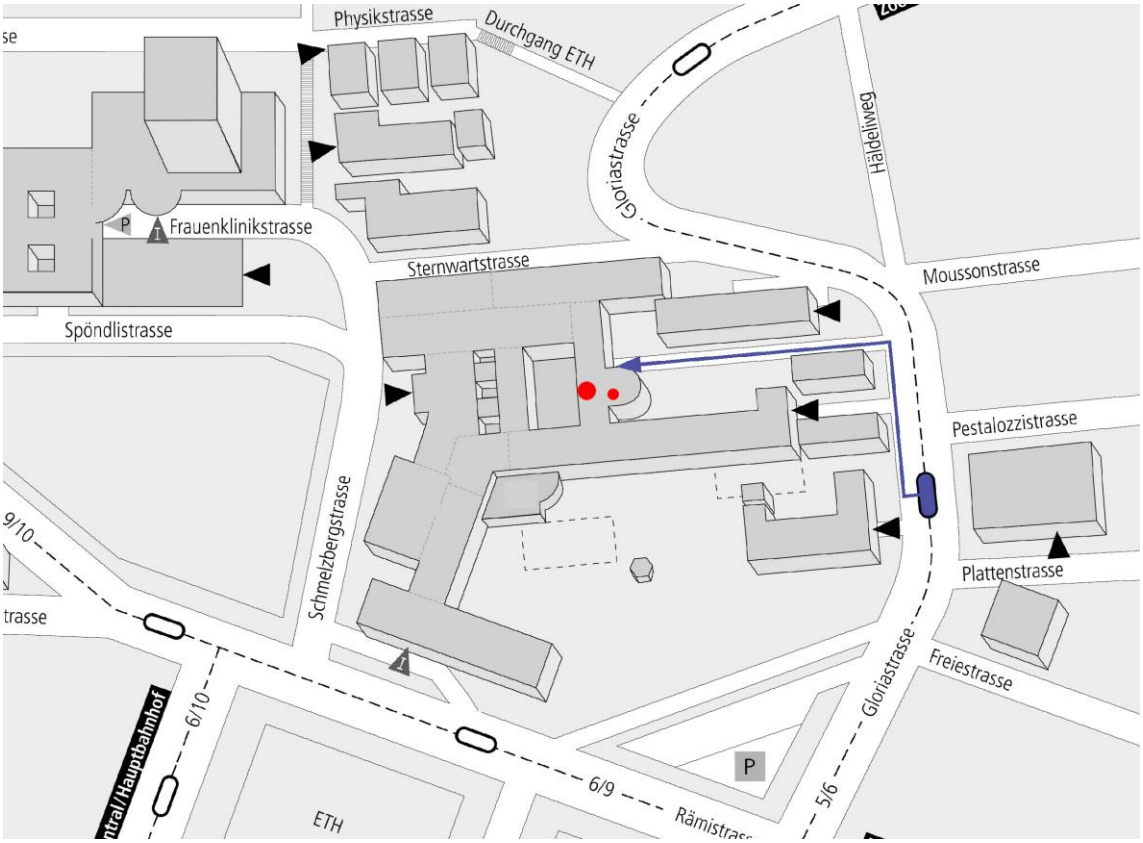


USZ Universitäts Spital Zürich